BEAM DYNAMICS AND OPTIMIZATION

Editors
E.P. Zhidkov
D.A. Ovsyannikov
I.P. Yudin

JOINT INSTITUTE FOR NUCLEAR RESEARCH

Proceedings of the 4th International Workshop

BEAM DYNAMICS AND OPTIMIZATION

October 13 - 17, 1997
Dubna, Russia

Editors
E.P. Zhidkov
D.A. Ovsyannikov
I.P. Yudin

Dubna 1998

Preface

The traditional International Workshop "Beam Dynamics and Optimization" was held in the Laboratory of Particle Physics, JINR, Dubna, near Moscow, Russia on October 13-17, 1997. The previous Workshops were BDO-94, BDO-95, BDO-96. The present Workshop (BDO'97) is organized by the Joint Institute of Nuclea· Research (Dubna), St.Petersburg State University(Faculty of Applied Mathematics & Control Processes and nstitute of Computational Mathematics & Control Processes), D.V.Efremov Institute of Electrophysical Apparatus (St.Petersburg), Institute of High Energy Physics (Protvino), Russian Research Center I.V. Kurchatov Institute (Moscow), Saratov State University, Peoples' Friendship University of Russia (Moscow).

PROGRAMME COMMITTEE: chairman - D.A. Ovsyannikov (Russia), V.A. Belyakov, B.I. Bondarev, N.V. Egorov, O.I. Nikonov, Yu.A Svistunov, I.P. Yudin, A.V. Zherebtsov (Russia), F. Meot (France), Yu. Tur (Ukraine), R. Ryne, A. Todd (USA), S. Kawata (Japan),

INTERNATIONAL ORGANIZING COMMITTEE: chairman - V.I. Zubov (Russia), co-chairman - E.P. Zhidkov (Russia), co-chairman - D.A. Ovsyannikov (Russia), S.N. Andrianov, Yu.A. Budanov, N.S. Edamenko, A.B. Kurzhanskii, B.P. Murin, V.V. Petrenko, V.P. Stepanchuk, V.A. Teplyakov, M.F. Vorogushin (Russia), A.N Dovbnya (Ukraine), H.Mais (Germany), M.Berz, G. Gillespie, R. Jameson (USA), Y. Yamazaki (Japan)

DUBNA LOCAL COMMITTEE: chairman - E.P. Zhidkov, vice-chairman - I.P. Yudin, A.V. Fedorov, G.G. Gulbekyan, I.N. Ivanov, V.D. Kekelidze, I.N. Meshkov, I.M. Melnichenko, R.V. Polyakova, I.A. Shelaev, G.D. Shirkov, A.P Korol

More than 80 scientiests attended the Workshop BDO'97 and 30 reports and short communications were presented.

The scientific topics cover the wide scope of mathematical problems including

• nonlinear problems of beam dynamics: mathematical modelling, nonlinear aberrations, including space charge forces; • the self-consistent distributions problem; • long time beam; • evalution, dynamic aperture and halo problems; • methods of control theory in the problems for the beam; • plasma dynamics optimization; • mathematical modelling of the electro- and magnetic fields; • computing problems for beam physics; • software for the beam dynamics and optimization.

This book containts refereed versions of the papers presented at the Workshop. We are grateful to all the authors for thier contributions.

We hope this book will be useful for other scientists, programmers, engineers and students.

The BDO'97 is sponsored by Russian Ministry of Science and Technologies and by Russian Foundation for Basic Research.

Editors:
E.P. Zhidkov, D.A. Ovsyannikov, I.P. Yudin

ISBN 5-85165-520-8

Contents

COMPUTER MODELLING OF A HIGH SOLID ANGLE MASS–SPECTROMETER [1]

S.N. Andrianov, N.S. Edamenko, D.A. Ovsyannikov

Bibliotechnaya 2, Computational Mathematics & Control Processes Institute, St.Petersburg State University, St.Petersburg, 198904, Russia
e-mail: vmpu@apmath.spb.su

W. Mittig

GANIL, Caen, France

Abstract

As an entrance focusing elements for mass–spectrometers we can use both quadrupole lenses and a solenoid lense. The first case can be realized using quadrupole lenses with high apperture. In the second case the lense aperture is more less. That is why for high solid angle mass–spectrometer design problem we consider the system which consists of two solenoids at the entrance and at the exit of the system, two electrostatic deflectors and two magnets separated by either a quadrupole lens or a solenoid. The central quadrupole lens can be used for focusing in Y–plane (the deflection plane) or in X–plane.

1 . Optical Structure of the Mass–Spectrometer. The above-mentioned structure should ensure the following conditions:

- *there must be kinetic achromatism;*
- *mass dispersion must be not less than 10 mm/%;*
- *resolution must be not less than 100.*

The most important condition is the first one. It means that all particles with different velocities for point source are focused into a point on the detector. The second condition guarantees mass separation in the pointed interval: two particles with masses M, $M + \Delta M$, $\delta M = \Delta M/M = 0.01$ are separated by the distance *10* mm. The third condition is closely connected with a finite emittance of the beam and is defined by a particle distribution function on the detector.

As usual, solution of the motion equations in linear approximation in the X–plane (this is a deflection plane) is presented in the form

$$x = r_{11}x_0 + r_{12}x'_0 + r_{13}y_0 + r_{14}y'_0 + r_{15}\delta v + r_{16}\delta m,$$

where $\mathbf{R} = \{r_{ik}\}$, $i,k = \overline{1,6}$ is the transfer matrix for our spectrometer, x, y are coordinates in X– and Y–plane corresponding y.

For our goal we must distinguish the coefficients r_{15} and r_{16}. Than we must create a procedure to vanish the coefficient $\mathcal{V} = r_{15}$ attached to the fractional deviation of velocity δ_v and simultaneously to increase the coefficient $\mathcal{D} = r_{16}$ attached to the deviation $\delta m = \delta_{M/Q}$ of the ratio mass/charge. This coefficient defines the mass

[1]Work supported by the Russian Foundation for Basic Research (grants No.96-02-17335, No.96-01-00926).

dispersion $\mathcal{D}$, which value is usually supposed equal to *1* to satisfy the usual requirement *10* mm/%.

As in this work we consider a linear model for the mass–spectrometer, then we use the matrix formalism for beam-line design. For this purpose computer algebra codes (CAC) are more preferable than pure numerical codes. The modern CAC furnished by vizualisation tools make design of beam lines more flexible. A designer can build $2D$– and $3D$–surfaces $\mathcal{V} = const$ and $\mathcal{D} = const$ in the parameters space.

Because the solenoids mix X– and Y–planes the structure of these surfaces becomes too complex. The visual modelling process admitted by such computer algebra code as *MAPLE V* [1] permits to select some appropriate systems more operative and then selected appropriate systems can be considered as starting systems for the next optimization process. The set of appropriate systems is necessary for the following process of high order aberrations investigation too.

2 . Interpretation of Results. For the mass–spectrometer design problem the FMA structure was chosen as an starting problem on which we tested our concepts and algorithms. The parameters for this system were taken from the paper [2]. This information is incomplete, that is why we make some modelling process. As an example we demonstrate the calculation results in corresponding pictures (see Figures 2–5) of the Appendix B.

For our mass–spectrometer with high solid acceptance we consider two solenoids instead of two doublets of quadrupole lenses (at the entrance and at the exit of the system) and two magnets separated by either a quadrupole lens or a solenoid instead of one magnet at the center, see Figure 1 in the Appendix B.

The central quadrupole lens can be used for focusing in X–plane (the deflection plane) or in Y–plane. In the case of focusing in X–plane the envelopes along the total system are acceptable. Because this case can be sensitive to influence of high order aberrations then this variant must be investigated more carefully in the frame of nonlinear model. In the case of focusing in Y–plane the envelope values are acceptable too, but the drift length d_2 (see Table 1 in the Appendix A) is almost on the boundaries of an admissible region for the system parameters. The variant with central solenoid seems promising. But this solenoid must be short (not greater than $0.4\ m$). Besides, the used solenoid as a central focusing element introduces more complex dependence on a set of the system parameters. This variant should be investigated for high order aberrations in detail . On Figures 4, 5 of the Appendix B one can see the dependences of d_2 (from the condition $\mathcal{V}(d_2) = 0$) and $\mathcal{D}$ on some essential parameters *omega*= ω and Bs2=B_{s_2}, where

$$\omega = \begin{cases} \sqrt{\frac{qG}{m_0 c\beta\gamma}} & \text{for the reduced gradient for the central quadrupole,} \\ \frac{B_0}{2m_0 c\beta\gamma} & \text{for the reduced magnetic field on a pole for the central solenoid,} \end{cases}$$

$$B_{s_2} = \frac{B_2}{2m_0 c\beta\gamma},$$

q, m_0, β, γ are a charge, a rest mass a reduced velocity and energy for a reference particle, G, B_0, B_2 are a gradient, magnetic fields for the corresponding lenses.

We should note that for achromatic system creation (with $\mathcal{V} = 0$) there are two ways: the corresponding distance d_2 is calculated from the achromatic condition for the total

system and this distance is calculated from similar condition for the truncated system when we do not consider last solenoid and last two drifts (with d_1 and d_4 as distances). The corresponding dependence d_2 on the system parameters has different forms. For the total system there is a ravine on a smooth slope (see Figure 4 in the Appendix B). For the truncated system condition we obtained the same smooth slope, without the ravine. The B_{s_2} values corresponding to the ravine location should be avoided for stability of the system working. On Figure 5 one can see the dependence of the beam spot size $X_{\max}$ on d_4. The character of such dependences is similar for quadrupole and solenoid as the central focusing elements. We should note that the similar behaviour there is for the FMA structure.

For the FMA system the beam has a crossover in center of the system in the deflection plane. This condition is one of possible conditions which can be imposed on the system. For the designed system we also consider different additional (besides main conditions for achromatism and mass–dispersion) conditions. This is necessary for next investigations including high order aberrations. The made investigations show that the system with desired characteristics exists. As an example we consider the variant when there is the crossover in the center of the system. For our system we have the crossover in both planes (compare with the FMA structure). The corresponding envelopes in the designed and the FMA systems are demonstrated on Figure 2). On that Figure one can see the beam spots on the detector for the corresponding structures too.

Our CAC for the procedure of parameters ranging are flexible and suitable for swithing from one model to another. These tools are based on symbolic formulae and their visual interpretations. As one can see from the corresponding Figures 4, 5 there are some problems attached to ranging of the final variant of the mass–spectrometer. In particular, the value of d_4 corresponding to $minX_{\max}$ is selected so that in the terminal solenoid there are no crossovers. What is more such ranging procedure should lead to a set of variants, which should be investigated including high order aberrations. Some model initial distributions of transverse phase coordinates are chosen for demonstrating distortion and resolution.

3 . Conclusion. Symbolic and numerical calculations demonstrate a principal opportunity of designing of High Solid Angle Mass–Spectrometer. But it is necessary to investigate an influence of high order aberrations on the basic system parameters (for example, dispersion, resolution). Decreasing of this influence can be realized including optimization methods and/or additional compensating structure elements (for example, sextupoles, octupoles).

Appendix A

The list of basic system and beam parameters.

Table 1

Geometrical parameters $[m]$		
d_0	distance between source and first solenoid	
d_1	distance between first solenoid and first electric dipole	
d_2	distance between electric dipole and magnetic dipole	
d_3	distance between magnetic dipole and central focusing element	
d_4	distance between second solenoid and target	
L_e	length of electric dipole	
L_m	length of magnetic dipole	
L_{s1}	length of first solenoid	
L_q	length of central quadrupole	
L_{s0}	length of central solenoid	
L_{s2}	length of second solenoid	
Field parameters		
E_0	field in electric dipole	$[kV/cm]$
B_0	field in magnetic dipole	$[T]$
B_{s1}	field in first solenoid	$[T]$
G	field gradient in central quadrupole	$[kG/cm]$
B_{s0}	field in central solenoid	$[T]$
B_{s2}	field in second solenoid	$[T]$
$\alpha_e = \alpha_m$	deflection angles in electric and magnet dipoles	
$E_{\rho 0}$	electric rigidity	$[MeV/Q]$
$B_{\rho 0}$	magnetic rigidity	$[Tm]$
Beam parameters at start		
X_m	X-size of beam spot $[mm]$	
Y_m	Y-size of beam spot $[mm]$	
$(dX/dZ)_m$	X-plane angular acceptance $[mrad]$	
$(dY/dZ)_m$	Y-plane angular acceptance $[mrad]$	
δ_p	momentum acceptance [%]	

The values of the basic system parameters:

Table 2

Geometry $[m]$	
d_0	0.200
d_1	0.200
d_2	2.110
d_3	0.300
d_4	1.600
L_e	1.496
L_m	0.244
L_{s1}	0.600
L_q	0.400
L_{s0}	—
L_{s2}	1.000

Table 3

Fields	
E_0	$50.00\,kV/cm$
B_0	$1.500\,T$
B_{s1}	$4.666\,T$
G	$3.000\,kG/cm$
B_{s0}	$-\ T$
B_{s2}	$1.900\,T$
$\alpha_e = \alpha_m$	$14.0°$
$E_{\rho 0}$	$20.00\,MeV/Q$
$B_{\rho 0}$	$1.100\,Tm$

The values of the basic beam parameters:

Table 4

Beam at start	
X_m	$\pm 0.5\,mm$
Y_m	$\pm 0.5\,mm$
$(dX/dZ)_m$	$\pm 120\,mrad$
$(dY/dZ)_m$	$\pm 120\,mrad$
δ_p	$\pm 10\%$

Table 5

Envelopes along the system $[cm]$							
	S_1	E_1	M_1	$Q\,(S_0)$	M_2	E_2	S_2
X_{max}	8.67	8.10	1.39	0.62	1.39	8.74	9.40
Y_{max}	8.67	8.10	1.40	0.78	1.40	8.75	9.48

Appendix B

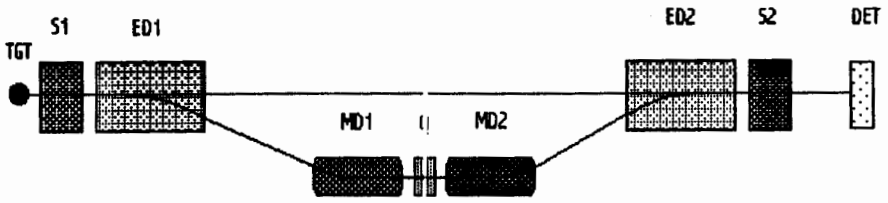

Figure 1

Schematic layout of the High Solid Angle Mass-Spectrometer
S1 , S2 - magnetic solenoids, ED1, ED2 - electric dipoles
MD1, MD2 - magnetic dipoles, Q - central quadrupole
TGT - target, DET - detector

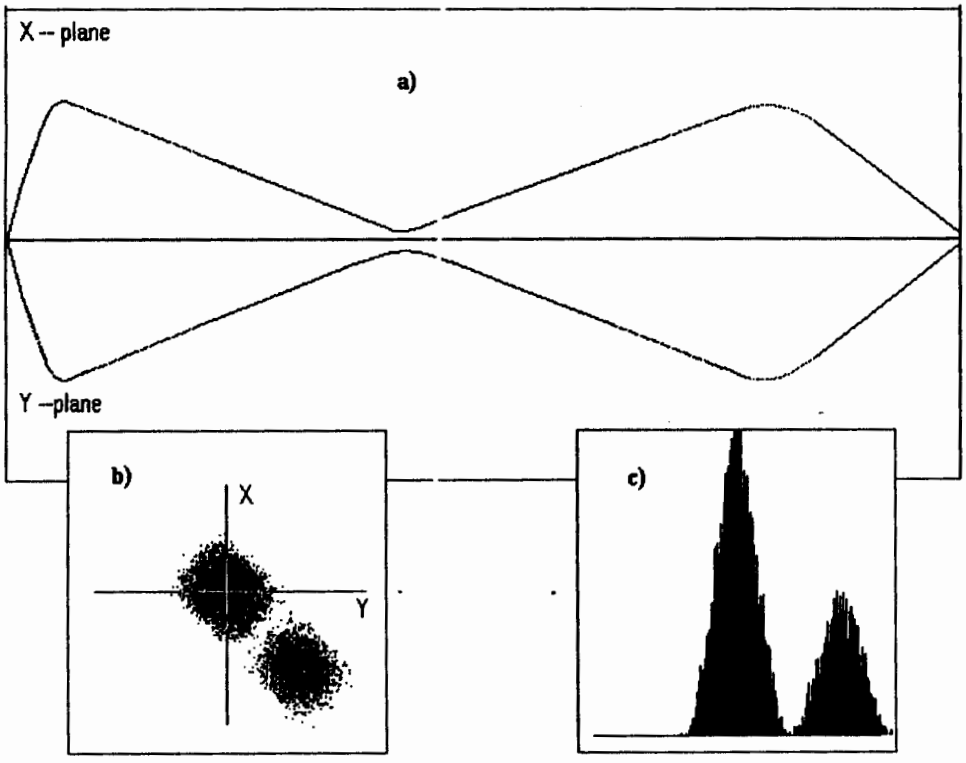

Figure 2

For the GMS structure

a) The envelopes in the X- and Y-planes;
b) The beam spots on the detector;
c) The beam distributions on the detector.

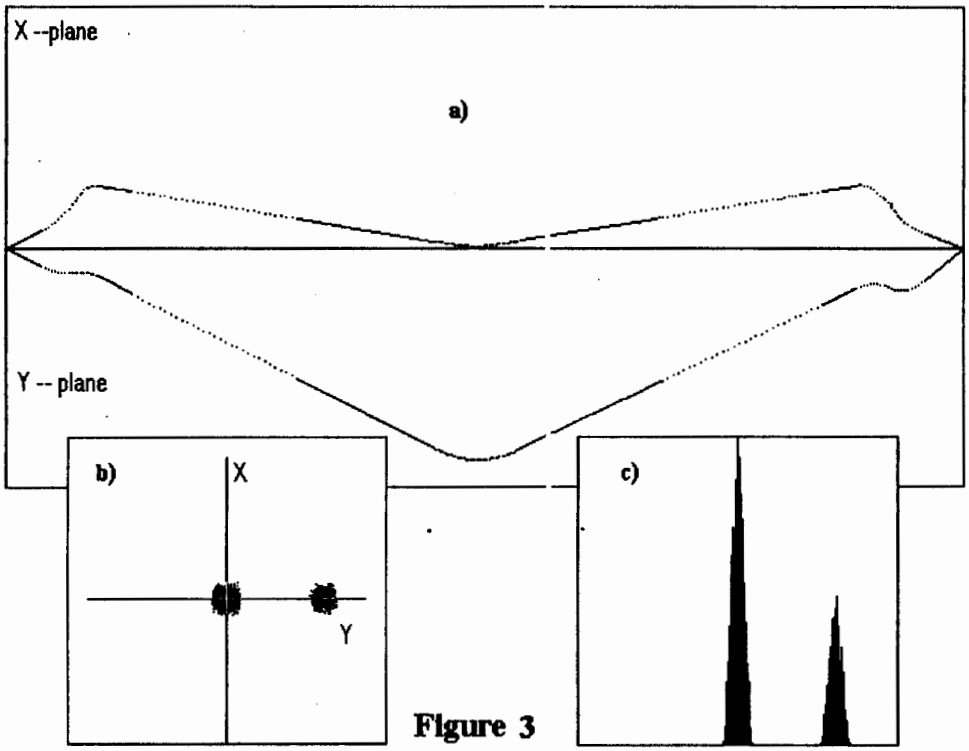

Figure 3

For the FMA structure
a) The envelopes in the X- and Y-planes;
b) The beam spots on the detector;
c) The beam distributions on the detector.

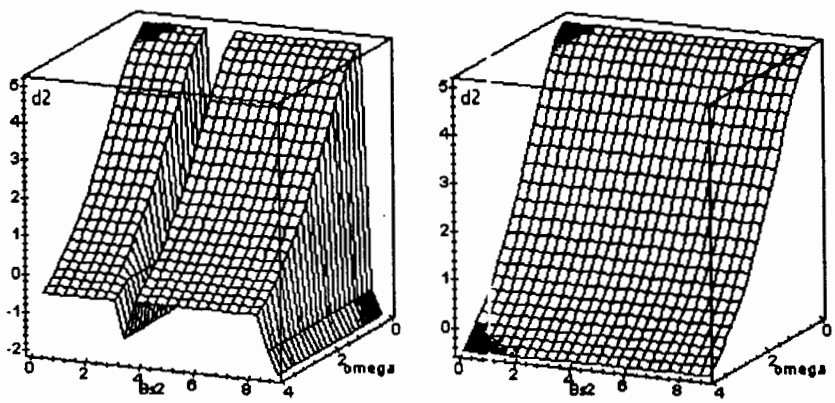

Figure 4

The dependence of the d2 on Bs2 and omega in the cases with and without the final focusing solenoid.

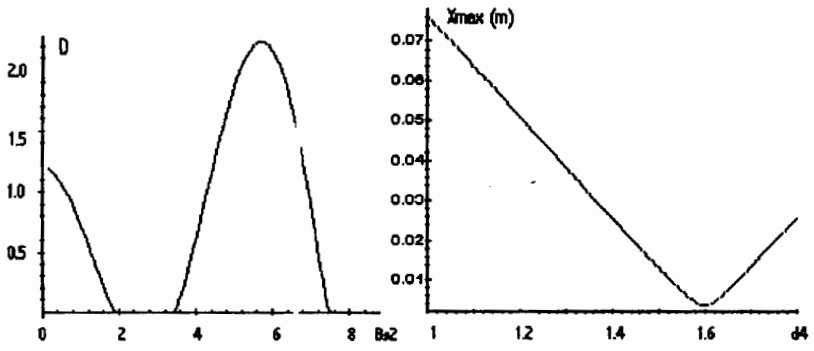

Figure 5

a) - the dependence of the dispersion D on Bs2;
b) - the dependence of the beam spot size Xmax on the final distance d4.

References

[1] A. Looking et al., *MAPLE V* **85**, (2) pp. 455–460, 1995.

[2] Davids C.N., Back B.B., Bindra K., Henderson D.J., Kutschera W., Lauritsen T., Nagame Y., Sugathan P., Ramayya A.V., Walters W.B., *Startup of the Fragment Mass Analyzer at ATLAS*, Nucl. Instr. and Meths., **B70**(1992), pp.358–365.

Software for the Solving of the Problems of Optimization of Beam Dynamics in Linear Accelerating and Focusing Structure *

O.I. Drivotin, D.A. Ovsyannikov
St.Petersburg State University, St.Petersburg, Russia

The main purpose of the present report is to show the possibility of application of mathematical methods of control theory for optimal choice of accelerating and focusing structures [1]. These methods can be called constructive methods of control theory. They are based on using of analytical expression of variation of functional which describes the quality of the structure. The variation, which is also functional in the space of infinite dimension, can be approximated by the functional defined in the space of finite dimension, namely, gradient of the functional on the parameters by which the control function can be parametrized. After that, minimization of the quality functional can be fullfiled with the usual methods of gradient descent.

Generally speaking, many problems of mathematical physics can be formulated as the problems of the control theory and solved with proposed methods. These methods require great amount of computations and so are not widely practiced. But recent development of computing devices allows to apply them. From our point of view the accelerating technology is the field where these methods can be used with great efficiency.

The mathematical and computational difficulties in modelling of the high intensity beams can be overcome when we use some simplified beam models. Let's concern one of such models. If the longitudinal motion is assumed not to depend on the transverse motion of the particles and the transverse forces acting on a particle are assumed to be linear on transverse coordinates, then the longitudinal and transverse coordinates can be considered separately and coordinates characterized at once some aggregate of the particles can be taken as the transverse coordinates. So, this particles aggregate represents a macroparticle.

In one of the simplest cases the control model will be the following. Assume that charged particles beam can be considered as a dynamical system described by the equations

$$\begin{cases} dZ/dt = f_1(t, Z, U) + \int_{M_{t,U}} f_2(Z, Z')\varrho(t, Z')\, dZ', \\ dX/dt = h(t, Z, X, U) \end{cases} \tag{1}$$

where Z, X are vectors characterizing longitudinal and transverse motion correspondingly, $U = U(t)$ is control vector, $Z \in R^n, X \in R^m, U(t) \in K \subset R^l, t \in [0, T]$, $T < \infty$. The

*Work supported by the Russian Foundation for Basic Research, grant 96-01-00926.

initial values of Z are supposed to fill some compact set $M_0 : Z(0) \in M_0 \subset R^n$ and $X(0) = X_0$. The image of the set M_0 at the mapping given by the system (1) is denoted by $M_{t,U}$. The integral term describes the interaction between macroparticles. $\varrho(t, Z)$ is macroparticles density and satisfies the equation

$$\frac{\partial \varrho}{\partial t} + \frac{\partial \varrho}{\partial Z} \cdot \frac{dZ}{dt} + \varrho\Big\{ div_Z f_1(t, Z, U) + \int_{M_{t,U}} div_Z f_2(Z, Z')\varrho(t, Z')\, dZ' \Big\} = 0,$$

which is partial integro-differential equation with characteristic lines described by the system (1). The initial condition for ϱ is $\varrho(0, Z) = \varrho_0(Z)$, $Z \in M_0$.

The problem is to minimize the functional

$$I(U) = \int_0^T \int_{M_{t,U}} g(t, Z_t, X_t)\varrho(t, Z_t)\, dZ_t\, dt + \int_{M_{T,U}} G(Z_T, X_T)\varrho(T, Z_T)\, dZ_T\,. \qquad (2)$$

where g and G are some integrable on t, Z and differentiable on Z and X functions characterizing the quality of the beam, $Z_t \equiv Z(t)$, $X_t \equiv X(t, Z_t)$.

For such problem we can apply general approach (see [1]) taking into account that integral on some components of the phase vector, namely X, is reduced to the only value of the integrand. The method of optimization is based on the expression for functional variation

$$\delta I = -\int_0^T \int_{M_{t,U}} \Big\{ \Psi_X(t, Z_t)\Delta_U h(t, Z_t, X_t\ U) + \Psi_Z(t, Z_t)\Delta_U f_1(t, Z_t, U) \Big\} \varrho(t, z_t)\, dZ_t\, dt\,. \quad (3)$$

where $\Delta_U h = h(t, Z, X, U(t) + \Delta U(t)) - h(t, Z, X, U(t))$. $\Delta_U f_1$ is expressed analogically. The auxiliary forms Ψ_X, Ψ_Z satisfy following differential equations and terminal conditions:

$$\begin{aligned}
\frac{d\Psi_X}{dt} &= -\Psi_X \frac{\partial h(t, Z, X, U)}{\partial X} + \frac{\partial g(t, Z, X)}{\partial X}, \\
\frac{d\Psi_Z}{dt} &= -\Psi_X \frac{\partial h(t, Z, X, U)}{\partial Z} - \Psi_Z \cdot \frac{\partial f_1(t, Z, U)}{\partial Z} + \int_{M_{t,U}} \frac{\partial f_2(Z, Z')}{\partial Z} \varrho(t, Z')\, dZ' \Big\} - \\
&\quad - \int_{M_{t,U}} \Psi(t, Z') \frac{\partial f_2(Z, Z')}{\partial Z'} \varrho(t, Z')\, dZ' + \frac{\partial g(t, Z, X)}{\partial Z},
\end{aligned}$$

$$\Psi_Z(T, Z_T) = -\frac{\partial G(Z, X)}{\partial Z}\Big|_{\substack{Z=Z_T \\ X=X(T,Z_T)}}, \quad \Psi_X(T, Z_T) = -\frac{\partial G(Z, X)}{\partial X}\Big|_{\substack{Z=Z_T \\ X=X(T,Z_T)}}.$$

The control model formulated above can be applied in the following important cases: radio frequency quadrupole (RFQ) channel and drift tubes channel with alternating phase focusing (APF).

Suppose that the beam entering to the RFQ channel is uniform along its longitudinal coordinate and has elliptical cross-section. It is convenient to approximate such beam

by the set of infinitely thin elliptic disks uniformely distributed initially in the segment $\gamma = \gamma_0, \varphi \in [-3\pi/2, \pi/2]$ in the phase plane of longitudinal motion (γ is reduced energy, φ is phase). Every thin disk is represented by the point of this segment.

The **equations** of longitudinal dynamics of these disks are

$$\begin{cases} d\varphi/d\zeta = 2\pi\gamma(\gamma^2-1)^{-1/2}, \\ d\gamma/d\zeta = \dfrac{2eU_0\lambda}{\pi m_0 c^2} k\Theta \cos\eta \cos\varphi + F_z . \end{cases} \tag{4}$$

Here $\zeta = z/\lambda$ dimensionless longitudinal coordinate, $\lambda = 2\pi c/\omega$ is the wavelength, e and m_0 are charge and rest mass of the beam particles, U_0 is intervane voltage, $k = 2\pi/(L/\lambda)$, L is modulation period of the electrodes, Θ is effectiveness of acceleration, $\eta = \int k\, d\zeta$ is modulation phase for which we have additional equation

$$d\eta/d\zeta = 2\pi\gamma_s(\gamma_s^2-1)^{-1/2} - d\Phi_s/d\zeta ,$$

where Φ_s is phase of synchronous particle relative to phase of the space modulation.

The term F_z is due to the longitudinal action of self field and determined from the expression for longitudinal component of electric field acting on $i-$th disk from $k-$th disk averaged on disk:

$$\overline{E}_{z_{ik}} = \frac{2q_i sign(z_i - z_k)}{\pi\varepsilon_0 R_i} \sum_{l=1}^{\infty} \frac{J_1(j_{0l}\frac{R_k}{a})}{R_k} \cdot \frac{J_1(j_{0l}\frac{R_i}{a})}{j_{0l}^2 J_1^2(j_{0l})} \frac{sh\frac{j_{0l}}{a}(\frac{L}{2} - |z_i - z_k|)}{sh\frac{j_{0l}L}{2a}} . \tag{5}$$

Here q_i, R_i, z_i are charge, average radius and longitudinal coordinate of $i-$th thin disk, a channel apperture.

Suppose also that transverse dynamics equations are linear and that motions in these planes are independent (i.e., angular momentum is neglected):

$$d^2x/dt^2 = Q_x x, \quad d^2y/dt^2 = Q_y y.$$

If initially particles fill some ellipses in the planes x, x' and y, y', then at all subsequent instants they fill some ellipses **described** by symmetrical matrices $B^{x,y}$: $X^*(B^x)^{-1}X \le 1$, $Y^*(B^y)^{-1}Y \le 1$, **where** $X = (x, x')^*$, $Y = (y, y')^*$. Therefore, we can introduce 6 variables which are elements of inverse matrices of these ellipses: s_{11}^x, s_{12}^x, s_{22}^x, s_{11}^y, s_{12}^y, s_{22}^y for every $Z \in M_{t,U}$. These variables have simple sense. For example, $\sqrt{s_{11}^{x,y}}$ are maximal values of x, y.

The equations for them are [1]

$$\begin{cases} \dfrac{ds_{11}^{x,y}}{dt} = 2s_{12}^{x,y}, \\ \dfrac{ds_{12}^{x,y}}{dt} = Q_{x,y}s_{11}^{x,y} + s_{22}^{x,y}, \\ \dfrac{ds_{22}^{x,y}}{dt} = 2Q_{x,y}s_{12}^{x,y}. \end{cases}$$

For RFQ channel [2]

$$Q_{x,y} = \frac{eU_0}{m_0\gamma}(\pm\frac{\chi}{a^2} + \frac{k^2\Theta}{\pi})\sin\eta)\cos\varphi + Q_{self\ x,y},$$

where $\chi = 1 - 4\Theta I_0(ka)/\pi$, and $Q_{self\ x,y}$ is coefficient accounting self field of the disk.

In the framework of the thin disks model $Q_{self\ x,y}$ can be taken in the form

$$Q_{self\ x,y} = \frac{e}{\pi\gamma^2\varepsilon_0 m_0 D}\sum_i \frac{q_i}{\sqrt{s_{11\,i}^{x,y}}(\sqrt{s_{11\,i}^{x}} + \sqrt{s_{11\,i}^{y}})}.$$

The summation is implemented on all disks in some interval which length is D and including the disk under consideration. The sum arises due to confusing of disks along $z-$axis.

The next three functions $u_1 = d\Phi_s/d\zeta$, $u_2 = \Theta$, $u_3 = \kappa/a^2$ can be taken as the components of the control vector. So, the dynamics equations in RFQ channel are analogous to the equations (1).

The second case when the control model under consideration can be used is drift tube channel with alternating phase focusing. In such case the longitudinal dynamics equations of thin disks can be written in the next simplified form

$$\begin{cases} d\varphi/d\zeta = 2\pi\gamma(\gamma^2-1)^{-1/2}, \\ d\gamma/d\zeta = \alpha(\zeta)\cos\varphi + F_z, \end{cases} \tag{6}$$

where $\alpha(\zeta) = e\lambda E_z(\zeta)/m_0 c^2$, and $E_z(\zeta)$ is longitudinal component of the electric field, for which can be taken various models, the simplest of them are piecewise constant and piecewise linear functions. The equations (6) are analogous to the equations (4). The term F_z accounting interaction between thin disks also can be calculated on the base of the expression (5).

The transverse particles dynamics equations in the simplest case are also linear:

$$\begin{cases} d\eta/d\zeta = \kappa, \\ d\kappa/d\zeta = -\frac{\gamma}{\gamma^2-1}(\kappa\alpha + \frac{1}{2}\eta\frac{d\alpha}{d\zeta})\cos\varphi + \pi(\gamma^2-1)^{-1/2}\eta\alpha\sin\varphi + Q_{tr}\eta. \end{cases} \tag{7}$$

Here $\eta = r/\lambda$, $\kappa = dr/dz$, r is radial coordinate. As in RFQ channel, here we can introduce the variables analogous to s_{11}, s_{12}, s_{22} mentioned above but regarded to radial motion:

$$(\eta \quad \kappa)\begin{pmatrix} s_{11} & s_{12} \\ s_{12} & s_{22} \end{pmatrix}^{-1}\begin{pmatrix} \eta \\ \kappa \end{pmatrix} \le 1.$$

We assume that initial values of η and κ fill ellipse, inverse matrix of which gives the initial values of s_{ik}. It follows from (7) that the variables s_{ik} satisfy the equations:

$$\begin{cases} \frac{ds_{11}}{dt} = 2s_{12}, \\ \frac{ds_{12}}{dt} = -\frac{\gamma}{\gamma^2-1}(s_{12}\alpha + \frac{1}{2}s_{11}\frac{d\alpha}{d\zeta})\cos\varphi + \pi(\gamma^2-1)^{-1/2}s_{11}\alpha\sin\varphi + Q_{tr}s_{11} + s_{22}, \\ \frac{ds_{22}}{dt} = -2\frac{\gamma}{\gamma^2-1}(s_{22}\alpha + \frac{1}{2}s_{12}\frac{d\alpha}{d\zeta})\cos\varphi + 2\pi(\gamma^2-1)^{-1/2}s_{12}\alpha\sin\varphi + 2Q_{tr}s_{12}. \end{cases}$$

$Q_{tr}\eta$ is the term accounting the beam self field and in the frame of thin disks model Q_{tr} can be approximated by the expression

$$Q_{self\ x,y} = \frac{e}{2\pi\gamma^2\varepsilon_0 m_0 D}\sum_i \frac{q_i}{s_{11\,i}}.$$

In this case the control vector has one component $u_1 = \alpha(\zeta)$. Therefore, the dynamics equations for this case also have the form (1).

So, both for RFQ channel and for APF channel we can use the mathematical control model described above. The wide choice of functional of the form (2) is possible. For example, we can take the functional (2) with functions g and G describing the capture of the particles in transverse and longitudinal motion correspondingly:

$$g(t, Z, X) = c_Z g_Z(Z) + c_X g_X(X).$$

Here c_Z, c_X are coefficients, and g_Z, g_X are given by expressions

$$g_Z(Z) = \begin{cases} (z_i - z_{u\,i})^{p_i}, & z_i > z_{u\,i}, \\ 0, \quad z_i \in [z_{l\,i}, z_{u\,i}], \\ (z_i - z_{l\,i})^{p_i}, & z_i < z_{l\,i}, \end{cases} \qquad g_X(X) = \begin{cases} (x_i - x_{u\,i})^{q_i}, & x_i > x_{u\,i}, \\ 0, \quad x_i \in [x_{l\,i}, x_{u\,i}], \\ (x_i - x_{l\,i})^{q_i}, & x_i < x_{l\,i}\ . \end{cases}$$

where p_i, q_i are some positive numbers, and $G(Z, X)$ has analogous form.

As mentioned above, the technique of optimization is based on approximation of components of control functions by functions depending on finite number of parameters. So, instead of functional variation which is also functional in the infinite dimensional space of control function variations we have its approximation, namely, gradient of the functional on the parameters. Then method of gradient descent can be applied [1]. Numerical realization included replacement of integration by summation and considering of systems (1) for discrete initial set instead of M_0. [3]

For the solving of beam dynamics modelling and optimization problems original software environment has been developed. This software is based on the modern object oriented programming technique. According to this approach, the program is the set of components and objects which are necessary for some class of problems. The possibility of customizing of that components and methods is supposed.

As an example, we consider the structure of the program for optimization of the RFQ channel. Program for APF channel optimization has analogous structure.

The main component in the program is the component of the type *TRFQAcceleration*, which is immediate descendant of the type *TDiskDistribution*. The base type *TDisk Distribution* has methods for forming of initial distributions of thin disks, graphical displaying of distributions, calculating of some characteristics of distributions and getting partial interval distributions on separate variables for given disk distribution. One of the fields of the type *TDiskDistribution* is *Evolution*, which type is *TDiskIntegrator*, the last being immediate descendant of the type *TIntegrator*. The main method of the base type *TIntegrator* - *Integrate* implements the integrating of the system of ordinary differential equations. The type *TDiskIntegrator* contains also additional method *RHSCalc* for calculating of the right-hand sides of equations being integrated. The type *TRFQAcceleration* compared with the type *TDiskDistribution* has additional fields and

methods, the most important of which are *Structure* of the type *TStructure* and method *FuncCalc* for calculation of the functional which is minimized in the optimization process. In its turn, the type *TStructure* has the field *Optimizer* of the type *TOptimizer*, the latest being the base object for implementation of optimization process and containing different methods of optimization.

Besides that, there are two additional types of objects: *TRFQDynamics* and *TRFQ Optimization*, which are descendants of the type *TThread*. On user call, i.e. choice of corresponding menu item on the program form, their instance is created and, in turn, creates a component of the type *TRFQAcceleration*, and after that their main method *Execute* is implemented. Such structure of the program allows user to work with many functionals and starting points of optimization at the same time because many components of types *TRFQDynamics* and *TRFQ Optimization* can be created simultaneously. The program form also can contain some windows for getting information on the course of optimization process, which are distributed among components and objects of the program.

The programs were tested on the known structures with the frequencies 148.5 MHz and 433 MHz. Results of modelling are satisfactory: close similarlity with known dynamics for these structures was obtained. During testing of the programs the output energy spread and transverse normalized emittance of the beam after optimization can be essentially decreased compared with ones before the optimization if their initial values were too great.

The described software allows to descend from some initial point of multidimensional parameter space to the local minimum point, which is not always permissible from the point of view of physical realization. So, working with the software demands sufficiently satisfatorily choice of initial point and using different functionals during the optimization process.

References

[1] D.A.Ovsyannikov, "Modeling and Optimization of Charged particle Beam Dynamics". Leningrad State University, Leningrad, 1990.

[2] I.M.Kapchinskij, "Theory of linear resonanse accelerators: beam dynamics". Moscow, Energoizdat, 1982.

[3] Drivotin O.I. "Numerical solution of the optimal control problem for charged particles beam". Proc. of Int. Workshop "BLO-94". St.-Petersburg,1994. P.63-67.

Simulation of the charge-state mixed ion beam transportation through the Low Energy Ion Beam Transport line (LEBT, CERN)

V.Alexandrov, Yu.Batygin*, N.Mironova, V.Mironov, V.Shevtsov, G.Shirkov
JINR, 141980 Dubna, Moscow Region, Russia.
* The Institute of Physical and Chemical Research (RIKEN), Hirosava, 2-1,
Wako-shi, Saitama, 351-01, Japan.

Abstract
Computer simulations for matching the high current, charge-state mixed ion beam in the real magnetic field are presented. 3 kinds of computer codes were used: the fast code based on the Root-Mean-Square (RMS) technique, the Particle-in-Cell (PiC) code, and Multi-Charge-Cords (MCC) code.

1. Computer Codes

The Particle-in-Cell (PiC) code /1/ and two PC codes realised on IBM PC in Visual Basic common interface were used. The PC codes are destined for the simulation and optimisation of beam dynamics. They are based on the successive and consistent use of two methods: the momentum method of distribution functions /2,3/ (RMS technique) and the method of Multi-Charge-Cords (MCC). The library allows to calculate the RMS parameters of electron and ion beams, passing through a set of quadrupoles, solenoids, bends, accelerating sections. It has a number of advantages:

- the initial beam and beam-line parameters are interactive defined and redefined using a display visualisation;
- the hard drive recording for the next simulations;
- the usage of an experimental field of real elements of magnetic structure;
- the calculation renewal at the beginning of a previous element after changing any element parameters while the simulation;
- the evolution of RMS beam dimensions (by using of RMS technique) or particle trajectories (if MCC) vs. distance is reflected while simulations are performed;
- four commonly used initial distributions (microcanonical, "water bag", parabolic and Gaussian) of particles /4/ are available for the MCC simulation.

The RMS code /5/ is a fast code very suitable for the first test, design and optimisation of the beam line parameters. The MCC code requires more time for execution but provides a high accuracy of simulation taking into account the space charge effects, aberrations and beam losses. One of the main advantages of MCC code presented here is an ability to simulate a real multicomponent beam of different masses and charged states of ions from ion sources.

2. Variants studied

Three variants are studied (see Table 1 and Fig. 1):

- present LEBT configuration /6/;
- optimised LEBT;
- ready-made SC solenoids.

The LEBT tantalum ion beam parameters are in Table 2.

Table 1. The parameters of 3 LEBT lattice variants.

		Drift 1	Solenoid 1	Drift 2	Solenoid 2	Drift 3
Present LEBT (60 mA)	L/R(cm) Bo (G)	17. / 5.	38. / 8.*) 6300.	93. / 5.	38. / 8.*) 8300.	15. / 5.
Optimised LEBT(60 mA)	L/R(cm) Bo (G)	24. / 5.	38. / 8.*) 8950.	86. / 5.	38. / 8.*) 10200.	15. / 5.
Ready made SC coils	L/R(cm) Bo (G)	24. / 7.	31. / 9.5*) 12600.	46. / 7.	31. / 9.5*) 13310.	18. / 7.

*) The middle radius of solenoid.

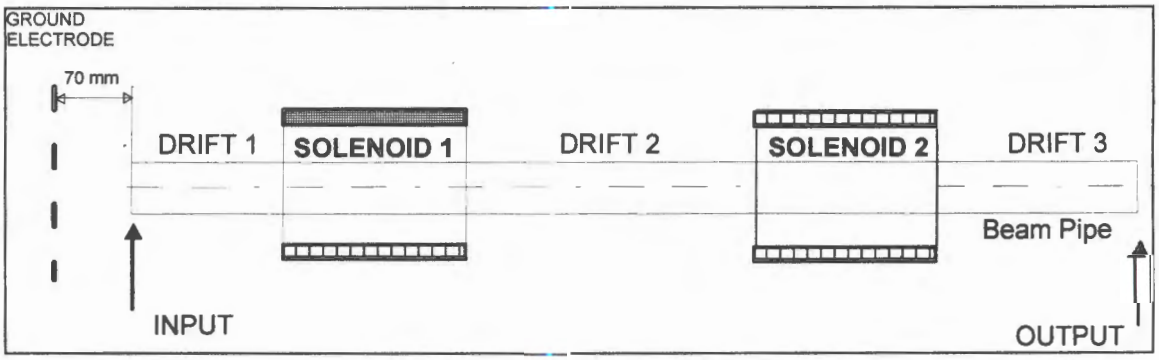

Fig. 1. The sketch of LEBT

Table 2. The ion beam parameters

	ε=4rms ε(u) cm·rad	α	β cm/rad	Δx cm	RMS x cm	Δx' rad	RMS x' rad
Input	0.025	-3.01	75.	1.37	0.685	0.055	0.0275
Output	0.020	0.85	3.7	0.272	0.136	0.0625	0.031

3. Simulation of the experimental results

The results of simulations by PiC code for the present LEBT configuration and Ta^{20+} 60 mA 60 keV are shown in Fig. 2.

RMS method has shown that the beam line is not matched in the best way with the beam now. MCC simulation gives the same results. Less than 30 % particles come through the LEBT. Figure 3 presents transverse phase space projections (a), trajectories and particle losses for each charge state (b) and the measured initial and calculated final charge distributions (c) simulated by MCC code for the charge-state mixed ion beam[1].

[1] It should be noted that the simulation was performed without taking into account the 6.5 mm input aperture of RFQ, therefore the final beam parameters can slightly differ from the values mentioned in Table 2.

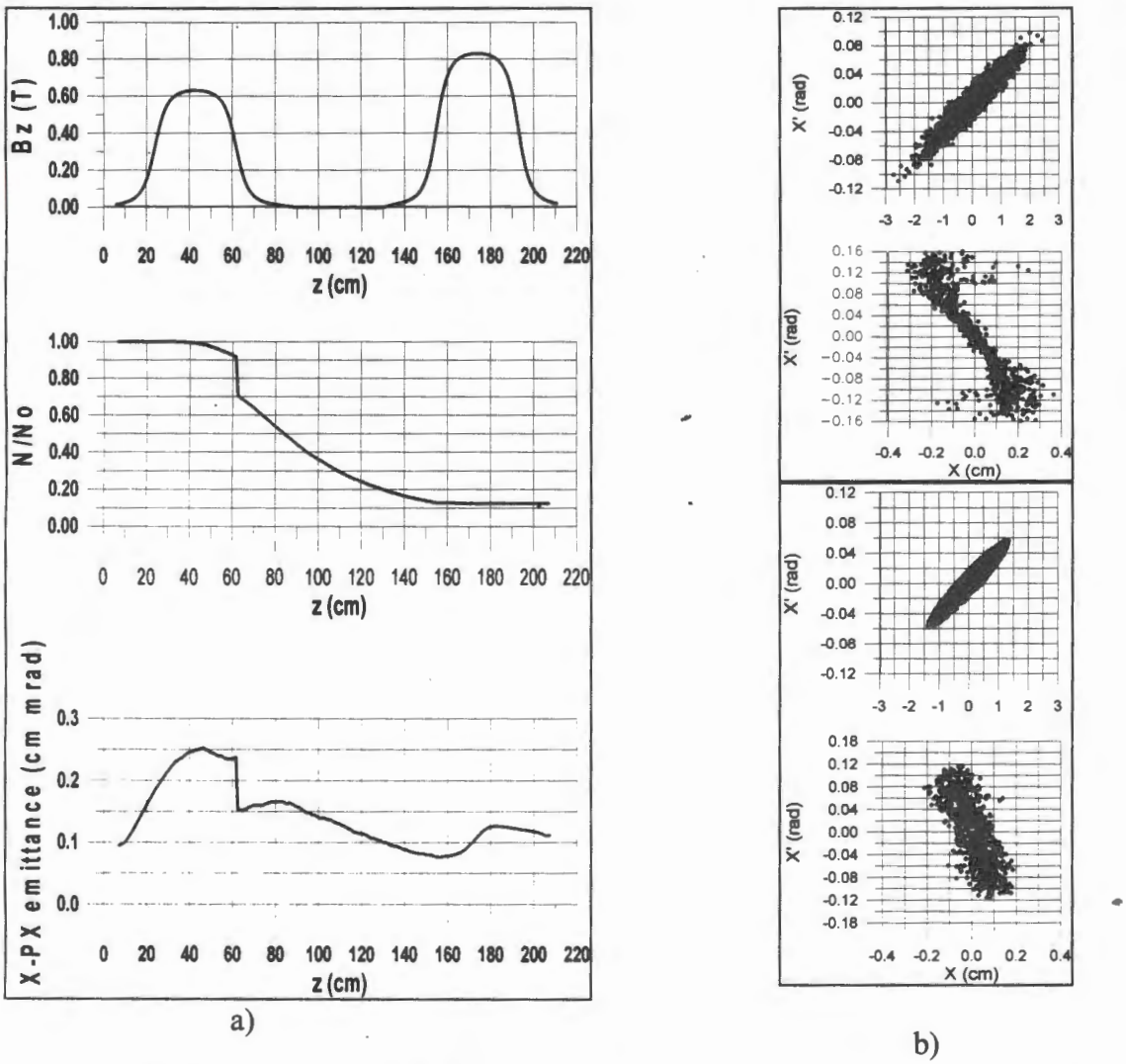

Fig. 2. a) The axial magnetic field B_z, number of particles N/N_o and the normalised emittance vs. distance, b) the transverse phase space projections at Gaussian (above) and Vladimirsky-Kapchinsky initial particle distributions.

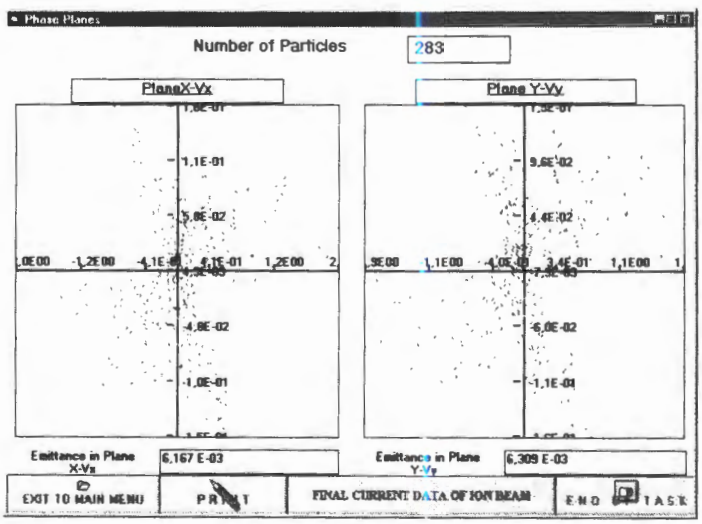

Fig. 3a. The final transverse phase space projections of the left particles.

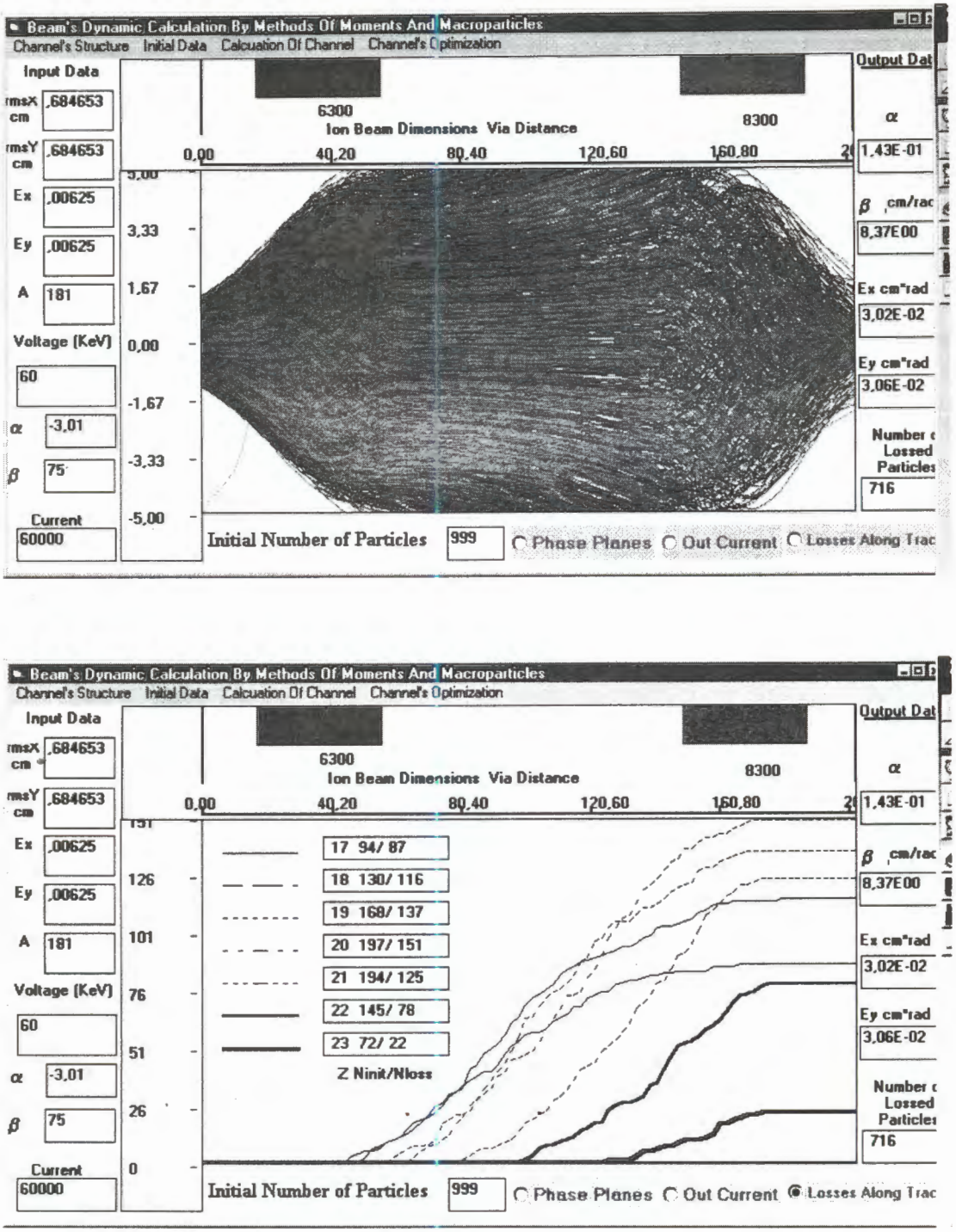

Fig. 3b. The trajectories (above) and particle losses for each charge state.

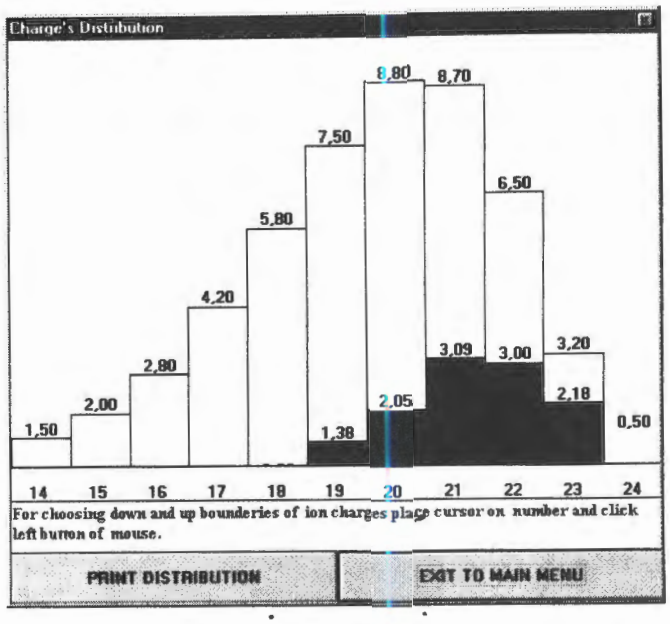

Fig. 3c. The initial (Z=17-23) and final (black) charge distributions.

4. LEBT optimisation

The optimisation is able to increase the efficiency of LEBT up to 90% for the only Ta^{20+} charge state beam of 60 mA and up to 70-75% for the total input current of 60 mA beam of Ta^{14+} - Ta^{23+} charged states. The significant improvement by the magnetic field increasing and slight adjustment of the coil positions could be done. One can see that the value of beam current is very close to the space charge limit in this "warm" variant of coils.

Figure 4 shows particle losses for each charge state (a) and the initial (Ta^{17+} - Ta^{23+}) and final charge distributions (b) for the experimental charge states and VK particle distribution.

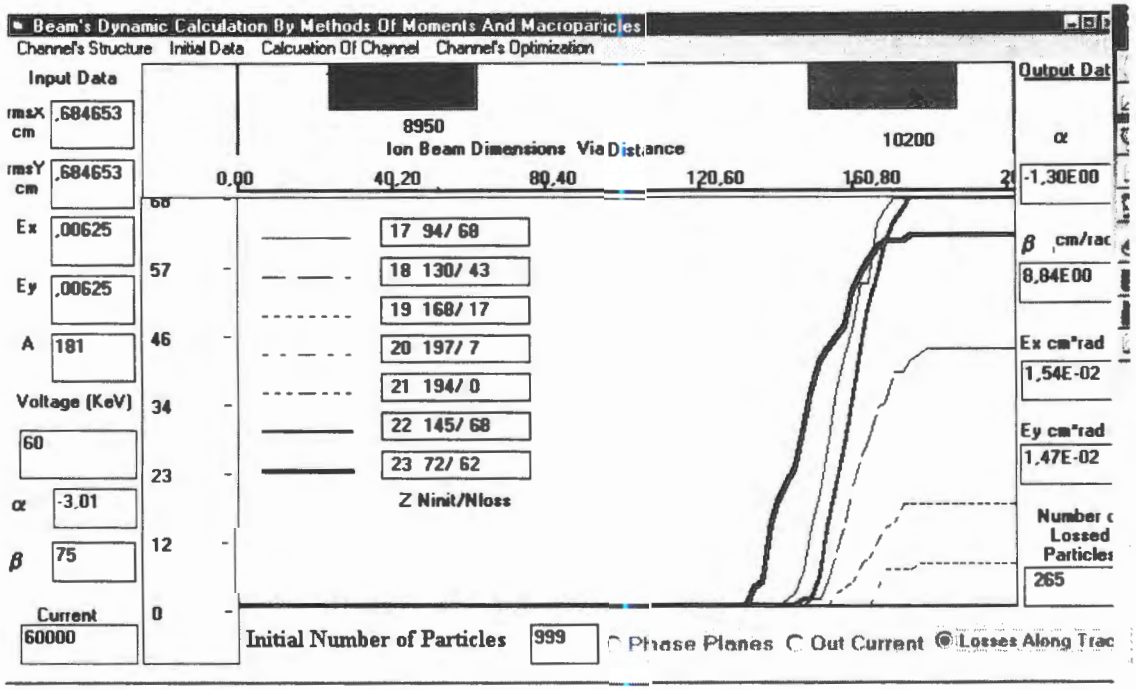

Fig. 4a. The particle losses for each charge state.

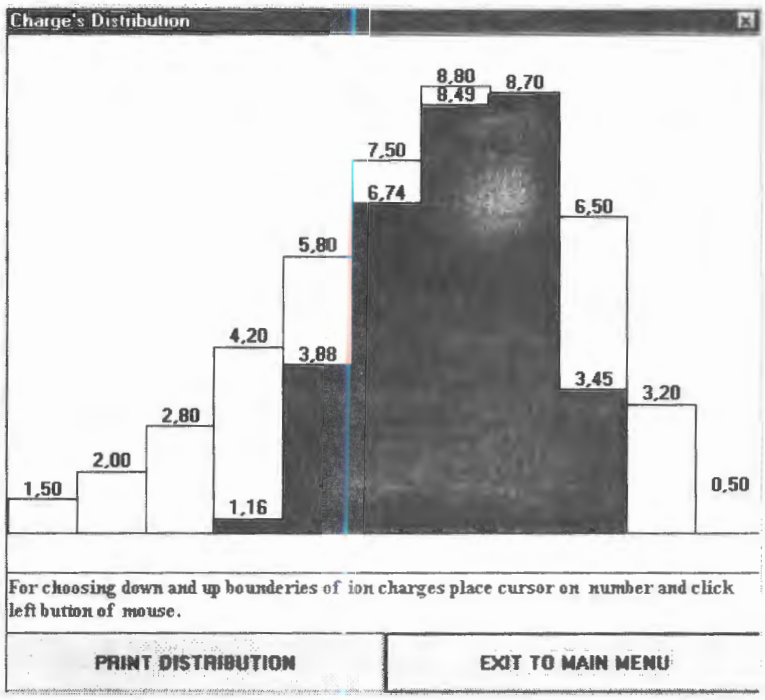

Fig. 4b. The initial (Z=17-23) and final (black) charge distributions.

5. SC LEBT sample

The next step to improve the situation is to increase the LEBT aperture and magnetic field value. The third kind of simulations has been made for the ready made SC coils and has shown that they are easily able to transport up to 100 mA and higher total beam current.

The ready made coils have 31 cm length, 15.8 cm inner tube diameter (without cryostat), 19 cm mean diameter of the coil. According to our estimations the maximum axis field is 3-4 T at the current of 60 A.

The results of simulation at VK initial particle distribution are shown in Fig. 5: the ion trajectories (a), the particle losses (b) and the initial and final charge states (c).

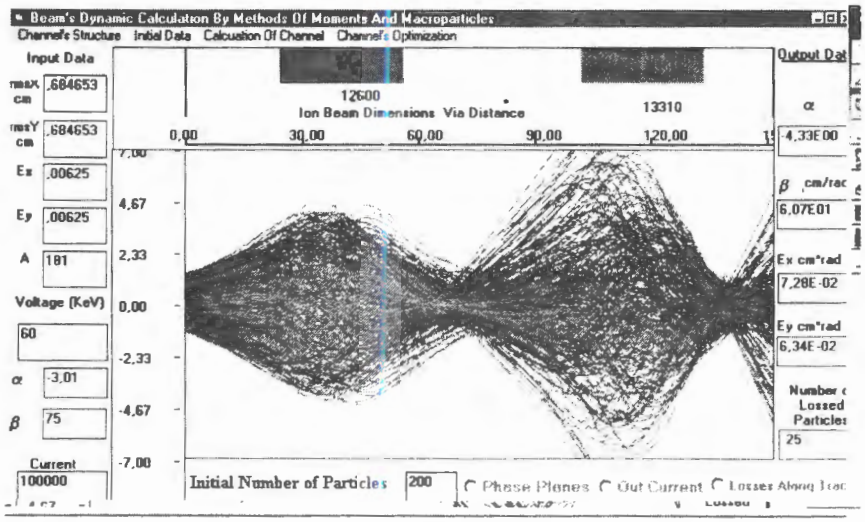

Fig. 5a. The ion trajectories.

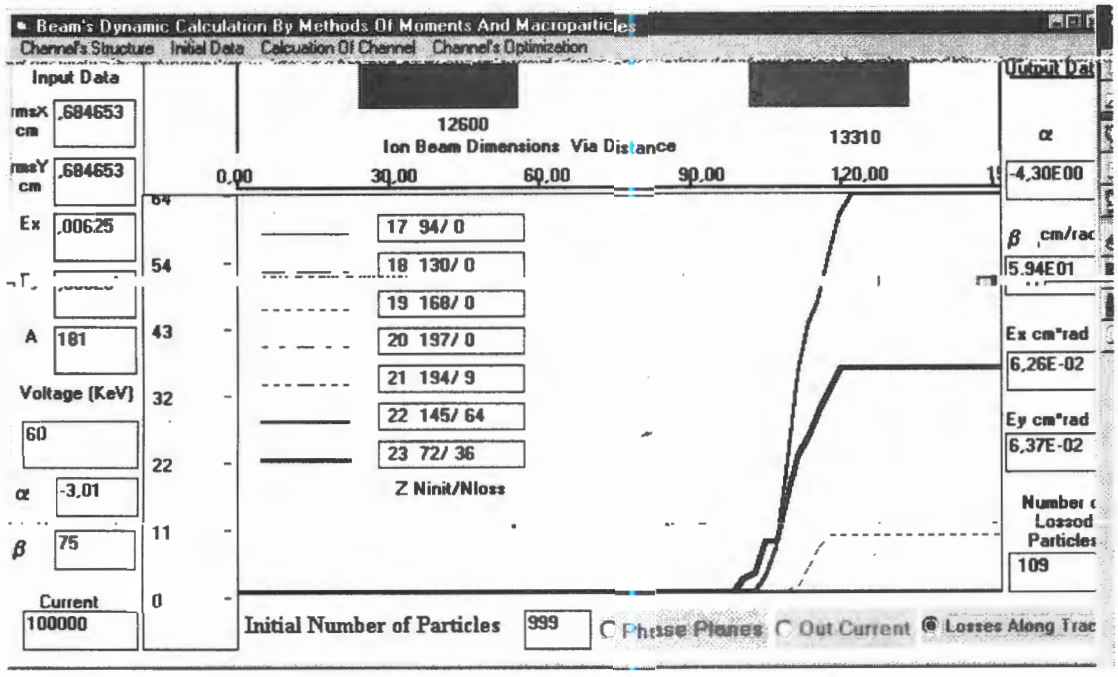

Fig. 5b. The particle losses at the 100 mA tantalum ion beam transportation.

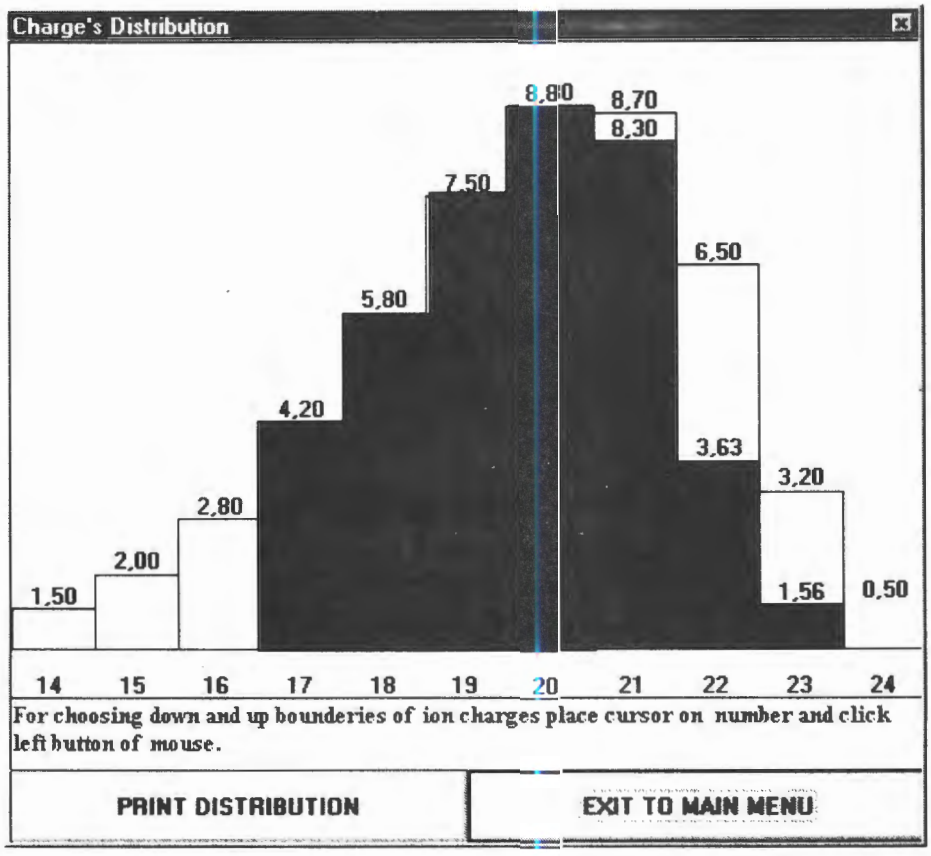

Fig. 5c. The initial (Z=17-23) and final charge states.

6. Conclusion

The simulation of the 60 mA 60 keV tantalum ion's transportation through the present LEBT configuration is in good agreement with the experimental results. The numerical optimisation has shown that the efficiency of LEBT could be significantly improved (by 3 times) by adjusting the coil positions and increasing the magnetic field. The higher current beam transportation requires to increase the LEBT aperture and the magnetic field level. A large inner solenoid diameter is also required to reduce spherical aberrations.

The simulation for ready-made SC coils with a larger aperture and higher field level has shown the possibility to transport the 100 mA (or more) total Ta^{14+} - Ta^{23+} beam current.

References

1. Y.Batygin. BEAMPATH: A Program Library for Beam Dynamics Simulation in Linear Accelerators. In: Proc. of the 3d European Particle Accelerator Conference (EPAC92), Berlin, 1992, p.822.
2. N.Yu.Kazarinov, E.A.Perelstein, V.F.Shevtsov. Moment Method in Charged Particle Beam Dynamics, Particle Accelerators, 1980, v.10, p.1. Preprint JINR, R9-10985, Dubna, 1977.
3. A.D.Dymnikov, E.A.Perelstein. Moment Method in Dynamics of Charged Particle Beams, Nucl.Instr. and Meth., 1978, 148(3), p.567. Preprint JINR R9-1020, Dubna, 1977. Preprint JINR R9-10620, Dubna, 1977.
4. Y.Batygin. Particle Distribution Generator in 4D Space. In: Proc. of the 3d European Particle Accelerator Conference (EPAC92), Berlin, 1992, p.822.
5. P.F.Beloshitsky, V.F.Shevtsov. Preprint JINR, Dubna, 1997.
6. M.Bourgeois at al., High Charge-State Ion Beam Production from a Laser Ion Source. In: Proc. of the Linac96, XVIII International Linac Conference, Geneva, Switzerland, 26-30 August, 1996.

EFFECTIVE DISTRIBUTION CONCEPT IN A MATHEMATICAL MODEL FOR SHADOWED SPUTTERING

L.A.Sevastianov[1]

Peoples' Friendship University of Russia

117198, 6, Miklukho-Maclay str., Moscow, Russia

E-mail: lsevastianov@mx.pfu.edu.ru

The practical sputtering of thin-film planar waveguide has shown the necessity of developing methods for the solution of certain problems, pertaining to shadowed sputtering:

A. Predicting the configuration of a layer obtained as a result of sputtering through the mask of a given shape (direct sputtering problem).

B. Defining the shape of a shadowing mask used for the sputtering of the layer of the given configuration (inverse sputtering problem).

Obviously the configuration of a sputtered layer depends not only on the mask shape but also on the entire complex of physical characteristics of sputtering of which the main are: the total time of sputtering, the source properties and operating conditions parameters, the properties of the physical medium (situated) between the source and the substrate, the laws of interaction of the sputtered particles with themselves and the medium particles as well as with the surfaces of the mask and the substrate. That's why the methods for solving the sputtering problems and calculating the formulas depend on the physical characteristics of the sputtering devices and are usually developed for a particular device.

In view of the complexity of the above physical phenomena no comprehencible account and their theoretical description has been achieved. Theoretical predictions of the sputtering results are proposed in a series of papers [1,2] and the mask shape necessary for the sputtering of a layer of a given configuration (particularly, of the waveguide Luneburg lens) and their theoretical calculations have been obtained [3,4]. However those results are valid only under conditions that can't be achieved so far in the existing sputtering devices [5,6].

This paper offers a description of all possible physical characteristics of the sputtering device by using a single function of six idependent variables that can be treated as the distribution of particles flow over coordinates, velocities and time and further termed an effective distribution.

The use of an effective distribution (concept) notion makes it possible to obtain a general formula and to develop a uniform method of calculating for sputtering processes with any source and a mask of any arbitrary shape (time-varied included). It appears besides that an effective distribution or its integral characteristics may be found for any concrete device by means of auxiliary sputtering experiments.

[1] Under support of Russian Foundation for Basic Research (grant N 94-01-01354a)

In order to introduce the concept of an effective distribution let us consider some mathematical characteristics of the sputtering process. Suppose that during the time of sputtering T, N sputtered particles passed through the inlet openings S_H of the mask in the direction of the substrate. Each particle at the moment of passing through the plane of the mask inlet opening is characterized by : the time $t \in [0, T]$, the two-dimensional coordinate vector $\vec{r}_H \in S_H$ and the three-dimensional velocity vector $\vec{V}$. The distribution of all N particles that passed through S_H over the coordinates, velocities and time may be given by the function $\rho_H^0(\vec{r}_H, \vec{V}, t)$ so that

$$N = \int_0^T dt \int_{S_H} d\vec{r}_H \int d\vec{V} \rho_H^0(\vec{r}_H, \vec{V}, t). \tag{1}$$

The distribution ρ_H^0 is determined by all the device parameters (the properties of the source, of the medium, of the substrate; by the influence of the mask, of the medium and of the substrate on the source etc.). On the other hand, ρ_H^0 in combination with the device parameters (the medium propertied, the interaction laws, the mask form,etc.) determine the sputtering result as a functional f:

$$h = f[\rho_H^0, M] \tag{2}$$

Here $h = h(\vec{r})$ is the thickness of the sputtered layer at the point $\vec{r}$ of the plane of the substrate, M is the mask shape. The concrete form of the functional f is determined naturally by all the totality of the device characteristics. It must be noted that the formula (2) cannot be used for calculating of concrete processes, because the complexity of the physical phenomena makes it impossible to predict both the form of the distribution ρ_H^0 and the form of the functional f. Since only the configuration of the sputtered layer h is measured experimentally the two above-mentioned quantities cannot be restored on the basis of the experimental results. Let us consider now the simplified problem. Suppose that the distribution ρ_H^0 is known and besides the reflecting capacities of the mask and of the substrate are equal to zero, there is a vacuum in the region L between the entrance of the mask and the substrate, the sputtered particles in this region do not interact with each other. In this case it is possible to trace the straight paths of the uniform movement of particles and to establish the linear functional dependence [7,8] of the thickness of the sputtered layer $h^0(\vec{r})$ (more precisely the number $N^0(\vec{r})$ of particles arriving at the point $\vec{r}$) over the distribution ρ_H^0 and the mask form M:

$$h^0 = f^0[\rho_H^0, M] \tag{3}$$

It's obvious that the configuration h^0 given by the formula (3) may essentially differ from the real configuration h determined by the relation (2). The comparison of formulas (2) and (3) clearly indicates that the calculation of all real influences of all the parameters of the device leading to the transformation from h^0 to h consists in the substitution of the functional f^0 by the functional f. Thus the real physical processes may be regarded as a perturbation of the model (simplified) functional dependence f^0. However it is possible to suppose that the transform from h^0 to h may be realized by the corresponding perturbation of the distribution ρ_H^0 (the transform from ρ_H^0 to ρ_H) so that the following relation would be valid

$$h = f^0[\rho_H, M]. \tag{4}$$

The auxiliary function ρ_H determined by the relations (2),(3) and (4), if it exists, will be named further an effective distribution. It is evident that an effective distribution exists if there is no interaction in the region L of the sputtering device. In this case f coincides with f^0 and consequently $\rho_H = \rho_H^0$. One may demonstrate that for a sputtering experiment with a concrete shadowing mask M there exists an infinite set $\{\rho_H\}_1$ of effective distributions. It allows to suppose that in the case of n experiments with near masks $M_1, ..., M_n$, in set $\{\rho_H\}_1, ..., \{\rho_H\}_n$ the unique distribution ρ_H for all those experiments may be found and to formulate the following assumption. For each fixed operating mode of the concrete sputtering device and for a finite number of shadowing masks with equal height H and similar forms M may be associated with a unique effective distribution of sputtered particles over coordinates, velocities and time in the plane of the mask entrance. It should be noted that the assumption formulated above is valid in the case of sputtering devices with negligible interaction in the region L. Note as well that in contrast to the real distribution ρ_H^0 the effective distribution ρ_H makes it possible to calculate the result h of sputtering with the shadowing mask M, because the functional f^0 in the formula (3) is known. Due to this reason the effective distribution itself may be calculated by means of data h_j of the series of experiments with the known mask M_j. For more accurate analysis of the influence of the interaction on the evolution of sputtered particles let us use the method, proposed in papers [9,10]. The particles movement in the process of sputtering has a stochastic character and so one may consider the process of sputtering by the statistical mechanics methods. The sputtered particle considered as a Brownian particle satisfied the Langevin equation [10]

$$m\ddot{\vec{x}} + \vec{f} = \dot{\vec{\varphi}}, \tag{5}$$

where m is a particle mass, $\vec{x}$ is its coordinate, $\vec{f}$ is the momentum of outside forces acting on a particle, $\dot{\vec{\varphi}}$ is a derivative of the Wiener process which is characterized by the temperature (dispersion) θ. The main task of the Brownian movement theory is evaluating of the probability density of the system's transition

from the state with the fixed value of the coordinate x_1 at the moment t_1, to the state with the coordinate value x_2 at the moment t_2. Knowing the probability density of the transition (the transition probability) $W(\vec{x}_1, t_1; \vec{x}_2, t_2)$ one may calculate the probability density $W(\vec{x}_2, t_2)$ of the given value x_2 at the moment t_2 if the probability density $W(\vec{x}_1, t_1)$ of the initial value x_1 at the moment t_1 is known. The above transition probability satisfies [10] the Einstein-Fokker-Plank equation

$$\frac{\partial W}{\partial t} = \frac{\partial}{\partial \vec{x}}\{\vec{f}W + \theta\frac{\partial W}{\partial \vec{x}}\}, \tag{6}$$

where $W = W(\vec{x}_1, t_1; \vec{x}, t)$. Thus the Brownian particle evolution is completely defined if the solution of equation (6) is known. To find the general form solution of equation (6), equation (5) is considered as the perturbation (not necessarily small) of the simpler Langevin equation

$$m\ddot{\vec{x}} + \vec{f}_0 = \dot{\vec{\varphi}} \tag{7}$$

to which corresponds the simplified Einstein Focker-Plank equation

$$\frac{\partial W_0}{\partial t} = \frac{\partial}{\partial \vec{x}}\{\vec{f}_0 W_0 + \theta\frac{\partial W_0}{\partial \vec{x}}\}, \tag{8}$$

which allow for simpler method of finding the solution. In this case solution of equation (6) follows from equation (8) solution with the help of the functional change of variables with the Jacobian

$$J[\vec{f}, \vec{f}_0] = exp\{\frac{1}{2}\int_{t_1}^{t_2} div(\vec{f} - \vec{f}_0)dt\}.$$

In order to use the above method in our specific problem let us denote by Σ the surface constraining the particle movement: Σ_1 is the entrance mask surface (secondary source of particles), Σ_0 is the substrate surface, Σ_M is a lateral surface. The Hamiltonian function of a given particle has the form

$$H = \frac{\vec{p}^2}{2m} + u(\Sigma) + \sum_j u_j(\vec{x}, \vec{x}_j).$$

Here $\vec{p}$ is the particle momentum, $u(\Sigma)$ is the potential energy of the interaction of a particle with the boundary surface Σ, $u_j(\vec{x}, \vec{x}_j)$ is the potential energy of the interaction of a given particle with another sputtered particle at point $\vec{x}_j$. The action's function of a given particle has the form

$$S(\vec{x}_1, t_1; \vec{x}_2, t_2) = \int_{t_1}^{t_2} (\vec{p}d\vec{q}) - Hdt .$$

And the relation [12] $m\dot{\vec{x}} = \vec{p} = \partial S/\partial \vec{x}$ is fulfilled. Thus the Langevin equation for a sputtered particle may be written in the form

$$m\dot{\vec{x}} - \frac{\partial S}{\partial \vec{x}} = \dot{\vec{\varphi}}, \tag{9}$$

where $\dot{\vec{\varphi}}$ is a three dimensional vector of non-correlated derivatives of the Wiener process with a temperature θ. To the Langevin equation (9) corresponds the Einstein-Fokker-Plank equation of a concrete form

$$m\frac{\partial W}{\partial t} + \frac{\partial}{\partial \vec{x}}\{W\frac{\partial S}{\partial \vec{x}} - \theta\frac{\partial W}{\partial \vec{x}}\} = 0, \tag{10}$$

where $W = W(\vec{x}_1, t_1; \vec{x}, t) \quad S = S(\vec{x}_1, t_1; \vec{x}, t)$

Let us consider a simplified problem for which the actior function $S_0(\vec{x}_1, t_1; \vec{x}, t)$ is chosen by the following specific mode. Let $\vec{x}_1$ be a point on surface Σ_1, $\vec{x}$ - a point cn surface Σ_0, $\ell(\vec{x}_1, \vec{x})$ - a straight line connecting the points $\vec{x}_1$ and $\vec{x}$. Let us assume $S_0 = (\vec{x}_1 - \vec{x})^2/4\pi\theta(t_1 - t)$ for the case when $\ell(\vec{x}_1, \vec{x})$ does not intersect the surface Σ_M and $S_0 = +\infty$ for a contrary case. Then the transition probability which is the solution of the equation

$$m\frac{\partial W_0}{\partial t} + \frac{\partial}{\partial \vec{x}}\{W_0\frac{\partial S_0}{\partial \vec{x}} - \theta\frac{\partial W_0}{\partial \vec{x}}\} = 0, \tag{11}$$

is concentrated on trajectories non-intersecting Σ_M. The particles movement along rectilinear trajectories is uniform. Equation (9) considered as a perturbed equation

$$m\dot{\vec{x}} - \frac{\partial S_0}{\partial \vec{x}} = \dot{\vec{\varphi}} \tag{12}$$

with a perturbation $\Delta = \partial S_0/\partial \vec{x} - \partial S/\partial \vec{x}$ leads to the functional change of variables with the Jacobian

$$J[S, S_0] = exp\{-\frac{1}{2}\int_{t_1}^{t} div(\frac{\partial S}{\partial \vec{x}} - \frac{\partial S_0}{\partial \vec{x}})dt\},$$

connecting the solution of the equation (10) with the solution of the equation (11). Thus

$$W(\vec{x}, t) = \int W(\vec{x}_1, t_1)W(\vec{x}_1, t_1; \vec{x}, t)d\vec{x}_1 = \int W(\vec{x}_1, t_1)J[S, S_0]W(\vec{x}_1, t_1; \vec{x}, t)d\vec{x}_1,$$

i.e., the resulting probability density $W(\vec{x}, t)$ is obtained from the initial probability density $W(\vec{x}_1, t_1)$ with the aid of the transition probability $W(\vec{x}_1, t_1; \vec{x}, t)$ as well as from the initial probability density

$$W_1[S, S_0](\vec{x}_1, t_1) = W(\vec{x}_1, t_1)J[S, S_0] \tag{13}$$

with the aid of the transition probability $W_0(\vec{x}_1, t_1; \vec{x}, t)$. Consequently the passage from the system description by using equations (9),(10) to its description with the help of equations (13), (11) does not lead

to the information loss when instead of the real initial distribution $W(\vec{x}_1, t_1)$ one considers the distribution $W_1(\vec{x}_1, t_1)$ connected by one-to- one correspondence (13) with the distribution $W(\vec{x}_1, t)$ and functionally depended on the total evolution of the particle in question. It is believed that the density of the particles distribution $\rho(\vec{x}_1, t)$ over coordinates $\vec{x}_1$ at the moment t_1 is proportional to the probability density. That is why the equations (6),(8),(10),(11) remain valid in the case of the replacement of $W(\vec{x}_1, t)$ by $\rho(\vec{x}_1, t)$ and one may describe the process of sputtering with the help of the transition probability W_0 which is the solution of equation (11) if instead of the real distribution $\rho(\vec{x}_1, t_1)$ of sputtered particles over the coordinates of the entrance mask surface Σ_1 one uses the distribution

$$\rho_1[S, S_0](\vec{x}_1, t_1) = \rho(\vec{x}_1, t_1) J[S, S_0]. \tag{14}$$

The distribution ρ_1 represented by the relation (14) and functionally dependent on the total evolution of particles in the process of sputtering, may well be termed an effective distribution. The function ρ_1 may be restored by the data of sputtering experiments because one knows an explicit expression for the transition probability W_0 satisfying the equation (11). That is why for computational modeling of the sputtering process it's much more preferable to working with the effective distribution ρ_1 instead of the real distribution ρ that cannot be restored by the experimental results of sputtering.

References

1. *Westwood D.B.* Calculation of deposition rates in diod sputtering systems. // J. Vac. Sci. Technol 1978,v.15,p.1.
2. *Yao S.K., Anderson D.B.* Shadow-sputtering difraction-limited waveguide Luneburg lenses. // Appl. Phys. Lett. 1978, v.33, p.307.
3. *Yao S.K.* Theoretical model of thin-film deposition profile with shadow-effect. // J. Appl. Phys., 1979, v.50, p.3390.
4. *Hatakoshi G., Inoue H., Naito K., Umegaki S., Tanaka S.* Optical waveguide lenses. // Optica Acta, 1979, v.26, p.961.
5. *Anikin V.I., Derugin L.N., Kuryshkin V.V., Sevastianov L.A.* Mathematical problems related with the process of sputtering. - Deposed in VINITI, N° 5175-82, 1982 (in Russian).
6. *Sevastianov L.A.* On shadowin of corpuscular fluxes. // Izv. Vuzov. Fizika. 1983,N° 7. p.126 (in Russian).
7. *Kuryshkin V.V., Sevastianov L.A.* Some questions of the corpuscular flows shadowing. Deposed in VINITI, N° 4403-81, 1981 (in Russian).

8. *Sevastianov L.A.* Mathematical model of the shadowing effect of non-intercting fluxes. // Math. Modeling , 1998, v.10, $N^{\underline{o}}$ 4 (in Russian).

9. *Beylinson A.A.* Using of functioal integration method to constract the fundamental solution of a Fokker-Plank-Kolmogorov equation. // DAN SSSR, 1959, v.123, $N^{\underline{o}}$ 5 (in Russian).

10. *Beylinson A.A.* On the relation of solutions of an Fol:ker-Plank-Kolmogorov equation and a Bloch-Schrödinger equation and the Kac-Feynman formula. – Deposed in VINITI, $N^{\underline{o}}$ 348-79, 1979 (in Russian).

СИНТЕЗ ЭКРАНИРУЮЩЕЙ МАСКИ ДЛЯ НАПЫЛЕНИЯ ТОНКОПЛЕНОЧНОЙ ЛИНЗЫ ЛЮНЕБЕРГА

Л.А.СЕВАСТЬЯНОВ[1]

Российский университет дружбы народов
117198, Москва, ГСП, ул.М.-Маклая, д.6, Россия
E-mail: lsevastianov@mx.pfu.edu.ru

Введение

К интегральной оптике относят научно-техническое направление, имеющее дело с распространением света в тонких слоях прозрачных материалов.Характерными интегрально-оптическими устройствами являются тонкопленочные линзы Люнеберга - участки многослойного диэлектрического волновода с цилиндрически симметричным утолщением верхнего слоя в круге радиуса R_0 плоскости волновода.

Для получения профиля напыленного слоя, близкого к теоретическому, в работах [1-3] предложена математическая модель экранируемого вакуумного напыления.

1. Каноническое уравнение процесса напыления цилиндрически симметричных пленок

В случае цилиндрической симметрии установки напыления и экранирующей маски с одним входным отверстием, т.е. в случае, когда установка и маска переходят в себя при повороте на произвольный угол вокруг вертикальной оси симметрии (такие условия выполняются при напылении участков тонкой пленки с круговой симметрией, например, линз Люнеберга), основная формула процесса напыления на плоскую подложку имеет вид (см. [3])

$$h(\vec{r}) = \frac{vT}{H^2} \iint_{-\infty}^{\infty} d\vec{r}_1 \int_{-\infty}^{0} du\, \rho_1(r_1, \frac{|\vec{r}_1 - \vec{r}|}{H} u, u) u^2 \Theta_M(\vec{r}_1, \vec{r}), \tag{1}$$

где

$$\Theta_M(\vec{r}_1, \vec{r}) = \prod_{z=0}^{H} \vartheta\left(R(z)^2 - |\vec{r} + \frac{z}{H}(\vec{r}_1 - \vec{r})|^2\right). \tag{2}$$

Здесь, как и в работе [3], v - элементарный объем, приходящийся на одну частицу напыленного вещества, T - время напыления, H - высота входа маски M, Θ_M - функция прозрачности маски M, $R(z)$ - радиус входного отверстия маски на высоте $z \in [0, H]$ над подложкой, $\vec{r}_1 = (x_1, y_1)$ - координаты точки плоскости входа маски, $\vec{r} = (x, y)$ - координаты точки плоскости подложки, $a = |\vec{a}|$ - норма вектора $\vec{a}$, ϑ - функция Хевисайда:

$$\vartheta(a) = \begin{cases} 1, & \text{если} \quad a \geq 0; \\ 0, & \text{если} \quad a < 0. \end{cases}$$

Выражения (1), (2) допускают замену переменных $\vec{r}_1 \longmapsto \vec{\eta} = \vec{r}_1 - \vec{r}$. Если дополнительно учесть, что распределение частиц на входе маски однородно по координатам $\rho_1(\vec{r}_1, \vec{v}, u) = \rho_1(\vec{v}, u)$, то соотношения (1), (2) в итоге приобретут вид

$$h(\vec{r}) = \frac{vT}{H^2} \iint_{-\infty}^{\infty} d\vec{r} \int_{-\infty}^{0} du\, \rho_1(\frac{u}{H}\eta, u) u^2 \tilde{\Theta}_M(\vec{r}, \vec{\eta}), \tag{3}$$

[1] Работа выполнена при поддержке РФФИ (грант N 94-01-01354a)

где

$$\tilde{\Theta}_M(\vec{r},\vec{\eta}) = \prod_{z=0}^{H} \vartheta\left(R(z)^2 - r^2 - (\frac{z}{H}\eta)^2 - 2\frac{z}{H}(\vec{r},\vec{\eta})\right). \tag{4}$$

Функция $\tilde{\Theta}_M$ в выражении (4) зависит от трех скалярных величин: $r, \eta, \varphi = arccos\frac{(\vec{r},\vec{\eta})}{r\,\eta}$:

$$\Theta_M(r,\eta,\varphi) = \prod_{z=0}^{H} \vartheta\left(R(z)^2 - r^2 - (\frac{z}{H}\eta)^2 - 2r\frac{z}{H}\cos\varphi\right),$$

а уравнение (3) записывается в виде

$$h(r) = \frac{vT}{H^2}\int_0^{\infty} d\eta\cdot\eta\int_0^{2\pi} d\varphi\int_{-\infty}^{0} du\,\rho_1(\frac{u}{H}\eta,u)u^2\,\Theta_M(r,\eta,\varphi). \tag{5}$$

В уравнении (5) функция Θ_M зависит от φ , но не зависит от u, а функция ρ_1, напротив, зависит от u, но не зависит от φ. Это позволяет перейти к описанию эффектов экранирования в процессе напыления с помощью интегральных характеристик установки напыления

$$\tilde{X}(\eta) = \eta\frac{vT}{H^2}\int_{-\infty}^{0} du\,\rho_1(\frac{u}{H}\eta,u)u^2 \tag{6}$$

и маски

$$\tilde{A}(r,\eta) = \int_0^{2\pi}\Theta_M(r,\eta,\varphi)d\varphi. \tag{7}$$

Уравнение (5) при этом запишется в виде одномерного интегрального уравнения

$$h(r) = \int_0^{\infty}\tilde{A}(r,\eta)\tilde{X}(\eta)d\eta. \tag{8}$$

Отметим вначале тот факт, что функция $\tilde{A}(r,\eta)$ обладает компактным носителем. Действительно, так как

$$\tilde{A}(r,\eta) = \int_0^{2\pi}\prod_{z\in 0}^{H}\vartheta\left(R(z)^2 - r^2 - (\frac{z}{H}\eta)^2 - 2r\frac{z}{H}\eta\cos\varphi\right), \tag{9}$$

то $\tilde{A}(r,\eta)\equiv 0$, если хотя бы для некоторого $z\in[0,H]$ выполняется неравенство

$$R(z)^2 - r^2 - (\frac{z}{H}\eta)^2 < 2r\frac{z}{H}\eta\cos\varphi$$

при любом угле $\varphi\in[0,2\pi]$.

Обозначим через

$$b(z;r,\eta) = \frac{R(z)^2 - r^2 - (\frac{z}{H}\eta)^2}{2r\frac{z}{H}\eta}.$$

Подынтегральное выражение в (7) не дает вклада в $\tilde{A}(r,\eta)$, если хотя бы при одном $z\in[0,H]$ выполняется неравенство

$$\cos\varphi \geq b(z;r,\eta).$$

Иными словами, вклад в интеграл (9) отличен от нуля для тех φ, при которых

$$\cos\varphi < \min_z b(z; r, \eta) \equiv b(r, \eta).$$

При этом

$$\tilde{A}(r, \eta) = 2\{\pi - \arccos b(r, \eta)\}.$$

Носитель функции $A(r, \eta)$ лежит в области $Q \subset R^2$, заданной неравенствами

$$0 \le r \le R(0), \quad 0 \le \eta\,;$$

$$H\frac{r - R(z)}{z} \le \eta \le H\frac{r + R(z)}{z}, \quad z \ne 0. \tag{10}$$

Ограничения (10) можно переписать в виде

$$\sup_{z\ne 0}\frac{r - R(z)}{z} \le \frac{\eta}{H} \le \inf_{z\ne 0}\frac{R(z) + r}{z}$$

и ввести канонические переменные, которые позволяют переписать уравнение (8) в каноническом виде. Положим

$$\mu = \inf_{z\ne 0}\frac{R(0) + R(z)}{z}, \quad \pi(z) = \frac{R(z)}{R(0)}, \quad \nu(z) = \frac{\mu z}{R(0)}.$$

Тогда канонические переменные

$$\sigma = r/R(0), \quad \rho = \eta/\mu H,$$

являющиеся безразмерными и превращающие неравенства (10) в неравенства вида

$$0 \le \sigma \le 1; \quad 0 \le \rho; \quad \max_z\frac{\sigma - \pi(z)}{\nu(z)} \le \rho \le \min_z\frac{\sigma + \pi(z)}{\nu(z)} \le 1\,.$$

Таким образом, в канонических переменных носитель ядра интегрального уравнения (8) лежит целиком в квадрате $[0, 1] \times [0, 1]$, а само уравнение записывается в виде

$$\int_0^1 A(\sigma, \rho)X(\rho)d\rho = Y(\sigma). \tag{11}$$

Здесь

$$Y(\sigma) = h(\sigma R(0)),\ X(\rho) = \tilde{X}(\rho\cdot\mu\cdot H),\ A(\sigma, \rho) = 2\{\pi - \arccos b(\sigma, \rho)\};$$

где

$$b(\sigma, \rho) = \min_z\frac{\pi(z)^2 - \sigma^2 - (\nu(z)\rho)^2}{2\sigma\nu(z)\rho}.$$

Ядро $A(\sigma, \rho)$ интегрального уравнения (11) зависит не от самой геометрической формы экранирующей маски, а от класса эквивалентности масок, заданного набором параметров:

$$\nu(z), \pi(z), z \in [0, H]\,.$$

Носители функции $Y(\sigma)$, задающей конфигурацию напыленного слоя, и подынтегральной функции $X(\rho)$, являющейся интегральной по отношению к эффективному распределению характеристикой установки напыления, лежат в единичном отрезке [0,1]. В итоге основное уравнение процесса напыления в канонических переменных записывается следующим образом:

$$Y(\sigma) = 2\int_0^1 \{\pi - \arccos[\min_z \frac{\pi(z)^2 - \tau^2 - (\nu(z)\rho)^2}{2\tau\nu(z)\rho}]\}X(\rho)\,d\rho.$$

2. Алгоритм восстановления функции источника разностным методом

Полученное в предыдущем пункте каноническое уравнение (11) является одномерным интегральным уравнением Фредгольма первого рода

$$\hat{A}X = Y$$

с квадратично-интегрируемым ядром $A(\sigma,\rho)$

$$A \in L_2(I^2), \quad Y \in L_2(I), \quad X \in C(I^2), \quad I = [0,1], \quad I^2 = [0,1]\times[0,1],$$

так что $\hat{A}$ - вполне непрерывный оператор.

Решение задачи (11) с приближенно заданными $\hat{A}_\sigma, Y_\gamma$ находим минимизацией тихоновского функционала [4]

$$M^\alpha[x] = \int_0^1 \{\int_0^1 A(\sigma,\rho)X(\rho)d\rho - Y(\sigma)\}^2 d\sigma + \alpha\int_0^1 \{q(\rho)X^2(\rho) + p(\rho)(\frac{dX}{d\rho}(\rho))^2\}d\rho. \tag{12}$$

Уравнением Эйлера для задачи (12) является интегродифференциальное уравнение

$$\int_0^1 A(\sigma,\rho)\{\int_0^1 A(\sigma,\tau)X(\tau)d\tau - Y(\sigma)\}d(\sigma) + \alpha\{q(\rho)X(\rho) - \frac{d}{d\rho}[p(\rho)\frac{dX}{d\rho}(\rho)]\} = 0. \tag{13}$$

с граничными условиями

$$X(0) = 0, \quad X(1) = 0. \tag{14}$$

Задачу (12) решаем с автоматическим выбором параметра регуляризации методом, изложенным в [5], т.е. отыскиваем точку равновесия по Нэшу пары функционалов:

$$M[X,\alpha] = \int_0^1 \{\int_0^1 A(\sigma,\rho)X(\rho)d\rho - Y(\sigma)\}^2 d\sigma, \tag{15}$$

$$N[X,\alpha] = \int_0^1 \alpha^2(\rho)\{q(\rho)X^2(\rho) + p(\rho)[\frac{dX}{d\rho}(\rho)]^2\}d\rho. \tag{16}$$

Одним из наиболее эффективных методов решения задачи (15), (16) является [6] итеративный поиск последовательности (X^k, α^k), сходящейся к паре (X^*, α^*), первая компонента которой X^* является решением задачи (12), т.е. искомой функцией источника. Этот поиск осуществляется пошаговой минимизацией функционалов:

$$r_k M[X,\alpha^k] + (r_k\alpha^k - 1)\int_0^1 \{X(\rho) - X^k(\rho)\}^2 d\rho,$$

$$r_k N[X^{k+1}, \alpha] + \int_0^1 \{\alpha(\rho) - \alpha^k(\rho)\}^2 d\rho$$

с параметрами τ_k, выбранными из условий сходимости итеративного поиска. Таким образом, на каждом шаге с номером k поиска решения (X^*, α^*) решается пара уравнений Эйлера:

$$\int_0^1 A(\sigma,\rho)\{\int_0^1 A(\sigma,\tau)X(\tau)d\tau - Y(\sigma)\}d\sigma + (\alpha^k(\rho) + \frac{1}{\tau_k})\{q(\rho)[X(\rho) - X^k(\rho)] - \frac{d}{d\rho}[p(\rho)\frac{d}{d\rho}(X(\rho) - X^k(\rho))]\} = 0, \tag{17}$$

$$\alpha(\rho)\{q(\rho)[X^{k+1}(\rho)]^2 + p(\rho)\ \frac{dX^{k+1}}{d\rho}(\rho)]^2\} + [\alpha(\rho) - \alpha^k(\rho)]\frac{1}{\tau_k} = 0. \tag{18}$$

Сходимость алгоритма и принадлежность решения X^* пространству непрерывных функций с квадратично-интегрируемыми производными обеспечивается, в частности, и при $\tau_k \equiv 1$, $q(\rho) \equiv 1$, $p(\rho) \equiv const$. Такие параметры были выбраны для численной реализации поиска функции источника.

Переход к дискретной модели осуществляется конечно-разностным методом. Область интегрирования по переменным ρ, τ разбивалась на N_1 участков равной длины $\Delta\rho = \Delta\tau = 1/N_1$, область интегрирования по σ разбивалась на $N_2 = N_1 - 2$ участков равной длины $\Delta\sigma = 1/N_2$. Интегралы заменялись интегральными суммами по формуле трапеций, а вторые производные - конечно-разностными выражениями:

$$[X(\rho_{j+1}) - 2X(\rho_j) + X(\rho_{j-1})]/(\Delta\rho)^2.$$

Граничные условия (14) позволяют разрешить два крайних уравнения возникающей при дискретизации уравнения (17) системы линейных алгебраических уравнений и привести систему к виду

$$\sum_{j=1}^{N_2}(A_{ij} + (\alpha_j^k + \frac{1}{\tau_k})B_{ij})X_j = U_i, \quad i = 1, ..., N_2. \tag{19}$$

Здесь $X_j = X(\rho_j)$, $\quad j = 1, ..., N_2$;

$$U_i = U(\rho_i) = \Delta\sigma\{\frac{1}{2}A(\sigma_1,\rho_i)Y(\sigma_1) + \sum_{j=2}^{N_2-1} A(\sigma_j,\rho_i)Y(\sigma_j) + \frac{1}{2}A(\sigma_{N_2},\rho_i)Y(\sigma_{N_2})\};$$

$$A_{ij} = \Delta\sigma\{\frac{1}{2}A(\sigma_1,\rho_i)A(\sigma_1,\rho_j) + \sum_{k=2}^{N_2-1} A(\sigma_k,\rho_i)A(\sigma_k,\rho_j) + \frac{1}{2}A(\sigma_{N_2},\rho_i)A(\sigma_{N_2},\rho_i)\};$$

$$B_{jj} = q + p/(\Delta\rho)^2, \quad j = 1, ..., N_2;$$

$$B_{j,j+1} = -p/(\Delta\rho)^2, \quad j = 1, ..., N_2 - 1; \quad B_{j-1,j} = -p/(\Delta\rho)^2, \quad j = 2, ..., N_2.$$

При дискретизации уравнения (18) получается система линейных алгебраических уравнений, которая с учетом граничных условий (14) приводится к виду

$$\alpha_j(X_j^{k+1}) - p^2\alpha_j(X_{j+1}^{k+1} - 2X_j^{k+1} + X_{j-1}^{k+1})/(\Delta\rho)^4 + \frac{\alpha_j - \alpha_j^k}{\tau_k} = 0. \tag{20}$$

Расчеты проводились с помощью пакета программ, реализующего указанный алгоритм на фортране. Предварительная обработка экспериментальных данных осуществлялась методом сплайн-

аппроксимации с помощью соответствующего комплекса программ. Все параметры r_k были выбраны тождественно равными 1, параметр q был выбран равным 1. Параметр p и начальное приближение α_0 параметра регуляризации варьировались при проведении серии численных экспериментов. В результате были найдены допустимые области выбора p и α_0. При любых p и α_0 из области допустимых значений решение задачи (11), (12) (дискретный аналог функции источника) получалось за число шагов, меньшее десяти.

3. Алгоритм отыскания формы экранирующей маски

Мы будем решать задачу в классе N-сегментных масок с отверстием, образованным набором сопряженных конических поверхностей с радиусами R_k на высотах z_k.

Замечание 1. В работе [1] показано, что такая экранирующая маска с кусочно-линейной функцией $R(z)$ при $n \to \infty$ приближает экранирующую маску с произвольной непрерывной функцией $R(z), z \in [0, H]$, и может служить хорошей моделью произвольной цилиндрически симметричной экранирующей маски с одним отверстием.

Замечание 2. Кусочно-линейная непрерывная выпуклая в сторону оси Oz функция $R(z)$: $R(z_k) = R_k$ задает ту же функцию маски $A[R(z)](\sigma, \rho)$ и ту же правую часть $Y[R(z)](\sigma)$, что и любая не выпуклая в сторону Oz функция $R'(z)$: $R'(z_k) = R_k$, т.е. и $A[R'(z)](\sigma, \rho) \equiv A[R(z)](\sigma, \rho) = A[R_k, z_k](\sigma, \rho)$ и $Y[R'(z)](\sigma) \equiv Y[R(z)](\sigma) = Y[R_k, z_k](\sigma)$.

А именно:функция маски

$$A[R_k, z_k](\sigma, \rho) = 2\{\pi - arccos\, b_N(\sigma, \rho)\}, \quad \text{где} \tag{21}$$

$$b_N(\sigma, \rho) = \min_{k \in \overline{1,N}} \frac{\pi_k^2 - \sigma^2 - (\nu_k \rho)^2}{2\sigma\nu_k\rho}, \quad \pi_k = \pi(z_k), \quad \nu_k = \nu(z_k), \text{а функция слоя}$$

$$Y[R_k, z_k](\sigma) = \int_0^1 A[R_k, z_k](\sigma, \rho) X(\rho) d\rho\,. \tag{22}$$

Вышеописанная N- сегментная маска с параметрами $\{R_k, z_k\}$, $k = 1, ..., N$ (так же, как и N-листовая маска с теми же параметрами) описывается $2N$-мерным вектором $w = (z_1, ..., z_N; R_1, ..., R_N)$. Соотношение (22) сопоставляет любому $2N$-мерному вектору w некоторую функцию $Y[w](\sigma)$. Если $H = z_N \geq z_{N-1} \geq ... \geq z_1 \geq 0$, функция $R(z)$: $R(z_i) = R_k$ - кусочно-линейная положительно определенная функция на $[0, H]$, то $w \in R^{2N}$ описывает экранирующую маску, а $Y[w](\sigma)$ описывает функцию слоя, напыленного через эту маску в круге радиуса R_0 . Обозначим через D_n замкнутое подмножество в R^{2N}

$$D_N = \{w = \{R_k, z_k\} : z_N \geq z_{N-1} \geq ... \geq z_1 = 0; \quad R_j \geq 0, j = 1, .., N\}\,.$$

Определим расстояние $\rho(Y, Y[w])$ между $Y(\sigma)$ и $Y[w](\sigma)$ в метрике $L_2[0, 1]$:

$$\rho^2(Y, Y[w]) = \int_0^1 \{Y[w](\sigma) - Y(\sigma)\}^2 d\sigma, \quad w \in D_N\,. \tag{23}$$

Назовем $\delta_N = \inf_{w \in D_N} \rho(Y[w], Y)$ максимально достижимой точностью приближения функций слоя, полученных с помощью N-сегментных масок. Ясно, что $\delta_1 \geq \delta_2 \geq ... \geq \delta_N \geq ... \geq 0$. Назовем $\delta = \lim_{N \to \infty} \delta_N$ предельно достижимой точностью. Задача состоит в том, чтобы приблизить в метрике (23) заданную функцию слоя $Y(\sigma)$ с некоторой априорно заданной точностью δ (такая задача имеет смысл при $\delta > \delta_0$) при дополнительных (технологических) ограничениях на синтезируемый профиль $w = \{R_k, z_k\}$. К таким ограничениям относятся и минимальность числа сегментов N, наличие минимально осуществимой толщины конического сегмента z_0: $z_j \geq z_{j-1} + z_0$, $j = 1, ..., N$. К ним можно отнести минимальность толщины маски, а значит, минимальность суммы $\sum_{j=1}^N z_j^2$; а также минимальность

отверстия маски, т.е. минимальность суммы $\sum_{j=1}^{N} R_j^2$. Если обозначить через $D_N^o = \{w \in D_N : z_j \geq z_{j-1} + z_0,\ j = 1, ..., N\}$ замкнутое подмножество $D_N \subset R^{2N}$, то задача состоит в минимизации функционала

$$F^\alpha[w] = \rho^2(Y[w], Y) + \alpha \sum_{k=1}^{N} (R_k^2 + z_k^2) \tag{24}$$

на множестве D_N^o при условиях

$$\rho(Y[w], Y) = \delta, \quad N = \min_{k=1,2,...} k \tag{25}$$

Дискретный аналог функционала (24) получается заменой интеграла (23) интегральной суммой по формуле трапеций

$$\begin{aligned} F_n^\alpha[R_k, z_k] = \Delta\sigma\{\frac{1}{2}[Y(\sigma_1) - Y(\sigma_1; R_k, z_k)]^2 + \sum_{j=2}^{L-1}[Y(\sigma_j) - Y(\sigma_j; R_k, z_k)]^2 + \\ + \frac{1}{2}[Y(\sigma_L) - Y(\sigma_L; R_k, z_k)]^2\} + \alpha \sum_{k=1}^{n-1}(R_k^2 + z_k^2), \end{aligned} \tag{26}$$

где

$$\Delta\sigma = 1/(L-1), \quad \delta\rho = 1/(L+1), \quad Y(\sigma; R_k, z_k) = \{\sum_{j=2}^{L-1} A(\sigma, \rho_j; R_k, z_k) X(\rho_j) \Delta\rho.$$

Последовательно увеличивая число N сегментов маски, находим такое N^*, при котором достигается заданная точность δ. После чего функционал $F_L^\alpha(w)$ минимизируется на $D_{N^*}^o$ с параметром α, выбранным из условия (25). Соответствующий минимизирующий вектор w_α^* существует, т.к. $D_{N^*}^o$ - замкнутое ограниченное подмножество конечномерного пространства.

Минимизацию функционала (26) проводим методом деформируемого многогранника [7] с дополнительным проектированием на область D_N^o допустимых значений параметов R_k, z_k. Проектирование осуществляется методом деформируемого многогранника и случайным способом [8], соответствующие способы известны под названиями: метод скользящего допуска и метод Бокса. Расчеты проводились обоими методами в классе трехсегментных масок.

ЛИТЕРАТУРА

1. *Л.А. Севастьянов.* Математическая модель экранирования невзаимодействующих корпускулярных потоков. //Матем. моделиование, 1998, т.10, N4.
2. *L.A. Sevastianov.* Effective distribution concept of a mathematical model for shadowed sputtering (ibid).
3. *Л.А. Севастьянов.* Математическая модель экранируемого напыления.//Матем. Моделирование, 1998, т.10, N4.
4. *А.Н. Тихонов, В.Я. Арсенин.* Методы решения некорректных задач. – М.: Наука, 1979.
5. *К.П. Ловецкий.* Об одном методе выбора параметра регуляризации. // В сб. Численные методы решения задач математической физики и теории систем. – М.: Изд.УДН, 1978, с.34-37.
6. *А. Бенсусан, Ж.-Л. Лионс, Р. Темам.* Методы декомпозиции, децентрализации, координации и их приложения. //В сб. Методы вычислительной математики. Новосибирск: Наука, 1975, с.144-274.
7. *Н. Химмельблау.* Нелинейное программирование. М.: Мир, 1969.
8. Численные методы условной минимизации. /Под ред. Ф.Гилла и У.Мюррея/. М.:Мир, 1977.

CALCULATION OF THE SP-94 MAGNET FIELD FOR EXCHARM SETUP *)

E.P. Zhidkov, S.V. Andreev, E.E. Perepelkin, R.V. Polyakova, T.V. Shavrina, I.P. Yudin

Joint Institute for Nuclear Research, 141980 Dubna, Moscow region, Russia
E-mail: mag@cv.jinr.ru

A distribution of the spectrometric SP-94 magnet field of the EXCHARM setup (Protvino, Russia) [1] has been investigated in order to study decay processes for charm and strange quarks.

A detailed field map has been calculated. The problem of obtaining a homogeneous field in a possibly large volume has been studied. An optimal configuration for adheared ferromagnet bars, which solve the present problem, has been found.

1. Introduction

IHEP (Protvino, Russia) plans ahead the new project of the EXCHARM II experiment with two spectrometric SP-40A [2] and SP-94 magnets (see fig.1).

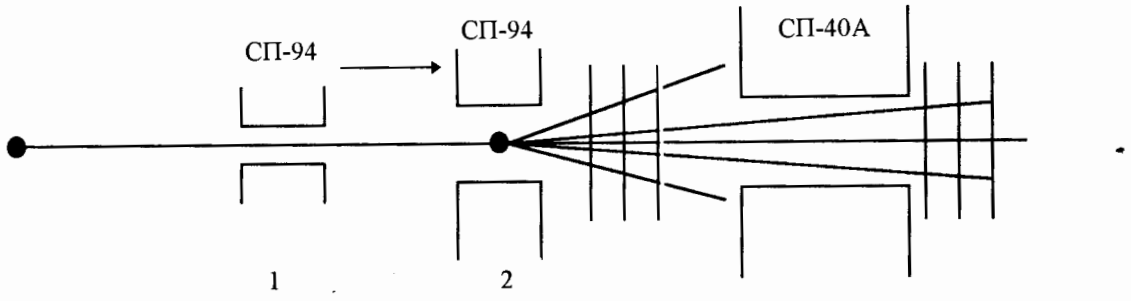

Fig.1. Layout of the EXCHARM II spectrometer.

At the present moment on the EXCHARM setup the SP-94 magnet is not connected and is located in position 1. The proposal exists to connect this magnet and to transfer it on position 2, as shown on fig.1. The reason is in the possibility of the registration of the larger number of multiparticle states consisting of complete tracks and half-tracks.

The aim of our paper is studying the field distribution of the spectrometric SP-94 magnet of the EXCHARM setup for an investigation of the hadroproduction and decay of charm and strange particles.

A detailed map of the field has been calculated. received by computative means. The problem of obtaining a homogeneous field in a maximally wide region is studied. The optimal configuration for adheared ferromagnet bars, which solve the present problem, has been found.

*) Work supported by the Russian Foundation for Basic Research (grants no.95-01-00737a and no.95-01-01467a) and supported in part by the Federal Centre "Integration" (project no.K0085)

2. Analysis of the numerical calculations

The numerical modelling of the SP-94 magnetic system of the EXCHARM setup was carried out by means of the CPMMS-v.1.1 program complex [3]. As a component, an accumulation of the data base of the investigated configurations of magnetic systems for the further graphic research of the obtained numerical result, is part of the program complex, which makes easier and faster the process of selection of the magnetic system configuration for its technical realization.

The calculation of the SP-94 magnet field in the 2-dimensional system of coordinates was performed in this paper with the help of the program POISCR [4], being a part of the CPMMS-v.1.1 codes.

The task was also solved by the method of vector potential by applying the method of boundary integral equations (the new origina VP2DBIE code). At a computer realization there was used the multigrid algorithm of calculations on the sequence of grids with 40x60, 80x120, 160x240, 320x480, 640x960 nodes.

The configuration of the 1/4 part of the SP-94 magnet is presented on fig.2 with accounting the dipole symmetry. The area of the pole of the SP-94 magnet with the adheared ferromagnetic bars is shown in fig.3.

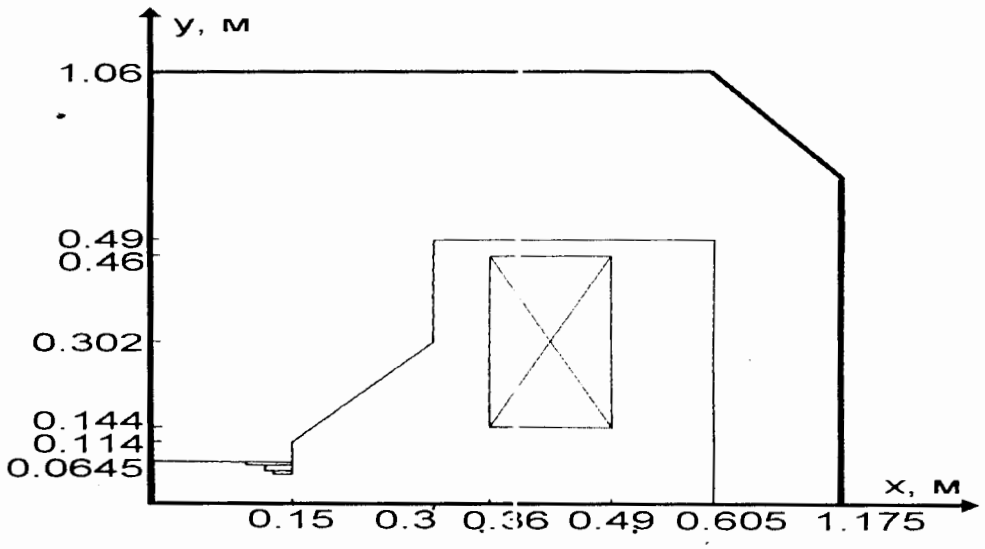

Fig.2.View of the 1/4 part of the SP-94 magnet.

The calculations of the magnet field for two configurations (with the adheared ferromagnetic bars and without it , see fig.2) were carried out. The graph of the magnetic field distribution for $y = 0, B_y(x)$ for the first configuration (without the adheared ferromagnetic bars) is given in fig.3. The sharp reduction of the $B_y(x)$ field is observed after $x = 10cm$ on the x-interval ($x = 10cm, x = 15cm$).

For formation of the good homogeneous field, the ferromagnetic bars were added to the pole of the ferromagnetic yoke. The graph of dependence of $B_y(x)$ for the different y-values are given in fig.4 after this addition.

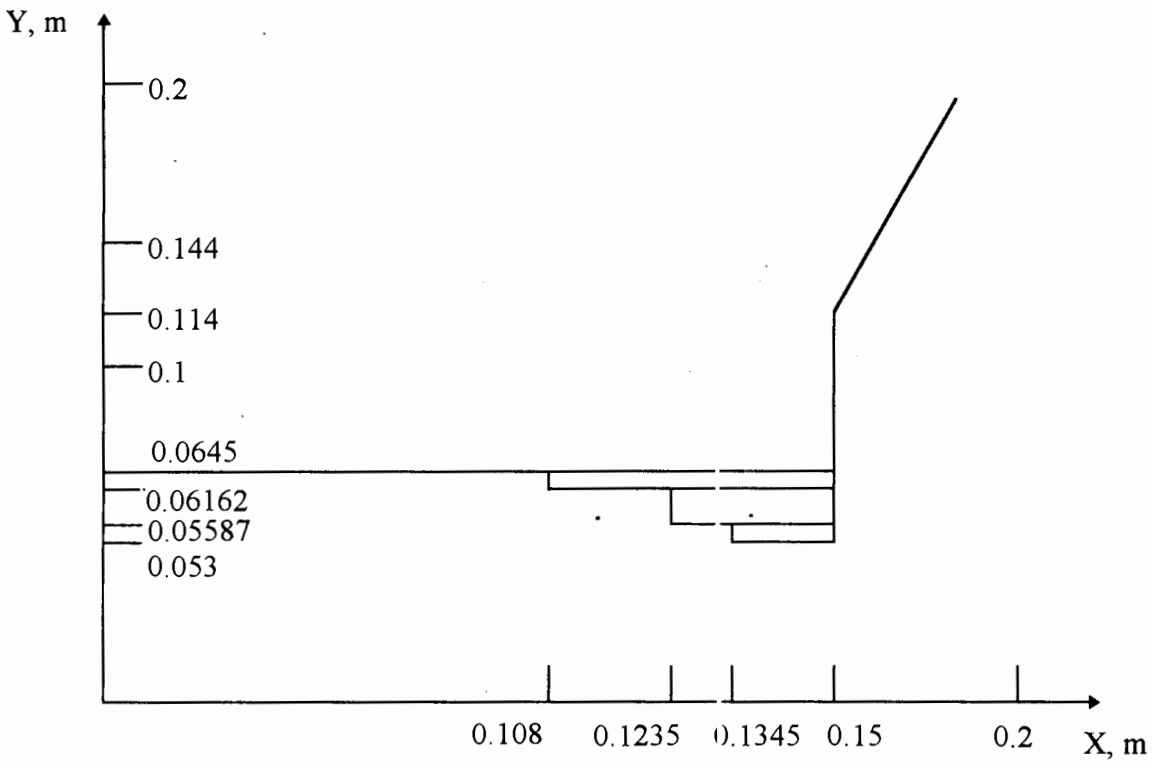

Fig.3. The area of the pole with the adheared ferromagnetic bars.

In particular, it is clear from the $B_y(x)$ graph for the 1-st (without the adheared ferromagnetic bars on the magnet pole, see fig.4) and 2-nd (with the adheared ferromagnetic bars on the magnet pole, see fig.5) configurations that the sharp reduction of the magnetic field begins with $x = 13\ cm$ in the second case. The bars added produce more homogeneous magnetic field in the magnet center. It is clear from comparison of the $B_y(x)$ graphs for the first and second configurations of the pole.

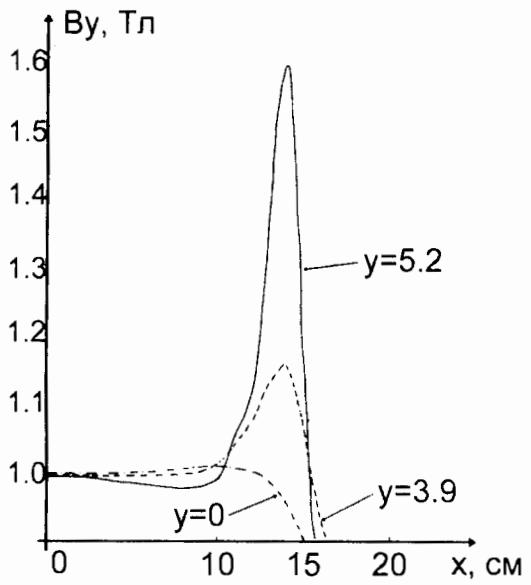

Fig.4.

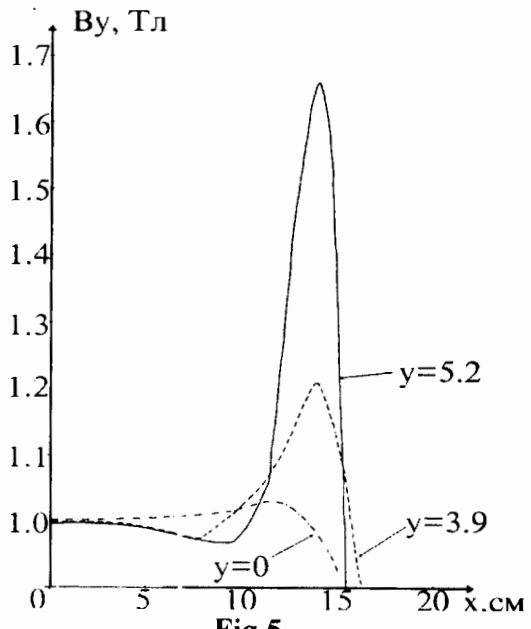

Fig.5.

3. Conclusions

1. Using CPMMS - v1.1 code (the Complex of Program for Modelling of Magnetic Systems), the field distribution is investigated for the SP-94 magnet of the EXCHARM spectrometer of charme and strange particles.
   The task was also solved by the method of vector potential by applying the method of boundary integral equations (the new original VP2DBIE code). At a computer realization it was used the multigrid algorithm of calculations on the sequence of grids with 40x60, 80x120, 160x240, 320x480, 640x960 nodes.
2. The configuration of the magnet is selected by means of numerical experiments. This magnetic field is homogeneous in the large half of the working area of the aperture.
3. The computer model of the SP-94 magnet is obtained and the map of the magnetic field for experimental physical data processing for the EXCHARM. II spectrometer is suggested.

References

1. Aleev A.N. et al. Observation of the Σ_C^0 charmed baryon in the experiment EXCHARM. - JINR Rapid Communications, No.3[77]-96, pp.31 - 46.
2. Zhidkov E.P. et al. Change of field distribution for spectrometric SP-40A magnet. - In present book, pp.
3. Zhidkov E.P., Lima S., Polyakova R.V., Fernandes Nodarse F., Yudin I.P. The Complex of Programs for the Modelling of Magnetic Systems. - Preprint JINR, P11-93-256, Dubna, 1993.
4. Holsinger R. F., Iselin C., POISCR-r604, User Guide, CERN, SPS/EMA, 1982.
5. Zhidkov E.P., Khoromsky B.N. Preprint CVM AN USSR, n 137, M., 1987, p.40.

THIRD ORDER BEAM OPTICS BY THE GREEN'S FUNCTION METHOD

V.V. Andreev, I. F. Yudin

Joint Institute for Nuclear Research, Dubna 141980, Russia
E-mail: MAG @ LCTA50. JINR. DUBNA. SU

Specification of the charged particles beam behaviour in optical magnetic and electrostatic systems of accelerators in terms of the transfer matrix is developed completely for the linear paraxial approach used not only linear motion equations, but «rectangular» or «integral» field models of elements in the beam transport channels.

But in practice it is necessary to take into account nonlinear *aberration* members of the motion equation because of the smooth field decreasing within fringe regions of the optical elements, as well as nonlinearity in the conservation laws being applied.

Often such a type of computation is produced by numerical methods (for example, by the Runge-Kutta method), or the motion equations are solved in integrals, that also requires significant timing and hardware resources, especially in multi-particle applications.

At present theoretical research and applicable charged beam dynamics simulation in the real optical magnetic and electrostatic elements within the *analytical solution approach* of the second order nonlinear differential equations and the transfer matrix evaluation of elements are carried out at the Laboratory of Particle Physics, JINR.

One of the solution techniques is the Green function method. The usage of this method is justified by the type of the obtained solutions and that is why it is quite reasonable.

We shall search for the solution of the plane trajectory equation defined by Lorentz force, operating on particle q in the external electrostatic $\boldsymbol{E}$ or magnetic $\boldsymbol{B}$ fields

$$\vec{F} = q(\vec{E} + [\vec{v} \times \vec{B}]), \tag{1}$$

in terms of the so-called *relative trajectory* because the time dependence is often beyond the scope of interests in these problems.

In some curvilinear coordinate system XYS we shall determine the following variables x, x', y and y' as phase-space coordinates defined from some selected relative trajectory, l - the path length difference between the relative trajectory and the considered one. The deviation from relative momentum p_0 is assumed as δ.

So, the solution to be found in this problem is 6-vector $\boldsymbol{X}$= (x, x', y, y', l, δ) with corresponding initial conditions. The main assumptions which are the base of the solution method, are as follows:

1. *There is some scalar potential symmetry.*
2. *There is a relative trajectory (i.e. it may be always selected).*

Here several optical magnetic and electrostatic systems are described: a dipole magnet, multi-pole lenses (up to the octupole), a solenoid, the axis-symmetrical electrostatic field

(for example, duoplasmotron), the toroidal focusing lens problem will be also touched upon.

Note, that only the dipole magnet obtains a relative trajectory specified as an arc with the definite curvature, as for all the listed elements, the relative trajectory is accepted as the central particle trajectory, that is easy to define equalising the initial conditions to zero with the known momentum.

Further assumption consists of negligible parameter deviations from the relative trajectory. Then the decomposition on the initial parameters accepts the following, so called TRANSPORT type (according to the name of a well-known program) [1]:

$$X_i(z) = \sum_{j=1}^{6} R_{ij}(z) X_j^0 + \sum_{j=1}^{6} \sum_{k=j}^{6} T_{ik}(z) X_j^0 X_k^0 + \sum_{j=1}^{6} \sum_{k=j}^{6} \sum_{l=k}^{6} U_{ijkl}(z) X_j^0 X_k^0 X_l^0. \tag{2}$$

This expression determines the transfer map from the initial vector $\boldsymbol{X^0}$ to the solution vector $\boldsymbol{X}$ and is fundamental for the matrix formalism evaluation. We shall define matrix **R** as the first order transfer matrix, and matrices **T** and **U** - as the second and the third orders, respectively.

Further we shall carry out the following:

1. *Decomposition of the field near the relative trajectory using Maxwell equations and scalar potential symmetry.*
2. *Then decomposition of the plane trajectory equation up to the necessary order.*
3. *Replacement of the field decomposition into the obtained equation.*
4. *Equalising the similar members coefficients, differential equations for aberration coefficients will be obtained.*
5. *Then linearly independent solutions of these obtained equations, Green's function, will be found. After this the Green's function will be integrated "order-by-order" with the right hand parts of the obtained equations.*

This procedure does not comprise sophisticated things, but requires only attention and time.

Let us take the linear equation. The magnetic field decomposition is known up to the third order in terms of «multi-pole» force:

$$B_y(x,0,s) = B_y(s)\left[1 - k_1 h x + k_2 h^2 x^2 + k_3 h^3 x^3 + \ldots\right], \tag{3}$$

where

$$k_n(s) = \frac{1}{h^n B_y(0,0,s)} B_y^{(n)}(x,0,s)$$

$$h = h(s) - \textit{the relative trajectory curvature}. \tag{4}$$

In the general case the linear equation of the plane trajectory in a curvilinear coordinate system is well known:

$$\begin{cases} x'' - (1 - k_1)h^2 x = h\delta, \\ y'' + h^2 k_1 y = 0. \end{cases} \tag{5}$$

The initial conditions are the following:

$$\begin{cases} x(0) = x_0,\ x'(0) = x_0', \\ y(0) = y_0,\ y'(0) = y_0'. \end{cases}$$

In the rotation plane let us determine two linearly independent solutions of the homogeneous equation for each coordinate and the partial solution of the inhomogeneous equation in the X-plane as follows:

The sin-like function $s_x(s)$: $s_x(0) = 0$, $s'_x(0) = 1$, $\delta = 0$.
The cosin-like function $c_x(s)$: $c_x(0) = 1$, $c'_x(0) = 1$, $\delta = 0$.
The dispersion function $d_x(s)$: $d_x(0) = 0$, $d'_x(0) = 0$, $\delta = 1$.
The sin-like function $s_y(s)$: $s_y(0) = 0$, $s'_y(0) = 1$, $\delta = 0$.
The cosin-like function $c_y(s)$: $c_y(0) = 1$, $c'_y(0) = 1$, $\delta = 0$.

These functions determine the so-called characteristic rays of an arbitrary magnetic system and all its aberration coefficients.

The general solutions of equation (5) in respect of the initial conditions, are the following

$$\begin{cases} x(s) = c_x(s) \cdot x_0 + s_x(s) \cdot x'_0 + d_x(s) \cdot \delta, \\ y(s) = c_y(s) \cdot y_0 + s_y(s) \cdot y'_0, \end{cases} \tag{6}$$

defining the next elements of matrix R: R_{11}, R_{12}, R_{16}, R_{33}, R_{34}.

From the general shape of the obtained solutions it follows that the Green's function

$$G(s, \xi) = s(s)c(\xi) - c(s)s(\xi), (s \geq \xi), \tag{7}$$

while the partial solution of the inhomogeneous equation of the following type:

$$g'' + k^2 g = f \tag{8}$$

is to be searched for via integral:

$$g(s) = \int_0^s G(s, \xi) f(\xi) d\xi. \tag{9}$$

The dispersion function $d_x(s)$ is:

$$d_x(s) = s_x(s) \cdot \int_0^s c_x(\xi) h(\xi) d\xi - c_x(s) \cdot \int_0^s s_x(\xi) h(\xi) d\xi. \tag{10}$$

One of the 6-vector elements l is equal by definition:

$$l = x_0 \cdot \int_0^s c_x(\xi) h(\xi) d\xi + x'_0 \cdot \int_0^s s_x(\xi) h(\xi) d\xi + \delta \cdot \int_0^s d_x(\xi) h(\xi) d\xi. \tag{11}$$

Then we can obtain the first order aberration coefficients of matrix R: R_{51}, R_{52}, R_{56}.

All aberration coefficients of matrices $T_{ijk}(s)$, $U_{ijkl}(s)$ are solutions of the inhomogeneous differential equations of type (8) with the initial conditions

$$g(0) = g'(0) = 0. \tag{12}$$

Substituting the decomposition (2) into the obtained equations, we shall obtain the following second order differential equations with non-zero right-hand parts:

$$X_i'' + k_i^2 X_i = \sum_j D_{ij}(s) X_j + \sum_j \sum_k E_{ijk}(s) X_j X_k + \sum_j \sum_k \sum_l F_{ijkl}(s) X_j X_k X_l, \tag{13}$$

where values X_i are components of the 6-vector $\boldsymbol{X}(z)$.

Thus, *driving forces* (i.e. the equation right-hand parts) to find the second order T_{ijk} elements are square forms from the first order aberration coefficients:

$$f_{ijk}^T(\xi) = \sum_m \sum_n E_{imn} R_{mj}(\xi) R_{nk}(\xi).$$

Driving forces for the third order U_{ijkl} elements have a more sophisticated appearance:

$$f_{ijkl}^U = \sum_m \sum_n E_{imn} R_{mj} T_{nkl} + \sum_m \sum_n E_{imn} T_{mjk} R_{nl} + \sum_m \sum_n \sum_p F_{imnp} R_{nj} R_{mk} R_{pl}. \tag{14}$$

The further calculations of aberration coefficients are associated with the integral type (9).

Note: the «angular» matrix elements *(i=2, 4)* are reevaluated by differentiation on *s* from the «position» matrix elements *(i=1, 3)* (the direct differetiation condition).

$$\begin{cases} R_{2j} = R_{1j}', R_{4j} = R_{3j}', \\ T_{2jk} = T_{1jk}', T_{4jk} = T_{3jk}', \\ U_{2jkl} = U_{1jkl}', U_{4jkl} = U_{3jkl}'. \end{cases} \tag{15}$$

Therefore, the obtained differential equations, their solutions and Green functions fully solve the problem how to find the aberration coefficients up to the third order. Further the integration results are described.

Dipole magnet

$$k_1 = k_2 = k_3 = 0.$$
$$h(s) = \rho_0^{-1} = const,$$
$$s_x = \rho_0 \cdot \sin(s/\rho_0), s_y = y,$$
$$c_x = \cos(s/\rho_0), c_y = 1.$$

The Green functions

$$\begin{cases} G_x(s, \xi) = \rho_0 \cdot \sin((s-\xi)/\rho_0), \\ G_y(s, \xi) = s - \xi, (s \geq \xi). \end{cases}$$

The dispersion function

$$d_x(s) = \rho_0(1 - c_x(s)).$$

So, the non-zero elements of matrix **R** (13 elements):

$$R_{11} = c_x, R_{12} = s_x, R_{16} = \rho_0(1 - c_x), R_{33} = 1, R_{34} = s, R_{44} = 1, R_{66} = 1,$$
$$R_{21} = -s_x/\rho_0^2, R_{22} = c_x, R_{26} = s_x/\rho_0, R_{51} = s_x/\rho_0, R_{52} = \rho_0(1 - c_x), R_{55} = s - s_x,$$

The nineteen non-zero elements of matrix **T** (10 are shown):

$$T_{111} = -(1 - c_x^2)/2\rho_0, T_{112} = s_x c_x/\rho_0, T_{116} = s_x^2, T_{66} = -s_x^2/2\rho_0,$$
$$T_{314} = (s \cdot s_x)/\rho_0, T_{324} = \rho_0 s \cdot (1 - c_x), T_{346} = s - s_x,$$
$$T_{122} = \rho_0 s_x \cdot (1 - c_x), T_{126} = s_x \cdot (1 - c_x), T_{144} = -\rho_0 \cdot (1 - c_x),$$

Thirty seven non-zero elements of matrix **U** (9 are shown):

$$U_{1111} = c_x^3 h^4 / 8 - c_x h^4 / 8 + c_x^5 h^2 / 8 - c_x^3 h^2 / 4 + c_x h^2 / 8,$$
$$U_{1112} = c_x^2 h^4 s_x / 8 + c_x^4 h^2 s_x / 8 - c_x^2 h^2 s_x / 8,$$
$$U_{1116} = ss_x h^3 / 2 - ss_x h / 2 - 11 c_x s_x^4 h^5 / 8 - s_x^4 h^5 / 2 + c_x^5 s_x^4 / 2 + c_x s_x^4 h^3 + 5 c_x s_x^2 h^5 / 8 -$$
$$-c_x^3 s_x^2 h^3 / 2 + s_x^2 h^3 + c_x^3 s_x^2 h / 2 + c_x^5 h / 4 + c_x^4 h / 2 - c_x^2 h / 2 - c_x h / 4,$$
$$U_{1122} = -ss_x h^2 / 4 - 3c_x^2 s_x h^2 / 8 - 3c_x^4 s_x / 8 - c_x^3 s_x / 8 - c_x s_x + 3s_x / 2 - c_x^3 h^2 / 8 +$$
$$+c_x h^2 / 8 - c_x^5 / 8 + c_x^3 / 3 + c_x^2 - 11 c_x / 8,$$
$$U_{1126} = -sc_x h / 2 + sc_x / 2h + c_x^4 s_x h^3 / 4 + c_x^4 s_x h / 4 - c_x^4 s_x / 4h - c_x^2 s_x / 4h,$$
$$U_{1144} = -s^2 s_x h^2 / 4 + ss_x h^2 / 2 + sc_x / 4 - s_x / 4 + c_x^2 / 2 - 1 / 2,$$
$$U_{1166} = -ss_x h^2 / 2 + ss_x / 2 + c_x s_x^4 h^4 + s_x^4 h^4 - c_x s_x^4 h^2 - c_x s_x^2 h^4 / 2 +$$
$$+c_x^3 s_x^2 h^2 / 2 + c_x s_x^2 h^2 / 2 - 2s_x^2 h - c_x^3 s_x^2 / 2 - c_x^4 + c_x^2,$$
$$U_{1222} = sc_x / 4 + c_x^2 s_x h^2 / 4 + c_x^4 s_x / 4 - s_x / 2 - 3c_x^5 / 8h^2 + 5c_x^3 / 4h^2 - c_x^2 / h^2 +$$
$$+c_x / 8h^2 - 3c_x^3 / 8 + 3c_x / 8,$$
$$U_{1226} = ss_x h / 4 + 3c_x^2 s_x h / 8 + 3c_x^4 s_x / 8h + c_x^2 s_x / 8h - c_x s_x / h + s_x / 2h + c_x^3 h / 8 -$$
$$-c_x h / 8 + c_x^5 / 8h - c_x^3 / 2h - c_x^2 / 2h + 7c_x / 8h,$$

Here the direct differentiation condition is executed.

Quadrupole

$$h(s) = k_2 = k_3 = 0.$$
$$k_1 = k = const,$$
$$s_x = 1/k \cdot \sin ks, s_y = 1/k \cdot sh\, ks,$$
$$c_x = \cos ks, c_y = ch\, ks.$$

The Green functions

$$\begin{cases} G_x(s,\xi) = 1/k \cdot \sin k(s-\xi), \\ G_y(s,\xi) = 1/k \cdot sh\, k(s-\xi), (s \geq \xi). \end{cases}$$

The dispersion function

$$d_x(s) = 0.$$

Thus, the non-zero elements (10 elements are shown) of matrix **R**:

$$R_{11} = c_x, R_{12} = s_x, R_{33} = c_y, R_{34} = s_y, R_{34} = k^2 s_y, R_{44} = c_y, R_{66} = 1. R_{55} = 1,$$
$$R_{21} = -k^2 s_x, R_{22} = c_x,$$

The four non-zero matrix T elements are chromatic (contributing on δ):

$$T_{116} = k^2 s s_x / 2,$$
$$T_{126} = (s_x - s c_x) / 2,$$
$$T_{336} = -k^2 s s_y / 2,$$
$$T_{346} = (s_y - s c_y) / 2.$$

The forty non-zero elements (4 are shown) of matrix **U:**

$$_{1111} = (3k^6 s_x s_x (4s) + 24k^6 c_x s_x^4 - 12k^6 s s_x) / 64,$$
$$_{2222} = -(3k^2 c_x s_x (4s) + (24 - 24c_x^4) s_x - 12k^2 s c_x) / 64,$$
$$_{3333} = (3k^6 s_y s_y (4s) + 24k^6 c_y s_y^4 - 12k^6 s s_y) / 64,$$
$$_{3444} = -(3k^2 c_y s_y (4s) - (24 + 24c_x^2) k^2 s_y^3 - 12k^2 s c_y) / 64.$$

Here the direct differentiation condition is executed.

Sextupole

$$h(s) = k_1 = k_3 = 0.$$
$$k_2 = k = const,$$
$$s_x = s_y = s,$$
$$c_x = c_y = 1.$$

The Green functions

$$G_x(s,\xi) = G_y(s,\xi) = s - \xi, (s \geq \xi).$$

The dispersion function

$$d_x(s) = 0.$$

The non-zero matrix **R** elements are equivalent to the drift space transfer matrix elements.

The ten non-zero matrix elements of matrix **T**:

$$T_{111} = -T_{133} = -2T_{313} = -k^2 s^2 / 2. T_{112} = -T_{134} = -T_{314} = -T_{324} = -k^3 s^3 / 3,$$
$$T_{122} = -T_{144} = -2T_{324} = k^2 s^4 / 12.$$

The sixty non-zero matrix elements of matrix **U** (11 are shown):

$$U_{1111} = U_{1133} = U_{3113} = U_{3333} = 21U_{1222} = k^4 s^4 / 12,$$
$$U_{1112} = \tfrac{6}{5}U_{1134} = -\tfrac{1}{5}U_{1233} = \tfrac{6}{5}U_{3123} = -\tfrac{1}{5}U_{3114} = U_{3334} = k^4 s^5 / 12.$$

Here the direct differentiation condition is executed.

Octupole

$$h(s) = k_1 = k_2 = 0.$$
$$k_3 = k = const,$$
$$s_x = s_y = s,$$
$$c_x = c_y = 1.$$

The Green functions

$$G_x(s,\xi) = G_y(s,\xi) = s - \xi, (s \geq \xi).$$

The dispersion function

$$d_x(s) = 0.$$

The non-zero matrix **R** elements are equivalent to the drift space transfer matrix elements.

Since the octupole field components don't have square members, all matrix **T** elements are equal to zero.

The forty non-zero matrix elements of matrix **U** (10 are shown):

$$U_{1111} = 3U_{1133} = 3U_{3113} = U_{3333} = -k^2 s^2 / 2,$$
$$U_{1112} = -2U_{1134} = -U_{1233} = -2U_{3123} = -U_{3114} = U_{3334} = -k^2 s^3 / 2.$$

Here the direct differentiation condition is executed.

Solenoid

A similar consideration is important for any axial symmetry systems. In this case we shall find 4-vector $X=(r, r', l, \delta)$ with the same definitions, but in a cylindrical coordinate system. Using the same assumptions and procedures, taking into account the condition of angular momentum conservation, the following nonlinear equation of a plane trajectory $r(z)$ up to the third order in the magnetic solenoid field is obtained

$$r'' = -k^2 r\left[1 - 2\delta - \frac{B''}{2B}r^2 + r'^2 + k^2 r^2 - \frac{B'}{B}rr' + 3\delta^2\right], \tag{16}$$

where $k=qB/2p_0$. Often the field $B(z)$ near the solenoid axis is represented as «bell-like». The linear optics of this element is clear enough:

$$s(z) = \tfrac{1}{k}\sin kz,$$
$$c(z) = \cos kz.$$

The Green function

$$G(s,\xi) = \tfrac{1}{k}\sin k(z - \xi), (s \geq \xi).$$

The six non-zero elements of the R matrix:

$$R_{11} = c, R_{12} = s, R_{21} = -k^2 s, R_{22} = c, R_{33} = 1, R_{44} = 1.$$

As in the quadrupole case, the six non-zero matrix T elements are chromatic (contributing on δ):

$$T_{114} = T_{224} = kzs, T_{124} = \tfrac{s}{k} - zc, T_{214} = ks + k^2 zc,$$
$$T_{311} = k^2 z / 2, T_{322} = z / 2.$$

The fifteen non-zero elements of matrix **U** (6 are shown):

$$U_{1111} = \tfrac{1}{8}\left(\tfrac{3B''}{2B} - 4k^2\right)kzc + k\tfrac{B'}{8B}kzc - k\tfrac{B'}{4B}s + \tfrac{B''}{32B}cs + k\tfrac{B'}{16B}ss(2kz),$$
$$U_{1211} = -\tfrac{1}{8k}\left(\tfrac{3B''}{2B} - k^2\right)kzc + \tfrac{1}{2k}\left(\tfrac{3B''}{8B} - k^2\right)s + \tfrac{B'}{8B}\left(kzs + \tfrac{3}{2}ss(2kz)\right) + \tfrac{3B''}{16kB}s^3,$$
$$U_{1122} = \tfrac{1}{8k^2}\left(\tfrac{3B''}{2B} - 4k^2\right)kzs - \tfrac{3B''}{32k^2B}ss(2kz) + \tfrac{B'}{8kB}kzc - \tfrac{B'}{8kB}s + \tfrac{3B'}{8kB}s^3,$$
$$U_{1144} = -\tfrac{1}{2}kzs - \tfrac{1}{2}k^2z^2c - \tfrac{1}{4}kzcs(2kz),$$
$$U_{1222} = \tfrac{1}{2k^3}\left(\tfrac{3B''}{8B} - k^2\right)(kzc - s) + \tfrac{B'}{8k^2B}kzs + \tfrac{B''}{16k^3B}s^3 - \tfrac{B'}{16k^2B}ss(2kz),$$
$$U_{1244} = -\tfrac{1}{2}zs.$$

Here the direct differentiation condition is executed.

It is useful to introduce the following formula for further computation:

$$\begin{pmatrix} r \\ r' \end{pmatrix} = \left[R + T_4 \cdot \delta + U_{22} \cdot r_0'^2 + U_{44} \cdot \delta^2\right] \cdot \begin{pmatrix} r_0 \\ r_0' \end{pmatrix}, where$$

$$R = \begin{pmatrix} R_{11} & R_{12} \\ R_{21} & R_{22} \end{pmatrix}, T_4 = \begin{pmatrix} T_{114} & T_{124} \\ T_{214} & T_{224} \end{pmatrix}, U_{11} = \begin{pmatrix} U_{1111} & U_{1211} \\ U_{2111} & U_{2211} \end{pmatrix}, U_{22} = \begin{pmatrix} U_{1122} & U_{1222} \\ U_{2122} & U_{2222} \end{pmatrix}, U_{44} = \begin{pmatrix} U_{1144} & U_{1244} \\ U_{2144} & U_{2244} \end{pmatrix}.$$

With a relation of a selected solenoid field model it is possible to build either the comprehensive resultant transfer map, or having chosen a small partitioning of the field action region, - to compute all transfer matrix elements within the chosen partitioning intervals, then to multiply the matrices in accurate correspondence using the matrix algebra rules.

Electrostatic lens

The beam optics in electrostatic fields is considered by the same method. The particularity of this problem consists of non conservativity of the electrostatic system, unlike all the others considered earlier. All assumptions are perfect here, but it is necessary to use the energy conservation law.

Abstracting the particle types after all the described steps in the cylindrical coordinate system, the following nonlinear plane trajectory equation $r(z)$ is obtained:

$$2sign(q) \cdot \Phi r'' - \Phi' r' - \frac{\Phi''}{2} r = \left(\frac{\Phi''^2}{8\Phi} - \frac{\Phi''''}{16}\right) r^3 + \left(\frac{\Phi'\Phi''}{4\Phi} + \frac{\Phi'''}{4}\right) r^2 r' + \frac{\Phi''}{2} r r'^2 + \Phi' r'^3. \quad (17)$$

The equation (17) does not depend explicitly on the q/m ratio. Thus, all particles with the same sign in the same field will have the same trajectories, but the particle velocity of passage through the transfer region will be differential. Due to this we shall restrict only an electron motion description by equalising $sign(q)=-1$.

Further solution of the motion equation is associated with the choice of the field model. We shall introduce the value

$$n = \sqrt{\frac{\Phi_1}{\Phi_0}}, \tag{18}$$

called the electron-optical index of refraction that is appropriate to Snellius' law, Φ_0 and Φ_1 are initial and final potential values in the interval from 0 up to D (D is the length of the acting field region). There is an important condition about n: the electron-optical index is equal to zero when the particle velocity is equal to zero only.

Now we shall consider the linear potential

$$\Phi(z) = \Phi_0(1 + \frac{z}{z_0}) = \Phi_0\bar{z},$$

where $z_0=D/(n^2-1)$.

The characteristic rays of the differential equation for the plane trajectory

$$2\bar{z}r'' + r' = 0,$$

with sufficient initial conditions

$$\begin{cases} r(1) = r_0, \\ r'(1) = z_0 \cdot r_0'. \end{cases}$$

are determined in the following way

$$\begin{cases} s(\bar{z}) = 2 \cdot \left[\sqrt{\bar{z}} - 1\right], \\ c(\bar{z}) = 1. \end{cases}$$

and the Green function

$$G(\bar{z}) = 2\sqrt{\bar{z}} - 1.$$

The known motion equation solution

$$\begin{cases} r(z) = r_0 + 2z_0r_0'\left[\sqrt{1 + z/z_0} - 1\right] \\ r'(z) = \dfrac{r_0'}{\sqrt{1 + z/z_0}}. \end{cases},$$

gives us five non-zero components of the linear transfer matrix **R**: R_{11}, R_{21}, R_{22}, R_{33} and R_{44}. The transfer matrix determinant is equal to $1/n$, that directly follows from Liouville's theorem of the phase volume conservation.

The non-zero components of the matrix T:

$$T_{322}(z) = \frac{z_0}{2} \cdot \ln(1 + z/z_0),$$
$$T_{422}(z) = \frac{1}{2(1+z/z_0)}.$$

The aberration coefficients of matrix U are obtained as an accurate analytical solution of the motion equation:

$$U_{1222}(z) = -z_0 \frac{(\sqrt{1 + z/z_0} - 1)^{3/2}}{\sqrt{1 + z/z_0}},$$
$$U_{2222}(z) = -\frac{z/z_0}{2(1 + z/z_0)^{3/2}}.$$

Here the direct differentiation condition is executed.

It is useful to introduce the following formula for further computation:

$$\begin{pmatrix} r \\ r' \end{pmatrix} = \left[R + U_{22} \cdot r_0'^2\right] \cdot \begin{pmatrix} r_0 \\ r_0' \end{pmatrix}, \text{where}$$

$$R = \begin{pmatrix} R_{11} & R_{12} \\ R_{21} & R_{22} \end{pmatrix}, U_{22} = \begin{pmatrix} 0 & U_{1222} \\ 0 & U_{2222} \end{pmatrix}.$$

This consideration allowed us to perform the series of important assumptions relatively initial parameters of the formed beam.

The relation between the plasma temperature, the electrode system geometrical sizes and electron-optical index brings up all coordinates of the phase ellipse basic points, the beam emittance initial value and others. A more sophisticated solution is obtained in consideration of the square potential of the following type

$$\Phi(z) = \Phi_0\left(1 \pm \bar{z}^2\right), \quad \text{where}$$

$$\bar{z} = z/z_0, z_0 = D/\sqrt{|n^2 - 1|}, (n \neq 1).$$

The sign $(\pm)$ corresponds to electron acceleration (+) and deceleration (-).

It is not so difficult to obtain the following differential equations for the plane trajectories

$$\eta'' \pm \frac{1}{2}\eta = 0,$$

if we perform substitutions:

$$\begin{cases} r(\bar{z}) = \eta(\xi), \\ \bar{z} = sh(\xi), (+) \\ \bar{z} = \sin(\xi), (-). \end{cases}$$

The linearly independent solutions of *the acceleration equation* are as follows:

$$\begin{cases} s(\bar{z}) = z_0 \sin(\frac{1}{\sqrt{2}} Arsh\ \bar{z}), \\ c(\bar{z}) = \cos(\frac{1}{\sqrt{2}} Arsh\ \bar{z}). \end{cases}$$

In this case the Green function is equal to:

$$G^{+}(\bar{z}, \tau) = z_0 \sin(\tfrac{1}{\sqrt{2}}(Arsh\ \bar{z} - Arsh\ \tau)).$$

Therefore, the obtained first order matrix elements R_{ij} are determined (6 ones).

The determinant of the first order transfer matrix R is equal to $1/\sqrt{2}n$.
The six non-zero (chromatic) elements of the matrix T are considered:

$$T^{+}_{411}(\bar{z}) = \frac{\sin^2 \zeta}{4z_0^2(1+\bar{z}^2)},$$

$$T^{+}_{412}(\bar{z}) = -\frac{\sin\zeta\cos\zeta}{2z_0(1+\bar{z}^2)},$$

$$T^{+}_{422}(\bar{z}) = \frac{\cos^2\zeta}{4(1+\bar{z}^2)}, \text{где } \zeta = \tfrac{1}{\sqrt{2}} Arsh\ \bar{z}.$$

The eight non-zero elements (2 are shown) of the matrix U:

$$U^{+}_{1111} = -\frac{\Phi_0}{2z_0^2}\left(\sin\zeta\ arctg\ \bar{z} - I_1 \sin\zeta + I_3 \cos\zeta\right),$$

$$U^{+}_{1112} = -\frac{\Phi_0}{2z_0}\left(\sqrt{2}\sin\zeta - I_1\cos\zeta - I_3\sin\zeta\right)$$

Here the direct differentiation condition is executed.
The similar calculations may be performed for particle deceleration in the electrostatic field.

It is useful to introduce the following formula for further computation:

$$\begin{pmatrix} r \\ r' \end{pmatrix} = \left[R^{\pm} + U^{\pm}_{22} \cdot \left(r_0^2 \pm r_0'^2 z_0^2\right)\right] \cdot \begin{pmatrix} r_0 \\ r_0' \end{pmatrix}, \text{where}$$

$$R^{\pm} = \begin{pmatrix} R^{\pm}_{11} & R^{\pm}_{12} \\ R^{\pm}_{21} & R^{\pm}_{22} \end{pmatrix}, U^{\pm}_{11} = \begin{pmatrix} U^{\pm}_{1111} & U^{\pm}_{1211} \\ U^{\pm}_{2111} & U^{\pm}_{2211} \end{pmatrix}.$$

Conclusion

Thus, we consider that the nonlinear third order beam optics is built in general for a wide list of different elements of the beam transport channels. Currently a self-coordinate space charge analysis is performed to integrate it into the considered model. The construction of the third order beam optics is near completion for toroidal focusing magnetic lens, too. All of the offered procedures are validated by real systems, full conformity correspondence with the results of numerical computation is presented.
The simplicity and completeness of the obtained results allow us to perform a qualitatively comprehensive aberration analysis and obtain important parameters of projected mountings and beams.

References

1. Brown K. L. et al. TRANSPORT. A Computer Program for Designed Charged Particle Beam Transport Systems. SLAC-91, Rev. 2 UC-28 (I/A). May 1977.

ADVANCED EQUATIONS FOR INVESTIGATION OF BEAM ENVELOPE AND EMITTANCE GROWTH

Yu. Zuev
D.V.Efremov Scientific Research Institute, St.Petersburg

Emittance growth is an important subject for accelerator dynamics and beam optics design. Until recently experimental data and computer tracing were the only tools for emittance growth estimation. Any estimations on the base of conventional coefficients of spherical aberration neglect space charge redistribution and associated field change [1-3]. Much used now the idea of relating emittance growth to the expected redistribution of the space charge [4-7] and to beam field energy released in this process allows an asymptotic estimation only [8]. The actual emittance growth is determined by details of the transition process. The simplest model for the transition process is described below.

In the general case a beam of charged particles is characterized by particle density in the phase space or by distribution function $f_6(\vec{r},\vec{v},t)$. Transfer of mass is handled with the local charge density $\rho(\vec{r},t) = qn(\vec{r},t)$ and local average velocity $\vec{V}$ referred also to mass-flow or directed one and defined as follows

$$\vec{V}(\vec{r},t) = \frac{1}{n(\vec{r},t)}\int_{-\infty}^{+\infty}\vec{v}\,f_6(\vec{r},\vec{v},t)d\vec{v}, \qquad n(\vec{r},t) = \int_{-\infty}^{+\infty} f_6(\vec{r},\vec{v},t)d\vec{v}.$$

A single particle velocity at the point $\vec{r}$ is assumed to be a random value with the expectation $\vec{V}$ and specified by the matrix of the second moments or covariance matrix $\left\langle(\vec{v}-\vec{V})(\vec{v}-\vec{V})^{T}\right\rangle$. Diagonal terms of the matrix are dispersions. Their sum in the case of equilibrium or Maxwellian distribution is related to temperature as follows:

$$\left\langle\frac{(v_X-V_X)^2}{2}\right\rangle+\left\langle\frac{(v_Y-V_Y)^2}{2}\right\rangle+\left\langle\frac{(v_Z-V_Z)^2}{2}\right\rangle=\frac{3}{2}\frac{k_BT}{m}.$$

For this reason the second order matrix is often referred as the temperature tensor

$$\hat{T}_{ps} = \begin{bmatrix} T_{XX} & T_{XY} & T_{XZ} \\ T_{YX} & T_{YY} & T_{YZ} \\ T_{ZX} & T_{ZY} & T_{ZZ} \end{bmatrix},$$

$$T_{ps} = \left\langle(v_p - V_p)(v_s - V_s)\right\rangle = \int_{-\infty}^{+\infty}\frac{(v_p - V_p)(v_s - V_s)\,f_6(\vec{r},\vec{v},t)}{n(\vec{r},t)}d\vec{v},$$

so the matrix trace is used as a measure of the particle heat motion in non-equilibrium configurations too:

$$\frac{k_BT_{eff}}{m} = \frac{\mathrm{Tr}\left[\hat{T}_{ps}\right]}{3} = \frac{T_{XX}+T_{YY}+T_{ZZ}}{3}.$$

Obviously, temperature tensor is involved to the pressure tensor, $\hat{P}(\vec{r},t) = mn(\vec{r},t)\hat{T}_{ps}(\vec{r},t)$, usually resolved into the sum of viscosity stress tensor

and diagonal one. Relationships between mass-flow velocity, charge density and temperature are known as the equations for transfer of mass, momentum and heat, and derived integrating the Boltzmann equation over the velocity space [9]. Single elements of temperature tensor can be found from the equations involving the third moments, which in turn include the fourth moments, and so on indefinitely.

Further charge particle flow is considered neglecting the third moments of the distribution function and non-diagonal terms of temperature tensor. Physical sense of the limitation will discuss later on. Furthermore the flow is assumed to consist of charge particles of an ideal gas, which interact to one another through common smoothed out electric field only (any pair collisions are absent). In this case the equation for internal energy is an equivalent of the entropy conservation law. For these assumptions the set of transport equations for axisymmetric beam with no magnetic field follows [10]:

$$\frac{d\rho}{dt} + \rho \,\mathrm{div}\vec{V} = 0, \tag{1}$$

$$\frac{dV_R}{dt} = \frac{F_R}{m} - \frac{1}{\rho}\frac{\partial(\rho T_{RR})}{\partial r} + \frac{T_{\theta\theta}}{r} - \frac{T_{RR}}{r}, \qquad \frac{dV_Z}{dt} = \frac{F_Z}{m} - \frac{1}{\rho}\frac{\partial(\rho T_{ZZ})}{\partial z}, \tag{2)-(3)}$$

$$\frac{dT_{RR}}{dt} = -2T_{RR}\frac{\partial V_R}{\partial r}, \quad \frac{dT_{\theta\theta}}{dt} = -2T_{\theta\theta}\frac{V_R}{r}, \quad \frac{dT_{ZZ}}{dt} = -2T_{ZZ}\frac{\partial V_Z}{\partial z}, \tag{4)-(6)}$$

where $T_{\theta\theta}$ is the rms spread in azimuthal velocity, $v_\theta = r\frac{d\theta}{dt}$; $F_Z = q\frac{\partial\Phi}{\partial z}$, $F_R = q\frac{\partial\Phi}{\partial r}$ are the forces from self-consistent electric field with the potential satisfying Poisson's equation

$$\frac{1}{r}\frac{\partial}{\partial r}\left(r\frac{\partial\Phi}{\partial r}\right) + \frac{\partial^2\Phi}{\partial z^2} = \frac{\rho}{\varepsilon_0}. \tag{7}$$

Substantial derivation along lines of flow in the case of axisymmetric stationary configuration is $d/dt = V_R\,\partial/\partial r + V_Z\,\partial/\partial z$. The flow lines are governed by the equation

$$\frac{V_R}{dr} = \frac{V_Z}{dz} \quad \text{or} \quad r' = \frac{dr}{dz} = \frac{V_R}{V_Z} \tag{8}$$

(tangent to the flow line specifies direction of the average speed vector $\vec{V}$ at the point of tangency, Fig.1). Notice that the line of flow here is no trace of a single particle due to heat motion in the beam.

By replacing independent variable, Eqs. (1),(4)-(6) can be rewritten in the form

$$\frac{d\rho}{\rho} + \frac{dr}{r} + \frac{dV_Z}{V_z} = \frac{1}{2}\frac{dT_{RR}}{T_{RR}}; \tag{9}$$

$$\frac{dT_{\theta\theta}}{T_{\theta\theta}} = -2\frac{dr}{r}; \quad \frac{dT_{ZZ}}{T_{ZZ}} = -2\frac{dV_Z}{V_Z}; \quad \frac{dT_{RR}}{T_{RR}} = -2\frac{dV_R}{V_R}, \tag{10)-(12}$$

and give along the flow lines the integrals of motion:

$$T_{\theta\theta}r^2 = const. \quad T_{ZZ}V_{ZZ}^2 = const. \quad T_{RR}V_{RR}^2 = const. \tag{13)-(15}$$

$$\rho = \frac{const.}{rV_RV_Z}, \quad \frac{\rho}{\sqrt{T_{\theta\theta}T_{RR}T_{ZZ}}} = const. \text{ or } \frac{\rho V_Z}{\sqrt{T_{\theta\theta}T_{RR}}} = const. \tag{16)-(17}$$

To solve Eqs. (1)-(7) in the general case one can use the method of series. Assuming that

$$V_R(r,z)=\sum_{n=0}^{\infty}\upsilon(z)_{2n+1}r^{2n+1},\quad V_Z(r,z)=\sum_{n=0}^{\infty}u(z)_{2n}r^{2n},$$
$$F_R(r,z)=\sum_{n=0}^{\infty}F_R(z)_{2n+1}r^{2n+1},\quad F_Z(r,z)=\sum_{n=0}^{\infty}F_Z(z)_{2n}r^{2n},\qquad(18)$$
$$\Phi(r,z)=\sum_{n=0}^{\infty}\Phi(z)_{2n}r^{2n},\quad \rho(r,z)=\sum_{n=0}^{\infty}\rho(z)_{2n}r^{2n},$$
$$T_{RR}(r,z)=\sum_{n=0}^{\infty}a(z)_{2n}r^{2n},\quad T_{\theta\theta}(r,z)=\sum_{n=0}^{\infty}b(z)_{2n}r^{2n},\quad T_{ZZ}(r,z)=\sum_{n=0}^{\infty}c(z)_{2n}r^{2n},$$
$$a_0=T_{RR}(0,z)=b_0=T_{\theta\theta}(0,z)=T_{\perp}(0,z),$$

substituting the series (18) into the original equations and equating terms of the same power r, one can obtain an infinite set of the equations with respect to the expansion factors. The truncated set of the equations:

$$\rho_0'=-\frac{\rho_0}{u_0}(2\upsilon_1+u_0'),\qquad \upsilon_1'=\frac{1}{u_0}\left(\frac{F_{R_1}}{m}+b_2-3a_2-\upsilon_1^2-\frac{2a_0\rho_2}{\rho_0}\right),$$
$$u_0'=\frac{1}{u_0}\left(\frac{F_{Z_0}}{m}-c_0'-c_0\frac{\rho_0'}{\rho_0}\right),\quad a_0'=-\frac{2a_0\upsilon_1}{u_0},\quad b_0'=-\frac{2b_0\upsilon_1}{u_0},\quad c_0'=-\frac{2c_0u_0'}{u_0},$$
$$\rho_2'=-\frac{1}{u_0}\left[\rho_2(4\upsilon_1+u_0')+\rho_0(4\upsilon_3+u_2')+\rho_0'u_2\right],\quad a_2'=-\frac{1}{u_0}\left[6a_0\upsilon_3+4a_2\upsilon_1+a_0'u_2\right],$$
$$\upsilon_3'=\frac{1}{u_0}\left[\frac{F_{R_3}}{m}-3\upsilon_1\upsilon_3-u_2\upsilon_1'-\frac{2a_2\rho_2}{\rho_0}+\frac{2a_0\rho_2^2}{\rho_0^2}\right],$$
$$c_2'=-\frac{1}{u_0}\left[2c_0u_2'+2c_2(\upsilon_1+u_0')+u_2c_0'\right],\qquad(19)$$
$$u_2'=\frac{1}{u_0}\left[\frac{F_{Z_2}}{m}-c_2'-c_2\frac{\rho_0'}{\rho_0}-c_0\left(\frac{\rho_2'}{\rho_0}-\frac{\rho_2}{\rho_0}\frac{\rho_0'}{\rho_0}\right)+\frac{u_2}{u_0}\frac{\rho_0'}{\rho_0}\right],$$
$$b_2'=-\frac{1}{u_0}\left[2b_0\upsilon_3+4b_2\upsilon_1+b_0'u_2\right],$$

where

$$F_{Z_0}=q\Phi_0',\ F_{Z2}=\frac{q}{2}\left(\frac{\rho_0'}{\varepsilon_0}-\Phi_0'''\right),\ F_{R1}=\frac{q}{2}\left(\frac{\rho_0}{\varepsilon_0}-\Phi_0''\right),\ F_{R3}=\frac{q}{4}\left(\frac{\rho_2}{\varepsilon_0}+\frac{1}{4}\left(\Phi_0^{IV}-\frac{\rho_0''}{\varepsilon_0}\right)\right),$$

can be numerically solved for given initial conditions and known axial potential $\Phi_0(z)$.

Adding some restrictions, the set of Eqs.(19) is possible to be reduced to the two equations, which describe the lines of flow near axis. For this purpose let rewrite the flow line equation (8) in the equivalent form

$$r''=\frac{\dfrac{dV_R}{dt}-r'\dfrac{dV_Z}{dt}}{V_Z^2}$$

and replace all the values by their expansions (18). As a result we obtain the non-linear equation

$$r''=C_1(z)r+C_2(z)r'+C_3(z)r^3+C_4(z)r^2r'+\dots .$$

Assuming small non-linearity, i.e., being limited within the paraxial approximation, let approach solution of the equation by the sum $r \approx r_0 + r_1$, where r_0 is a solution to the homogeneous equation

$$r_0'' + C_1(z)r_0 + C_2(z)r_0' = 0, \tag{20}$$

and r_1, usually named as aberration, is a solution to the perturbed one

$$r_1'' + C_1(z)r_1 + C_2(z)r_1' = C_3(z)r_0^3 + C_4(z)r_0^2 r_0'. \tag{21}$$

Let ξ be a marker or Lagrangian variable marking initial positions of flow lines on the phase plane (r, r'). If the initial positions lie on the straight line:

$$\begin{cases} r_0(0) = \xi R_0, \\ r_0'(0) = \xi R_0', \quad 0 \le \xi \le 1, \\ r_1(0) = r_1'(0) = 0 \end{cases} \tag{22}$$

(R_0, R_0' are constants), then the flow lines due to linearity of Eqs. (20)-(21) are curves of the single-parametric family:

$$\begin{cases} r(z) = \xi R(z) + \xi^3 \chi(z), \\ r'(z) = \xi R'(z) + \xi^3 \chi'(z). \end{cases} \tag{23}$$

Here $R(z)$ is a solution of Eq.(20) with the initial conditions (22) at $\xi = 1$ and $\chi(z)$ is that of Eq.(21). According to the formulae (23), Eq.(20) represents the beam with geometrically similar flow lines, whereas Eq.(21) describes distortion of initial beam structure. Among all flow lines specified by the value of ξ one can select the line most remote from the axis at the given point z to treat this line as the beam envelope R_b:

$$R_b(z) = R(z) + \chi(z), \quad \text{for } R(z) \ge -3\chi(z), \tag{24}$$

$$\begin{cases} R_b(z) = \dfrac{2}{3\sqrt{3}} \dfrac{R^{3/2}(z)}{\sqrt{(-\chi(z))}}, \quad \text{for } R(z) < -3\chi(z),\ R(z)\chi'(z) \ne R'(z)\chi(z) \\ R(z) > 0 \end{cases} \tag{25}$$

The ratio $R = -3\chi$ indicates origin of so-called fold (in terms of [11]) or agitating in the flow lines.

As beam accelerated the particle heat spread in longitudinal velocities decreases according to the integral (14) representing the Liouville theorem. In standard ion sources for accelerators, mass-flow velocity on a plasma emissive surface ranges up to several volts in energy units [12]. Considering beam after an extracting optics, when particle energy reaches units or tens keV, one can neglect the temperature of longitudinal motion, put $c_0(z) = c_2(z) = 0$ in the model and use for charge-transport velocity the relation $V_Z(z) \approx \sqrt{\dfrac{2q}{m}\Phi(r, z)}$. This relation is extensively exploited in the paraxial optics and valid for relatively slow variation in the beam envelope and axial potential [13]. Notice that the longitudinal velocity of flow lines will be the same across the beam if only the external field will compensate exactly repulsion of the space charge ρ.

To find relations between other expansion factors and beam envelope for the case with no fold, the integrals (13)-(17), expansions (18), single-parametric representation (23) are used omitting χ to the 2nd power and higher and χ adjacent to R. Charge distribution across the beam in the form

$\rho(r,z) \approx \rho_0(z) + \rho_2(z)r^2$ is easy derived from the current density

$$J_0(z) = \frac{J_0(0)R^2(0)}{R^2(z)}, \quad J_2(z) = \frac{J_2(0)R^4(0)}{R^4(z)} - \frac{4\chi(z)J_0(0)R^2(0)}{R^5(z)},$$

presuming the full current constancy

$$I \approx \pi R_b^2(z)\left[J_0(z) + J_2(z)R_b^2(z)/2\right]$$

($J_0(0)$, $J_2(0)$, $R(0)$ are constant values defined by initial beam state). Being equal at the axis, radial and azimuthal temperatures are related to R as follows:

$$a_0(z) = b_0(z) = T_\perp(0,z) = \frac{C_\perp}{R^2(z)},$$

where $C_\perp = a_0(0)R^2(0) = T_\perp(0,0)R^2(0)$ is a constant too. In considered conditions of collisionless rare plasma, beam transport in a transversely limited channel occurs with momentary losses of the particle from the tail of like-Maxwellian distribution so with forming a limited phase volume of beam particles. If radial temperature tends to zero at the beam edge, then

$$a_2(z) = \frac{1}{2}\left(\frac{\partial^2 T_{RR}}{\partial r^2}\right)_{r=0} \approx -\frac{C_\perp}{R^4(z)}\left(1 - \frac{2\chi(z)}{R(z)}\right). \tag{26}$$

The radial distribution of azimuthal temperature can be found from the integral (13) representing the angular momentum conservation:

$$b_2(z) = \frac{1}{2}\left(\frac{\partial^2 T_{\theta\theta}}{\partial r^2}\right)_{r=0} = -\frac{C_\perp}{R^4(z)}\left(1 + \frac{2\chi(z)}{R(z)}\right). \tag{27}$$

Different effect of aberration χ is required to point comparing the formulae (26) and (27). Only vanished χ gives the same radial and azimuthal temperatures.

Based on the established relations Eqs.(20-21) for the envelope first approximation and aberration can be rewritten in the form:

$$\begin{cases} R'' = -\dfrac{\Phi_0' R'}{2\Phi_0} - \dfrac{\Phi_0'' R}{4\Phi_0} + \dfrac{\tilde{C}_p}{4\Phi_0^{3/2}R} + \dfrac{2\tilde{C}_\perp}{\Phi_0 R^3}\left(1 - \dfrac{\rho_2 R^2}{\rho_0} - \dfrac{4\chi}{R}\right), \\ \chi'' = \dfrac{\Theta_1}{u_0^2}\chi - \dfrac{\Theta_0}{u_0^2}\chi' + R^3\left(\dfrac{\Theta_3}{u_0^2} - \dfrac{2u_2}{u_0}\dfrac{\Theta_1}{u_0^2}\right) + R^2 R'\left(\dfrac{2u_2}{u_0}\dfrac{\Theta_0}{u_0^2} - \dfrac{\Theta_2}{u_0^2}\right), \end{cases} \tag{28)-(29}$$

$$R(0) = R_b(0), \; R'(0) = R_b'(0), \; \chi(0) = \chi'(0) = 0$$

$$\frac{\Theta_0}{u_0^2} = \frac{\Phi_0'}{2\Phi_0}, \qquad \frac{\Theta_1}{u_0^2} = \frac{R''}{R} + \frac{1}{2}\frac{\Phi_0' R'}{\Phi_0 R}, \qquad \frac{\Theta_2}{u_0^2} = -\frac{1}{8}\left(\frac{\Phi_0''}{\Phi_0} + \frac{1}{2}\frac{\Phi_0'\tilde{C}_p}{\Phi_0^{5/2}R^2} - \right),$$

$$\frac{\Theta_3}{u_0^2} = \frac{\Phi_0^{IV}}{32\Phi_0} + \frac{\tilde{C}_p}{32\Phi_0^{3/2}R^2}\left(\frac{4\rho_2}{\rho_0} - \frac{\rho_0''}{\rho_0}\right) + \frac{2\tilde{C}_\perp}{\Phi_0 R^4}\frac{\rho_2}{\rho_0}\left(1 - \frac{2\chi}{R} + \frac{\rho_2 R^2}{\rho_0}\right),$$

$$\frac{u_2}{u_0} = \frac{1}{8}\left(\frac{\tilde{C}_p}{\Phi_0^{3/2}R^2} - \frac{\Phi_0''}{\Phi_0}\right), \quad \frac{\rho_2}{\rho_0} = \frac{1}{R^2}\left(\frac{2P_2}{P_0} - \frac{4\chi}{R}\right) - \frac{u_2}{u_0}, \quad \frac{\rho_0''}{\rho_0} = \frac{3}{4}\left(\frac{\Phi_0'}{\Phi_0}\right)^2 - \frac{\Phi_0''}{2\Phi_0} - \frac{2R''}{R},$$

$$\tilde{C}_p = \frac{J_0(0)R_b^2(0)}{\varepsilon_0\sqrt{2q/m}}, \quad \tilde{C}_\perp = \frac{T_{RR}(0,0)R_b^2(0)}{2mq} = \varphi_T(0)R_b^2(0), \quad \frac{P_2}{P_0} = \frac{J_2(0)R_b^2(0)}{2J_0(0)}.$$

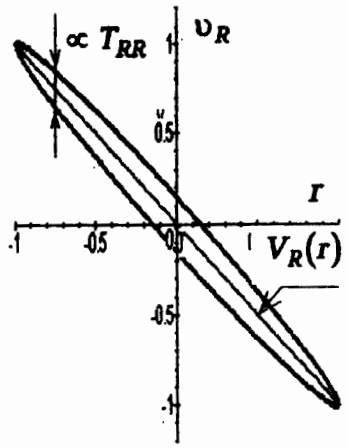

Fig.1. $E^2_{rms} = E^2_t$

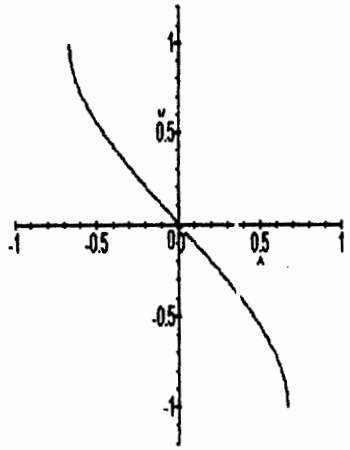

Fig.2. $E^2_{rms} = E^2_h$

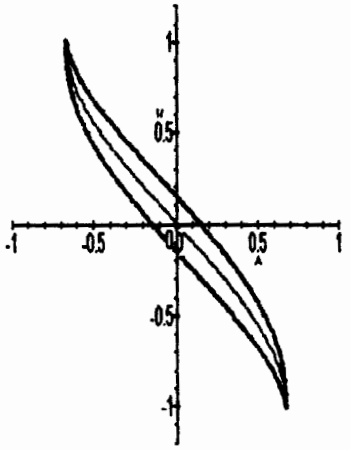

Fig.3. $E^2_{rms} = E^2_t + E^2_h$

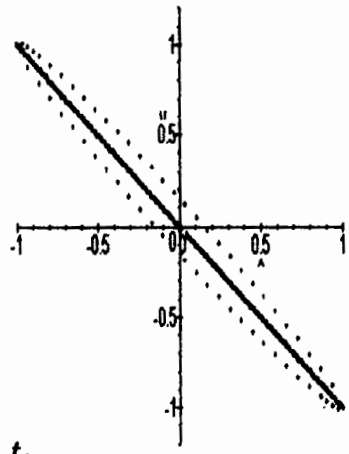

Fig. 4.1

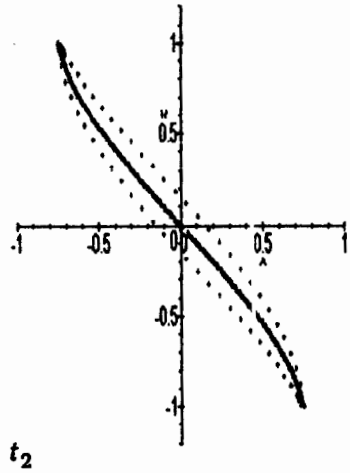

Fig. 4.2

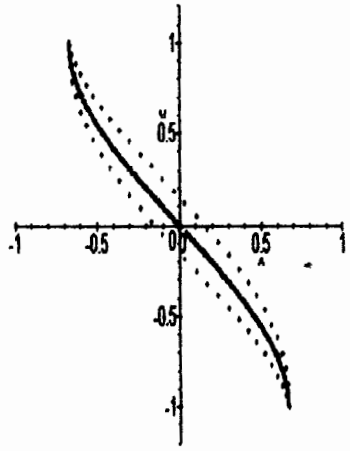

Fig. 4.3

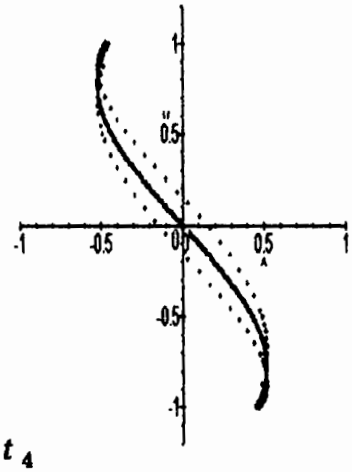

Fig. 4.4

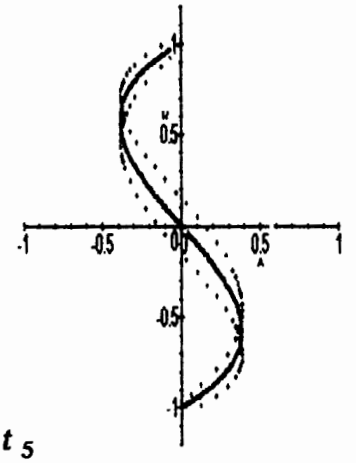

Fig. 4.5

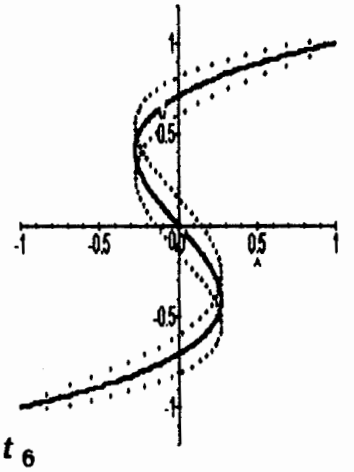

Fig. 4.6

Here $J_0(0)$ is the initial current density on the axis, P_2/P_0 is the input beam nonuniformity; $\varphi_T(0) = k_B T_\perp(0,0)/q$ is the initial temperature of beam on the axis in energy units.

Beam optics quality is most often evaluated by the change in rms emittance. Concept of the rms emittance comes from statistical analysis of the particle spread in the phase space. When the particle coordinates are considered as random values and covariance matrix is calculated for them, then the rms emittance is proportional to the square root of the matrix determinant. Being properly factored, it equals to the area (volume) occupied by the particles in the phase space. [21].

It can be shown [7] that square of the rms emittance defined as follows

$$E_{rms}^2 = \frac{< r^2 >< v_R^2 > - < r v_R >^2}{(\gamma\beta c)^2},$$

is the sum

$$E_{rms}^2 = E_t^2 + E_h^2,$$

where E_h is the fluid or hydrodynamic part,

$$E_h^2 = \frac{< r^2 >< V_R^2 > - < r V_R >^2}{(\gamma\beta c)^2},$$

and E_t is the heat one in the full sense,

$$E_t^2 = \frac{< r^2 >< T >}{(\gamma\beta c)^2}.$$

Here <> denotes an average across the beam, β is the beam velocity in term of speed of light c, γ is the relativistic mass-factor. For a cold beam with no fold $T_{RR}(r) \equiv 0$, $v_R(r) \equiv V_R(r)$, so emittance is completely determined by the term E_h (see Fig.2). If $V_R(r) \propto r$, then $E_{rms} = E_t$ (Fig.1). In other words, the value πE_t can be interpreted as an area of a figure fixed on the phase curve of flow lines $V_R(r)$ (Fig.3). Contour of the figure outlines the actual projection of the particle phase volume. Under the model assumptions the figure area is conserved, so the rms emittance heat term can be approximated as:

$$E_t^2(z) = E_t^2(0)\frac{\Phi_0(0)}{\Phi_0(z)}.$$

The single-parametric representation of flow lines (23) allows the average <> to be calculated analytically and the rms emittance fluid part to be expressed in the terms of R and χ:

$$E_h^2 = \kappa(\alpha)\frac{(R\chi' - R'\chi)^2}{72}.$$

The factor $\kappa(\alpha)$ closes to unity, being dependent on the radial distribution of the space charge :

$$\kappa(\alpha) \approx 1 + \frac{1}{5}\frac{\left(\alpha + \alpha^2/4\right)}{\left(1 + \alpha + \alpha^2/4\right)}, \qquad (30)$$

where $\alpha = 4\chi/R + \rho_2 R^2/\rho_0$. If averaging is taken over current density instead of density of charge, then $\alpha = J_2(0)R_b^2(0)/J_0(0)$ and approximate equality in the equation (30) becomes the rigorous one.

In the expansion for phase curve of flow lines

$$r'(r) = V_R(r)/V_Z(r) = C_1 r + C_3 r^3 + \cdots$$

the non-linearity factor C_3 is possible to relate with the fluid part of rms emittance:

$$E_h^2 = \kappa(\alpha)\frac{\left(C_3 R^4\right)^2}{72}. \qquad (31)$$

Factors of the inverse expansion

$$r(r') = c_1 r' + c_3 r'^3 + \cdots$$

take the form $c_1 = R/R'$, $c_3 = (\chi R' - \chi' R)/(R')^4$ and can be interpreted as the focal length f_{eff} and spherical aberration coefficient C_s of an equivalent thin lens [14], which are calculated now with consideration for internal beam process. By using those, the relationship (31) is rewritten as follows

$$E_h^2 = \frac{\kappa(\alpha)}{72}\left(\frac{C_s R^4}{f_{eff}^4}\right)^2$$

(compare with [2]). More rigorous examination of the flow lines phase portrait in relation to solutions of the advanced envelope equations (28)-(29) confirms the condition

$$R\chi' = R'\chi,$$

as the required one for linear, i.e., non-distortion transfer of the phase volume. The condition without perturbation, $\chi = \chi' = 0$, is only a particular case.

Evidently, Eq.(28) for the envelope first approximation is the conventional paraxial equation for the boundary particle trajectory in a cold beam, when the current density and the longitudinal speed of particles are assumed to be uniform across the beam [13]. The microcanonical distribution of particle phase density [15] has different projections on the planes (r, υ_R),(r, υ_θ), but exhibits common radial dependence in azimuthal and radial temperatures:

$$T_{\theta\theta}(r, z) = T_{RR}(r, z) = T_\perp(0, z)\left(1 - r^2/R_b^2(z)\right).$$

Substitution of the temperatures into the expansion (19) reduces Eq.(28) to well-known K-V equation in the form of paper [1], because $T_\perp(0, z) = \dfrac{E^2}{2R_b^2(z)}$, where πE is the ellipse area covering K-V distribution on the planes (r, υ_R), (r, υ_θ), (x, υ_X) or (y, υ_Y).

As stated above, the assumed set of Eqs.(1)-(6) eliminates from consideration such phenomena as particle pair collisions, dissipation of energy, heat exchange with surroundings and corresponds to an adiabatic plasma transport with entropy conservation. Pair collisions are of considerable importance in highly compressed beams (as those in probe devices), in particle flows extending through dense gas (beam in extracting gap of plasma source, gas neutralizer, welding equipment, etc.), in long life beams (storage rings). It is because of typical for other optics insignificant role of the pair collisions that beam distri-

bution function is highly non-equilibrium: the temperature gradient across the beam occurs, temperatures of transverse and longitudinal motion are substantially different.

Dissipation is always associated with irreversibility of motion and entropy growth. So-called viscosity process or internal friction, described with non-diagonal elements of temperature tensor occurs only when the substance motion proceeds along the flow lines with different velocities. In this case there are moving of the flow parts relative to each other and interchange energy of the directed motion by heat migration of beam particles. In other words, viscosity takes effect of the transfer of the directed motion energy from place with higher flow velocity to that with lower one and dissipation of the energy into heat, i.e., increasing particle speed spread. Handling of the collisionless dissipation requires the equation for non-diagonal terms of temperature tensor, $T_{ZR} = T_{RZ}$, and appropriate additions to be included in the model. Analysis of this equation [10]

$$\frac{dT_{ZR}}{dt} = -T_{ZR}\left(\frac{\partial V_R}{\partial r} + \frac{\partial V_Z}{\partial z}\right) - T_{ZZ}\frac{\partial V_R}{\partial z} - T_{RR}\frac{\partial V_Z}{\partial r}$$

near the axis shows that heating of the beam due to internal friction decreases with increasing speed of particles and is negligible in the quasi-parallel beams of low temperature. In particular, K-V beam conserves transverse emittance as long as all beam particles have the same longitudinal velocity.

The entropy conservation requires in addition to low viscosity some conditions for eliminating the heat flow, which are associated with a certain symmetry in the distribution function or, more precisely, with zero third moment [10,16,17]. From this viewpoint the approximation used consists in replacing actual speed distribution by a symmetric one. However, the analysis of full set of equations points surely that conservation of the distribution symmetry is possible, if only density of moving particles and their temperature remain properly coupled all time, as it is in so-called self-model distributions [1,11,15].

On the other hand, it is known [18,19] that entropy growth in adiabatic flows can result from irreversible losses of the directed motion energy, when the losses are accompanied by forming surfaces of discontinuity (jump) in temperature, pressure or density. Such a surface with moment flow through it is usually referred as a shock wave or shock wave front [20]. The time and place of shock wave forming can be determined mathematically. Let us consider the flow line phase portraits shown in Fig.4 Dissimilar speed of phase point motion results in changing shape of the curve $V_R(r)$. Eventually, the curve can be crooked so much that it occurs many-valued. It is evident that multivaluedness of the mass-flow, i.e., average velocity is physically impossible. In reality the mass-flow velocity is a single-valued function of distance from the axis with jump at shock wave. The particle density and temperature exhibit similar discontinuous.

Obviously, shock wave forming is followed by the fold with typical for it asymmetry in distribution function about local average velocity. For this reason and requirement to conserve a certain ratio between solution to the first approximation envelope equation (20) and its perturbation (21), application of the advanced envelope equations (28)-(29) is limited within the range $R \geq 3|\chi|$.

The fold in flow can arise from ordinary, non-singular initial conditions. Forced elimination of the fold is made difficult by multivaluedness of the flow line phase curve, then by necessity for selected action on the group of particles located at the same point of the configuration space. In the absence of electric field an asymptotical straightening of the fold is possible always and associated with beam cooling on expanding, i.e., transformation of the particle heat energy into the work of pressure forces (some examples see [7,11] and Fig.5)

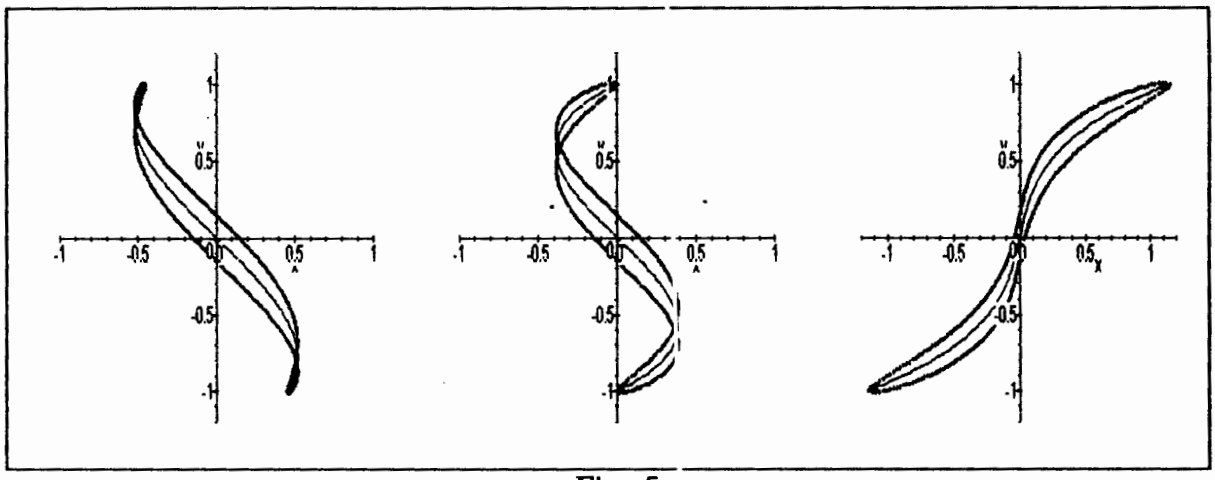

Fig. 5

REFERENCES

[1] J.D.Lawson, The Physics of Charged Particle Beams (Clarendon, Oxford,1977)
[2] Y.Batygin, A.Goto, Y.Yano //EPAC96, Barselona, (1996)
[3] M.J.Rhee //Physics of Plasma, V.2, N.2, (1990), p.452
[4] J.Struckmeier, J.Klabunde, M.Reiser //Part. Accel., 15, 47 (1984)
[5] T.P.Wangler, K.R.Crandall, R.S.Mills, M.Reiser // IEEE Trans. Nucl. Sci. 32 (5), 2196 (1985)
[6] I.Hofmann //Proc. 1986 Linear Accelerator Conference, (1986)
[7] O.A.Anderson // Part. Accel., 21 (3-4), 197 (1987)
[8] M.Reiser //J.Appl.Phys. 70(4), 1919 (1991)
[9] Braginsky S.I. // The Problems of Plasma Theory , ed. by acad. M.A.Leontovich, V.1 (Atomizdat, Moscow, 1963), pp.183-272
[10] J.E.Carroll //J.Electronics and Control, 14(4), 1963, p.403
[11] I.B.Zeldovich, A.D.Mishkis, The Elements of Mathematical Physics (Science, Moscow,1973)
[12] A.T.Forrester, Large Ion Beams (Willey, New York, 1988)
[13] S.I.Molokovsky, A.D.Sushkov, Intense Electron and Ion Beams (Energy,Leningrad,1972)
[14] P.W.Hawkes, E.Kasper, Principles of Electron Optics, Vol.2 (Academic Press, London,1989)
[15] I.M.Kapchinsky, Theory of Resonance Linear Accelerators (Harwood, Chur, 1985)
[16] I.Hofmann //Adv. Electron. and Electron Physics, Suppl.13C (1983), Part C, p.49
[17] I.Hofmann // IEEE NS-26, N.3, 1979
[18] L.I.Sedov, Mechanics of the Continuum (Science, Moscow, 1976)
[19] M.A.Lavrentiev, B.V.Shabat, The Problems of Hydrodynamics and Their Mathematical Models (Science, Moscow, 1977)
[20] L.Landau, E.Lifshitz, Hydrodynamics (Science, Moscow, 1986)
[21] J.Buon //Proc. 1993 IEEE Part. Accel. Conf. (IEEE, Washington, D.C.,1993),p.469

AN INVESTIGATION OF HIGH ORDER ABERRATIONS IN A HIGH SOLID ANGLE MASS–SPECTROMETER [1]

S.N. Andrianov, A.I.Dvoeglazov, N.S. Edamenko, D.A. Ovsyannikov

Bibliotechnaya 2, Institute of Computational Mathematics & Control Processes, St.Petersburg State University, St.Petersburg, 198904, Russia
e-mail: vm.pu@apmath.spb.su

W. Mittig

GANIL, Caen, France

Abstract

This work is a continuation of the work [1] devoted to the problem of optical structure selection for the high solic angle mass–spectrometer. Here we consider influences of high order (second– and third–orders) aberrations on the achromatism property, mass– dispersion and resolution in this system. For this purpose the matrix formalism for Lie algebraic tools is used. Some results of the investigation are demonstrated.

1. Introduction

The work [1] is devoted to the ranging problem for linear approximation of the mass–spectrometer system. This linear optic investigation allowed us to build a set of appropriate prototypes of the mass–spectrometers. As mentioned in the [1] for the high solid angle system it is necessary to study influences of high order aberrations of different kind. First of all a designer should consider high order chromatic aberrations. This investigation must be developed both for separate system elements and for the total system. Among the systems studied in the linear approximation we should select the more appropriate system – the system with the least high order aberrations. The geometric aberrations in such systems are not essential so that is why should be studied on the second step.

2. Formulation of the Problem

As distinct from the linear modeling here the main criterion is the size and distribution of the beam spots on the detector. For this purpose some model functions of particle distribution on the target are generated. For obviousness here we consider two masses beam with masses M and M+ΔM, δm := ΔM/M=0.01. The value of the mass–resolution R=M/dM must be equal to 100 on the half of the maximal height of the central (which corresponds to the mass M) pick (see Fig.11 in the Appendix). On this picture the values L and L + Δ L correspond to the locations of the beam spots for particles with the mass M and M+ΔM correspondingly. The value dL corresponds to a mass derivation dM in the resolution R definition. Simultaneously we monitor other properties, for example,

[1]Work supported by the Russian Foundation for Basic Research (grants No 96-02-17335, No 96-01-00926).

focusing properties. We should note that these criteria and high solid angle acceptance condition should be considered as goal functions for the modeling and optimization process. Different kinds of aberrations in the mass-spectrometer must be considered thoroughly, and a designer should separate aberrations into groups of essential and unessential aberrations. As a support system we consider the linear model mentioned in [1].

The selection of the set of focusing and deflecting elements, their forces and geometrical parameters depend on properties of particles of the initial beam, among them we should mention the following parameters: *central energy* and *energy spread* (or *central impulse* and *impulse spread*), *central mass* and *mass spread*, *central charge* and *charge spread*. The other set of particles parameters envelopes such parameters as *magnetic* and *electric rigidities*. These parameters are important for estimation of capabilities of the mass–spectrometer to work in the given reaction region. The estimations of these parameters can be obtained from the works similar to [2]. Total modelling process we separate into the following steps:

- creation of achromatic linear structure for some variants of focusing and deflecting elements;
- investigation of the stability and sensitivity selected variants (for linear model);
- inclusion and investigation of linear aberrations, such as fringing fields, displacement of the structure elements (in transverse and longitudinal directions) and so on;
- step–by–step inclusion of high order aberrations: on the first step for a separate element and than for the total system;
- conclusion about an influence of these aberrations on optical beam characteristics, first resolution and sizes of a beam image;
- inclusion of correction elements, for example sextupole lenses for compensating of chromatic aberrations;
- optimization procedure for achievement of required characteristics.

In this report we monitor distribution functions for the terminal beam spot for different combinations of aberrations in the mass-spectrometer elements for the generated parameters set for the linear models.

3. Chromatic Aberrations in the Quadrupole and Solenoids

Fig.1 demonstrates the beam envelope along the system in $X-$ and $Y-$ planes, the image for two mass values ($\delta m = 0.01$) (the down and left picture) and corresponding picks for distribution functions (the down and right picture) for one of the linear models

as a support picture. We study nonlinear aberrations for separate structure elements for detection what kind of aberrations and what kind of elements produce a greatest contribution to beam distortions. After this the common contribution is investigated also. The nature of *chromatic aberrations* in solenoids and quadrupoles allows us to investigate this kind of aberrations in all orders. On Fig.2, as an example, the influence of chromatic aberrations (in all order) in the solenoids and the quadrupole is shown. The separate influence of chromatic aberrations in the quadrupole is not significant. One can see a small shift the pick for $M + \Delta M$, $\Delta M = 0.01$.

4. Second Order Aberrations

On the first step of the investigation we consider the influence of the second order aberrations (geometrical and chromatic) separately for every structure element and compare their influences. The geometrical and chromatic aberrations of the second order in the electrostatic deflector (ED) lead to the shift of the picks from the center. On Fig.3 one can see this shifting for some example of parameters. In particular, geometrical aberrations lead to the shift of the central pick equal to *7.2 mm* and chromatic aberrations lead to the same shift and distortion of the first and second picks widths approximately up to three times (see Fig.5). On Fig.4 the influences of the geometrical and chromatic aberrations in the bending magnets are demonstrated, without aberrations induced by the ED. Separately these types of aberrations lead to the following distortions (in comparison with Fig.1):

- for geometrical aberrations: the central pick is the same and the neighboring pick width grows two times.
- for chromatic aberrations: the growth of both the picks widths has the factor 3/2 (see Fig.6).

All aberrations influences without chromatic aberrations in magnetic and electric dipoles are shown on Fig.7, and with chromatic aberrations in magnetic and electric dipoles are shown on Fig.8.

These pictures in the full measure demonstrate the influence of second order aberrations in the mass–spectrometer. Certainly it is necessary to study these influences in more detail for some selected variants of the system.

5. Third Order Aberrations

Third order aberrations should be separated into two parts:

- Geometrical aberrations in *focusing* elements (in the solenoids and the quadrupole). Only chromatic aberrations induced by these elements we investigate in all orders (see Section 3).
- Chromatic and geometric aberrations in *deflecting* elements: electrostatic and magnetic elements.

Appendix

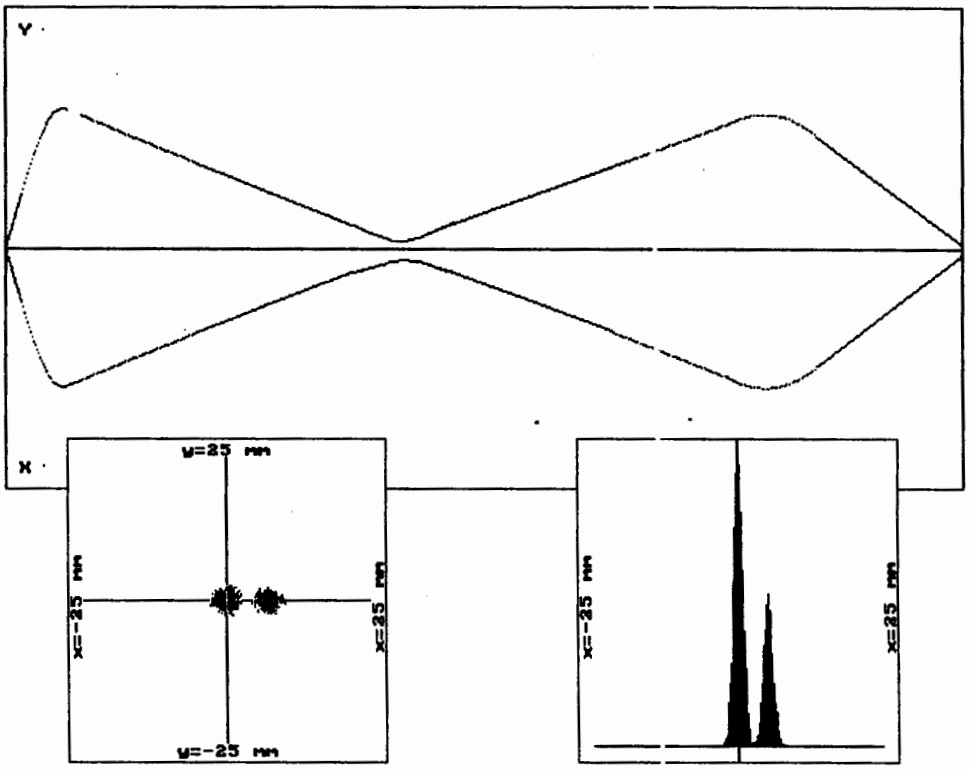

Figure 1

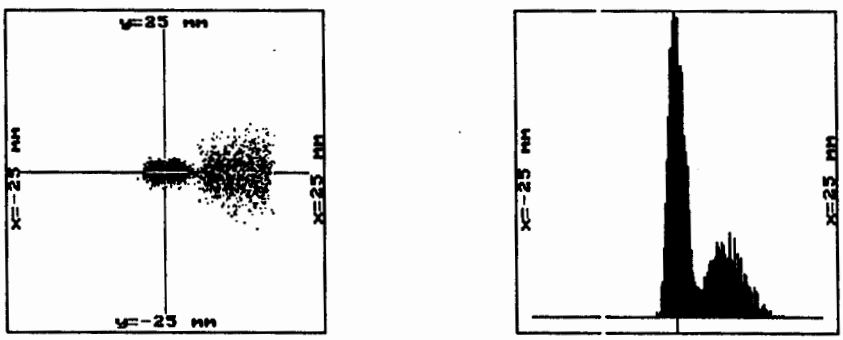

Figure 2

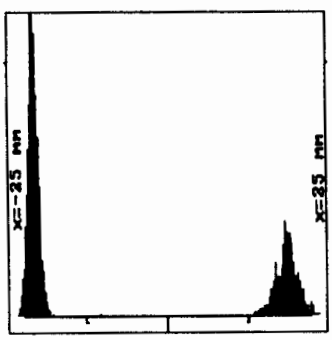

Figure 3

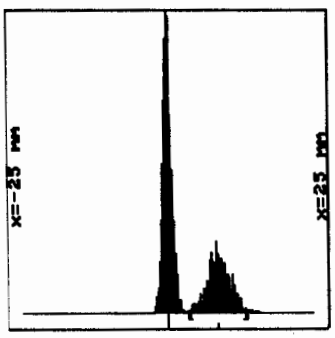

Figure 4

In particular, geometrical aberrations of the third order in the solenoids lead to the growth of the first pick width 1.2 tirnes. For the quadrupole geometrical aberrations the first pick has the same width bu the second pick width has the factor 1.1 (see Figures 9,10).

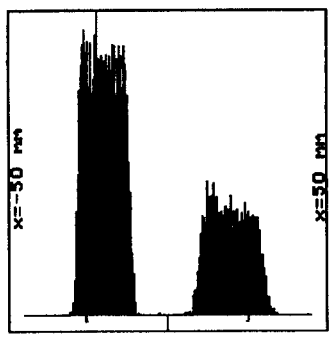

Figure 5

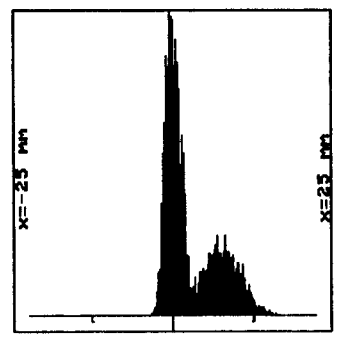

Figure 6

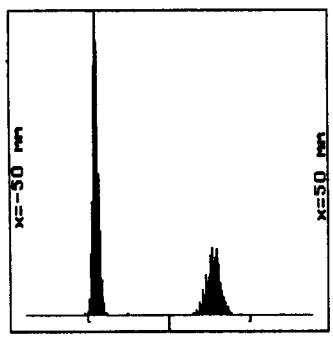

Figure 7

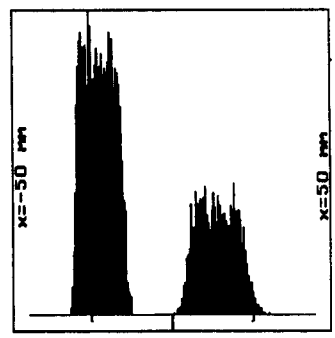

Figure 8

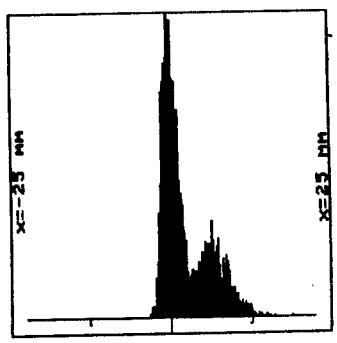

Figure 9

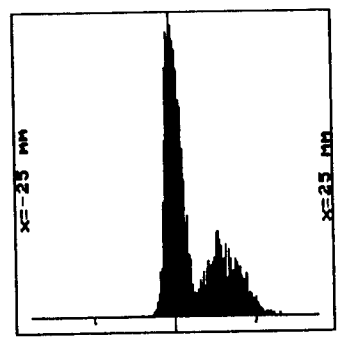

Figure 10

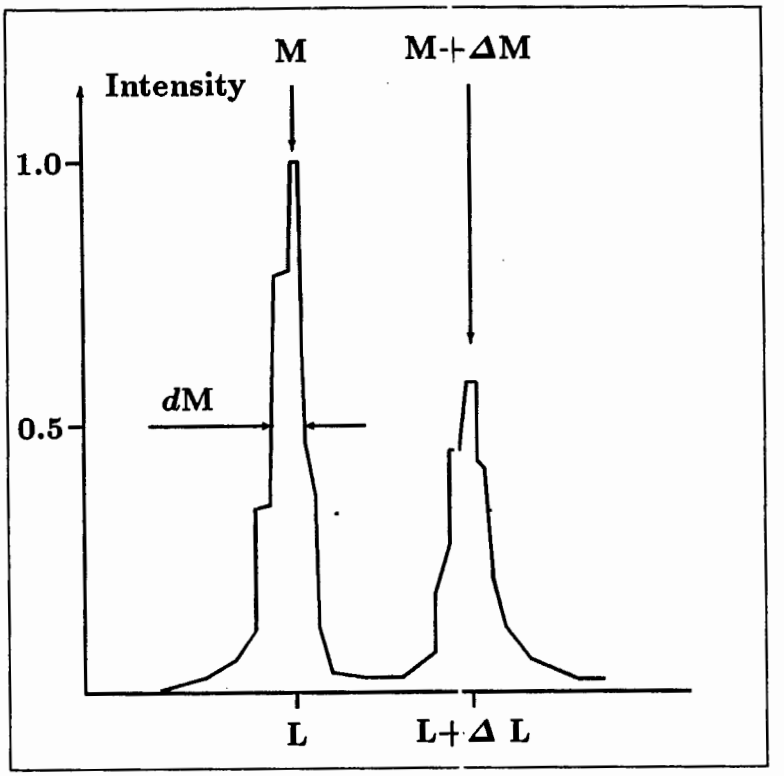

Figure 11

6. Conclusion

The developed calculations demonstrate that the chromatic aberrations exert greater influence upon the terminal distribution function in comparison with the geometrical aberrations. This allows us to declare that only chromatic aberrations should be compensated. In particular, for example, we can note that such system should contain sextupoles for correction chromatic aberrations in the bends (for example, after the first bend and before the second).

References

[1] Andrianov S.N., Edamenko N.S., Ovsyannikov D.A., Mittig W., *Computer Modeling of a High Solid Angle Mass–Spectrometer*, in this Proccedings.

[2] Drouhet Fl. *Calcul d'un Spectrométre de Grande Acceptance*, Universite de CAEN, CAEN, 1996.

One Variational Method for Solution of Magnetostatic Problems

M.V. Aljeshin

Moscow State Technical (Bauman) University, Russia

The Formulation of Problem and Estimate of Error of Its Approximate Solution

Investigated physical system – ferromagnetic in the field of the coil with current. Magnetic occupies the domain of space D, the magnet wire of coil – D', the density of current $\vec{j}$. The system equation is presented in integral form

$$\vec{H}(\vec{r}) + \vec{\nabla}\left(\frac{1}{4\pi}\int_D (\vec{M}(\vec{r}', \vec{H}(\vec{r}')) \cdot \vec{\nabla}') \frac{1}{|\vec{r} - \vec{r}'|} d\vec{r}'\right) = \vec{H}_s(\vec{r}),$$

where $\vec{H}$ – the strength of magnetic field, $\vec{M}$ – the magnetization of magnetic and right part $\vec{H}_s(\vec{r}) = [\vec{\nabla} \times \frac{1}{4\pi}\int_{D'} \frac{1}{|\vec{r} - \vec{r}'|} \vec{j}(\vec{r}')\, d\vec{r}']$. Here as a variable is considered $\vec{H}$, function $\vec{M}(\vec{H})$ and the density of current $\vec{j}$ are believed known.

In order to define field outside the magnetic, it's enough to solve the system equation inside domain D. The solution maybe is found on space $\vec{L}_2(D)$ of square-integrated measurable on D vector-functions. Confining to this space, we shall write down the equation in operatorial type $\vec{H} + J\vec{M}(\vec{H}) = \vec{H}_s$. It admits the estimate of the error of any its approximate solution without the precise value of $\vec{H}$. This estimate permits to denote the method of the solution of the investigated problem possessing stop-criterion of computations.

We shall begin with the properties of operator J. On $\vec{L}_2(D)$ it is continuous and self-adjoint. For finite D with Lipschitz boundaries the range of values of J is $\vec{V} = \vec{\nabla}[W_2^1(D)]$. Here $W_2^1(D)$ — the space that is measurable on D functions which are square-integrated together with its weak derivatives. The contraction $J\downarrow\vec{V}$ is positive definite. The substantiation of all the above-mentioned properties may be found in [1].

We shall exclude out of consideration infinite magnetics and magnetics with boundaries, not satisfying the Lipschitz condition. Such pace permits to introduce orthogonal projector P from $\vec{L}_2(D)$ on $\vec{V}$ and operator K, inverse $J\downarrow\vec{V}$. Making up of them non-linear operator $R(\vec{H}) = M(\vec{H} - \vec{H}_s) + P\vec{M}(\vec{H})$, we shall present the investigated problem by the

system of equations $(1-P)(\vec{H}-\vec{H}_s)=0$, $R(\vec{H})=0$. Obviously R has positive definite on $\vec{V}$ strong derivative. Just this circumstance makes possible the potential estimate of the error of the approximate solution of the problem [2]. It defines as well the existence of sole exact solution.

We shall pass on to real situation when all physical magnitudes are known with finite precisions. Obtained in an outcome of measurements the current density will be designated $\vec{j}+\delta\vec{j}$. It originates $\vec{H}_s(\vec{r})+\delta\vec{H}_s(\vec{r})=[\vec{\nabla}\times\frac{1}{4\pi}\int\limits_{D'}\frac{1}{|\vec{r}-\vec{r}'|}(\vec{j}(\vec{r}')+\delta\vec{j}(\vec{r}'))\,d\vec{r}']$. As an approximation of the strength of field inside D we shall choose $\vec{H}+\delta\vec{H}$ – an arbitrary element of $\vec{L}_2(D)$. The approximation of magnetization replying this element, will be designated $\vec{M}+\delta\vec{M}$. Its association with $\vec{H}+\delta\vec{H}$ shall be specified below. Then the field strength outside domain D is $\vec{H}_s(\vec{r})+\delta\vec{H}_s(\vec{r})+\vec{\nabla}(\frac{1}{4\pi}\int\limits_{D}((\vec{M}(\vec{r})'+\delta\vec{M}(\vec{r})')\cdot\vec{\nabla}')\frac{1}{|\vec{r}-\vec{r}'|}d\vec{r})'$. Its error in any point $\vec{r}$ does not exceed as to absolute value

$$\frac{1}{3}(\int\limits_{D}\frac{d\vec{r}'}{|\vec{r}-\vec{r}'|^6})^{1/2}\,\|(\vec{M}+\delta\vec{M})[\vec{H}+\delta\vec{H}]-\vec{M}(\vec{H})\|+\|[\vec{\nabla}\times\frac{1}{4\pi}\int\limits_{D'}\frac{1}{|\vec{r}-\vec{r}'|}\delta\vec{j}(\vec{r}'))\,d\vec{r}']\|.$$

(the symbols of norm and further scalar product relate to $\vec{L}_2(D)$). Thus, it is necessary to evaluate $\|(\vec{M}+\delta\vec{M})[\vec{H}+\delta\vec{H}]-\vec{M}(\vec{H})\|$.

If for $\vec{j}+\delta\vec{j}$ to retain the property of a current preservation, then $[\vec{\nabla}\times(\vec{H}_s+\delta\vec{H}_s)]=0$ on D. Respectively $(1-P)(\vec{H}_s+\delta\vec{H}_s)=0$ [3] and having required $(1-P)(\vec{H}+\delta\vec{H})=0$, it may be introduced as an approximation of the operator R

$$(R+\delta R)(\vec{H}+\delta\vec{H})=K(\vec{H}+\delta\vec{H}-\vec{H}_s-\delta\vec{H}_s)+P(\vec{M}+\delta\vec{M})[\vec{H}+\delta\vec{H}].$$

Admitting onward into attention equality $R(\vec{H})=0$, we shall receive

$$(R+\delta R)(\vec{H}+\delta\vec{H})=K(\delta\vec{H}-\delta\vec{H}_s+P((\vec{M}+\delta\vec{M})[\vec{H}+\delta\vec{H}]-\vec{M}(\vec{H})).$$

Such form of operator prompts representation

$$(\vec{M}+\delta\vec{M})[\vec{H}+\delta\vec{H}]-\vec{M}(\vec{H})=((\vec{M}+\delta\vec{M})[\vec{H}+\delta\vec{H}]-\vec{M}(\vec{H}+\delta\vec{H}))+$$

$$+(\vec{M}(\vec{H}+\delta\vec{H})-\vec{M}(\vec{H}+\delta\vec{H}-\delta\vec{H}_s))+(\vec{M}(\vec{H}+\delta\vec{H}-\delta\vec{H}_s)-\vec{M}(\vec{H})).$$

The first two residuals in the right part of this identity from $\vec{H}$ do not depend. In order to estimate the third residual, take advantage of relation $(1-P)(\delta\vec{H}-\delta\vec{H}_s)=0$ and $\|\delta\vec{H}-\delta\vec{H}_s\|^2\leq(\delta\vec{H}-\delta\vec{H}_s,\,K(\delta\vec{H}-\delta\vec{H}_s))$ [1].

According to the properties of Lebesque integral [4] and positive perceptibility of magnetic (the maximal value of perceptibility is designated $\bar{\nu}$),

$$\|\vec{M}(\vec{H}+\delta\vec{H}-\delta\vec{H}_s)-\vec{M}(\vec{H})\|=\|\int_0^1((\delta\vec{H}-\delta\vec{H}_s)\cdot\frac{\partial}{\partial\vec{H}})\vec{M}(\vec{H}+t(\delta\vec{H}-\delta\vec{H}_s))\,dt\|\le$$

$$\le\int_0^1\|((\delta\vec{H}-\delta\vec{H}_s)\cdot\frac{\partial}{\partial\vec{H}})\vec{M}(\vec{H}+t(\delta\vec{H}-\delta\vec{H}_s))\|\,dt\le$$

$$\le\bar{\nu}^{1/2}\int_0^1(\delta\vec{H}-\delta\vec{H}_s,\,((\delta\vec{H}-\delta\vec{H}_s)\cdot\frac{\partial}{\partial\vec{H}})\vec{M}(\vec{H}+t(\delta\vec{H}-\delta\vec{H}_s)))^{1/2}dt\le$$

$$\le\bar{\nu}^{1/2}(\delta\vec{H}-\delta\vec{H}_s,\int_0^1((\delta\vec{H}-\delta\vec{H}_s)\cdot\frac{\partial}{\partial\vec{H}})\vec{M}(\vec{H}+t(\delta\vec{H}-\delta\vec{H}_s))\,dt)^{1/2}=$$

$$=\bar{\nu}^{1/2}(\delta\vec{H}-\delta\vec{H}_s,\,\vec{M}(\vec{H}+\delta\vec{H}-\delta\vec{H}_s)-\vec{M}(\vec{H}))^{1/2}\le$$

$$\le\xi(\delta\vec{H}-\delta\vec{H}_s,\,K(\delta\vec{H}-\delta\vec{H}_s)+P(\vec{M}(\vec{H}+\delta\vec{H}-\delta\vec{H}_s)-\vec{M}(\vec{H})))/\|\delta\vec{H}-\delta\vec{H}_s\|\le$$

$$\le\xi(\|(R+\delta R)(\vec{H}+\delta\vec{H})\|+\|(\vec{M}+\delta\vec{M})[\vec{H}+\delta\vec{H}]-\vec{M}(\vec{H}+\delta\vec{H})\|+$$

$$+\|\vec{M}(\vec{H}+\delta\vec{H}-\delta\vec{H}_s)-\vec{M}(\vec{H}+\delta\vec{H})\|)\le$$

$$\le\xi(\|(R+\delta R)(\vec{H}+\delta\vec{H})\|+\|(\vec{M}+\delta\vec{M})[\vec{H}+\delta\vec{H}]-\vec{M}(\vec{H}+\delta\vec{H})\|+\bar{\nu}\|\delta\vec{H}_s\|).$$

Here ξ – is constant satisfying the inequality

$$\nu^{1/2}/\xi\le\|\delta\vec{H}-\delta\vec{H}_s\|/(\delta\vec{H}-\delta\vec{H}_s,\,\vec{M}(\vec{H}+\delta\vec{H}-\delta\vec{H}_s)-\vec{M}(\vec{H}))^{1/2}+$$

$$+(\delta\vec{H}-\delta\vec{H}_s,\,\vec{M}(\vec{H}+\delta\vec{H}-\delta\vec{H}_s)-\vec{M}(\vec{H}))^{1/2}/\|\delta\vec{H}-\delta\vec{H}_s\|.$$

Because the right part of the inequality is not less than 2, then $\xi=\bar{\nu}^{1/2}/2$. As a result

$$\|(\vec{M}+\delta\vec{M})[\vec{H}+\delta\vec{H}]-\vec{M}(\vec{H})\|\le(\bar{\nu}^{1/2}/2)\|(R+\delta R)(\vec{H}+\delta\vec{H})\|+$$

$$+(1+\bar{\nu}^{1/2}/2)\|(\vec{M}+\delta\vec{M})([\vec{H}+\delta\vec{H}]-\vec{M}(\vec{H}+\delta\vec{H})\|+(\bar{\nu}+\bar{\nu}^{3/2}/2)\|\delta\vec{H}_s\|.$$

Discretization of Problem

Received estimate permits to transform the solution of magnetostatic problem in digital procedure minimizing this estimate. The real implementation of such procedure assumes discretization of the problem. We take advantage of the certain variant of piecewise-constant discretization. Volume of the magnetic will be approached by polyhedron which, in its turn, will be parted on terahedrons. The characteristic functions of the tetrahadrons will be designated η_i. The strength of magnetic field suitable to search in the

form $\vec{H}+\delta\vec{H}=\vec{H}_s+\delta\vec{H}_s+J\vec{c}_i\eta_i$ with constant $\{\vec{c}_i\}$ (on repeated indices summing is conducted). Chosen form $\vec{H}+\delta\vec{H}$ simplifies construction $(R+\delta R)(\vec{H}+\delta\vec{H})$, but makes difficult the magnetization computing. Therefore we shall introduce $\vec{G}=<\vec{H}+\delta\vec{H}>$ – either approximation $\vec{H}+\delta\vec{H}$, constant inside the tetrahedrons. To namely this approximation will match also piecewise-constant $(\vec{M}+\delta\vec{M})[\vec{H}+\delta\vec{H}]=\vec{M}(\vec{G})+\delta\vec{M}(\vec{G})=\vec{s}_i\eta_i$.

After the above-made improvements we have

$$(R+\delta R)(\vec{H}+\delta\vec{H})=KJ\vec{c}_i\eta_i+P\vec{s}_i\eta_i=P(\vec{c}_i+\vec{s}_i)\eta_i,$$

$$\|(\vec{M}+\delta\vec{M})[\vec{H}+\delta\vec{H}]-\vec{M}(\vec{H}+\delta\vec{H})\|\le\|\vec{M}(\vec{G})-\vec{M}(\vec{H}+\delta\vec{H})\|+\|\delta\vec{M}(\vec{G})\|\le$$

$$\le\bar{\nu}\|\vec{H}_s+\delta\vec{H}_s-<\vec{H}_s+\delta\vec{H}_s>\|+\bar{\nu}\|J\vec{c}_i\eta_i-<J\vec{c}_i\eta_i>\|+\|\delta\vec{M}(\vec{G})\|,$$

$$\|(\vec{M}+\delta\vec{M})[\vec{H}+\delta\vec{H}]-\vec{M}(\vec{H})\|\le(1+\bar{\nu}^{1/2}/2)(\bar{\nu}\|\vec{H}_s+\delta\vec{H}_s-<\vec{H}_s+\delta\vec{H}_s>\|+$$

$$+\|\delta\vec{M}(\vec{G})\|+\bar{\nu}\|\delta\vec{H}_s\|)+(\bar{\nu}^{1/2}/2)\|P(\vec{c}_i+\vec{s}_i)\eta_i\|+(\bar{\nu}+\bar{\nu}^{3/2}/2)\|J\vec{c}_i\eta_i-<J\vec{c}_i\eta_i>\|.$$

Values $\|\delta\vec{M}\|$, $\bar{\nu}\|\delta\vec{H}_s\|$ are dependent on the precision of the measurements of current and magnetization. They dictate requirements for a smallness of the remaining addends of the right side of last inequality. Rather fine initial partition of D permits to satisfy this requirement in respect to $\bar{\nu}\|\vec{H}_s+\delta\vec{H}_s-<\vec{H}_s+\delta\vec{H}_s>\|$. The further procedure is reduced to a construction $\{\vec{c}_i\}$ for initial and fineer partitions of the magnetic. According to positive definiteness $J\downarrow\vec{V}$, the purpose of similar procedure may be to elect diminution $\Phi\{\vec{c}_i\}=\|J^{1/2}(\vec{c}_i+\vec{s}_i)\eta_i\|+\bar{\nu}\|J\vec{c}_i\eta_i-<J\vec{c}_i\eta_i>\|$. Advantages of this functional will be explicit below.

Algorithm of Solution

Let $\vec{c}_i\to\vec{c}_i+d\vec{c}_i$. Such substitution leads to

$$d(\|J^{1/2}(\vec{c}_i+\vec{s}_i)\eta_i\|)=((\vec{c}_i+\vec{s}_i)\eta_i,\ Jd(\vec{c}_j+\vec{s}_j)\eta_j)/\|J^{1/2}(\vec{c}_{i'}+\vec{s}_{i'})\eta_{i'}\|=$$

$$=((\vec{c}_i+\vec{s}_i)\eta_i,\ J(d\vec{c}_j\eta_j+\vec{e}_\gamma\eta_j\theta^j_{\gamma\gamma'}(\vec{e}_{\gamma'}\eta_j,\ Jd\vec{c}_{i'}\eta_{i'})))/\|J^{1/2}(\vec{c}_{j'}+\vec{s}_{j'})\eta_{j'}\|,$$

$$d(\|J\vec{c}_i\eta_i-<J\vec{c}_i\eta_i>\|)=(J\vec{c}_i\eta_i,\ (Jd\vec{c}_j\eta_j-<Jd\vec{c}_j\eta_j>))/\|J\vec{c}_{i'}\eta_{i'}-<J\vec{c}_{i'}\eta_{i'}>\|.$$

Here $\theta^j_{\gamma\gamma'}$ is the magnetic perceptability depending on $\vec{G}$. Direction of the quickest decrease of $\Phi\{\vec{c}_i\}$ can be defined by the equations $d\vec{c}_i=-(\vec{c}_i+\vec{s}_i)\,dt$ under conditions $dt>0$ and $-\frac{d}{dt}(\|J^{1/2}(\vec{c}_i+\vec{s}_i)\eta_i\|)\ge\frac{d}{dt}(\bar{\nu}\|J\vec{c}_i\eta_i-<J\vec{c}_i\eta_i>\|)$ (t – arbitrary parameter). In order

the equations make sense on the finite interval of variations t, we shall add their requirement $-\frac{d}{dt}(\| J^{1/2}(\vec{c}_i + \vec{s}_i)\eta_i \|) \geq 10\frac{d}{dt}(\bar{\nu}\| J\vec{c}_i\eta_i - <J\vec{c}_i\eta_i>\|)$ in initial moment t=0. To This requirement may be satisfied, if approximation $<J\vec{c}_i\eta_i>$ will correspond to a finer partition of D, than $\{\vec{c}_i\}$.

For construction $\vec{c}_i(t)$ the differential equations it is convenient to transform in integral $\vec{c}_i(t) = \vec{c}_i(0)\, e^{-t} - \int_0^t \vec{s}_i(t)' e^{-(t'-t')}dt'$. Last equations belong to Volterra type and are solved by iterative procedure: $\vec{c}_i^{(0)}(t) = \vec{c}_i(0)\, e^{-t}$, $\vec{c}_i^{(\kappa+1)}(t) = \vec{c}_i(0)\, e^{-t} - \int_0^t \vec{s}_i^{(\kappa)}(t')\, e^{-(t-t')}dt'$, where $\vec{s}_i^{(\kappa)}\eta_i = \vec{M}(\vec{G}^{(\kappa)}) + \delta\vec{M}(\vec{G}^{(\kappa)})$, $\vec{G}^{(\kappa)} = <\vec{H}_s + \delta\vec{H}_s + J\vec{c}_j^{(\kappa)}\eta_j>$. The convergence of this procedure is specified by easily receivable estimate

$$\int_D |(\vec{c}_i^{(\kappa+1)}(t) - \vec{c}_i^{(\kappa)}(t))\eta_i|^2 d\vec{r} \leq \frac{t}{\kappa!}(\bar{\nu}^2 \int_0^t t'dt')^\kappa \int_0^t dt' e^{-2(t-t')} \int_D |\vec{s}_i^{(0)}\eta_i|^2 d\vec{r} \leq$$

$$\leq (t^2/2\pi\kappa)^{1/2}(\bar{\nu}^2 t' e/2\kappa)^\kappa \int_0^t dt' e^{-2(t-t')} \int_D |\vec{s}_i^{(0)}\eta_i|^2 d\vec{r}.$$

The second inequality is explained by Stirling formula [5].

By now the suggested algorithm of the solution of the magnetostatic problem may be described on the whole. As already was said, initial partition of the magnetic is chosen so, that piecewise-constant approximation of the current field $\vec{H}_s + \delta\vec{H}_s$ is rather exact. On this approximation the magnetization of the magnetic is defined and its value in each subregion of the partition is identified with $(-\vec{c}_i)$. Thereby, we get initial field $\vec{H} + \delta\vec{H}$, and with it $\vec{G}$, $\{\vec{s}_i\}$ and Φ. The case of small value Φ shall be considered below. If Φ is large, then it is necessary to construct new $\{\vec{c}_i\}$.

We shall clear up in the beginning whether the entry condition is fulfilled

$$-\frac{d}{dt}(\| J^{1/2}(\vec{c}_i + \vec{s}_i)\eta_i \|) \geq 10\frac{d}{dt}(\bar{\nu}\| J\vec{c}_i\eta_i - <J\vec{c}_i\eta_i>\|).$$

Its non-observance compels to pass to a fineer partition of the magnetic. By a sequential choice we shall discover a partition, for which the entry condition is performed. To it are matched their own $\{\vec{s}_i\}$. Further from the integral equations, $\vec{c}_i^{(1)}$ is found and from functional equation $\frac{d}{dt}(\| J^{1/2}(\vec{c}_i^{(1)} + \vec{s}_i^{(1)})\eta_i \|) - \frac{d}{dt}(\bar{\nu}\| J\vec{c}_i^{(1)}\eta_i - <J\vec{c}_i^{(1)}\eta_i>\|)$ its nearest to zero root t_1 is found. If t_1 will turn out to be more or comparable with $1/\bar{\nu}$, then we shall pass on to $\vec{c}_i^{(2)}$ and shall continue procedure. Otherwise for new value $\vec{c}_i$ we shall admit $\vec{c}_i^{(1)}(t_1)$. On step κ we will solve the equation

$$\frac{d}{dt}(\|J^{1/2}(\vec{c}_i^{(\kappa)} + \vec{s}_i^{(\kappa)})\eta_i\|) = -\frac{d}{dt}(\bar{\nu}\|J\vec{c}_i^{(\kappa)}\eta_i - <J\vec{c}_i^{(\kappa)}\eta_i>\|)$$

and compare its root t_κ with $(\kappa/\bar{\nu}^2)^{1/2}$.

The search for roots can be finished before Φ will is found to be enough small. Then we shall pass to a fineer partition of D having restored the entry condition $-\frac{d}{dt}(\|J^{1/2}(\vec{c}_i + \vec{s}_i)\eta_i\|) \geq 10\frac{d}{dt}(\bar{\nu}\|J\vec{c}_i\eta_i - <J\vec{c}_i\eta_i>\|)$. At such passage a variation of the functional $\Phi'\{\vec{c}_i\} - \Phi\{\vec{c}_i\}$ does not exceed on an absolute value

$$\|J^{1/2}(\vec{s}_i'\eta_i' - \vec{s}_i\eta_i)\| + \bar{\nu}\|J\vec{c}_i\eta_i - <J\vec{c}_i\eta_i>'\| - \bar{\nu}\|J\vec{c}_i\eta_i - <J\vec{c}_i\eta_i>\| \leq$$

$$\leq \|\vec{s}_i'\eta_i' - \vec{s}_i\eta_i\| + \bar{\nu}\|J\vec{c}_i\eta_i - <J\vec{c}_i\eta_i>'\| - \bar{\nu}\|J\vec{c}_i\eta_i - <J\vec{c}_i\eta_i>\| \leq$$

$$\leq \bar{\nu}\|<J\vec{c}_i\eta_i>' - <J\vec{c}_i\eta_i>\| + \bar{\nu}\|J\vec{c}_i\eta_i - <J\vec{c}_i\eta_i>'\| - \bar{\nu}\|J\vec{c}_i\eta_i - <J\vec{c}_i\eta_i>\| \leq$$

$$\leq 2\bar{\nu}\|J\vec{c}_i\eta_i - <J\vec{c}_i\eta_i>'\|$$

(the prime marks magnitudes, concerning a new partition). As a result it may be attained that $|\Phi'\{\vec{c}_i\} - \Phi\{\vec{c}_i\}|$ has not exceed one tenth of the functional variation at expense of the previous optimization $\{\vec{c}_i\}$. Further everything continues as it is described above.

Eventually $\|J^{1/2}(\vec{c}_i + \vec{s}_i)\eta_i\| + \bar{\nu}\|J\vec{c}_i\eta_i - <J\vec{c}_i\eta_i>\|$ will become so small, as far as it is necessary. But we have $\|J^{1/2}(\vec{c}_i + \vec{s}_i)\eta_i\| \leq \|P(\vec{c}_i + \vec{s}_i)\eta_i\|$ [3], therefore one needs separate research $\|P(\vec{c}_i + \vec{s}_i)\eta_i\|$. This magnitude coincides with a minimum of the functional $(\|(\vec{c}_i + \vec{s}_i)\eta_i\|^2 - 2((\vec{c}_i + \vec{s}_i)\eta_i, \cdot) + \|\cdot\|^2)^{1/2}$ on orthogonal complement of $\vec{V}$ and with a maximum $(2((\vec{c}_i + \vec{s}_i)\eta_i, J(\vec{c}_i + \vec{s}_i)\eta_i + \cdot) \|J(\vec{c}_i + \vec{s}_i)\eta_i + \cdot\|^2)^{1/2}$ on the gradients of harmonic functions from $W_2^1(D)$ (the range of values of $P - J$ is the space of similar gradients [3]). Any element of the orthogonal complement of $\vec{V}$ can be approached by piecewise-polynomial vectors, any harmonic function from $W_2^1(D)$ — a potential of a simple layer with a piecewise-constant density [6]. These circumstances permit to construct upper and lower evaluations of $\|P(\vec{c}_i + \vec{s}_i)\eta_i\|$, the residual of which can be made small as is wished. The computations stop, as soon as the upper evaluation becomes less admissible error. If in any moment the lower evaluation exceeds an admissible error, it is necessary to come back to minimising $\|J^{1/2}(\vec{c}_i + \vec{s}_i)\eta_i\| + \bar{\nu}\|J\vec{c}_i\eta_i - <J\vec{c}_i\eta_i>\|$. Thus, from a practical point of view the advantage of the explained method is the availability of the stop-criterion of computations.

References

1. Friedman M. J., Pasciak J. E. Spectral Properties for the Magnetization Integral Operator. – Math. Comp. 1984, v. 43, no. 168, p. 447-453.

2. Михлин С. Г. Вариационные методы в математической физике. – М.: Государственное издательство технико–теоретической литературы. 1957.

3. Ладыженская О.А. Математические вопросы динамики несжимаемой жидкости. – М.: Наука. 1970.

4. Колмогоров А.Н. Фомин С.В. Элементы теории функций и функционального анализа. – М.: Наука. 1990.

5. Бронштейн И. Н., Семендяев К. А. Справочник по математике. – М.: Наука. 1986.

6. Бесов О. В., Ильин В. П., Никольский С. М. Интегральные представления функций и теоремы вложения. – М.: Наука. 1975.

CHANGE OF FIELD DISTRIBUTION FOR THE SPECTROMETRIC SP-40A MAGNET *)

S.V. Andreev, V.A. Panacik, E.E. Perepelkin, R.V. Polyakova, T.V. Shavrina, I.P. Yudin, E.P. Zhidkov.

Joint Institute for Nuclear Research, 141980 Dubna, Moscow region, Russia
E-mail: mag@cv.jinr.ru

A significance of the numerical modeling for research in magnet systems is defined by the known advantages of computational experiment and the fact, that a measurement of magnet field is a laborious and expensive problem. Therefore, sometimes one has to use the magnet field measured in one working mode of the physical setup for other working modes, accordingly, having recalculated it.

In this paper a problem of recalculation of the SP-40 magnet field of the EXCHARM spectrometer [1] in another working mode is considered. The field distributions for these working modes are received by computation. At that the experimental data are available for the first of them. It is carried out a comparison of the computed distribution with the experimentally measured ones which turned out to be satisfactory. From the comparison of these two distributions, an algorithm of the recalculation of the field distribution from the mode of the known experimental data to another mode, is received. The magnet field maps are composed for two modes of the EXCHARM experiment. One of them is the mode of measurements for the field $B_0 = 0.7840T$ in the center and the other is one (session N 10, 1995) for the field in the center, which is equal to 0.85 of the magnitude $B_0 = 0.7840T$. The results of this paper are aimed to process of the experimental physical information having received in the session N 10 of the EXCHARM experiment.

1. Field distribution for first work mode

The SP-40A magnet field measurements of the EXCHARM spectrometer [2] carried out in March 1996 [3] have been processed and used for the receiving of the magnet field map. This map is applicable for the experimental physical information processing at present and in the sessions of the EXCHARM experiment carried out before. Two work modes of the spectrometer magnet are interesting at present. Namely, the mode with the field $B_0 = 7840Гс$, in the center of magnet, is the 1-st mode, and it is the mode of measurements. The graphs of the components B_x, B_y and B_z of the measured magnet field are presented in [3]. And the 2-nd mode is one with the field $B_0 = 6664Гс$, that is equal to 85 % of the first value.

The numerical modeling of the SP-40A magnet of the spectrometer (the configuration of the 1/4 part is given on fig.1) was performed by the CPMMS-v.1.1 complex of programs [4], including such programs as POISCR [5] for numerical modeling of two-dimensional magnetic fields, and other codes for solving of the Poisson equation (of Laplace equation) in two- and three-dimensional cases. Besides, the CPMMS-v.1.1 complex of programms includes as a

*) Work supported by the Russian Foundation of Basic Research (grants no.95-01-00737a and no.95-01-01467a) and supported in part by the Federal Centre "Integration" (project no.K0085).

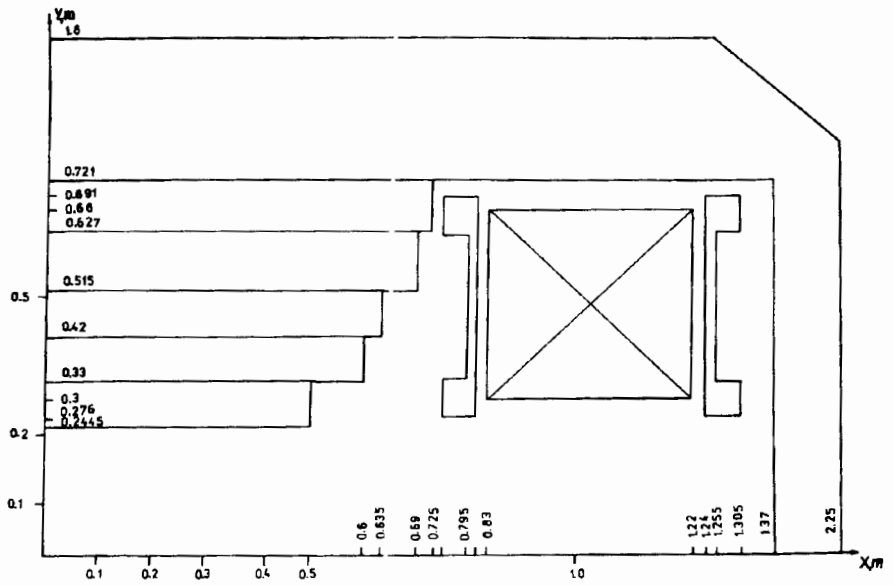
Y,m
1.6
0.721
0.691
0.66
0.627
0.515
0.42
0.33
0.3
0.276
0.2445
0.5
0.2
0.1
0.6
0.635
0.69
0.725
0.795
0.83
1.22
1.24
1.255
1.305
1.37
2.25
0.1
0.2
0.3
0.4
0.5
1.0
X,m

Fig. 1

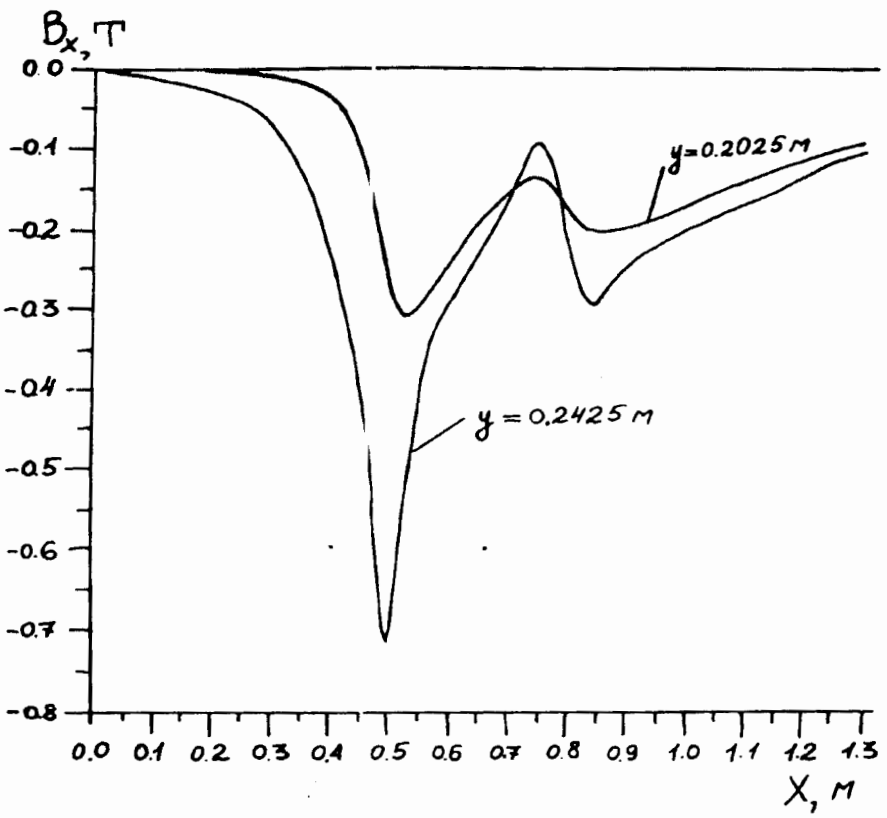
B_x, T
0.0
-0.1
-0.2
-0.3
-0.4
-0.5
-0.6
-0.7
-0.8
y=0.2025 м
y = 0.2425 м
0.0 0.1 0.2 0.3 0.4 0.5 0.6 0.7 0.8 0.9 1.0 1.1 1.2 1.3
X, м

Fig. 2

constituent part the data base of the configurations of magnet systems for graphic examination of obtained numerical results that makes considerably easier and accelerates the process of selecting configurations of the magnet system for its technical realization.

Let us designate the components of the measured field as $B_x^{(э)}(x,y,z)$, $B_y^{(э)}(x,y,z)$ and $B_z^{(э)}(x,y,z)$ where the field in the center of magnet is $B_0 = 0.7840T$. The results of the field calculation are presented in fig.2 (B_x component) and in fig.3 (B_y component) depending on x at $z = 0$ and $y = 20cm$ and $y = 24cm$, where inhomogeneity of the field look especially greatly. The field is more homogeneous for $y < 20cm$.

Let us designate the computational values corresponding to the first work mode, as N1 and $B_x^{(1)}$, $B_y^{(1)}$, and also the field in the center as $B_0^{(1)}$,. Here $B_0^{(1)} = B_0^{(э)}$.

In fig.4 these computational curves are compared with experimental values (they are labelled by thick points) in the characteristic region of the magnet field. Analyzing the computational and measured fields, one may say about a good consent of the computational model of the field with experimental data.

2. The field distribution in the second work mode

The problem of using the obtained map of the measured field for physical data processing in other sessions of the experiment EXCHARM, where winding current differed from its value in carrying out measurements [2], is topical.

Let us investigate a mode with the field in the center of the magnet

$$B_0^{(1)} = \alpha \cdot B_0^{(э)} \qquad (1)$$

where $\alpha = 0.85$ in our case.The received calculation values of the magnetic field components for this mode are designated as $B_x^{(2)}(x,y,z)$ and $B_y^{(2)}(x,y,z)$. Further, the differences are determined as

$$\begin{cases} \Delta B_x(x,y,z) = B_x^{(2)}(x,y,z) - \alpha \cdot B_x^{(1)}(x,y,z) \\ \Delta B_y(x,y,z) = B_y^{(2)}(x,y,z) - \alpha \cdot B_y^{(1)}(x,y,z). \end{cases} \qquad (2)$$

The graphs of these values are given in fig.5.

3. The field map for the second work mode

For experimental physical data processing received under the conditions of the second work mode, one can suggest the following computed map of the magnet field:

$$\begin{cases} B_x(x,y,z) = \Delta B_x(x,y,z) + \alpha \cdot B_x^{(э)}(x,y,z) \\ B_y(x,y,z) = \Delta B_y(x,y,z) + \alpha \cdot B_y^{(э)}(x,y,z) \end{cases} \qquad (3)$$

where $\alpha = 0.85$, and $\Delta B_x(x,y,z)$ and $\Delta B_y(x,y,z)$ are determined from (2).

The computed map lets to use measured magnet field,and also take into account nonlinear effects of the real magnet field.

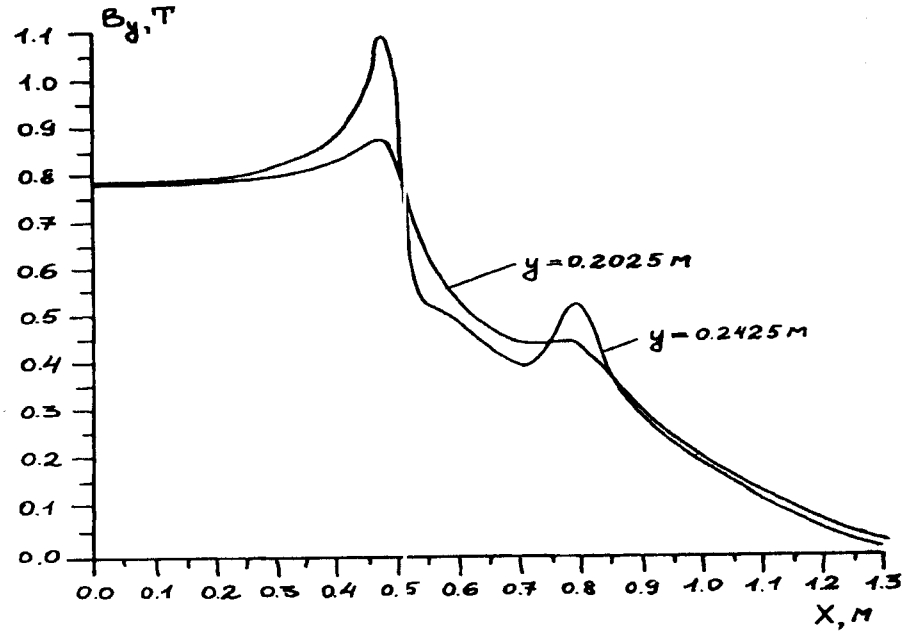

Fig. 3

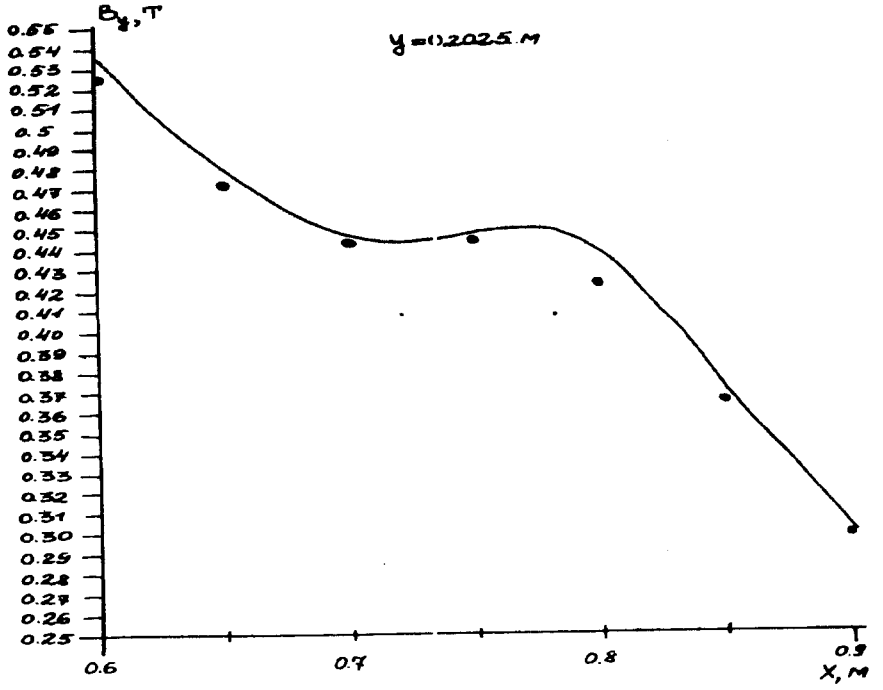

Fig. 4

4. The precision condition $u(\infty) = 0$

It should be noted, that the last version of the CPMMS-v.1.1 complex of programs [4] includes an algorithm for studying the magnetic field behavior at infinity. It has considerably expanded the region of the application of this program.

In the process of the numerical calculations of the SP-40A magnet field the complementary monitoring of the approximation accuracy of the $u(\infty) = 0$ condition is performed on the base of methods, using by anology with [6], an extrapolation according to the parameter R^{-1}, where

$$R = \max(l_x, l_y) \qquad (4)$$

and l_x and l_y are the lengths of the sides of rectangle limitting computative region Ω. It is supposed, that the error of the approximation of the boundary condition $u(\infty) = 0$ can be expanded in a series by power of parameter R^{-1}. For the considered task the following algorithm was used. The boundary value problems are solved for the sequence of widenned regions Ω_k, $k = 1, \ldots, M$, having in pairs different values R_k from Eq.(4). Then the values of $u_k(p)$ solutions (at various K) are compared in the check points P of the computative region Ω. If for this chosen $\varepsilon > 0$, the condition

$$\|u_k(p) - u_{k+1}(p)\| \le \varepsilon, \quad p \in \Omega \qquad (5)$$

is fulfilled, we suppose that condition $u(\xi)$, where ξ belongs to the boundary of the computative region, will satisfactorily approximate the boundary condition $u(\infty) = 0$. If one apriori supposes that there is a the regular expansion in series by power of parameter R^{-1} for the approximation error of the condition on infinity:

$$u_R(p) = u(p) + \frac{1}{R^{\gamma}} g(p) + O(R^{-\beta}), \quad \beta > \gamma > 0 \qquad (6)$$

where $u(p)$ is the exact solution of the Poisson equation, and a function $g(p)$ does not depend on R, then one can exclude the second term in Eq.(6) by means of extrapolation. For this purpose we will define numbers γ_1, γ_2 from the system of equations

$$\gamma_1 + \gamma_2 = 1, \quad \gamma_1 R_1^{-\gamma} + \gamma_2 R_2^{-\gamma} = 0, \quad R_1 \neq R_2 \qquad (7)$$

where R_1, R_2 correspond to two various computative regions. Then the linear combination

$$\tilde{u}(p) = \gamma_1 u_{R_1}(p) + \gamma_2 u_{R_2}(p) \qquad (8)$$

satisfies the estimation

$$\|u(p) - \tilde{u}(p)\| \le O(R^{-\beta}) \qquad (9)$$

i.e. approaches the condition $u(\infty) = 0$ with a high accuracy then each of u_{R_1} and u_{R_2}.

Using the described numerical algorithm, the configuration of the magnet SP-40A was calculated for two radiuses R_1 and R_2, parameter γ was taken equal to 2.

The solution (the magnitude of potential $u(p)$ was founded by using formula (8). That gave us a more exact coincidence with the experimental values of the magnet field.

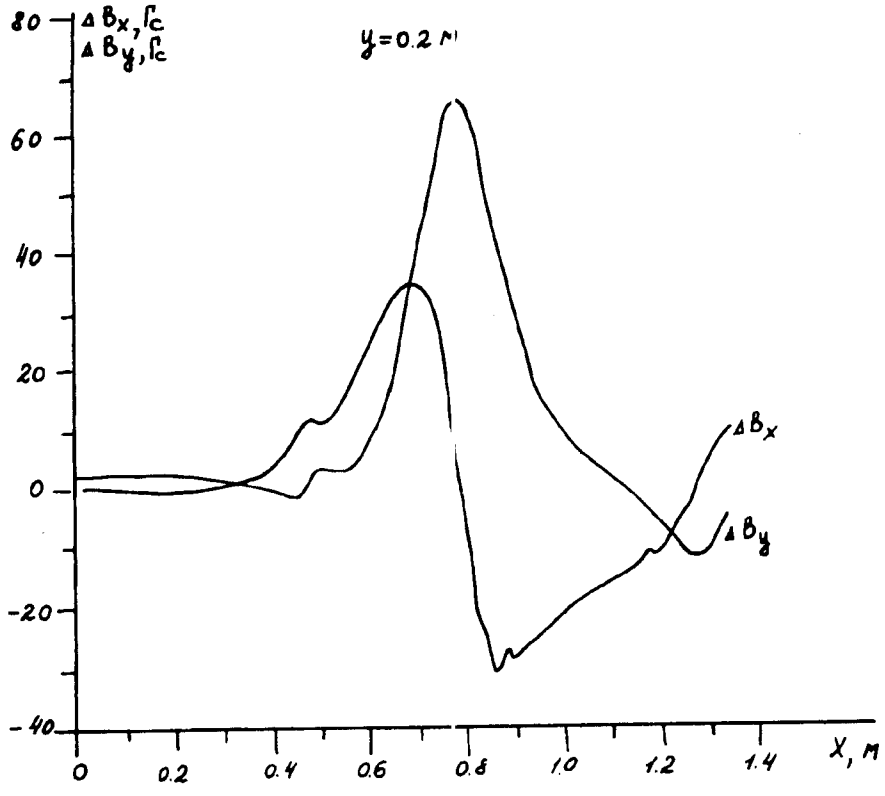

Fig. 5

5. Conclusions

1. The behavior of magnet SP-40A field for two work modes of spectrometer EXCHARM is investigated by using the complex of programs for the calculation of the magnet systems (CPMMS - v1.1).
2. The good consent of our computational model with the available experimental data has been received.
3. The magnet field map is suggested for experimental physical data processing that in the conditions of the second work mode of the SP-40A magnet of spectrometer EXCHARM (for session N 10).

References

1. Aleev A.N. et al. Observation of Σ_C^0 Charmed Baryon in the Experiment EXCHARM. - JINR Rapid Communication, 1996, No.3 [77] -- 96, pp. 31 --46.
2. Zhidkov E.P. et al. Calculation of the SP-94 magnet field for EXCHARM setup. - In present book, pp.
3. Potrebenikov Yu.K., Yudin I.P. et al. Measurements of the magnet field of spectrometer EXCHARM. - In Proceedings of XV Conference on Charged Particles Accelerators, (October 22--24, 1996, Protvino, Russia), IHEP, Protvino, 1996. vol.2, pp.186-190.
4. ZhidkovE.P., Lima S., Polyakova R.V , Fernandes Nodarse F., Yudin I.P. - The complex of programs for the modelling of magnetic systems, P11-93-256, Dubna, 1993.
5. Holsinger R. F., Iselin C., POISCR-r604, User Guide, CERN, SPS/EMA, 1982.
6. Zhidkov E.P., Khoromsky B.N. Preprint OVM AN USSR, n 137, M., 1987, p.40.

Calculation of Planar Systems for Proton Beam Transportation to the Patient

M.M. Kats , K.K. Onosovsky

Institute of Theoretical and Experimental Physics, Moscow, Russia.

The system for transportation of a beam used for proton therapy is suggested. In this system a prone patient is placed perpendicularly to the beam axis. The beam is bent and focused in the vertical plane in such a way that makes possible patient irradiation from any direction. Three versions of such a system are discussed. All of them give the opportunity to transport protons with energy up to 250 MeV and R*R'. up to 10 mm*mrad to targets with linear size in the interval between 10 and 300 mm. As compared to systems described in this paper have smaller weight of movable equipment, occupy less space and consume less power.

It is know that for successful application of proton beam therapy it is necessary to have the system for the proton beam transportation from the accelerator to the lying patient witch permit target irradiation from various direction. These systems have to transport proton beams with energies from various 70 to 250 MeV and transversal phase volume characteristic. for the slow extraction of the beam from the proton synchrotron [1]. At the same time they have to provide active formation of necessary dose fields using three-designed and introduced into medial practice [2,3]. However these systems have some features that put obstacles into the way of wide introduction into medical practice. These features are their size (5 x 13 x 13 m), weight of the movable equipment (up to 90 tons) and necessary electric power (the field of 15 kGs turns the beam to the angle of 360 degrees at the magnet cross0section of about 50 x 50 mm).

Trying to solve this problem, we have since 1993 designed several versions of the PLANE GANTRY [4,5,6,7]. In the traditional systems the patient is placed along the proton beam axis (towards the center of the irradiate target) by the magnet system placed on the rotating platform (Figure 1a) We proposed to place the patient perpendicularly to the beam axis and to turn anc focus the beam in the vertical plane (Figure 1b). We used a vertical concrete wall as a main constructive supporting element. We used beam focusing by the quadrupole's lenses to diminish magnet field volume and to provide necessary beam size on the target. We supposed that for target irradiation from various directions it is possible to rotate the table with patient around the vertical axis to 180 degrees. We supposed that active scanning of the long targets can be provided in the pane of beam turns by one scanning magnet, along the patient axis – by the show (about 1 cm/s) movement of the procedure table and in the depth – by the corresponding alteration of proton of proton energy and by using filters.

All the versions of PLANE GANTRY described here are preliminary. All the versions were calculated by using programs TRANPORT [8] and REVMOC [9] to let through the proton beam with energy up to 250 MeV and transversal half-size up to X*X'=Y*Y'=2mm*5mR and dP/P=0.1%.

In the paper [6] the version of PLANE GANTRY was described in witch only part of the magnet equipment is movable and the procedure table with the patient is stationary (Figure 2). In this version the proton beam is first transported through one of the nine stationary magnetic channels. The platform with movable magnets moves along the rails placed on the vertical wall. Beam direction is defined by its turns in the last stationary and the last movable magnets. It is supposed that the proton beam was focused in the initial point 1. Then stationary quadrupole lenses refocus it into the

center of the stationary bending magnets (in this way small cross-section of the beam in these magnets and thus small size, weight and consumed power are provided). The scanning magnet, two quadrupole lenses and the last magnet with enlarged cross-section are placed on the trolley. In comparison with traditional systems this system takes up less space in the building. The system needs less electric power (bending angles are up 200 degree at magnet cross-section of 20 x 80 mm). The weight of movable magnetic equipment is small enough – of about 3 tons.

It is worth noting two significant medical advantages of this system. Medical personnel is able to reach the lying patient from every side right before and after irradiation. Thus it is possible to think about partial combination of functions of the operation and the procedure tables. Beside there is a possibility to irradiate the patient from the directions not lying in the plane perpendicular to the patient axis by using table rotation in horizontal plane. This may permit to wide the possibilities of the proton therapy usage.

In the paper [7] the sample version of PLANET GANTY is described in which all magnetic equipment is stationary and only the table with patient and accompanying medical equipment are movable (Figure 3.). The necessity to move the table is a significant and obvious defect of such construction. This system may however be useful if there is few room or the height of the building is less than necessary because this system has relatively small size (3 x 7 x 8 m). It is worth noting that movable table was used before (PSI) and is sometimes considerate in designing such systems [3].

The compromise version of PLANET GANRTY is shown in Figure 4. In it all magnetic equipment is stationary, the system takes up few space and electric power and small weight. The necessity to move the table with the patient a little (with the platform for the medical personnel and accompanying medical equipment) doesn't interfere much with the medical work. Its construction resembles the one shown in Figure 2. Nine magnetic channels are placed on the vertical wall and they work one at a time. Each channel can transport the beam to the target in the limits of its direction interval (30 degrees) using beam turn in the last magnet and the corresponding shift of the procedure table axis in the vertical plane. (This shift doesn't exceed 70 cm.) As the platform moves together with the table axis medical personnel has circular access to the patient at all irradiation direction. In this version there is also a possibility to irradiate the patient from the directions not laying in the plane perpendicular to the patient axis. For the irradiation from the lower hemisphere the platform has a slot witch is opened only in time of irradiation. The cross-section of the stationary bending magnets gap is 20 x 80 mm, maximum beam turn angle is 200 degrees maximum magnetic field is 15 kGs. Stationary quadrupole lenses with product of aperture diameter to the lens length d x l of 60 x 300 mm are used in stationary magnetic channels. The total weight of movable equipment doesn't exceed 500 kg. The place necessary for the magnetic equipment is 1 x 15 m at a height of 14 m and beside it is necessary to have 5 x 5 x 6 m for the procedure table, medical equipment and medical personnel.

It seems to us that in designing new medical centers for proton therapy it is useful to consider the systems like PLANET GANTRY along with traditional systems for beam transportation.

The authors are grateful to V.S. Khoroshkov, V.M. Breev, L.L. Goldin for useful discussion of this paper.

K.K. Onosovsky died in 1995. He was the leader of the ITEP proton synchrotron. He was the inventor of H- accelerator in medical purpose. PLANE GANTRY is his last work.

a Usual GANTRY

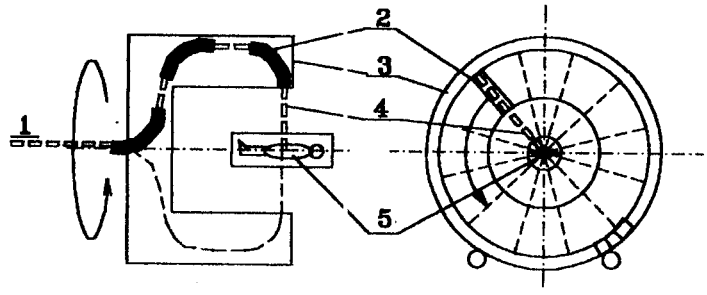

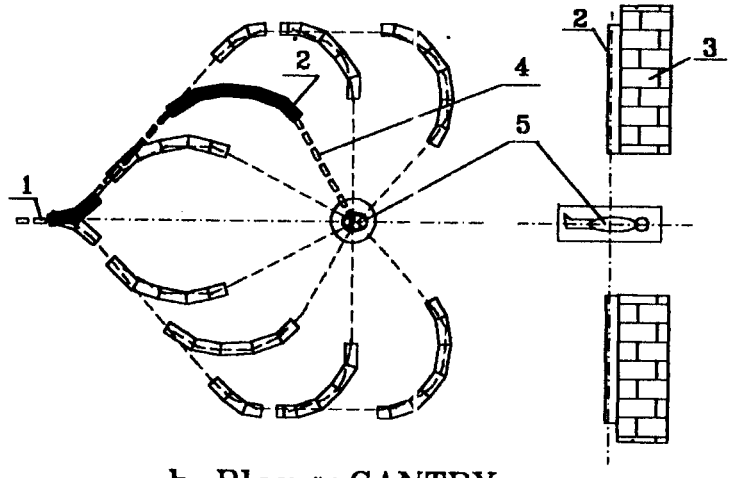

b Planar GANTRY

c Planar GANTRY with movable patient

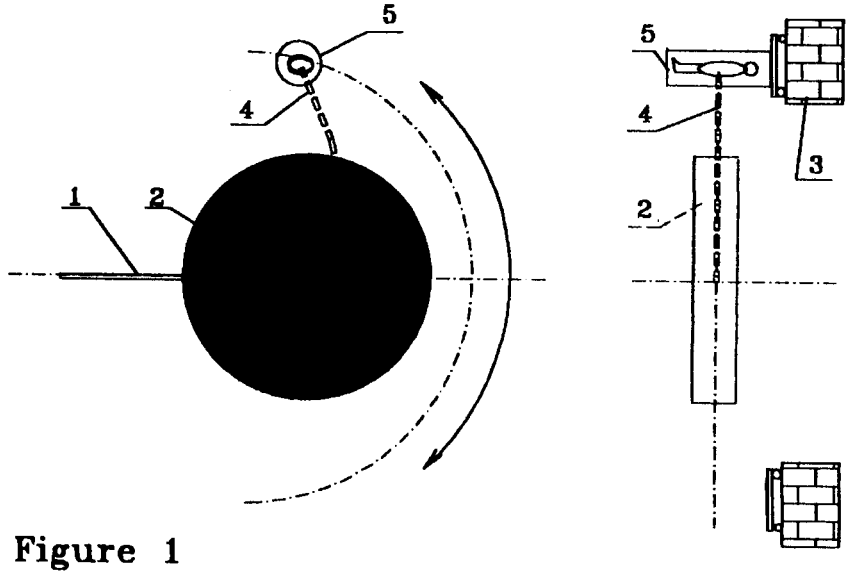

Figure 1

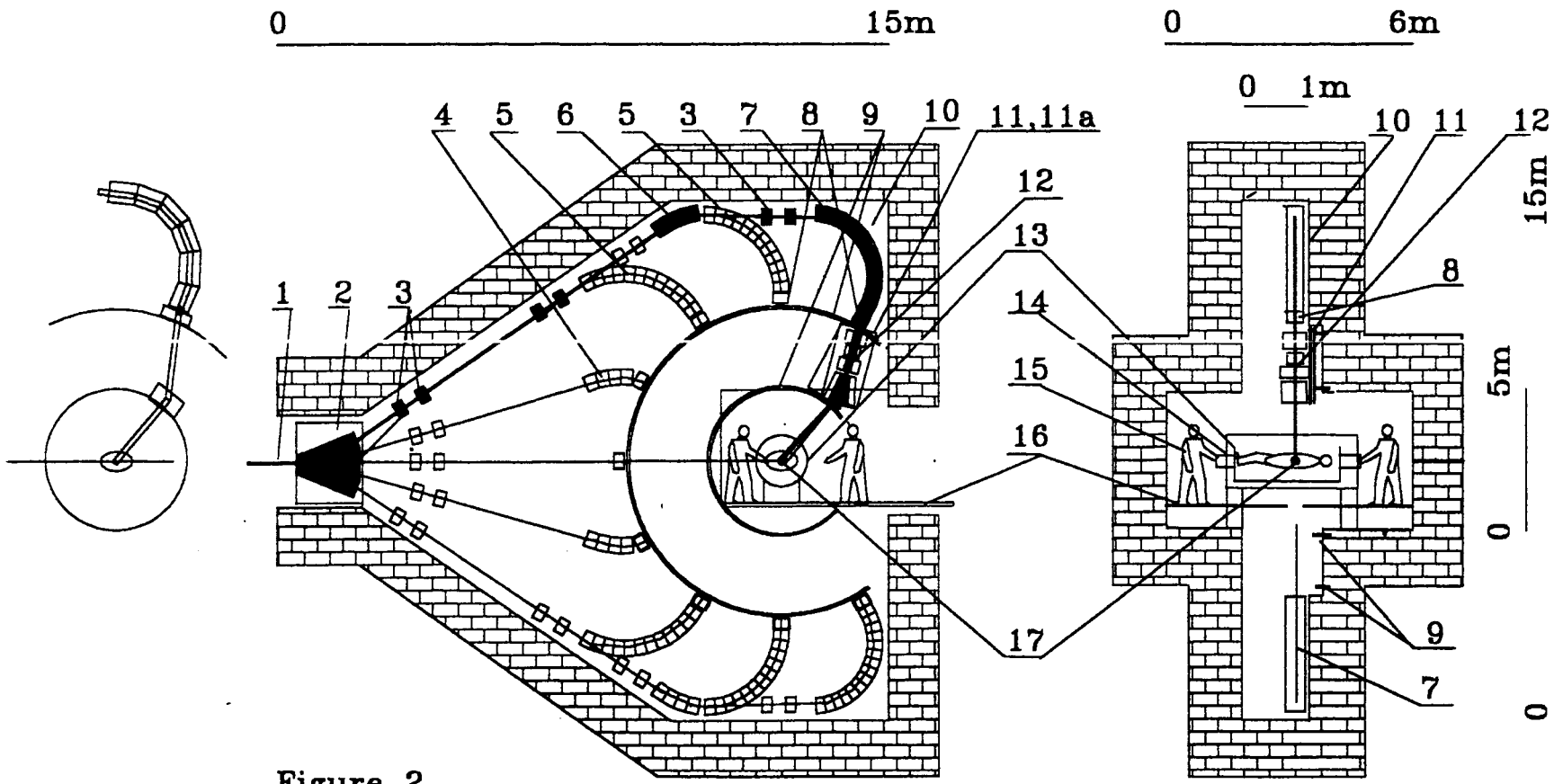
0
15m
0
6m
0 1m
4 5 6 5 3 7 8 9 10 11,11a
12
13
14
15
16
17
1 2 3
10 11 12
8
9
7
15m
5m
0
0

Figure 2

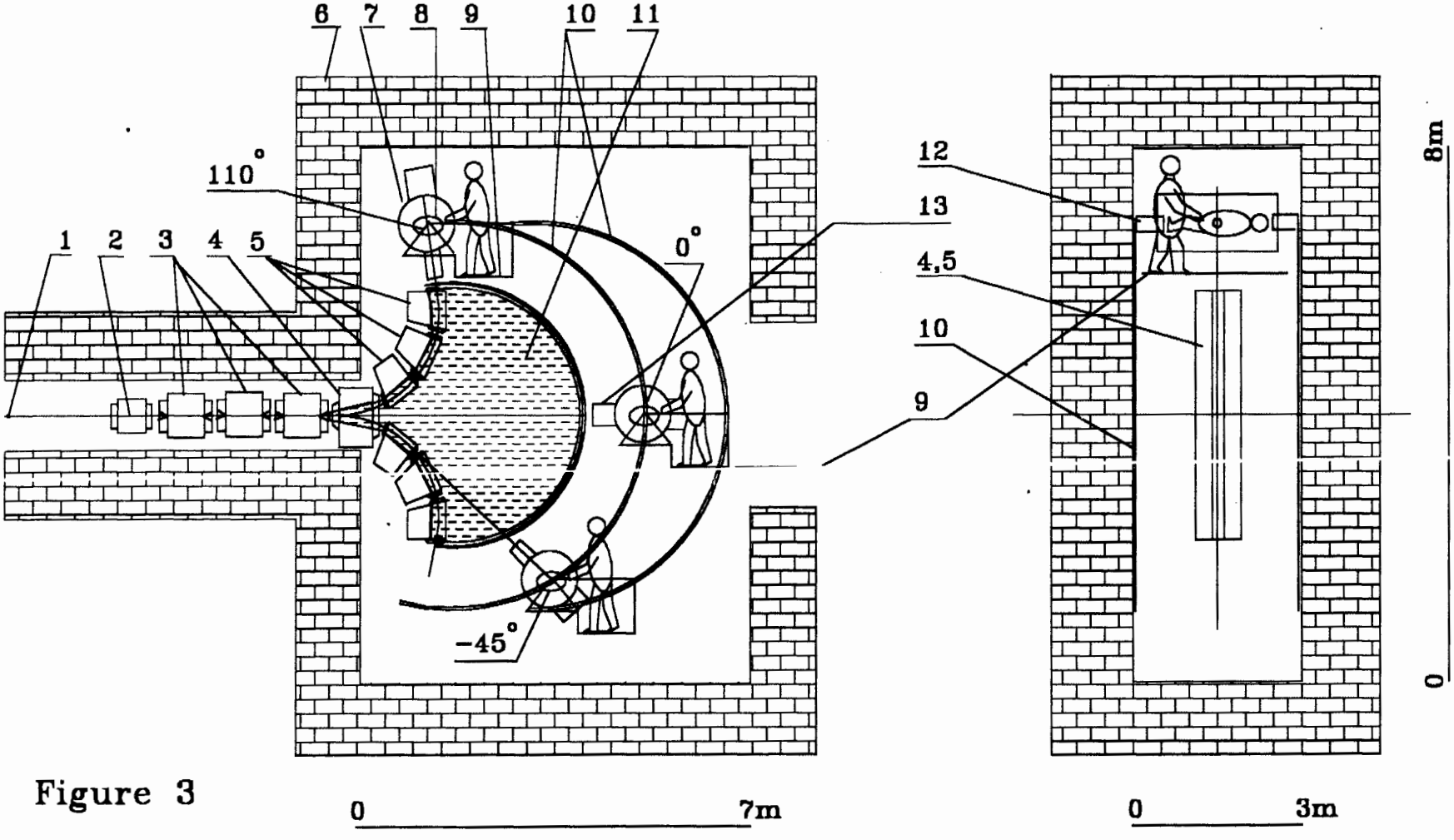

Figure 3

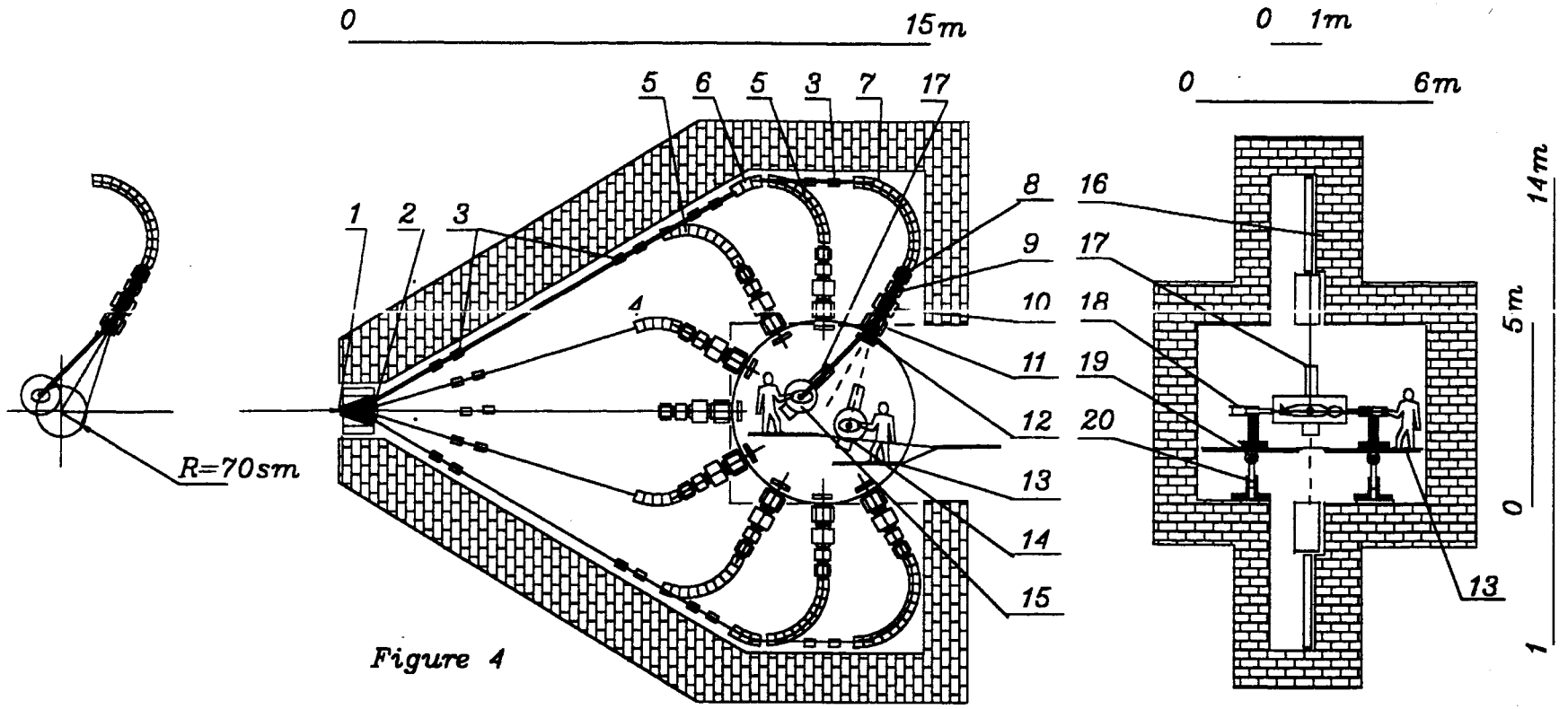
0
15m
0
1m
0
6m
5
6
5
3
7
17
1
2
3
4
8
9
10
11
12
13
14
15
16
17
18
19
20
R=70sm
14m
5m
0
1
13

Figure 4

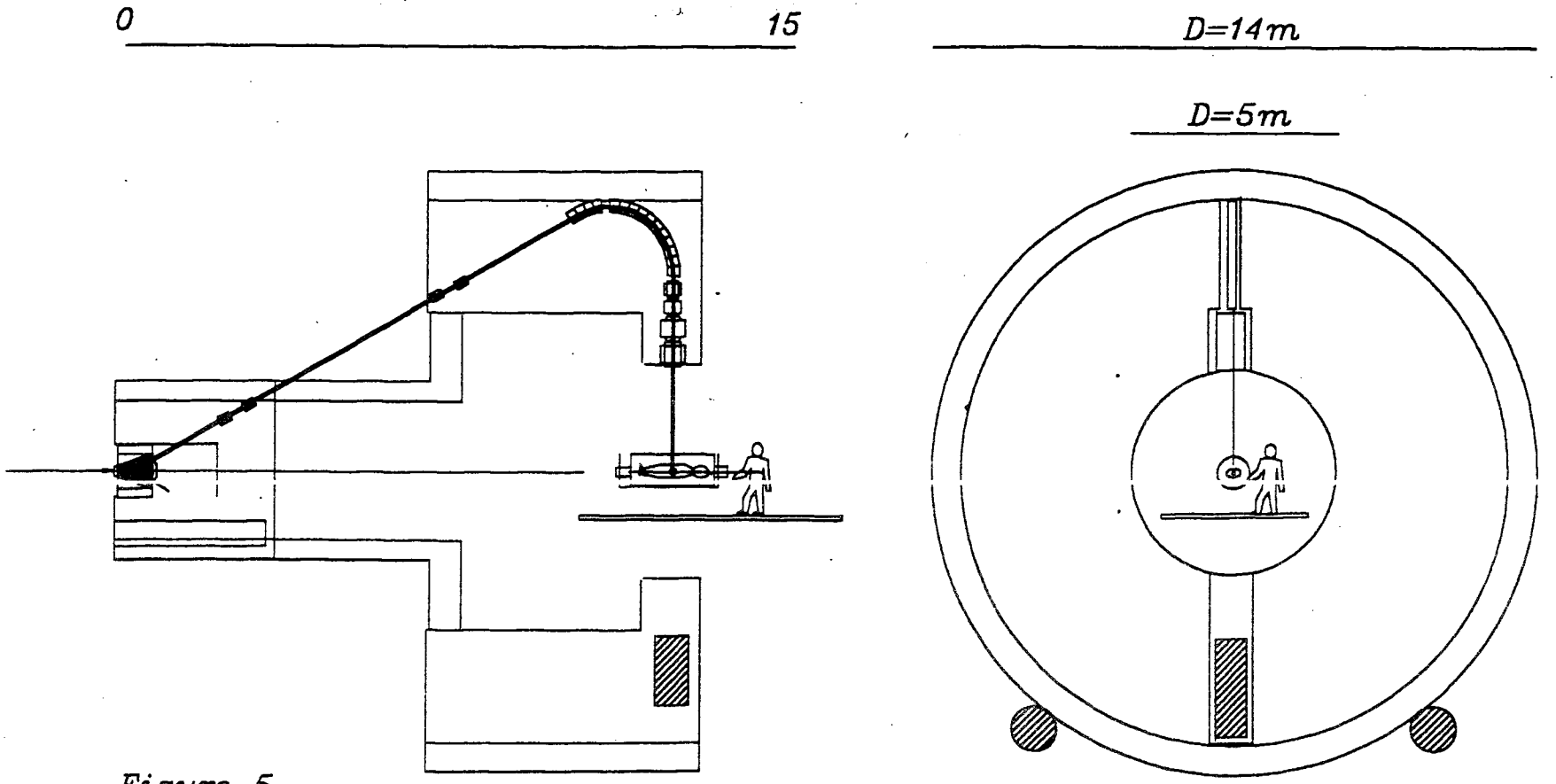

Figure 5

Figure 1a. The layout of the beam transportation in usual GANTRY
1. Direction of the proton beam.
2. Magnets.
3. Rotated frame.
4. Direction of the beam transportation.
5. The procedure table with the patient

Figure 1b. The layout of the beam transportation in the PLANAR GANTRY
1. Direction of the proton beam.
2. Magnets.
3. Vertical wall.
4. Directions of the beam transportation and working magnet channel.
5. The procedure table with the patient

Figure 1c. The layout of the beam transportation in the PLANAR GANTRY with movable patient
1. Direction of the proton beam.
2. Magnets.
3. Vertical wall.
4. Directions of the beam transportation and working magnet channel.
5. The procedure table with the patient.

Figure 2. The layout of the PLANAR GANTRY with partially movable magnetic equipment
1. The point of focusing of the proton beam.
2. The magnets bending the beam by the angles up to 30 degrees.
3. Quadrupole lenses.
4. The magnet with the bending angle of 45 degrees.
5. The magnet with the bending angle of 90 degrees.
6. The magnet with the bending angle of 30 degrees.
7. The magnet with the bending angle of 120 degrees.
8. The last stationary magnet with bend angle less than 12 degrees.
9. The rails along which the platform moves.
10. The vertical wall to which all magnets and rails are attached.
11. The platform that can be fixed with the step of 30 degrees moving along the circular rails.
11a. The frame that can turn by the angles up to 15 degrees with respect to the platform
12. Movable magnetic equipment: the scanning magnet, two quadrupole lenses with enlarged cross-section and the magnet that bends the beam by the angles up to 25 degrees.
13. Procedure table with the patient.
14. The mechanism of the axial shift of the procedure table.
15. Medical personnel.
16. The platform for the medical personnel.
17. The irradiated target.

Figure 3. The layout of the PLANET GANTRY with minimum size and movable procedure table.
1. The point of focusing of the proton beam.
2. The scanning magnet.
3. Quadrupole magnet.

4. The distributing magnet bending the beam by the angle up to 25 degrees.
5. C-shaped magnets with the winding pole : in each of them the beam is bent by the angle up to 25 degrees.
6. Radiation protection around the insallation.
7. The procedure table.
8. The patient.
9. The platform for the medical personnel witch is moved to the necessary position with the procedure table.
10. The rails attached to the vertical wall.
11. Plane vacuum camber in which proton beam is transported after its the magnets by the necessary angle.
12. The mechanism of the axial shift of the procedure table.
13. **Medical equipment.**

Figure 4. The layout of the PLANET GANTRY with stationary magnetic equipment and slightly movable procedure table.

1. The point of focusing of the proton beam/
2. The distribution magnet bending the beam by the angles to 30 degees.
3. Quadropole leses.
4. The magnet with bending angles of 45 degrees.
5. The magnet with bending angles of 30 degrees.
6. The magnet with bending angles of 90 degrees.
7. The magnet with bending angles of 120 degrees.
8. The scanning magnet.
9. The quadropole lens with enlarged cross-sect on.
10. The quadropole lens with enlarged cross-sect on.
11. The magnet with the bending angle of 15 degrees.
12. Beam monitor.
13. The platform for the medical personnel witch is shift together with the procedure table. During the irradiation from below a slit is open in the platform.
14. Position of the procedure table with the patient during the irradiation from the direction of 115 degrees.
15. Position of the procedure table with the patient during the irradiation from the direction of 115 degrees.
16. Vertical wall with stationary magnetic equipment attached to it .
17. The frame with movable medical equipment.
18. The mechanism of the axial shift of the procedure table during the irradiation.
19. The mechanism of the horizontal shift of the platform during the change of irradiation direction.
20. The mechanism vertical shift of the platform during the change of irradiation direction.

Reference

1. Cho W.T., Staples. J.E., Ludewigt. B.A. et al. Performance Specifications for Proton Melity, BNL report #33749, March 1993.

2. Slater. J. E., Archameau. J.O., SlaterJ.D. Proc. Int. Workshop on Heavy Charged Particle The Related Subjects, Chiba. Japan, 1991.

3. Mitschal K.B., Koehler A.M., Sisterson J.M. and Wanger M.S. Proc. Proton Radio the Workshop at PSI, Switzeland, PSI Report, p. 111.

4. Kats M.M. Onosovskii K.K. Prib. Tekh. Exp., 1993, #4, p.163-166
Kats M.M. Onosovskii K.K. Prib. Tekh. Exp., 1994, #4, p.157-160
Kats M.M. Onosovskii K.K. Prib. Tekh. Exp., 1996, #1, p.142-146
Kats M.M. Onosovskii K.K. Prib. Tekh. Exp., 1996, #1, p.147-149

5. Brown K.L., Carry D.C., Iselin Ch., Rotacher F. TRANSPORT, CERN 80-04,1980.

THE SIMULATOR OF MICROTRON [1]

V.P.Gorbachev, S.V.Yerokhin, V.P.Stepanchuk, V.V.Shlyapin

Department of Physics, Saratov State University, Astrakhanskaya 83, Saratov 410601 Russia.
E-mail: serg@sgu.ssu.runnet.ru

The program packet, simulating the work of microtron with microwave supply system on the base of magnetron, has been described. Its basis is the program for the calculation of the transition processes in microwave supply system of the microtron. While woking with the packet the calculated pulses of injection current from cathode microtron and accelerated current are being displayed at the monitor screen. The values of main parameters of accelerator systems are also being shown on the screen and may be immediately changed. The programme packet may be used for training of microtron operators and teaching of students of physics of electron accelerator specialization.

The software package is designed to simulate the work of microtron with microwave supply system on the base of magnetron connected with accelerating cavity through ferrite isolating unit.

The packet consists of: a program-shell and a program Lar-Sim that calculates transition prosseses in microwave supply system of microtron (including pulses of injection current from microtron cathode and accelerated current), and three files with the data necessary from the mentioned above program.

The program-shell designed to simulate a control mechanism of an accelerator is written in Fox-Pro 2.6 language with the use of its standard means and intended for work in Windows environment. At the monitor screen is displays pulses of injection from microtron cathode and accelerated current of the target, calculated by Lar-Sim program and also, main six parameters of microtron (average anod current of magnetron, generation frequency, "phase" and attenuation of accelerating cavity-reflected wave, current magnitude of injection from microtron cathode and driving magnetic field magnitude), also average current of injection and accelerated current. The main parameters are digitalized and can be changed promptly with the help of "mouse". After that the program-shell repeats the submit of Lar-Sim program and displays at the monitor newly calculated pulses of accelerated current and injection current. The results of the previous submit of a Lar-Sim program are also displayed at the monitor but their color is different.

Lar-Sim program is based on the program described in [1]. The following models of system units have been included: magnetron generator and accelerating cavity have been represented as single oscillators. These oscillators loaded on long lines where wave processes occur. Electron conductivity of magnetron is the function of anode voltage and microwave voltage at the corresponding circuit. Thus, the finite duration of the edge of puls of anode voltage supply and hard excitation of magnetron generator are taken into account. Electron load of accelerating cavity in [1] was represented as a model of beam with lag of "relay" type [2]. The power of accelerated electron beam of all orbits

[1] Work supported by the Russian Foundation for Basic Research (grants No 96-02-16360A).

(and its current) at moment t is defined by the value of the amplitude of oscillations at time $t - \tau_e$ (where τ_e–time of electron path from the first to the last orbit). It has been assumed that interaction between beam and cavity takes place only at the first harmonic. Phase shift between the accelerating voltage and first harmonic of the current of **all orbits** in the frame work of this model is determined immediately. The elements of waveguide system have been represented as multipoles with corresponding matrices of scattering. The generalized equivalent circuit diagram of microwave supply system [1] on the base of mentioned above model representation has been drawn. Oscillation processes in it are described by the system of differential nonlinear equations with lag argument. To integrate the system the program achieving algorithm of Runge–Cutt of the fourth order is used. The program has been adapted for FORTRAN–51 that makes possible to use it in IBM compatible with PC.

The modifications introduced by us for model representation described in [1] concern primarily microtron beam model. Further development of the model with lag of "relay" type [2] has been carried out. Microtron orbits have been devided into three groups $(1 - N_1)$, $(N_2 - N_1)$, $(N_3 - N_2)$. At $N_3 = 20$ – is a number of microtron orbits $N_2 = 12$, and $N_1 = 6$. The summarized current that loads the accelerating cavity can be represented as:

$$I_e = I_{e1} + I_{e2} + I_{e3} + \alpha_k I_k \ , \tag{1}$$

where:

I_{e1} – is current of "first" $(1 - N_1)$ orbits;

I_{e2} – is current of "middle" $(N_1 - N_2)$ orbits;

I_{e3} – is current of "last" $(N_2 - N_3)$ orbits;

α_k – is a coefficient defined by the value of the power of cathode electron beam with accelerating cavity field interaction.

Current I_{e1}, I_{e2} and I_{e3} is connected with the current injected from microtron cathode as following:

$$I_{20} = K I_k \quad I_{e3} = K I_k (N_3 - N_2) \ , \tag{2}$$

where:

I_{20} – is current of accelerated electrons of the 20^{th} orbits;

K – is a capture coefficient;

I_k – is injection current from microtron cathode.

Using the curve of current distibution over the orbits for certain mode one can obtain coefficients connecting current of "first" and "middle" orbits with the "last" ones. In this case, as shown in fig.1. a smooth curve is replaced by a bar graph.Thus, (1) becomes:

$$I_e = I_k K [K_{13} N_1 + K_{23} (N_2 - N_1) + (N_3 - N_2)] \ , \tag{3}$$

where K_{13},K_{23} are coefficients connecting current of different groups of orbits.

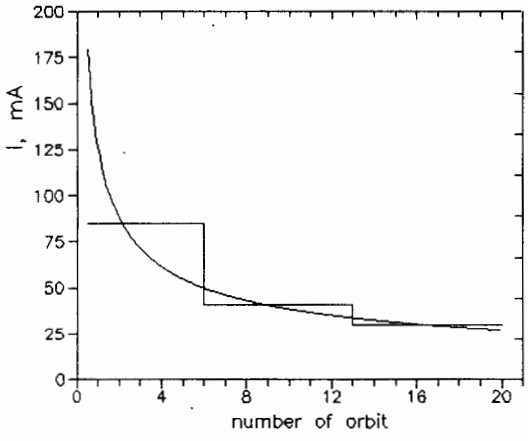

Fig.1. The dependance of accelerated current value on the number of orbit

The dependences of stationary value of the beam intensity on the oscillation ampitude in accelerating cavity have been calculated by calculation technique [2] for each group of orbits. The obtained dependences have been normalized on the maximum for each of their values. Thus, the functions $i_{e1}(v), i_{e2}(v), i_{e3}(v)$ describing the dependences of the beam current of three groups of orbits on the accelerating voltage have been obtained. Current of all orbits can be represented as followir g:

$$I_e(v) = I_k K \left[K_{13} N_1 i_{e1} + K_{23} (N_2 - N_1) i_{e2} + (N_3 - N_2) i_{e3}\right] \qquad (4)$$

$$i_{e1} = i_{e1}(v(\tau - \tau_{e1})) \quad i_{e2} = i_{e2}(v(\tau - \tau_{e2})) \quad i_{e3} = i_{e3}(v(\tau - \tau_{e3}))\,,$$

where: τ_{e1}, τ_{e2}, τ_{e2} are lag time corresponding to the three groups of orbits.

The values of I_e (4) and the average phase of a beam are used for the calculation of active and reactive conductivities of electron beam that is in equations describing oscillation processes in microwave supply system of microtron. Current of the 20^{th} orbit is estimated by equation (2).

The software package demands 520 Kbites. Recently the parameters of microtrone with 20 orbit have been introduced into data entry file. This S–band microtron has acceleration mode of $\Omega = 1,2$. Microwave supply system of microtron is made on the base of magnetrone MI–202. The form of modulator pulse is modified (nonuniformity of the plateau has been neglected). But in case of need the parameters of any of the microtron with any acceleration mode can be introduced to the data entry file of the package. The described software package can be used to train students specializing in physics and mechanics of accelerator and, probably, to train microtron operators.

References

[1] N.V. Vladimirov at all., The Simulation of Transition Processes in Microwave Supply Systems of Microtron. Saratov. 1991. *Dep. in VINITI*, **No 1837-B92 Dep.** 03.06.92.

[2] E.L.Kosarev. *JTF.* **Vol LXII**,(10) pp.2239-2247,1972.

MICROTRON WITH AUTOGENERATIVE MICROWAVE SUPPLY SYSTEM ON THE BASE OF AMPLITRON [1]

I.V.Alekseyev, N.V.Vladimirov, V.P Gorbachev, V.P.Stepanchuk

Department of Physics Saratov State University, Astrakhanskaya 83, Saratov 410601 Russia.

E-mail: serg@sgu.ssu.runnet.ru

The modernized microtron with autogenerative microwave supply system on the base of amplitron has been described in the paper. It has been desined for experimental research on the process of the acceleration and oscillation in microwave system at values of the relative electron conduction in the range of 2 – 10. The usage of acceleration mode with small increase of electron energy (Ω = 0.62 and Ω = 0.36) provides the increase of values of electron load.

Use of experience of microtron with autogenerative microwave supply system on the base of amplitron [1] shows that its main merit is simple and fast putting into operation. The system once tuned doesn't need any adjustment in subsequent turning on. Yet, up to now transition processes and steady state in such accelerators have been investigated at value of relative conductivity of the electron beam not exceeding 2. The beam of electrons of all orbits is nonlinear load of accelerating cavity with a lag response to the change of field amplitude in it. The increase of electron load can cause the change in acceleration process and the character of auto-oscillation processes in microwave supply system. The calculation results obtaned by us [2], prove the possibility of automodulation current in the beam of accelerated electrons to exist in the microtron. The present paper contains the description of a modernized microtron [1] that is planned to be a means for experimental research on the process of acceleration and oscillation in the autogenerative system when relative beam power is increased. The increase of relative power of electron beam is achieved due to realization of acceleration modes with $\Omega = 0.62$ and $\Omega = 0.36$ instead $\Omega \approx 1$. The first one has been suggested and obtained in Scientific Research Institute of Mechanics and Physics, Saratov State University [3]. It is applied in all X-band microtrons. The acceleration mode with Ω = 0.36 has been found experimentally [4] and up to now has not gained wide acceptance. The use of these acceleration mode will allow to achieve the values of relative conductivity of beams equal to 4 and 10, respectively.

An accelerator has 24 orbits, it corresponds to the finite energy of electrons – 8.6 and 4.3 MeV due to the acceleration mode. Driving magnetic field is induced by electromagnet of armour type. Vacuum chamber is made as a copper ring enclosed between electromagnet poles that are its sides. The copper shell has a rubber seal. Electromagnet is placed on a metalwork with vacuum system pumps and stabilized power inside it. The last provides the stability of the current of electromagnet with accuracy 0.5% and adjustment within the limits of 20% from assigned values that are specified depending on the applied acceleration mode.

The scheme of autogenerative microwave supply system that has been applied in accelerator is shown in fig.1. The key element of this scheme is amplitron – V1 with positive feedback circuit including accelerating cavity of passing type–W5. Amplitron output has

[1] Work is supported by the Russian Foundation for Basic Research (grants No96-02-16360 A).

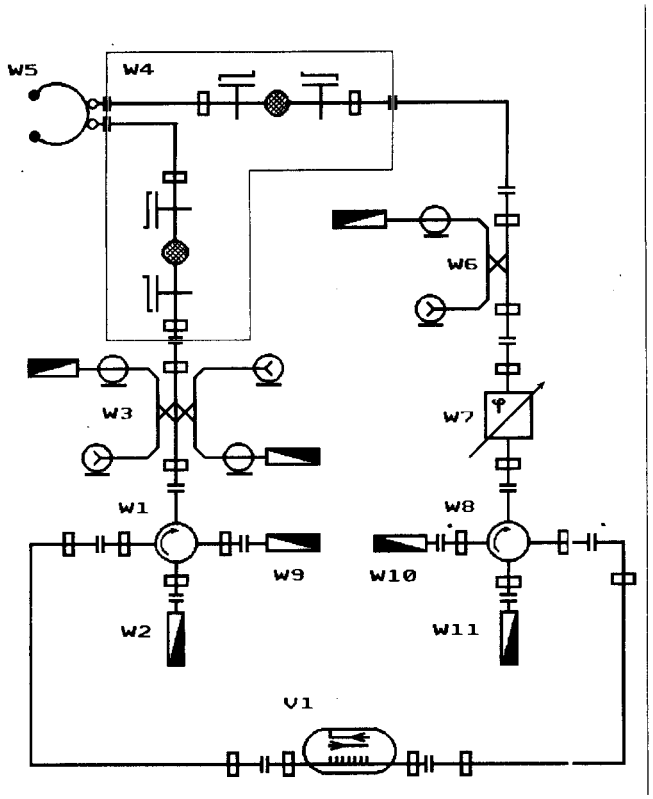

Figure 1: *The scheme of autogenerative microwave system on base of amplitron; V1 – amplitron; W1,W8 – circulators; W2,W9,W10,W11 – waveguide matched loads; W3,W6 – directional couplers; W4 – waveguide unit with ceramics windows; W5 – accelerated cavity; W6 – phas-shifter.*

been matched cavity input with the help of a circulator – W1. To measure the power reflected from cavity to the third channel of the circulator – W1, instead of load – W4, a measuring load of the wattmeteer M3–13 can be switched. The values of the power supplying cavity, reflected from cavity and passed through it are measured by wattmeter M3–51, where signals from directional coupler – W3,W6. Phase shifter – W7 allows to find optimal conditions for generation at the eigenfrequency of cavity. To avoid a parasite autoexcitation of the amplitron its input and output of cavity are isolated from each by circulator –W8. The application of circulator is connected with planned experiments with big feedback coefficients and abrupt increasing of an output power of the cavity without electron beam load. An attenuator can be connected to the circuit between the cavity output and amplitron input. The measurements of oscillation parameters and the observation on their enveloping have been carried out with the help of spectrum analyzer C4–27 and cavity waveguage. Accelerating cavity – W5 must provide the assigned modes

of the work of accelerator and autogeneiator. It has two coupling windows. The main window provides the connection with a wavegiude by which cavity is supplied by microwave power.The power which is needed for auto-oscillation mode is got from cavity through the second window. The coefficient power transmission through cavity at resonance frequency is defined by formula:

$$\tau = \frac{4\,\beta_1\,\beta_2}{(\beta_1 + \beta_2 + \eta_e)^2},$$

where:

β_1, β_2 – the coupling factor of cavity with input and output waveguides;

η_e – relative conductivity (power) of electron beam.

The values $\beta_1, \beta_2, \eta_e^0$ – according to the assigned coefficient of the cavity transmission – τ can be defined by the technique [5] (here η_e^0 is the value of relative electron power at which the cavity is matched on the waveguide input side. This technique gives good results at $\tau = 0.1 - 0.2$ (it takes place when microtron is in use [1]). During experiments the value of τ assums to be varied in the limits of 0.1 – 0.5. In this case for engineering calculation of the cavity parameters it is advantageous to use the obtained from [5]:

$$\beta_2 = \frac{K_{oc}\,P_g}{P_r(1 - K_{oc})}$$

$$\eta_e^0 = \frac{P_g\,S_1}{P_r\,(1 - K_{oc})} - 1 - \beta_2$$

$$\beta_1 = \frac{P_g\,S_1}{P_r\,(1 - K_{oc})},$$

$$K_{oc} = S_1\,S_2\,\tau$$

where:

P_r is the power of loss by the cavity surface, which is necessary for acceleration mode realization;

P_g is the power of oscillations, induced in retarded system of amplitron by an electron flow (it is found experimentally at an assigned feedback coefficient and anode current corresponding to the quenching of oscillations in the second zone);

K_{oc} is a feedback coefficient at an assigned load of cavity;

S_1, S_2 are the coefficients of the power transmission of output and input circuit of amplitron, respectively.

The accelerating cavity is made of a vacuum copper, it consists of a case cooled by water and a cover attached to it screw heads. On the cover there is a directly heated cathod made of $La\,B_6$ of a cylinder form. It is put deeper into the cover surface and placed in cone hole as has been suggested in [6]. The size of the cone hole, the cathode and the depth of the hole have been estimated according to the results given in [7]. It has allowed to increase the size of emitting surface as twice and hence to get the larger injection current. Coupling windows are made on the generatrix of a cylinder cavity in a line. To connect the

cavity with other autogenerative scheme units a special waveguide element– W4 is used. It consists of two waveguides having one common side. The waveguide connected to the cavity input has a standard cros section, while the size of narrow side of the waveguide, where the signal is divided into a feedback circuit, is reduced. The Chebyshev's transition to the normal cross section is placed in vacuum. The vacuum part of both waveguides is separated by ceramic windows. Electric contact between the cavity and waveguides is implemented by leed plates. To cool the system elements a double–coutour system of the water–cooled with thermostat coolant is used. In non–vacuum part of microwave track the exceeding power of 2 atm occurs.

Recently the optimization of acceleration mode with $\Omega = 0,62$ has been completed. The feedback circuit has been disconnected, while an amplitron has been connected according to scheme of a classic stabilitron. Pulses beam current of the 20^{th} orbit equals 12 mA at $\eta_e \approx 4$. After feedback circuit has been connected, the investigation on the process of acceleration in microtron with autogenerative microwave system at the increased values of electron load can be started.

References

[1] I.V.Alekseyev et al., *Proc. of the 8^{th} All Union Conference on Charged Particle Accelerators.* Protvino, Okt 19–21, 1982. JINR, Dubna, **Vol.2.** pp. 41–43, 1983.

[2] V.P.Gorbachev et al.,*Proc.of Second International Workshop "Beam Dynamic and Optimization"*. St.-Petersburg State University Press. p.16, 1995.

[3] F.V. Rodionov, V.P. Stepanchuk. *JTF.* **Vol. 41** pp. 999–1001, 1971.

[4] I.P. Petryajev et al., *In Book: The Problems of Theoretical and Nuclear Physics. Electromagnetic Interactions (Elementary Particles and Atomic Nuclear).* Saratov University Press. **Issue.8.** pp. 5–8, 1982.

[5] N.V. Vladimirov et al., *In Book: The Problems of Theoretical and Nuclear Physics. Electromagnetic Interactions (Elementary Particles and Atomic Nuclear).* Saratov University Press. **Issue.8.** pp. 27–38, 1982.

[6] M.A.Zakharov et al., *JTF.* **Vol.47** pp.593–599, 1977.

[7] A.Ju.Balayev et al., *Proc. of the 12^{th} All Union Conference on Charged Particle Acceleerators.* Moscow, Okt 3–5, 1990. JINR, Dubna, **Vol.2** pp. 35–36. 1992.

ON THE AUTOMODULATION OF THE BEAM CURRENT IN MICROTRON WITH AUTOGENERATIVE MICROWAVE SYSTEM AT THE AMPLITRON [1]

V.P. Gorbachev, V.P. Stepanchuk

Department of Physics, Saratov State University, Astrakhanskaya 83, Saratov 410601, Russia.
E-mail: serg@sgu.ssu.runnet.ru

The calculation results showing the possibility of amplitude automodulation of accelerating beam current in microtron with autogenerative microwave system on the base of amplitron have been obtained in more precise form. The model of microtron beam with the lag of "relay" type has been modified. This alowed to take into account the influence of the electrons that are lost at the first orbits.

Use of experience of microtron with autogenerative microwave supply system on the base of amplitron [1] has shown that its main advantage is the simple and immediate putting into operation. The system once tuned does not need any adjustment in consequent turning on. Recently, transition process and steady state in such accelerators have been investigated at values of relative conductivity of beam not exeeding 2. Electron beam at all orbits is nonlinear load of accelerating cavity with a lag response to the change of the amplitude in it. The increase of electron load can result in the qualitative changes of accelerating process and the character of oscillation processes in microwave system. Calculation results [2] obtained by us prove the occurrence of the automodulation of beam current in microtron with autogenerative microwave system on the base of amplitron. The aim of this paper is to precise the result obtaned in [2].

In autogenerative systems amplitron is chained by a positive feedback circuit which includes accelerating cavity and matching elements. The autogenerative microwave supply system with external feedback circuit is schematically shown in Fig.1. It includes

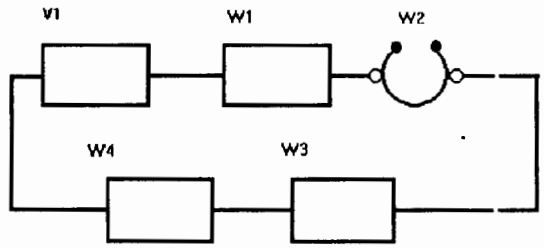

Fig.1. The scheme of autogenerative microwave system of microtron with external feedback circuit, connected through accelerated cavity: V1 - amplitron; W1,W4 - ferrite isolating units; W2 - accelerating cavity with two coupling elements; W3 - phase-shifter.

amplitron - V1, ferrite isolation units - W1,W4; accelerating cavity with two coupling elements - W2 and phase-shifter - W3. The amplitude conditions of generation are proved by the choice of the coefficient of cavity transmission whereas phase conditions - by the valteration of the position of phase-shifter - W3. A detailed description of this system can be found in [3].

[1] Work supported by the Russian Foundation for Basic Research (grants No 96-02-16360 a).

To describe oscillation process in microwave system, model representations analogous to [4,5] have been used. The cavity with two coupling elements has been represented as single lumped circuit connnected with two long lines and loaded by the current of electron beam. It has been assumed that interaction between beam and cavity takes place only at the first harmonic. The amplitron has been considered as a four-pole with assigned amplitude characteristics. Other system units have been described by matrices of scattering and lag time. These model representations have allowed to get the system of differential equations for oscillation processes in autogenerative microwave supply system of microtron. The equation given below has been obtained for the autogenerative system with external feedback circuit (their orders have been reduced by the method of slowly changing amplitudes).

$$\begin{cases} \frac{dV}{d\tau} + (\alpha + G_e)\,V - [C\,V(\tau-\tau_1) - D\,U(\tau-\tau_1)]\cos(\Psi(\tau-\tau_1) - \theta_1 - \Psi) = 0 \\ \frac{d\Psi}{d\tau} + \Delta\Omega + B_e - [C\,\frac{V(\tau-\tau_1)}{V} + D\,\frac{U(\tau-\tau_1)}{V}]\sin(\Psi(\tau-\tau_1) - \theta_1 - \Psi) = 0 \end{cases} \quad (1)$$

$$\alpha = 0,5\,\omega_0\,(\beta_1 + \beta_2 + 1)/\omega_s Q_0 \quad \Delta\Omega = 1 - \omega_0/\omega_s \quad \tau = \omega_s\,t.$$

where:

C,D – are constant defined by cavity parameters and losses in microwave system units;

V – is slowly changing normalized amplitude microwave voltage at the cavity (the normalization has been carried out into voltage amplitude corresponding to the power of acceleration mode losses);

U – is the slowly changing normalized amplitude of voltage induced in slow-wave system of amplitron by its electron flow;

Ψ – is slowly changing phase of oscillations in cavity;

θ_1 – is electric length of ring in waveguide system of autogenerator;

τ_1 – is summarized lag in the ring;

ω_0,ω_s – is resonance frequency of cavity and frequency of steady state oscillations in the system;

Q_0, – is q-factor of accelerating cavity;

β_1, β_2 – are coupling factor of cavity with input and output waveguides;

G_e, B_e – are active and reactive conductivities of electron beam (are to be discussed later).

Electron load of accelerating cavity has been described by the suggested model of microtron beam with lag of "relay" type [6]. The power of beam of all orbits at moment τ defined by the oscillation amplitude in cavity at moment $\tau - \tau_e$. Lag τ_e approximates the time of electron flight from the first to the last orbit. Phase shift between the first harmonic of beam current and accelerating voltage is determined immediately. Then active and reactive electron conductivities can be expressed as following :

$$G_e = (\eta_e + \frac{db_e}{d\tau})/2Q_0 \quad B_e = (b_e + \frac{d\eta_e}{d\tau})/2Q_0\,, \quad (2)$$

where:

$$b_e = \eta_e(V(\tau - \tau_e))\, tg(\varphi_e) \quad \eta_e = \eta_e(V(\tau - \tau_e)) \quad \eta_e = P_e/P_r$$

P_e – is the power of accelerated electron beam;

P_r – is the power of loss in accelerating cavity;

η_e, b_e – are the relative active and reactive powers (conductivity) of electron beam;

φ_e – is a phase shift between accelerated voltage and the first harmonic of beam current.

The lag value of the last orbit, here in (2) is attributed to the beam spread over all orbits of microtron. So, the contribution of the first orbits to the reaction of the beam to the oscillation amplitude changing in cavity is estimated not exactly enough. For the further development of the model [6] microtron orbits (it was suggested that there are twenty of them) have been devided into three groups: the "first" – from the 1^{th} to 6^{th}, "middle" – from the 7^{th} to the 12^{th} and "the last"– from the 13^{th} to the 20^{th}. The value of electron load is distibuted between the groups according to the curve of distribution over the orbits, as shown in Fig.2.

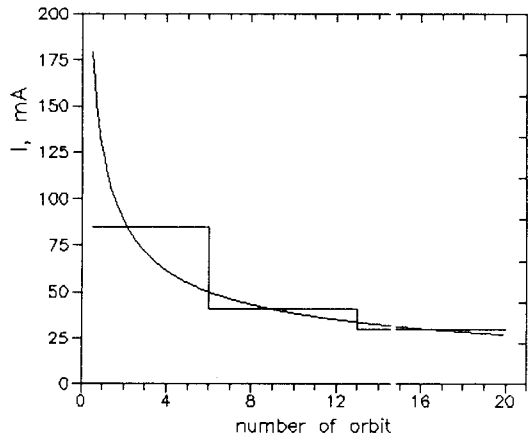

Fig.2.The dependence of accelerated current value on the number of orbit.

The lag for each group is equal to the time of electron fligth from the first orbit to the last one in the group. Then relative power of the beam can be written as:

$$\eta_e = \eta_{e1}(V(\tau - \tau_{e1})) + \eta_{e2}(V(\tau - \tau_{e2})) + \eta_{e3}(V(\tau - \tau_{e3})). \qquad (3)$$

where:

$\tau_{e1}, \tau_{e2}, \tau_{e3}$ – are the times of electron flight to the 6^{th}, 12^{th} and 20^{th} orbits.

Further, steady state of oscillations have been considered.It was assumed, that their frequency values are equal to the resonance of cavity and low deviations of amplitude from stationary values have been studied.

$$V = V_0 + V_1(\tau) \quad V_1 = V_1^0\, e^{(j\nu_1 + \nu_2)} \quad V_1 \ll V_0,$$

where:

V_0 – stationary solution of equation system (1);

$V_1(\tau)$ – is low disturbance of amplitude oscillation;

V_1^0 – is amplitude of low disturbance:

ν_1, ν_2 – is frequency and increment of low disturbance.

The system of equations has been linearized and characteristic equations with roots equal to frequencies and increments of amplitude disturbance have been obtained:

$$\begin{cases} \sum_{k=1}^{3} F_k \cos(\nu_1 \tau_{ek}) + \sqrt{\beta_1 \beta_2}\, e^{\nu_2} \cos(\nu_1 \tau_1) + \beta_1 + \beta_2 + 1 - 2\nu_2 Q_0 = 0 \\ \sum_{k=1}^{3} F_k \sin(\nu_1 \tau_{ek}) - \sqrt{\beta_1 \beta_2}\, e^{\nu_2} \sin(\nu_1 \tau_1) + 2\nu_1 Q_{=}0 \end{cases} \tag{4}$$

$$F_k = (\eta_{ek} + V_0 \frac{d\eta_{ek}}{dV})\, e^{-\nu_1 \tau_{ek}}.$$

We have analyzed the indices of increments of amplitude disturbance. In cases when roots are real ($\nu 1 = 0$) the values have been obtained by calculation. To define increment indices of complex roots the method D-splitting has been used [7]. The main specified parameters of steady state of system are:electron load – η_e, the amplitron gain at a working point K_a and an equilibrium phase – φ_s. The parameters of cavity with two coupling elements have been chosen according to the calculation technique [3].

Main results are as follows: In the system under consideration aperodical increase of disturbance of oscillation amplitude. Typical dependences of increment of electron load to series of values are shown in Fig.3. At the increasing η_e dependence of increment increases

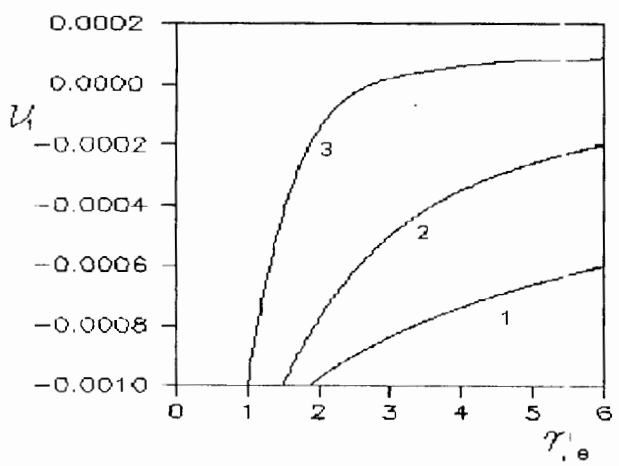

Fig.3. The dependences of increment of low disturbances of amplitude from the relative beam power. $\tau_1 = 50$, $N = 20$, $K_a = 10dB$. *Curves 1* – $\varphi = 0.15$; *curves 2* – $\varphi = 0.2$; *curves 3* – $\varphi = 0.25$.

monotonically. Positive value can be obtained at $\varphi_s > 0.25$. The values of the positive increment correspond to amplitude alteration of 5-10% during the pulse of the enveloping of microwave oscillations duration. Apparently it will result in the shortening of pulse of accelerated current.

Complex root of system of equations (4) corresponds to the oscillation disturbances. Positive values of increment indicate the increase of oscillation disturbances and the occurrence of amplitude automodulation The results presented in [1] were obtained by the use of beam model [6]. Autogenerative system shown in Fig.1. and the system made in accordance with the scheme of inverted stabilotron have been considered there [8]. In microtrons with autogenerative microwave systems the occurrence of amplitude automodulation is possible at the excess of the threshold value by the beam power. The threshold value of electron conductinvity depends on the scheme of turning on of amplitron, its gain in a working point and an equilibrum phase. Fig.4. shows the typical dependences of threshold on the value of equilibrum phase for values gain in a working point. Curves 1-3 estimated considered system whereas curves 4-5 for the inverted stabilotron. Solid lines show the curves obtained in this paper, dashed lines – the curves obtained in [2]. It also shows the curves obtained by the use of a modified beam model. It is not difficult to note that more precise estimation of the contribution of "the first" orbit results in the 10-20% increase of threshold values of beam power according to the steady state and system parameters. It is easy to note that the threshold value of the occurrence of automodulations in the inverted stabilotron is lower than in the system with external feedback circuit.

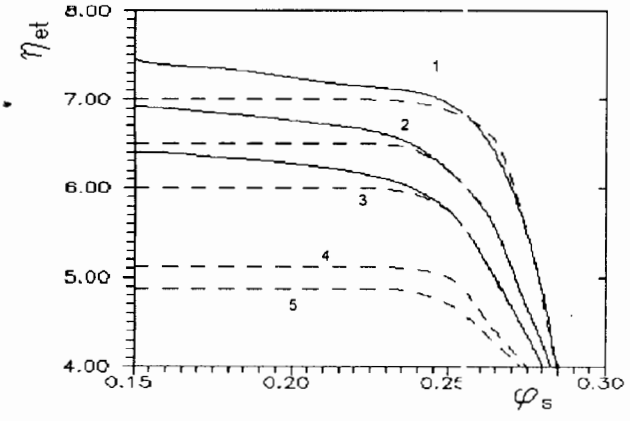

Fig.4. The dependences of threshold values of relative beam power on the value of equlibrium phase. $\tau_1 = 50$, $N = 20$.
1 – $K_a = 10dB$,
2 – $K_a = 6dB$,
3 – $K_a = 3dB$,
4 – $K_a = 10dB$,
5 – $K_a = 5dB$.

It is connected with fact that electron load of cavity in inverted stabilotron influences the value of oscillation amplitude in the feedback circuit more than in the autogenerative system under consideration. In all systems the threshold value of electron load is much reduced at $\varphi_s > 0.25$. There is a sector of "volt ampere" characteristics of cavity which has negative differential conductivity [6]. The increase of the feedback coefficient (which is equivalet to the decrease of amplitron gain) also results in the decrease of threshold value of electron load. The work of the low amplitron gain causes the increase of energy accumulated in the system. The output power of amplitron consists of power induced by its electron flow and input power passed through lag system. The power induced by the electron flow of amplitron has weak dependence from the input power value and hence, from electron load of accelerating cavity. The value of power circulating in the system is defined by the electron load of the cavity. With increasing of its part in amplitron output power, the effect of the beam on itself in the lag feedback circuit, increases.

The use of a modified beam model with lag of "relay" type has allowed to reveal the possibility of aperiodic increase of amplitude disturbances which can cause the shortening of accelerated current pulses. The obtained data on the threshold values of relative beam conductivity has been precised. The excess of the values causes the occurrence of amplitude automodulation. The question, whether the beam reached the last orbit under such conditions has no reply as yet.

Further, more detailed estimations are planned to be carried out. Equations (1) are to be integered with initial conditions and autogenerative system parameters assigned on the basis of results obtained in the present paper.

References

[1] I.V.Alekseyev et al., *Proc. of the 8th All Union Conference on Charged Particle Accelerators.* Protvino, Okt 19-21, 1982. JINR, Dubna, **Vol.2.** pp. 41-43, 1983.

[2] V.P.Gorbachev et al.,*Proc.of Second International Workshop "Beam Dynamics and Optimization".* St.-Petersburg State University Press. p.16, 1995.

[3] I.V.Alekseyev et al., Microtron with Autogenerative Microwave Sypply System on the Base Amplitron.**In pres. Proc.** pp.

[4] N.V. Vladimirov et al., The Simulation of Transition Processes in Microwave Supply Systems of Microtron. Saratov. 1991. *Dep. in VINITI,* **No 1837-B92 Dep.** 03.06.92.

[5] V.P.Gorbachev et al., The Simulator of Microtron. **In pres. Proc.** pp.

[6] E.L.Kosarev. *JTF.* **Vol LXII,**(10) pp.2239-2247,1972.

[7] L.E. Elzgolz. Introduction to the Theory of Differencial Equations with Deviation Argument. M: "Nauka", 1964.

[8] V.P. Gorbachev et al., *Eletronnay Tecknicka, SVCh Tecknicka (in Russian).* **Issue 4** (464) pp.25-27, 1994.

Mechanical and Thermodynamical approach to Halo creation problem

Yu.Senichev

Aarhus University, Denmark

Abstract

During last decade the halo creation problem became one of the most popular problems. It can be explained by the highest interest to intense proton machines for Kaon, Neutron Factories and the linac for the transmutation technology. At present three accelerators of such a class, JHF in KEK, ESS in Europe and SNS in Oak Ridge are under design and construction. In two of them the author took part. The halo creation is most serious problem in such machines, since it restricts the intensity of the beam and the life time of the facility. In this work the halo creation problem is investigated using the non-linear mechanics apparatus and the numerical modelling. The author considers two conceptions, the mechanical and the thermodynamical ones and gives the estimation of their applicability frame.

1 Introduction

During the last decade the problem of the halo creation in the high intense proton accelerators is widely discussed in all accelerator centres. First R.Jameson brought up this important problem[1]. Later the significant contribution in the investigation of this problem has been done by K.R.Crandall, R.L.Gluckstern, I. Hofmann, L. Laslett, G. P.Lawrence, S. Machida, R.S.Mills, M. Reiser, J. Struckmeier, T. Wangler, for instance, [2-5] and certainly I. M.

Kapchinsky and F.J.Sacherer. The author of this article made the series of works dedicated to some particular problems of halo creation in the intense beam as well [6-9].

At present there are two conceptions explaining the halo creation and behavior. The first one is the "mechanical" conception based on the analysis of the mechanical equation. The method uses the linearized equation of the motion and introduces the so-called "free" energy concept. The second one is the "thermodynamical" conception explaining this phenomena by means of the thermodynamical equations. It was based on the statistic physics with the use of the thermodynamical equations, what allows to easier find the equilibrium distribution proceeding from the temperature equality for all directions.

However, both the conceptions explain just the behavior of the second moments only, what is not enough for the understanding of the halo creation phenomena. Simultaneously in the method of the "free" energy the time dependence of Hamiltonian is not taken into account. It is not quite correct, since any channel with the alternative gradient has the explicit dependence of Hamiltonian on time due to the external focusing and defocusing forces. Some conclusions based on the thermodynamical consideration do not take into account such important characteristics as the ratio between the relaxation and acceleration time, what makes the scale to the process.

Definitely, the halo creation problem is a very complicate phenomena and to solve it we need to make some simplifications, but they have not to be in a contradiction with the phenomena itself. The author uses the analytical methods of the nonlinear mechanics together with the numerical calculations. Firstly, to avoid the misunderstanding we consider the system, where the external structure resonances are absent, what it is easy to get in the practice. Secondly, we can assume the halo does not affect the main part of the beam, since it is usually assumed to be 90-95% of the beam. The most strong assumption in our analytical model is the axial symmetry of the beam. But in reality we can check it by the numerical calculation and understand how it is strong. The numerical simulations are carried out on the rectangular grid with the metallic boundary and the requirement of the symplectical condition.

The paper integrates the previous results of author and develops the self consistent imagination about the halo creation problem.

2 The motion equation with the space charge

The distribution with the axial symmetry is represented in the common form of the binomial polynomial:

$$\rho(r) = \frac{enm}{\pi b^2}\left[1 - \frac{r^2}{b^2}\right]^{m-1} \tag{1}$$

with the dispersion $\sigma = \frac{b}{\sqrt{2m+2}}$, where m is the order of the binomial distribution, en is the linear density of the charge in the beam. The force of the space charge affecting any particle $F = e(E - vB)$ is determined from the Poisson equation solution:

$$F(r) = \frac{e^2 n}{2\pi\varepsilon_0 r\gamma^2}\left\{1 - \left[1 - \frac{r^2}{2(m+1)\sigma^2}\right]^m\right\}, \tag{2}$$

where γ - Lorentz factor.

Taking into account the external focusing forces, the final equation is represented in the form:

$$\frac{d^2r}{ds^2} + K(s)r - \frac{e^2 n\lambda^2 k^2}{2\pi\varepsilon_0 m_0 c^2\gamma^3 r}\left\{1 - \left[1 - \frac{r^2}{2(m+1)\sigma^2(s)}\right]^m\right\} = 0, \tag{3}$$

where $K(s) = \pm\frac{eG(s)L^2}{p}$ -the focusing-defocusing term, $L = k_f\beta\lambda$ is the focusing period length with the multiplicity k_f and $s = z/L$ is the new normalized longitudinal coordinate, which plays the role of time. Obviously, the dispersion $\sigma(s)$ depends on the time and this dependence is determined by the envelope equation. As a remark, we should say the space charge influence in the linear accelerators goes down as γ^3, but not as $\beta^2\gamma^3$ in the circular accelerators. The last one means the space charge effect in the linear accelerators remains to be strong during all time of acceleration. Let us rewrite the equation (3) in the form:

$$\frac{d^2r}{ds^2} + K(s)r = F(r,s), \tag{4}$$

where $F(r,\tau) = C_{sc}\frac{1}{r}\left\{1 - \left[1 - \frac{r^2}{2(m+1)\sigma^2(s)}\right]^m\right\}$ is the right part of the equation dependent on the coordinate r and the time s. The multiplier

$C_{sc} = \frac{e^2 n S^2 \lambda^2}{2\pi\varepsilon_0 m_0 c^2 \gamma^3}$ depends on the intensity of the beam and the parameters of the accelerator and practically does not depend on the energy.

The solution of the equation (4) can be represented in the form $r = \eta \cdot \widehat{\beta}^{1/2}$, where $\eta(\tau) = \cos \int_0^\tau \frac{ds}{\widehat{\beta}(s)}$ is the new function dependent on the coordinate τ. Following the Courant Snyder formalism [10], we get the equations system:

$$\eta'' + \mu^2 \eta = \mu^2 \widehat{\beta}^{3/2}(\tau) F(r,\tau)\left(\widehat{\beta}^{1/2}\right)' + K(\tau)\widehat{\beta}^{1/2} - \frac{1}{\widehat{\beta}^{3/2}} = 0, \qquad (5)$$

where μ is the phase advance per the unit period determined by the expression $\mu\tau = \int_0^\tau \frac{ds}{\widehat{\beta}(s)}$, and $\widehat{\beta} = \beta/L$. Then $\frac{r^2}{\sigma^2} = \frac{r^2}{\widehat{\beta} L \varepsilon_{rms}}$ or $\frac{r}{\sigma} = \frac{\eta}{\varepsilon_n^{1/2}}$, where $\varepsilon_n = \varepsilon_{rms} L$. Since the emittance ε_{rms} is changed along the focusing channel as $1/\beta\gamma$ and L as β, the normalized emittance almost does not depend on the relative velocity β in the energy region approximately up to 1 GeV. Substituting the new variables in the equation (5), we have

$$\eta'' + \mu^2 \eta = C_{sc}\mu^2 \frac{\widehat{\beta}(\tau)}{\eta}\left\{1 - \left[1 - \frac{\eta^2}{2(m+1)\varepsilon_n}\right]^m\right\}. \qquad (6)$$

The polynomial between the brackets multiplied $1/\eta$ can be represented through a Teylor series:

$$\frac{1}{\eta}\left\{1 - \left[1 - \frac{\eta^2}{2(m+1)\varepsilon_n}\right]^m\right\} = \sum_{n=1}^{m} \frac{(-1)^{n-1} m!}{(m-n)!n!2^n (m+1)^n \varepsilon_n^n} \cdot \eta^{2n-1}. \qquad (7)$$

If the coefficients of the series denote as c_n, the equation has the form:

$$\eta'' + \mu^2 \eta = C_{sc}\mu^2 \widehat{\beta}(\tau) \sum c_n \eta^{2n-1}. \qquad (8)$$

So, in order to get the final solution of the problem, we have to solve the system consistent of the equation (8) and the envelope equation.

3 The envelope equations

Firstly, since the structure resonances are assumed to be avoided, the stationary solution for the envelope has to exist. Secondly, the behavior of the

$C_{sc} = \frac{e^2 n S^2 \lambda^2}{2\pi\varepsilon_0 m_0 c^2 \gamma^3}$ depends on the intensity of the beam and the parameters of the accelerator and practically does not depend on the energy.

The solution of the equation (4) can be represented in the form $r = \eta \cdot \widehat{\beta}^{1/2}$, where $\eta(\tau) = \cos \int_0^\tau \frac{ds}{\widehat{\beta}(s)}$ is the new function dependent on the coordinate τ. Following the Courant Snyder formalism [10], we get the equations system:

$$\eta'' + \mu^2 \eta = \mu^2 \widehat{\beta}^{3/2}(\tau) F(r,\tau)\left(\widehat{\beta}^{1/2}\right)' + K(\tau)\widehat{\beta}^{1/2} - \frac{1}{\widehat{\beta}^{3/2}} = 0, \qquad (5)$$

where μ is the phase advance per the unit period determined by the expression $\mu\tau = \int_0^\tau \frac{ds}{\widehat{\beta}(s)}$, and $\widehat{\beta} = \beta/L$. Then $\frac{r^2}{\sigma^2} = \frac{r^2}{\widehat{\beta} L \varepsilon_{rms}}$ or $\frac{r}{\sigma} = \frac{\eta}{\varepsilon_n^{1/2}}$, where $\varepsilon_n = \varepsilon_{rms} L$. Since the emittance ε_{rms} is changed along the focusing channel as $1/\beta\gamma$ and L as β, the normalized emittance almost does not depend on the relative velocity β in the energy region approximately up to 1 GeV. Substituting the new variables in the equation (5), we have

$$\eta'' + \mu^2 \eta = C_{sc}\mu^2 \frac{\widehat{\beta}(\tau)}{\eta}\left\{1 - \left[1 - \frac{\eta^2}{2(m+1)\varepsilon_n}\right]^m\right\}. \qquad (6)$$

The polynomial between the brackets multiplied $1/\eta$ can be represented through a Teylor series:

$$\frac{1}{\eta}\left\{1 - \left[1 - \frac{\eta^2}{2(m+1)\varepsilon_n}\right]^m\right\} = \sum_{n=1}^{m} \frac{(-1)^{n-1} m!}{(m-n)!n!2^n (m+1)^n \varepsilon_n^n} \cdot \eta^{2n-1}. \qquad (7)$$

If the coefficients of the series denote as c_n, the equation has the form:

$$\eta'' + \mu^2 \eta = C_{sc}\mu^2 \widehat{\beta}(\tau) \sum c_n \eta^{2n-1}. \qquad (8)$$

So, in order to get the final solution of the problem, we have to solve the system consistent of the equation (8) and the envelope equation.

3 The envelope equations

Firstly, since the structure resonances are assumed to be avoided, the stationary solution for the envelope has to exist. Secondly, the behavior of the

envelope does not depend on the particles in the halo, since it is the small part of the beam . Appositively; the trajectory of any particle in the halo is determined by the core. Therefore, knowing the solution for the envelope we can find the solution for any particle in the halo. So, first of all we should find the solution for the envelope. Following by Kapchinsky [11], we find the solution in the form:

$$\widehat{\beta}^{1/2} = R \cdot (1 + q)\,, \tag{9}$$

where R and q are the slow and fast oscillating functions correspondingly. Taking into account the linear part of the space charge B_a, we get the envelope equation

$$R'' + \mu^2 R - \frac{1}{R^3} - \frac{B_a}{R} = 0, \tag{10}$$

where we would like to emphasize the fact, that μ is the phase advance per the period for the case without the space charge. Obviously, for the matched beam $R'' = 0$ and the radius is determined by the expression:

$$R^2 = \frac{B_a + \sqrt{B_a^2 + 4\mu^2}}{2\mu^2}. \tag{11}$$

It is the expression, which has been got by Kapchinsky. However, we are interested, in the case, when the beam is mismatched with channel due to some reason, for instance, the space charge. Unfortunately, the equation (10) has not the analytical solution. Therefore we use the perturbation method and seek the solution in the form $\tilde{R} = R + \triangle r$. Substituting the last one and remembering, the equation (10) is fulfilled for R, we get the equation for Δr :

$$\triangle r'' + \mu^2 \triangle r + \frac{3}{r^3} \cdot \frac{\triangle r}{r} + \frac{B_a}{r} \cdot \frac{\triangle r}{r} = 0. \tag{12}$$

Using Kapchinsky's parameter $n = \frac{B_a}{2\mu}$, the equation (12) is derived to the simplest form:

$$\triangle r'' + \triangle r \cdot \mu^2 \left[2 \cdot \left(1 + \frac{1}{p^2}\right)\right] = 0, \tag{13}$$

where $p = h + \sqrt{1+h^2}$. In result we get the important expression for the oscillation frequency of the envelope $\widetilde{\mu}$ with allowance for the space charge:

$$\widetilde{\mu} = \mu \left[2 \cdot \left(1 + \frac{1}{p^2} \right) \right]^{1/2}. \tag{14}$$

At the small current, when $h \to 0$ and $p \to 1$ the envelope frequency equals the double value of the oscillation frequency of the particles in the core of the beam $\widetilde{\mu} = 2 \cdot \mu$. In the intensive beam $h \to \infty$,then $p \to \infty$ and the ratio (14) has the different meaning $\widetilde{\mu} = \sqrt{2} \cdot \mu$. This result is enough unexpected for us, that the frequency of the envelope does not tend to zero with the intensity growth and it is stabilized around the final value. Solving the equation (13), we can say the envelope breaths with the frequency $\widetilde{\mu}$:

$$\triangle r = \triangle r_m \cos \widetilde{\mu} \tau, \tag{15}$$

where the maximum ratio of the mismatching is determined by the expression $\triangle r_m / R = \sqrt{\sqrt{1+h^2} + h} - 1$. The meaning of q in the equation (9) can be found by the method of the averaging. We quote here the solution for FD meander case:

$$q(\tau) = \frac{1}{\pi^3} \sum_{l=0}^{\infty} \frac{(-1)^l}{(2l+1)^3} \cos 2(2l+1)\pi\tau. \tag{16}$$

So, we have found the solution for the envelope in the form through Δr and q:

$$\widehat{\beta} = \widehat{\beta}_0 \cdot \left(1 + 2 \cdot \frac{\triangle r_m}{R} \cos \widetilde{\mu}\tau + 2 \cdot q(\tau) \right). \tag{17}$$

Now we have every thing in order to solve the equation for the particles locating in the halo and executing a motion around the core with the changing sizes in an accordance with (17).

4 The beam halo creation

Let us denote the right part of the equation (8) as $\widetilde{F}$ and represent it through the sum of two components depending and not depending on the time τ:

$$\widetilde{F}(\eta,\tau)=\widetilde{F}_0\left(\eta,\eta^3,\ldots\eta^{2n-1}\right)+\widetilde{F}_1\left(\eta,\eta^3,\ldots,\eta^{2n-1},\tau\right), \tag{18}$$

where

$$\mu^2\widetilde{F}_0\left(\eta,\eta^3,\ldots,\eta^{2n-1}\right)=C_{sc}\mu^2\widehat{\beta}_0\sum_{n=1}^{m}c_n\eta^{2n-1}, \tag{19}$$

$$\mu^2\widetilde{F}_1\left(\eta,\eta^3,\ldots,\eta^{2n-1}\right)=C_{sc}\mu^2\widehat{\beta}_0\frac{\triangle r_m}{R}\sum_{n=1}^{m}c_n\eta^{2n-1}\cos\mu\tau. \tag{20}$$

In accordance with [12] the solution is seek in the form

$$\eta=a\cdot\cos\Theta, \tag{21}$$

where the amplitude and the phase are described by the expressions:

$$\begin{aligned}\tfrac{da}{d\tau}&=-\tfrac{\mu}{2\pi}\int_0^{2\pi}\widetilde{F}_0\left(\cos\Theta,\cos^3\Theta,\ldots,\cos^{2n-1}\Theta\right)\cdot\sin\Theta d\Theta-\\&-\tfrac{\mu}{2\pi}\int_0^{2\pi}\widetilde{F}_1\left(\cos\Theta,\cos^3\Theta,\ldots,\cos^{2n-1}\Theta,\cos\mu\tau\right)\cdot\sin\Theta d\Theta,\end{aligned} \tag{22}$$

$$\begin{aligned}\tfrac{d\Theta}{d\tau}&=\mu-\tfrac{\mu}{2\pi a}\int_0^{2\pi}\widetilde{F}_0\left(\cos\Theta,\cos^3\Theta,\ldots,\cos^{2n-1}\Theta\right)\cdot\cos\Theta d\Theta-\\&-\tfrac{\mu}{2\pi a}\int_0^{2\pi}\widetilde{F}_1\left(\cos\Theta,\cos^3\Theta,\ldots,\cos^{2n-1}\Theta,\cos\mu\tau\right)\cdot\cos\Theta d\Theta\end{aligned} \tag{23}$$

Since the average value of the product $\langle\cos^{2n-1}\Theta\cdot\sin\Theta\rangle$ for any n equals zero, the function $\widetilde{F}_0$ does not cause the growth of the amplitude a, but just causes the amplitude fluctuation around the value of a only. However, the same function $\widetilde{F}_0$ brings in the frequency $\frac{d\theta}{d\tau}$ nonlinear dependence on the amplitude a, since $\langle a^{2n-1}\cos^{2n}\Theta\rangle=b_n a^{2n-1}$, where $b_n=\frac{(2n)!}{4^n(n!)^2}$, from where we can find the dependence of the frequency versus the amplitude:

$$\frac{\Delta\mu(a)}{\mu}=C_{sc}\widehat{\beta}_0\sum_{n=1}^{m}c_n b_n a^{2n-2}. \tag{24}$$

The first term $n=1$ gives the linear part of the frequency shift. It depends on the distribution and in the case of the uniform distribution, when $m=1$

coincides with Laslett tune shift. The second term $n = 2$ gives the positive cubic frequency dependence.

Now let us consider the term $\widetilde{F}_1$. Substituting the function $\widetilde{F}_1$ in the equations (22,23) and taking into account the simple relation $\cos^{2n-1}\Theta \cdot \sin\Theta = \sum_{k=1}^{2n-2} d_k \cos(2k-1)\Theta \sin\Theta$,we get the equation system:

$$\frac{da}{d\tau} = -\mu C_{sc}\widehat{\beta}_0 \frac{r_m}{R} c_k d_k a^{2k-1} \sin 2k\psi, \tag{25}$$

$$\frac{d\psi}{d\tau} = \mu - \Delta\mu(a) - \frac{\widetilde{\mu}}{2k-2} - \mu C_{sc}\widehat{\beta}_0 \frac{r_m}{R} c_k d_k a^{2k-2} \cos 2k\psi, \tag{26}$$

where $\Delta\mu(a)$ and $\widetilde{\mu}$ are determined by the expression (24) and (14) correspondingly.. From all spectrum we extracted the resonant harmonic $(2k-2)$ only, which is assumed to be the nearest to the total frequency $\widetilde{\mu}$. If such a harmonic exists, we can derive the slow phase for this harmonic $2k\psi = (2k-2)\Theta - \widetilde{\mu}\tau$.

From the equation (26) we can find the "frame-work" curve of the nonlinear resonance:

$$\mu - \Delta\mu(a) = \frac{\widetilde{\mu}}{2k-2}. \tag{27}$$

Additionally we can find the phase invariant curves determining the particles motion. Let us suppose under some value of a we have resonance. Then we can expand the derivatives of a and ψ in the vicinity of this point $a = a_0 + \delta a$ and $\psi = \psi_0 + \delta\psi$:

$$\frac{d\delta a}{d\tau} = 2k\mu C_{sc}\widehat{\beta}_0 \frac{r_m}{R} c_k d_k a_0^{2k-1} \cos 2k\psi, \tag{28}$$

$$\frac{d\delta\psi}{d\tau} = \left(-\frac{d\Delta\mu(a)}{da}\right)_{a=a_0} \cdot \delta a - \mu C_{sc}\widehat{\beta}_0 \frac{r_m}{R} c_k d_k a_0^{2k-3} (2k-2) \cos 2k\psi \cdot \delta a. \tag{29}$$

Taking into account the first order terms only, we have the equation of the nonlinear resonance:

$$\frac{d^2\delta a}{d\tau^2} + \Omega_k^2 \cos 2k\psi \cdot \delta a = 0, \tag{30}$$

where $\Omega_k^2 = 2k\mu \left(\frac{d\Delta\mu(a)}{da}\right)_{a=a_0} C_{sc} \widehat{\beta}_0 \frac{r_m}{R} c_k d_k a_0^{2k-1}$ is the frequency of the small oscillation in the vicinity of the resonance. From these expressions it is easy to find the maximum amplitude changes δa:

$$\delta a = \left(\frac{4k\mu C_{sc} \widehat{\beta}_0 \frac{r_m}{R} c_k d_k a_0^{2k-1}}{\left(\frac{d\Delta\mu(a)}{da}\right)_{a=a_0}} \right)^{1/2} . \tag{31}$$

Thus, the amplitude of the oscillation is changed, but it is restricted by the final value. It means the halo is created and then stabilized with the maximum size δa.

We have considered the problem in the "one resonance" approximation, when only one harmonic in the spectrum of the beam envelope oscillations affects. However, the function $q(\tau)$ has the wide spectrum. If the distance between two harmonics Δa less the resonance width δa we have the superimposing of resonances and in accordance with Chirikov's criterium the stochastic layer is formed with width[13]:

$$\frac{a - a_0}{a_0} \propto \frac{\Delta r_{rl}}{R} \exp\left(-\frac{\pi}{\mu - \Delta\mu(a_0)} \right). \tag{32}$$

However, in our case, when the phase advance equals $30^0 - 45^0$, the layer is extremely small value $\simeq 10^{-10}$.

So, we have got the analytical description of the halo creation phenomena in the mechanical approach.

5 The thermodynamical approach to the halo creation

The thermodynamical equilibrium consideration is based on the determination of the condition, when the temperature is equal for all three directions in the three dimensional bunch:

$$T_\perp = T_\parallel, \tag{33}$$

what means through the emittance definition:

$$\frac{\varepsilon_{nr}}{\varepsilon_{nz}} \cdot \frac{a_z}{a_r}\gamma = 1, \tag{34}$$

where ε_{nr}, ε_{nz} and a_r, $a_z$are the transverse and longitudinal emittances and the semi-axes of ellipsoidal bunch correspondingly.. To follow this ratio we should keep the transverse wave number equal to:

$$k_r \propto \frac{1}{\beta_s^{3/2}\gamma_s^{3/2}}, \tag{35}$$

where the index s means the synchronous particle. In accordance with the thermal equilibrium, if we follow this condition, we have to have the minimum growth of emittance. It is the truth for the stationary stage, therefore we should estimate what is the relaxation time of this process described by the equation:

$$\frac{d\left(T_\perp - T_\parallel\right)}{dt} = -\frac{1}{\tau_c}\left(T_\perp - T_\parallel\right). \tag{36}$$

For not strong coupled plasma the relaxation time is defined by the expression:

$$\frac{1}{\tau_c} = 0.06\omega_p\Gamma^{3/2}\ln\Lambda, \tag{37}$$

where $\omega_p$is the plasma frequency:

$$\omega_p = \sqrt{\frac{Z^2e^2n}{m\varepsilon_0}}, \tag{38}$$

Γ is the parameter of one component plasma, determined by the ratio of the interparticle potential energy and the thermal energy :

$$\Gamma = \frac{Z^2e^2}{\varepsilon_0 4k_BT\pi}\left(\frac{n4\pi}{3}\right)^{1/3}, \tag{39}$$

and the Coulomb logarithm:

$$\ln\Lambda = \ln\frac{3}{\Gamma^3}. \tag{40}$$

Let us consider the case with the parabolic distribution of the charge density:

$$n = \frac{3I}{r^2 l_{bunch} 2\pi}. \tag{41}$$

At the average current $I = 30mA$, the emittance $\varepsilon_{x,y} = 2 \cdot 10^{-6}$, the charge density $n = 3 \cdot 10^{15} p/m^3$ and $k_B T = 1.4 \cdot 10^{-17}$the parameters of the plasma will be equal to: $\Gamma = 4.0 \cdot 10^{-6}$, $\omega_p = 0.76 \cdot 10^8$, $\ln \Lambda = 40$ and the relaxation time $\frac{1}{\tau_c} = 1.5$. But on the other hand, the acceleration time in the linear accelerator up to 1 GeV has the scale of 5 μsec, consequently $\frac{t_{ac}}{\tau_c} = 10^{-5}$. The last ratio means we cannot reach the thermal equilibrium for such short time and the nature of equipartition has to be explained by the different way. Nevertheless many authors can object to this assertion, since they did the simulation by the code and observed transient process for the emittance growth. Let us estimate the parameters of the model plasma. For instance we take 3000 "particles" in each bunch and under the same current the parameter $\Gamma = 0.015$, the Coulomb logarithm $\ln \Lambda = 14$ and the plasma frequency retains the same value. Then the modelling relaxation time equals 10 μ sec. The simple calculation shows the possible growth of emittance could be around 50%, but it is the artificial effect, what in reality is not observed.

6 The results of the numerical calculation

The numerical model is based on the grid method of Poisson equation solution with the boundary condition. The calculation is done with the symplectic condition, what is the most important for so-called "long term instability" effect.

Since the main purpose is the study of the halo creation, we avoided any structure resonances /6,7/ and considered the simplest unit of the periodicity FODO cell. In this simple model we adjusted the channel with some phase advance per cell, for instance 80 degrees, and varied the current value to change the tune shift due to the space charge. The detuning value we took as the parameter of intensity.

We could observe the halo creation phenomena at the different intensity of the beam. The figures 1 and 2 show the behavior of the rms beam size and the rms emittance versus the FODO cells number at the different tune shift (a-zero current, b-30% tune shift, c-90% tune shift). We can see from

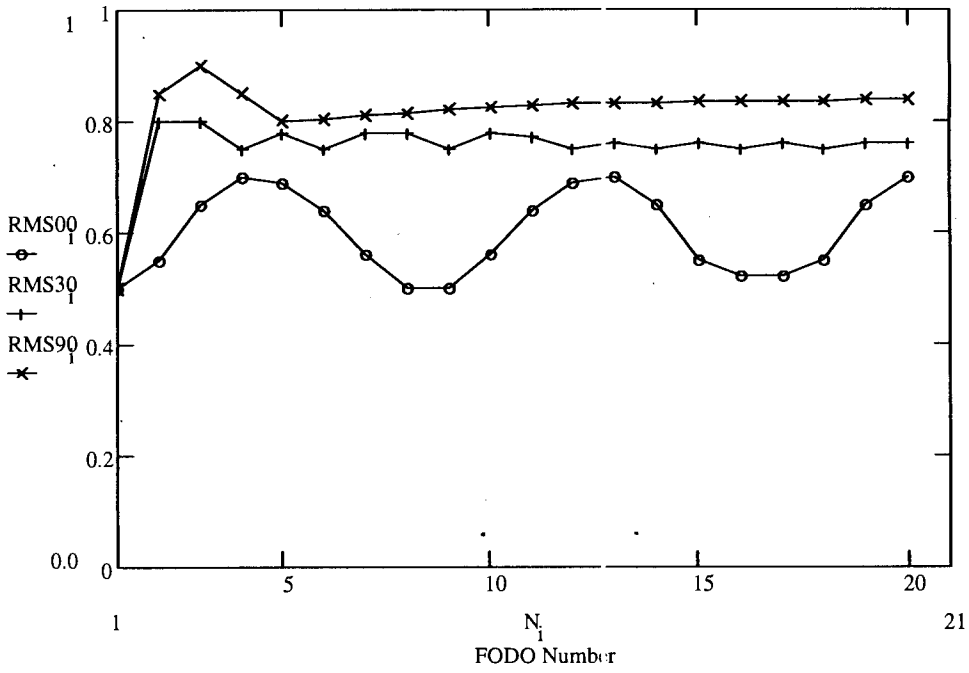

Figure 1. The RMS size of the beam vs the FODO cells number at the different intensity of the beam.

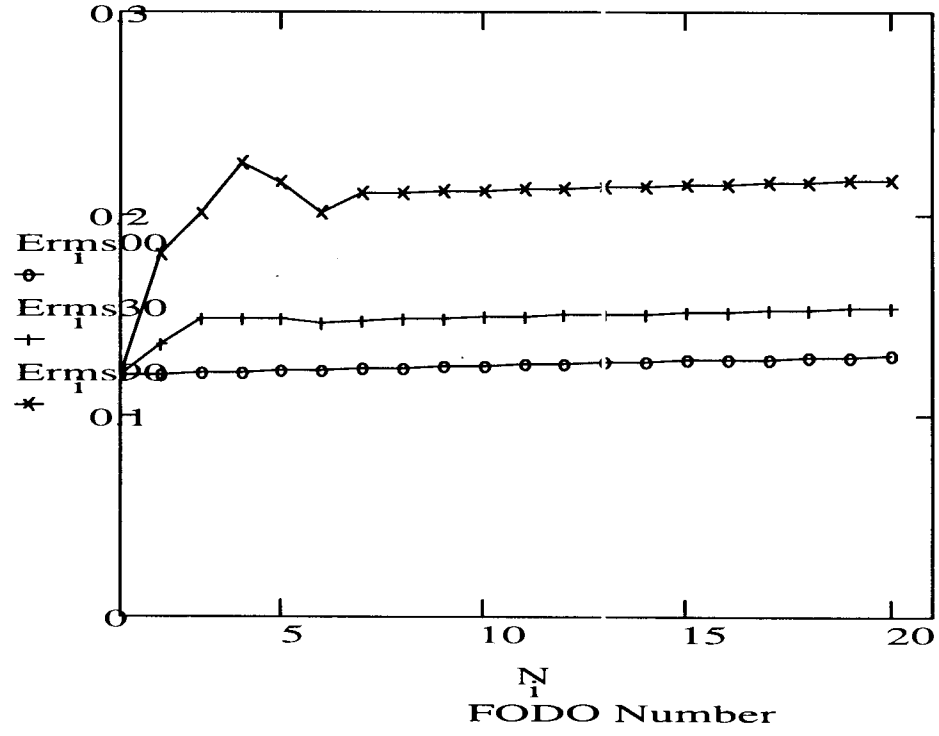

Figure 2. The RMS emittance vs the FODO cells number at the different intensity of the beam.

the first picture the different character of the processes without and with the space charge. In all cases the beam is mismatched with the channel, but in the zero intensity case the envelope has the oscillating character and follows the Kapchnsky's equations. In another two cases the envelope has the initial growth and then it is saturated practically without any oscillations. It can be explained, following by the theory expounded above. For zero case we have a good prediction in accordance with Kapchinsky's equations, since they coincide with the module solution behavior. In the case of the strong space charge we could split the process on two parts. In the first part we observe the resonant behavior exactly in accordance with the equations (28,29), when the particle amplitude grows due to the oscillation of the beam core. But the resonant condition (27) is performed for the small part of the particles located enough far from the centre. In the same time for the main part of the beam the space charge acts as the octupole, spreading the particles in the phase plane and stabilizing the instability (eq. 24, n=2). This natural octupole forms the new core with the new ratio between the rms size and the rms divergence determined by the effective tune equal to $\mu - \Delta\mu\,(a)$.Obviously, the time of the fist stage is proportional to $\propto 1/\Delta\mu\,(a)$ .To convince in the nature of the "octupole" space charge action the author has done the numerical experiment with the space charge "octupole" compensating by the real octupoles up to the zero effective chromaticity [14]. These results confirmed this explanation.

After the first stage of the new nuclear formation we get the stationary process without any beating of the envelope, which now could be described by Kapchinsky's equations. The emittance slightly grows due to the self-heating process. This part of the process follows the thermodynamical description, when the beam is heated due to the envelope oscillation. The last one could be described by both the mechanical and thermodynamical models. Since the envelope oscillation will exist always, the heating process has to be observed always as well.

7 Conclusion

We have described the model of the halo creation. Obviously, the equipartition, as phenomenon, exists and we can observe experimentally how the global growth of emittance is stabilized at some final value. This value depends on many factors. For instance in the simplest case, when we have not external resonance, the beating of envelope could be such a source for the emittance growth. In common case the nonlinearity due to space charge is

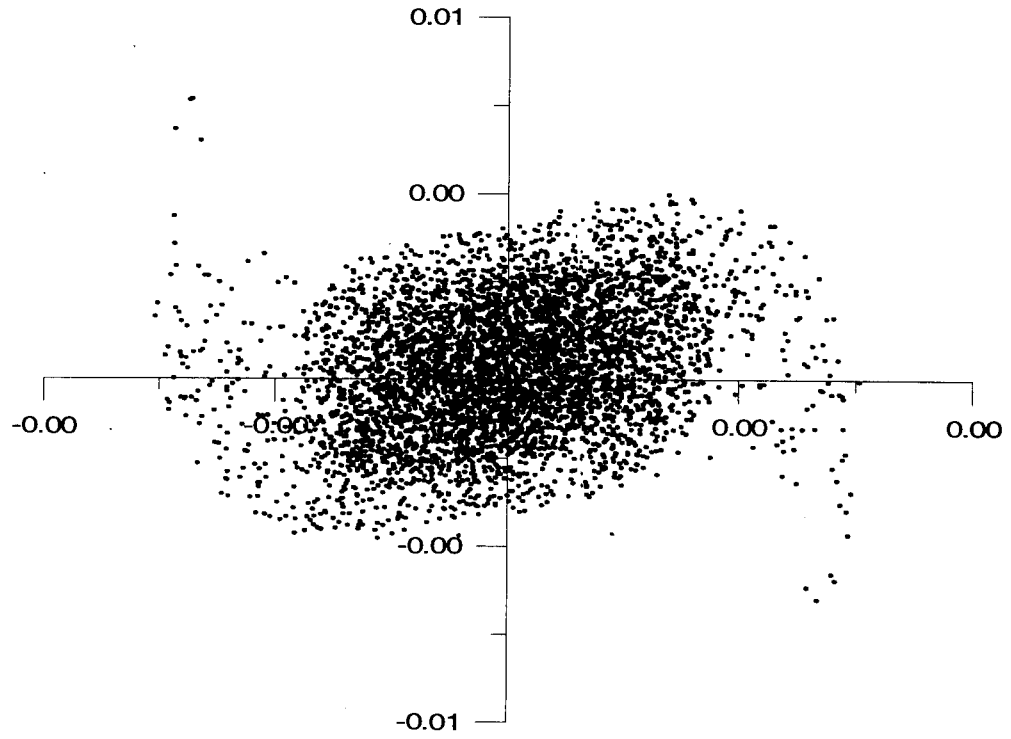

Figure 3. The phase portrait of the beam at the initial stage.

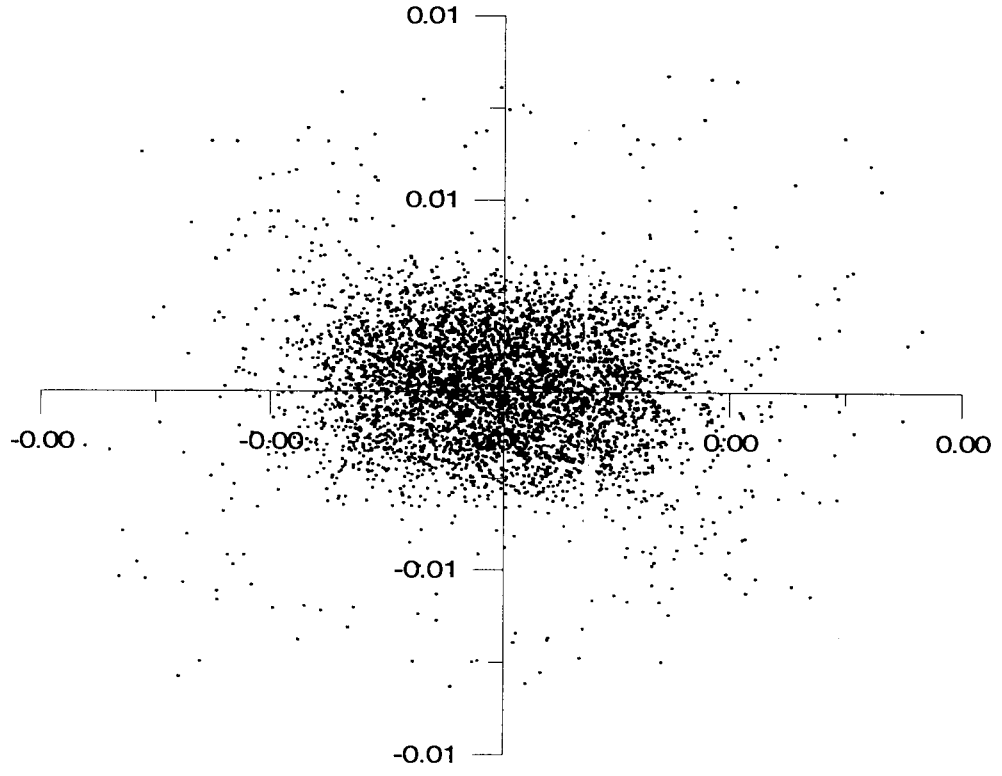

Figure 4. The phase portrait of the beam at the final stage.

the main reason of the emittance growth. In each particular case it is either the parametric resonance due to the space charge itself, or due to the external resonance crossing. We have shown what size of the halo could be expected. But later the halo continue to grow. This growth is very small and could be estimated by the thermodynamical equations.

References

[1]

[2] R.A.Jameson, IEEE Trans.Nucl.Sci. 28, pp.2408-2412, 1981.

[3] I. Hofmann, Negative energy oscillations and instability of intense beams, Particle Accelerator, 1980 V.10, pp. 253-258.

[4] Hofmann, J.Struckmeier, Generalized three-dimensional equations for the emittance and field energy of high-current beams in periodic focusing structures,Particle Accelerator, 1987, v. 21, pp.69-98.

[5] J.Struckmeier, Improved envelope and emittance description of particle beams using the Fokker-Planck approach, Particle Accelerator, 1994, v. 45, pp. 229-252.

[6] M. Reiser, Design of equipartitioned high-current RF linacs, Linac Conference, 1994

[7] Yu. Senichev, V.Balandin, Space Charge and Emittance Growth in some applications of accelerator, Proceeding of Workshop of Emittance Growth and Space Charge, Tsukuba, KEK, 1995

[8] Yu. Senichev, A.Budzko, Study of space charge effects close by half-integer resonances, HEACC-92, Hamburg.

[9] Yu. Senichev, Passing through Half-Integer Resonance due to Space Charge under Different Initial Distribution, PAC, Washington, 1993.

[10] Yu. Senichev, V.Balandin, The Space Charge Effect in Slow Extraction by Third Integer Resonance, EPAC London 1994.

[11] E.D. Courant, H.S.Snyder Theory of the alternating-gradient synchrotron, Annals of physics. 3, pp. 1-48, 1958.

[12] I.Kapchinsky, Dynamic of particles in linear resonant accelerators, Atomizdat, 1966.

[13] N.Bogoljubov,Yu. Mitropolsy, Asymptotic methods in the theory of nonlinear oscillation,M.: Science, 1974.

[14] Chirikov B. Investigation in the theory of nonlinear resonance and stochastic, preprint INF 267, 1969.

[15] Yu.Senichev, V.Balandin, The space charge effect in Slow Extraction by third integer resonance, EPAC London, 1994.

THE LOW ENERGY POSITRON (ELECTRON) STORAGE RINGS WITH LONGITUDINAL MAGNETIC FIELD

I.N. Meshkov, A.O.Sidorin,

JINR, Dubna, Russia

The general parameters of the low energy positron storage ring for positronium generation and the electron one dedicated to electron cooling are described.

The methods of the intense positronium streams generation is based on positron storage ring equipped with electron cooling device. The positron beam energy in the range of several keV is mostly interesting. The use of longitudinal magnetic field is very attractive way for positron focusing. In this case the long term stability of the positron beam can be provided with additional spiral coils, which form a quadrupole magnetic field, similar to the "stellarator" one. The same scheme of a storage ring for electrons permits to avoid the problems of the traditional configuration of an electron cooling system for ion energy of several tens of GeV/amu (electron energy is of several MeV). For this purpose the ion storage ring is to be equipped with an additional electron one, which is periodically filled up with new portion of cold electrons. The electron beam circulates in longitudinal (quasitoroidal) magnetic field. Using induction acceleration one can accelerate the electron beam without distortions caused by RF system of linear accelerators.

The particle dynamics and the ring design are discussed.

Introduction

For generation of antihydrogen atoms an antiproton source (like the AA at CERN or the antiproton source at FNAL) has to be supplemented by two small rings – one to store low energy antiprotons and another to store positrons, respectively. The first ring is a conventional strong focusing storage ring for antiprotons with an energy in the range of 0.5 – 50 MeV. The positron ring is proposed [1] to have a focusing system with longitudinal magnetic field and spiral quadrupole field. Such a magnetic system is similar to the one used in a modified betatron [2] and its modification called 'stellatron" [3]. The rings have a common section, where the recombination of antiprotons and positrons occurs. Electron cooling is used for both antiprotons and positrons. In the electron cooling section of the positron ring the positronium is generated by recombination of the positrons with cooling electrons and orthopositronium beam leaves the magnetic system. This means that the positron ring is a source of orthopositronium, which gives additional possibilities for physics experiments.

A storage ring with longitudinal magnetic field for electrons permits to avoid the problems of the traditional configuration of an electron cooling system for ion energy of several tens of GeV/amu (electron energy is of several MeV) [4, 5]. For this purpose the ion storage ring is equipped with an additional electron one, which is periodically filled up with new portion of coold electrons. Using induction acceleration one can accelerate the electron beam without distortions caused by RF system of linear accelerators. The scheme proposed in Ref.[1] differs from earlier researches [2,3] by the injection method, which permits to inject a "magnetized" positron (electron) beam from a source immersed in longitudinal magnetic field.

1. Storage ring for positronium generation

The low energy positron toroidal accumulator (LEPTA) designed in JINR for positronium generation [6] has 2 toroidal solenoids and 2 straight ones, connected together as a racetrack. To obtain the longitudinal field homogeneity the common magnetic shielding surrounds all solenoids. The first of straight solenoids, so-called "septum", is used for superposition and separation of the cooling electron beam and the circulating positron one by the horizontal drift of the electron beam in transverse magnetic field, which is produced by special coils. Beams superposition and separation in the vertical plane are produced by centrifugal drift of electrons in the toroidal solenoids. The positron injection is performed by special kicker coil. After injection the orbit of the positron beam circulating inside the ring is placed between the septum coils, where the transverse magnetic field is absent. The spiral quadrupole coil is wound around vacuum chamber of the positron beam inside the septum. The ring circumference is about 12 meters. Positron energy can be varied from 5 to 20 keV. Longitudinal magnetic field value lies in the range of 300 - 1000 G.

2. Particle dynamics

Unlike the stellatron [3] the focusing system of the rings described here is nonuniform: the quadrupole spiral winding occupies only some parts of the ring circumference. The focusing system of the positron ring (Fig 1) consist of three basic elements: two toroidal solenoids with additional coils forming bending field, straight solenoid with spiral quadrupole coil and straight solenoid of the electron cooling section.

To estimate the general parameters of the focusing system we consider the particle dynamics inside the basic elements of the ring.

In assumption that the longitudinal particle velocity $r\dot{\alpha} = v$ is much larger of the transverse one, the equations of motion in the toroidal $B_\alpha = B_0 R_0 / r$ (B_0 is the longitudinal field

on the particle trajectory, R_0 – major toroid radius) and the uniform bending B_z=B_t=*const* fields can be written as:

$$\begin{cases} \dfrac{d^2x}{d\alpha^2} - x(1+2\dfrac{R_0}{\rho}\dfrac{B_t}{B_0}) + \dfrac{R_0}{\rho}\dfrac{dz}{d\alpha} = R_0(1+\dfrac{R_0}{\rho}\dfrac{B_t}{B_0}) \\ \dfrac{d^2z}{d\alpha^2} - \dfrac{R_0}{\rho}\dfrac{dx}{d\alpha} = 0 \end{cases}, \quad \rho = \frac{mc^2\beta\gamma}{eB_0}, \tag{1}$$

where $x = r - R_0$, z, α are polar coordinates.

Positron current is limited by the intensity of low energy positron source and lies in the range from 100 μA to 1 mA. Therefore, one can neglect, in first approximation, the beam field influence. When the bending magnetic field satisfies the condition

$$B_t = -\frac{mc^2\beta\gamma}{eR_0}, \tag{2}$$

the positron drift velocity inside the toroid is given by the following expression:

$$\left(\frac{dz}{d\alpha}\right)_{drift} = -\frac{\rho}{R_0}\left(\frac{\rho}{R_0}\left(\frac{dz}{d\alpha}\right)_0 + x_0\right). \tag{3}$$

The spiral quadrupole coil is used to compensate this drift and to form the equilibrium positron trajectory. Spiral coil consists of two pairs of conductors with opposite current directions, which form the rotating quadrupole field:

$$\begin{aligned} B_x &= -G(x\sin 2ks - z\cos 2ks) \\ B_z &= G(x\cos 2ks + z\sin 2ks) \end{aligned} \tag{4}$$

Here G is the focusing field gradient value, k=2π/h, h – the spiral step.

If the longitudinal positron velocity is much larger of the transverse one, the motion equations can be written as the following

$$\begin{cases} x'' + \dfrac{1}{\rho}z' - \dfrac{1}{\rho}\dfrac{G}{B}(x\cos 2ks + z\sin 2ks) = 0 \\ z'' - \dfrac{1}{\rho}x' - \dfrac{1}{\rho}\dfrac{G}{B}(x\sin 2ks - z\cos 2ks) = 0 \end{cases}, \tag{5}$$

where $(\,)' = \dfrac{d}{ds}$, B- the longitudinal magnetic field.

When the condition $\frac{G}{Bk}<1$ is satisfied, the solution of the system (5) is the sum of three oscillations:

1) the fast Larmor rotation;

2) the quadrupole oscillations with wave number of

$$q = 2k - \left(\frac{G}{B}\right)^2 \frac{1}{2k};$$

3) the slow betatron oscillations.

From initial conditions we have:

$$\begin{aligned}
x(s) &\approx x_0\left(\left(1-\frac{1}{2}\frac{G}{Bk}\right)\cos Qs+\frac{1}{2}\frac{G}{Bk}\cos qs\right)\\
&-z_0\left(\left(1+\frac{1}{2}\frac{G}{Bk}\right)\sin Qs-\frac{1}{2}\frac{G}{Bk}\sin qs\right)+\rho x'_0\sin\frac{s}{\rho}+\rho z'_0(\cos\frac{s}{\rho}-1)\\
z(s) &\approx x_0\left(\left(1-\frac{1}{2}\frac{G}{Bk}\right)\sin Qs+\frac{1}{2}\frac{G}{Bk}\sin qs\right)\\
&+z_0\left(\left(1+\frac{1}{2}\frac{G}{Bk}\right)\cos Qs-\frac{1}{2}\frac{G}{Bk}\cos qs\right)-\rho x'_0(\cos\frac{s}{\rho}-1)+\rho z'_0\sin\frac{s}{\rho},
\end{aligned} \tag{6}$$

where $Q=\left(\frac{G}{Bk}\right)^2\frac{k}{2}$ is the betatron wave number.

Moving in the ring, a positron rotates with fast Larmor frequency $\omega_L = eB/\gamma mc$ around the field line and drifts – inside the toroidal section in vertical direction and inside the focusing section around the axis of the spiral coil. Let us consider now the positron dynamics as a drift motion of "the Larmor circle". One can describe the transformation of the coordinates of the Larmor circle center with the transfer matrixes:

$$M_{Tor}=\begin{pmatrix}1 & 0\\ -\frac{\pi\rho}{R_0} & 1\end{pmatrix},\quad M_Q=\begin{pmatrix}\cos QL & -\sin QL\\ \sin QL & \cos QL\end{pmatrix}, \tag{7}$$

where M_{Tor} is the transfer matrix for toroidal section, M_Q - for focusing section with quadrupole coil (when $L \neq nh/2$, n is integer). The matrix of the focusing period can be

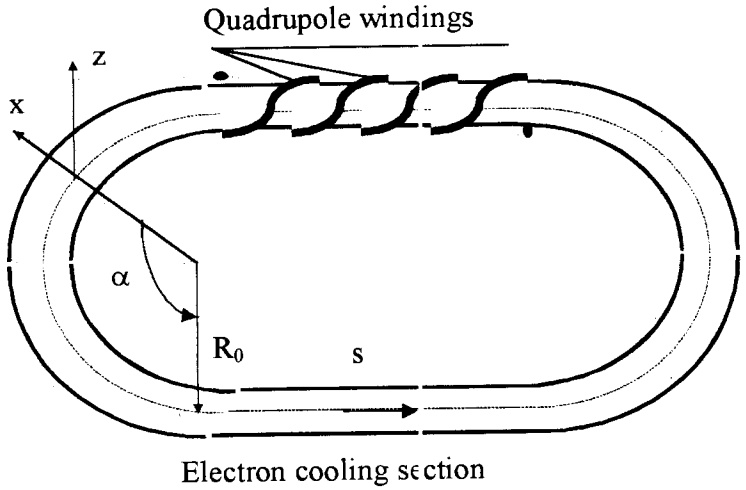

Fig 1. The focusing system of the low energy positron accumulator.

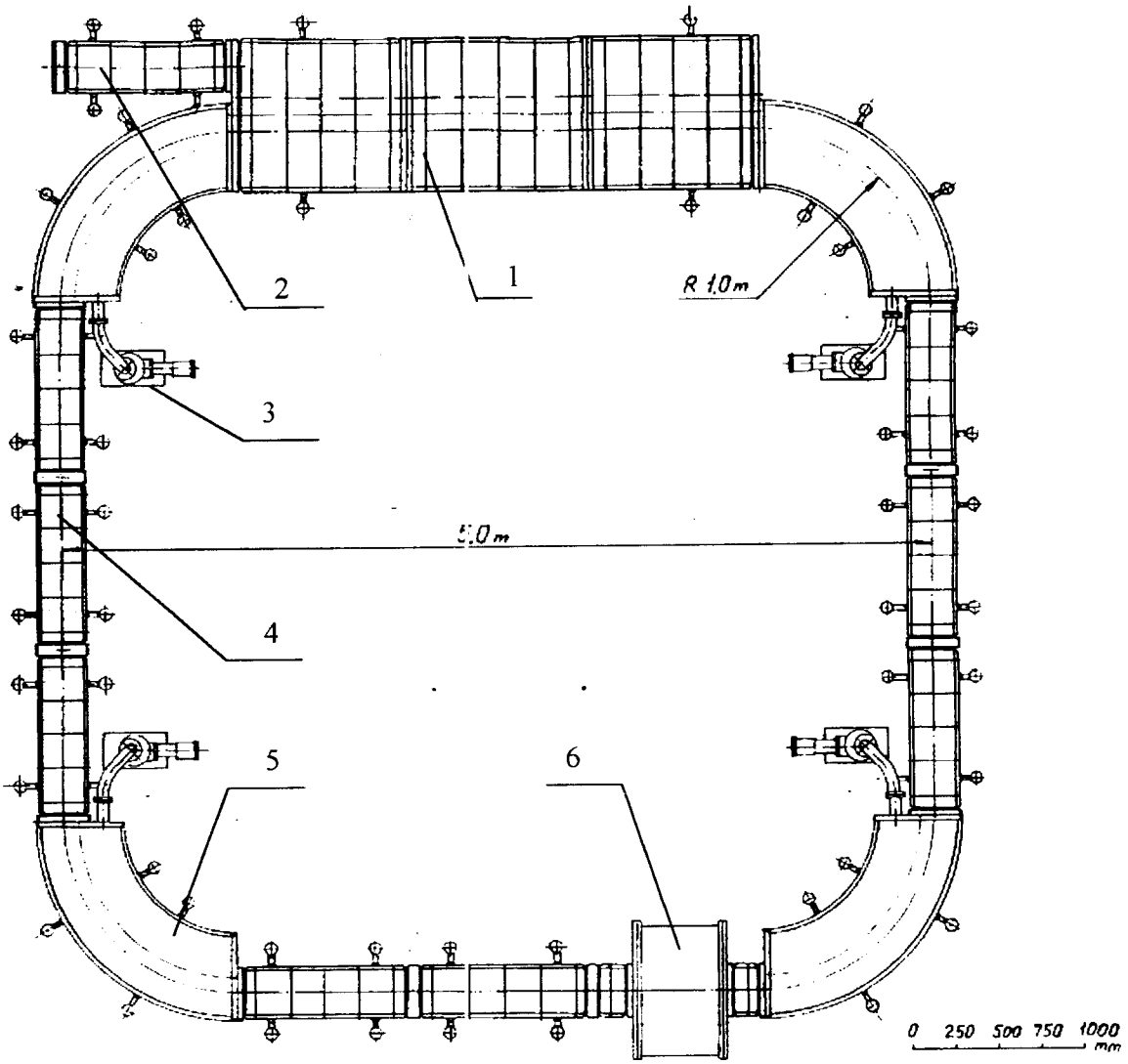

Fig. 2. Schematics of the Modified Betatron Prototype: 1 – kicker, 2 - electron gun, 3 - vacuum pump, 4 - section with quadrupole spiral coil, 5 - toroidal section, 6 – inductor.

obtained by multiplication of the matrices of the elements.The drift motion is stable, when the following condition is satisfied:

$$\left|\sqrt{1+\left(\frac{\pi\rho}{R_0}\right)^2}\cos(QL - a\tan\frac{\pi\rho}{R_0})\right| < 1 \cdot \qquad (8)$$

Then the Larmor circle crosses the electron cooling section (for instance) in the points, which lie on the canonical ellipse with eccentricity given by expression

$$\frac{a}{b} = \sqrt{1-\left(\frac{\pi\rho}{R_0}\right)^2 - 2\frac{\pi\rho}{R_0}\cdot c\tan QL}\,. \qquad (9)$$

Such a simple two-dimensional model permits to estimate the minimal gradient value of the spiral focusing coil required for stability of the particle drift motion and to calculate the beam crossection inside the different elements of the ring. However, a correct solution of the problem of the particle motion stability and obtaining of the beam characteristics during acceleration and storing requires the numerical simulation of the particle dynamics in six-dimensional phase space (in progress presently).

3. The prototype of the modified betatron dedicated to electron cooling

In order to test the medium energy electron cooling system based on modified betatron the design of the prototype of such a system was started in the JINR. The focusing system of the prototype (Fig 2) consists of two focusing periods. The septum coils of the injection system are not necessary because only one beam accelerates and circulates in the ring. General parameters of the Modified Betatron Prototype are given in the Table. The relation between the frequencies of the electron revolution and of the accelerating induction field determines the energy spread of electrons due to acceleration. Its value is about 10^{-5} [4], which satisfies the requirements to a cooling system. We plan to study experimentally with the prototype the following questions: the optimal parameters of the spiral focusing system for different electron energies, the space charge effects, the resonance phenomena, the electron momentum

Table. General parameters of the Modified Betatron Prototype.

Ring parameters and electron beam		
Circumference	m	18.28
Maximal energy	MeV	4.36
Revolution period	nsec	367-50
Longitudinal magnetic field	KG	1.0
Bending magnetic field	G	2.6-160
Major radius of the toroids	m	1
Electron gun		
Injection energy	keV	10
Maximal beam current	A	0.5
Electron beam radius	cm	1.2
Quadrupole spiral coils		
The length of the coil	m	3
Max gradient of quadrupole magnetic field	G/cm	12
The number of spiral winding		3
Acceleration cycle		
Induction accelerating voltage amplitude	V	50
Acceleration repetition frequency	Hz	1
Acceleration cycle duration	msec	10
Diameter of vacuum chamber	Cm	5
Residual gas pressure	Torr	10^{-9}

spread at induction acceleration, the longitudinal coherent instability threshold and some others. Presently the technical design of the standard section of the straight solenoid of the ring is completed and manufacturing of the ring elements is started.

This work is supported by the Russian Foundation for Basic Research (Grant N 92-02-17211).

References

1. I.Meshkov and A.Skrinsky, Preprint JINR E9-95-130, Dubna (1994), NIM A379 (1996) 41-49.

2. Rostoker N., Part. Accel. 1973, v 5, N 7, pp. 93-97

3. Robertson C.W., Mondelli A., Chernin D., Phys. Rev. Lett., 1983,v 50, N 7, pp. 507-510.

4. I.N.Meshkov, A.O.Sidorin Proc of the International Workshop on Medium Energy Electron Cooling, Budker INP, Novosibirsk, 1997, 183-188.

5. G.P. Jackson "Modified betatron approach to electron cooling." ibid, 171-182.

6. I.N.Meshkov, A.O.Sidorin, NIM A391 (1997) 205-209.

ON THE PARTIAL STABILITY OF SOLUTIONS OF NONAUTONOMOUS SYSTEMS

A.Yu. Aleksandrov

St.Petersburg State University,
Bibliotechnaya pl. 2, Petrodvorets, St.Petersburg, 198904 Russia
e-mail: alex@vrm.apmath.spb.su

Abstract

Using the Lyapunov direct method, the sufficient conditions of the asymptotic stability of solutions of nonlinear nonstationary systems with respect to a part of the variables are obtained.

Consider the system of differential equations

$$\dot{X} = Y, \quad (m\dot{Y}) = qE + qY \times B. \tag{1}$$

System (1) describes the motion of charged particle of mass m and charge q in an electromagnetic field [1]. This field is determined by the magnetic induction vector $B(t, X)$ and by the electric field strength vector $E(t, X)$; X and Y are respectively the position and velocity of the moving particle.

According to Zubov's theorem of universality of the electrodynamic equations of Maxwell [2], for a given velocity field

$$\dot{X} = \eta(t, X)$$

there exist vector-valued functions $B(t, X)$ and $E(t, X)$ that satisfy Maxwell's equations and such that system (1) admits the existence of the integral manifold

$$Y = \eta(t, X) \tag{2}$$

in the phase space of the moving charged particles. The integral manifold (2) has the property that an arbitrary charged particle situated on it at $t = t_0$ remains on this manifold for all times during its motion.

The important problem is that of stability of the integral manifold (2). It can be reduced to the investigation of partial stability of an auxiliary differential equations system [3].

The aim of the present paper is to obtain some conditions of partial stability of solutions of nonlinear nonautonomous systems.

Let the system be given

$$\begin{aligned} \dot{X} &= \frac{\partial W}{\partial X} + G(Y)X, \\ \dot{Y} &= H(X). \end{aligned} \tag{3}$$

Here X is a m-vector, Y is a p-vector; $H(X)$ is continuous p-vector defined for $X \in E^m$, and $H(0) = 0$; $W(X)$ is continuously differentiable negative definite homogeneous function of order $\mu + 1$, $\mu > 1$; and $G(Y)$ is a skew-symmetric matrix of the order m defined and continuous for $Y \in E^p$.

Consider the function

$$V(X) = \frac{1}{2}\|X\|^2. \quad \left(\|X\| = \sqrt{x_1^2 + \ldots + x_m^2}\right). \tag{4}$$

Its derivative with respect to system (3) has the form

$$\frac{dV}{dt} = (\mu + 1)W(X).$$

Hence, the zero solution of system (3) is asymptotically stable with respect to X [4].

Side by side with system (3), we will consider the perturbed system

$$\begin{aligned} \dot{X} &= \frac{\partial W}{\partial X} + G(Y)X + B_1(t)R_1(X), \\ \dot{Y} &= H(X) + B_2(t)R_2(X), \end{aligned} \tag{5}$$

where the elements of the l and k-vectors $R_1(X)$ and $R_2(X)$ are continuously differentiable homogeneous functions of order μ; the $(m \times l)$ and $(p \times k)$-matrices $B_1(t)$ and $B_2(t)$ are continuous and bounded for $t \geq 0$ as well as the integral

$$\int_0^t B_1(\tau)\, d\tau.$$

Let us suppose that $G(0) = 0$, and vector $H(X)$ satisfies the inequality

$$\|H(X)\| \leq A\,\|X\|^{\lambda}, \quad A > 0, \quad \lambda > 0,$$

in some vicinity of the point $X = 0$.

Theorem 1. *Under the condition $\lambda > \mu - 1$ the zero solution of system (5) is stable with respect to (X, Y) and asymptotically stable with respect to X.*

Proof. Construct the Lyapunov function for system (5) in the form

$$V_1(t, X) = V(X) - X^* \int_0^t B_1(\tau)\, d\tau\ R_1(X), \tag{6}$$

where $V(X)$ is defined by (4).

Differentiate V_1 with respect to (5):

$$\begin{aligned} \frac{dV_1}{dt} = (\mu + 1)W(X) - \left(\frac{\partial W}{\partial X} + G(Y)X + \right. \\ \left. + B_1(t)R_1(X)\right)^* \frac{\partial}{\partial X}\left(X^* \int_0^t B_1(\tau)\, d\tau\ R_1(X)\right). \end{aligned}$$

The inequalities

$$\begin{aligned} a_1\|X\|^2 - a_3\|X\|^{\mu+1} \leq V_1(t, X) \leq a_2\|X\|^2 + a_3\|X\|^{\mu+1}, \\ \frac{dV_1}{dt} \leq -b_1\|X\|^{\mu+1}(1 - b_2\|G(Y)\|), \quad \|B_2(t)R_2(X)\| \leq b_3\|X\|^{\mu} \end{aligned}$$

are valid for all $X \in E^m$, $Y \in E^p$. Here a_1, a_2, a_3, b_1, b_2, b_3 are positive constants. Therefore, there exists a $\delta > 0$ such that the conditions

$$\|X(t)\| < \delta, \quad \|Y(t)\| < \delta, \quad t \in [t_0, t_1],$$

imply the inequalities

$$|y_s(t)| \le |y_s(t_0)| + \int_{t_0}^{t} \left(A\|X(\tau)\|^{\lambda} + \|X(\tau)\|^{\mu}\right) d\tau, \quad s = 1, \ldots, p,$$

$$\frac{a_1}{2}\|X(t)\|^2 \le V_1(t, X(t)) \le \frac{3a_2}{2}\|X(t)\|^2,$$

$$\frac{dV_1(t, X(t))}{dt} \le -\frac{b_1}{2}\|X(t)\|^{\mu+1}, \quad t \in [t_0, t_1].$$

Here $(X(t), Y(t))$ is a solution of (5).

Utilising the method of estimations [5], we get that all the solutions of (5) starting at $t = t_0$ from the point close enough to the $(X, Y) = (0, 0)$ satisfy the inequalities

$$\|X(t)\| \le c_1 \left(1 + c_2\|X(t_0)\|^{\mu-1}(t - t_0)\right)^{-\frac{1}{\mu-1}},$$

$$|y_s(t)| \le |y_s(t_0)| + c_3 \left(\|X(t_0)\|^{\lambda+1-\mu} + \|X(t_0)\|\right), \quad s = 1, \ldots, p,$$

for any $t \ge t_0$. Here c_1, c_2, c_3 are positive constants. That completes the proof.

Corollary. *Consider in (5) the perturbation of the type*

$$B_1(t)R_1(t) = b(t)\frac{\partial}{\partial X}\left(\|X\|^{\mu+1}\right),$$

where scalar function $b(t)$ and its integral $\int_0^t b(\tau)\,d\tau$ are continuous and bounded for $t \ge 0$. Then for all $\mu > 1$, $\lambda \ge 0$ the zero solution of system (5) is asymptotically stable with respect to X.

Consider now the system

$$\dot{X} = \frac{\partial W}{\partial X} + G(X)X + B(t)R(X). \tag{7}$$

Here X is a m-vector; $W(X)$ is continuously differentiable negative definite homogeneous function of order $\mu + 1$, $\mu > 1$; $G(X)$ is skew-symmetric matrix defined and continuous for all $X \in E^m$ and satisfying the inequality

$$\|G(X)\| \le A\|X\|^{\lambda}, \quad A > 0, \quad \lambda > 0,$$

in some vicinity of the point $X = 0$; the elements of the l-vector $R(X)$ are continuously differentiable homogeneous functions of order σ, $\sigma > 1$; the $(m \times l)$-matrix $B(t)$ and its integral $\int_0^t B(\tau)\,d\tau$ are continuous and bounded for $t \ge 0$.

It is known [5], that in case where $\sigma > \mu$, the zero solution of (7) is asymptotically stable.

This condition can be strengthened if we use function (6). We get

Theorem 2. *If the inequalities*

$$2\sigma > \mu + 1, \quad \sigma + \lambda > \mu$$

are valid, then the zero solution of system (7) is asymptotically stable.

To prove the theorem, one has to verify the conditions of Lyapunov's asymptotic stability theorem for the function $V_1(t, X)$ constructed by formula (6).

References

[1] Bo Lehnert, *Dynamics of charged particles*, North-Holland, Amsterdam, and Interscience, New York, 1964.

[2] V. I. Zubov, *Oscillations and waves*, Leningrad Univ., Leningrad, 1989 (in Russian).

[3] V. I. Zubov, *Theory of oscillations*, Vyssh. Shkola, Moscow, 1979 (in Russian).

[4] V. V. Rumyantsev, A. S. Oziraner, *Stability and stabilization of motion with respect to a part of the variables*, Nauka, Moscow, 1987 (in Russian).

[5] V. I. Zubov, *Methods of A. M. Lyapunov and their application*, Noordhoff, Groningen, 1964.

On Application of Multiobjective Optimization to the Problem of Beam Dynamics Control *)

L.V. Vladimirova, I.D. Rubtsova, M.V. Sukhomud

St. Petersburg University, Russia

In the earlier published works [1,2,3] the problem of beam dynamics optimization was reduced to minimization or maximization of the criteria connective

$$K = \sum_{j=1}^{J} c_j K_j(u) \tag{1}$$

with certain factors c_j, $j = \overline{1,J}$. Here $K_j(u)$, $j = \overline{1,J}$, are the criteria characterizing device quality, u is the control function. The factors c_j, $j = \overline{1,J}$, are assigned with allowance of criteria significance; $\sum_{j=1}^{J} c_j = 1$. In [1] the explicit expression of functional (1) gradient is obtained. The experience of numerical optimization shows that the requirements laid on the beam are often contradictory and the improving of optimization results is reached as compromise between these requirements. For example, the requirements of high bunching quality and small energy dispersion are conflicting. After realization of several initial optimization steps the following situation may occur: the further increase of phase bunching quality entails increase of energy dispersion, and on the other hand, at a drop of energy spread the bunching worsens. Therefore in such situation it is advisable to apply the multicriterial approach. In this paper the solution of optimal control problem by the method of vectorial optimization is offered.

We shall introduce some necessary definitions [4]. The criteria vector $K = (K_1, K_2, \ldots, K_J)$ is defined in the domain D of parameters space ($D \subset E^s$).

Assume that we are interested in a minimum (maximum) on each criterion.

Definition 1. The point $A' \in D$ is called unconditionally better than point $A \in D$ if for any ν

$$K_\nu(A') \le K_\nu(A) \quad (K_\nu(A') \ge K_\nu(A)) \tag{2}$$

and at least for one $\nu = \nu_0$

$$K_{\nu_0}(A') < K_{\nu_0}(A) \quad (K_{\nu_0}(A') > K_{\nu_0}(A)). \tag{3}$$

Definition 2. A point $A \in D$ is said to be effective point if there is no point $A' \in D$ to be unconditionally better than A.

The set of all effective points is designated by E.

Definition 3. The set P (in criteria space) which consists of points corresponding to all points $A \in E$ is named Pareto set.

A set of Pareto points in two-dimensional criteria space ($J = 2$) is named compromise curve (trade-off curve).

Now we explain the method of approximate compromise curve construction. Consider

*) Work supported by the Russian Foundation for Basic Research, grant no. 96-01-00926.

a point $A(\alpha_1,\alpha_2,\ldots,\alpha_s)\in D$. Let parameters α_i, $i=\overline{1,s}$ satisfy the conditions

$$\alpha_i^* \le \alpha_i \le \alpha_i^{**}, \quad i=\overline{1,s}.$$

These limitations determine parallelepiped Π in parameters space. In addition to parametric constraints, the problem formulation usually contains the criterial constraints

$$K_\nu(A) \le K_\nu^{**}, \quad \nu=\overline{1,J}. \tag{4}$$

The value K_ν^{**} is the worst of the allowable values of a criterion $K_\nu(A)$.

For the construction of approximate Pareto set we select trial points A_i from Π and calculate the values of all criteria $K_1(A_i),K_2(A_i),\ldots,K_J(A_i)$. The points A_i satisfying the condition (4) compose the finite set D_N. Approximately effective points $\tilde{A}$ are chosen from D_N by rules (2), (3). The points $\tilde{B}=(K_1(\tilde{A}),K_2(\tilde{A}),\ldots,K_J(\tilde{A}))$ corresponding to approximately effective points $\tilde{A}\in E_N$ compose the approximate Pareto set in the criteria space. For $J=2$ the polygonal line connecting approximately Pareto points is the approximate compromise curve P_N.

We shall describe the algorithm of finding of approximately effective points in D_N. Let's mark any $A_{i_1}\in D_N$. Comparing it with all remaining points from D_N we eliminate all points A_j which are unconditionally worse than A_{i_1} (for A_{i_1} and A_j the conditions (2), (3) are checked up). Then we choose A_{i_2} from the remainder of points and mark it. Comparing A_{i_2} with all points remained and with A_{i_1}, we reject the points which are unconditionally worse than A_{i_2}, etc. After a finite number of steps we'll have only marked points that compose a set of approximately effective points E_N.

The geometric interpretation of this algorithm is as follows. May B_{i_1} in criteria space be the transform of the point A_{i_1}. We exclude the points A_j if their transforms B_j get a quadrant with the top B_{i_1}. The illustration of the algorithm is represented at fig.1 for the case of both criteria minimization. The convergence of E_N to E is proved in [4].

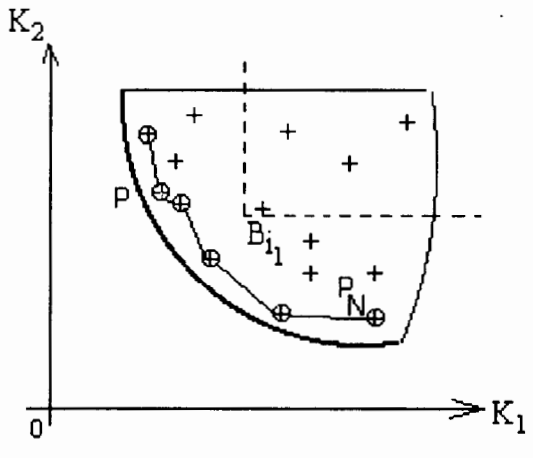

Fig. 1

We present the application of the method of vectorial optimization for obtaining of optimized parameters of two devices. The first is traveling wave linear accelerator of electrons LEA-15-M with the following main specifications: initial energy of particles is $W_0=40keV$, the length of accelerator is $L=78cm$. The dynamics of a charged particle in such a structure is described by equations [1]

$$\frac{d\gamma}{d\xi} = -\alpha(\xi)\sin\varphi$$
$$\frac{d\varphi}{d\xi} = 2\pi\left(\frac{1}{\beta_{ph}} - \frac{\gamma}{\sqrt{\gamma^2-1}}\right) \qquad (5)$$

Here the control functions are as follows: the pure value of amplitude parameter of accelerating wave intensity

$$\alpha(\xi) = \frac{eE_0\lambda}{m_0c^2} \qquad (6)$$

and the reduced phase velocity of accelerating wave:

$$\beta_{ph} = \frac{v_{ph}}{c}. \qquad (7)$$

From here on e, m_0 are the charge and rest-mass of electron, c is the velocity of light, λ is the accelerating wave length, $\xi = \frac{z}{\lambda}$ is reduced longitudinal coordinate (the axis Oz coincides with the channel symmetry axis), γ is reduced energy, φ is the phase of a particle, E_0, v_{ph} determine

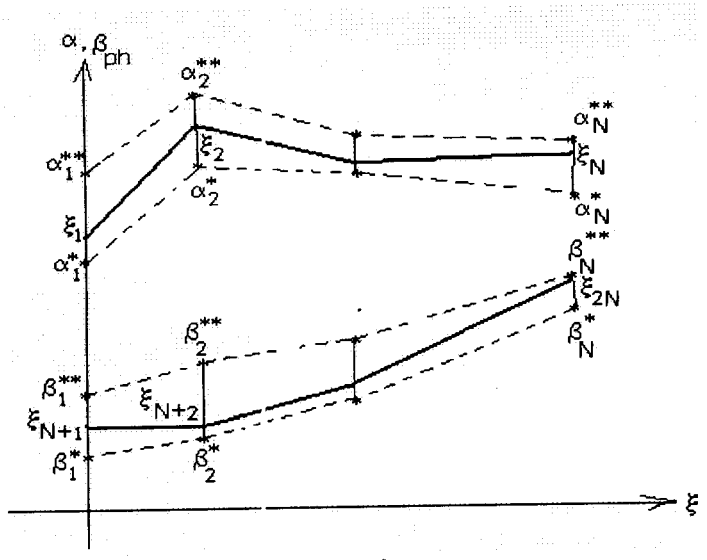

Fig.2

a basic harmonics of accelerating wave. The initial data set for (5) is $M_0 = \left\{\gamma_0^{(i)}, \varphi_0^{(i)},\ i = \overline{1,M}\right\}$, where $\gamma_0^{(i)}, \varphi_0^{(i)} (i = \overline{1,M})$ are the initial phase and energy values of M model particles. The initial energy is supposed to be identical for all particles and equal to $\gamma_0^{(i)} = \bar{\gamma}_0 = 1 + \frac{W_0}{m_0c^2}$, $i = \overline{1,M}$, (because of small dispersion of initial energies). We consider the initial phases $\varphi_0^{(i)}$ of particles to belong a segment $[-\pi, \pi]$. The results are represented for $M = 20$.

The problem of optimization of beam dynamics in the accelerator is to determine the controls (6), (7) providing the minimal beam energy spread and minimal phase dispersion at maximal capture coefficient. Therefore we introduce the following criteria

$$K_1(u) = \max_i \varphi_i^e - \min_i \varphi_i^e,$$
$$K_2(u) = \max_i \gamma_i^e - \min_i \gamma_i^e, \qquad (8)$$
$$K_3(u) = \frac{\Delta\varphi}{2\pi},$$

where $u = (\alpha(\xi), \beta_{ph}(\xi))$ is the control vector , $\Delta\varphi$ is initial phase interval, φ_i^e, γ_i^e are the values of phase and energy of i -th particle at accelerator exit .

The controls (6), (7) are defined by the values in N grid points: $\alpha(\xi_i), \beta_{ph}(\xi_i)$, $i = \overline{1,N}$. So we have $2N$ optimization parameters, which assume the values in parallelepiped

$$\Pi = \left\{X : \alpha_i^* \le \alpha_i \le \alpha_i^{**}, \beta_i^* \le \beta_{ph,i} \le \beta_i^{**}, i = \overline{1,N}\right\}.$$

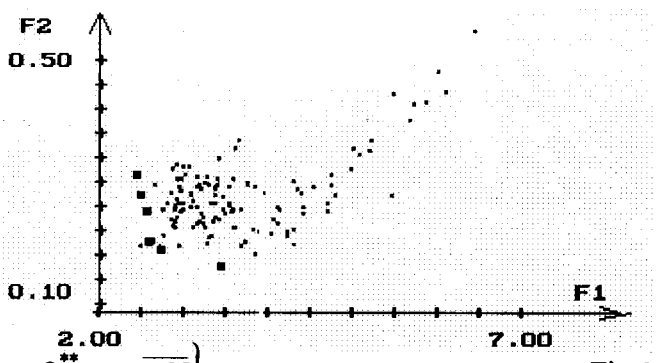

Fig.3

The point in Π determines one control (6) and one control (7).

We shall construct the Pareto set for criteria (8) under the condition

$$K_3^* \le K_3 . \qquad (9)$$

Let's select control u as a random point from Π

$$\xi = \left(\xi_i = (\alpha_i^{**} - \alpha_i^*)x_i + \alpha_i^*; \xi_{N+i} = (\beta_i^{**} - \beta_i^*)x_{N+i} + \beta_i^*, i = \overline{1,N}\right),$$

where x is $2N$-dimensional vector with components uniformly disrtibuted in [0,1] (Fig.2).

After numerical intergration of the system (5), we compute values of criteria (8) and check the condition (9). If it is satisfied we receive a point in the criteria space, otherwise we compute a new point ξ. We apply the described above method of approximate compromise curve construction. At first we receive the set of approximately effective points in Π. In our case it is the set of effective controls (6),(7) which provide the required beam parameters, in particular, the capture coefficient not less than preassigned value K_3^*.

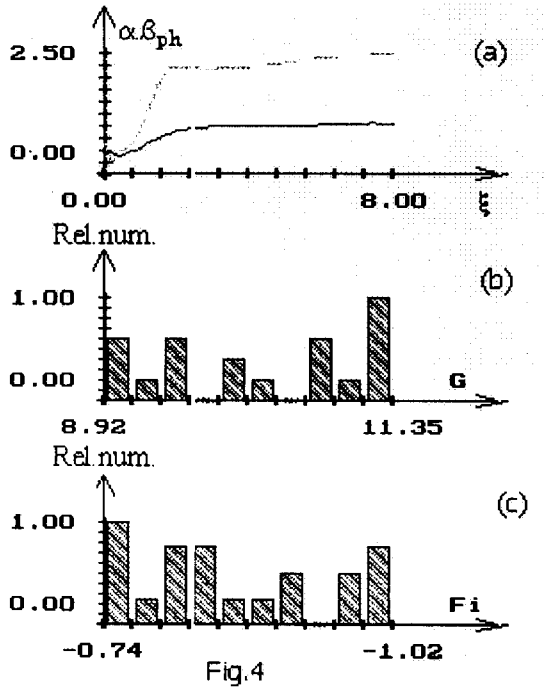

Fig.4

Tab.1

K_1	K_2	K_3
2.5178	0.2655	0.8947
2.6450	0.2016	0.8947
2.5647	0.2641	0.8947
2.4514	0.2829	0.9474
2.5835	0.2120	0.8947
3.3902	0.1736	0.8947
2.5709	0.2423	0.8947

On fig.3 the points of approximate compromise curve for the circumscribed device are shown at $K_3^* = 0.7$. The values of three criteria for all points of a compromise curve are given in table 1. Fig.4 represents the controls (a), energy spectrum (b) and phase spectrum (c) for Pareto point which corresponds to the effective controls $\alpha(\xi), \beta_{ph}(\xi)$ providing maximal capture.

The next device to be discussed is buncher of klystron type. Longitudinal dynamics of relativistic particle in bunching system is described by equations:

$$\frac{dz}{d\tau} = \frac{p}{\sqrt{1+p^2}}$$
$$\frac{dp}{d\tau} = \frac{e}{m_0 c^2}\left(\sum_{n=1}^{N} E_n(\tau, z, u) + E_p(\tau, z)\right). \qquad (10)$$

Here $\tau = ct$, t is the time, z, p are longitudinal coordinate and reduced momentum of particle, N is the total number of resonators of buncher, $E_n(\tau, z, u)$ is longitudinal component of RF field intensity in n-th resonator, $E_p(\tau, z)$ is longitudinal component of Coulomb field intensity. We suppose the coordinate axis Oz to be aligned with channel symmetry axis. Control vector u is introduced as a vector of device parameters, namely, the mismatches of resonators and drift tube lengths (excluding modulator and drift tube preceding it). The investigation of longitudinal beam dynamics in such a structure is carried out with due account of Coulomb repulsion and the excitation of RF fields in resonators.

We designate phase vector of a particle as $x = (z, p)^T$. Let M_0 be the set of initial phase states $x_0 = (z_0, p_0)^T$ of particles of one or several consequent bunches. At fixed control u the system (10) defines the ensemble of trajectories $x = x(\tau, x_0, u)$ emerging from the set M_0.

We investigate the problem of bunching system parameters optimization. The purpose of optimization is to maximize the share of particles of a bunch satisfying some restrictions on phase and energy at the device exit. These restrictions are as follows:

$$|\varphi| \le \Delta\varphi, \quad \frac{|W - W_0|}{W_0} \le b.$$

Here $\varphi \in [-\pi, \pi]$, W are accordingly phase and energy of particles at the exit ; W_0 is initial energy of particles; the constants $\Delta\varphi$, b characterize required phase width and reduced energy dispersion of a bunch.

Let us introduce the following optimization criteria characterizing bunching quality on phase and energy correspondingly:

$$K_1(u) = \int_0^T \int_{M_{\tau,u}} \Phi_1(\tau, z_\tau)\Phi_3(z_\tau - z_{ex}(u))dz_\tau dp_\tau, \qquad (11)$$

$$K_2(u) = \int_0^T \int_{M_{\tau,u}} \Phi_2(\tau, z_\tau)\Phi_3(z_\tau - z_{ex}(u))dz_\tau dp_\tau \,. \qquad (12)$$

Here T/c is the time necessary for model particles to pass the struture; $M_{\tau,u} = \{x_\tau = x(\tau, x_0, u) : x_0 \in M_0\}$ is τ-cutset of trajectory bundle of system (10) for the control u; $z_{ex}(u)$ is device exit coordinate. The integrands in formulae (11), (12) are determined by expressions:

$$\Phi_1(\tau, z) = \begin{cases} \cos\left(\frac{2\pi}{\Delta\varphi}\varphi(\tau, z)\right) + 1 & |\varphi(\tau, z)| \le \frac{\Delta\varphi}{2} \\ 0, & |\varphi(\tau, z)| > \frac{\Delta\varphi}{2} \end{cases},$$

$$\Phi_2(p) = 1 - \left(\frac{2}{bW_0}\left(\left(\sqrt{1+p^2} - 1\right)m_0c^2 - W_0\right)\right)^2,$$

$$\Phi_3(\xi) = \begin{cases} \cos\left(\frac{2\pi}{\Delta z}\xi\right) + 1, & |\xi| \le \frac{\Delta z}{2} \\ 0, & |\xi| \le \frac{\Delta z}{2} \end{cases}.$$

The function $\Phi_3(z - z_{ex}(u))$ is different from zero only in neighbourhood $\left(z_{ex} - \frac{\Delta z}{2}, z_{ex} + \frac{\Delta z}{2}\right)$. That's why a particle makes nonzero contribution to quality functional in only case: the particle is in the given neighbourhood. The size Δz is preassigned for every numerical problem. The values of functions $\Phi_1(\tau, z)$, $\Phi_2(\tau, z)$ increase with lowering of deviation of phase and energy of particle from mear values 0 and W_0 correspondingly. The function $\Phi_1(\tau, z)$ vanishes if the particle does not get the required phase interval at device exit.

Vectorial optimization of device parameters with criteria (11),(12) was carried out for the buncher with following main characteristics: the number of resonators $N = 4$, $W_0 = 500keV$, $\lambda = 0.1m$, mean value of beam current $I_0 = 10A$ channel aperture radius $a = 0.006m$, bean radius $R = 0.003m$, input power $p_0 = 0.3kVt$. The optimization parameters are resonator mismatches $\left(\frac{\Delta f_2}{f}, \frac{\Delta f_3}{f}, \frac{\Delta f_4}{f}\right)$ and drift tube lengths (l_2, l_3, l_4, l_5). So the control vector $u = \left(\frac{\Delta f_2}{f}, \frac{\Delta f_3}{f}, \frac{\Delta f_4}{f}, l_2, l_3, l_4, l_5\right)^T$.

For construction of Pareto set 150 trial points were used. The coordinates of the points and corresponding criteria values are represented in table 2. In this table the values of the following beam characteristics at device exit are given: relative value I_1/I_0 of the

amplitude of beam current first harmonics; relative value $\Delta W/W_0$ of energy dispersion; the percentage η of particles (of a bunch), which got into the required intervals of phases and energies at device exit. The total buncher length L is presented in the last column of the table.

The values of the same parameters, criteria and characteristics for the device before optimization are given in the last line of the table for a comparison.

Table 2

Optimization parameters							**Criteria**		**Characteristics**			
mismatches of resonators			drift tube lengths									
$\Delta f_2/f$	$\Delta f_3/f$	$\Delta f_4/f$	L2	L3	L4	L5	K1 (u)	K2 (u)	I1/I0	$\Delta W/W_0$	η	L
0.0020	0.0088	0.0101	0.19	0.34	0.25	0.82	2.57	2.21	1.07	0.170	75	1.74
0.0025	0.0091	0.0151	0.34	0.71	0.38	0.66	2.93	0.69	1.35	0.246	50	2.24
0.0022	0.0088	0.0122	0.18	0.68	0.34	0.91	2.88	1.55	1.30	0.206	68	2.25
0.0025	0.0076	0.0154	0.22	0.60	0.32	0.87	2.88	1.82	1.25	0.191	80	2.14
0.0018	0.0107	0.0131	0.22	0.34	0.34	0.81	2.65	2.13	1.13	0.174	75	1.85
0.0026	0.0094	0.0137	0.29	0.69	0.26	0.85	2.91	1.33	1.31	0.217	59	2.22
0.0018	0.0072	0.0105	0.25	0.61	0.45	0.62	2.96	1.03	1.39	0.29	47	2.08

The controls obtained (as a result of multicriteria optimization) provide high level of bunching at system exit. One can choose the proper device among the structures corresponding the Pareto points.

References

1. Ovsyannikov D.A. Modelling and Optimization of Charged Particle Beam Dynamics. L.: Leningrad University, 1990.
2. Vladimirova L.V., Svistunov Yu. A., Ovsyannikov D.A. The Optimization of Particle Capture in Acceleration Regime for Large Currents in LEA // The Problem of Atomic Science and Technology. Series: Electrophysical Apparatus, issue 26, 1993.
3. Olemskoy I.V., Rubtsova I.D. Modeling and Optimization of Beam Dynamics in Resonance Bunching and Decelerating Systems. Proceedings of the International Workshop: Beam Dynamics and Optimization, July 4-8, 1994, St.-Petersburg, Russia; St.-Petersburg, 1995, pp.143-153.
4. Sobol I.M., Statnikov R.B. Optimal Parameters Determination in Multicriteria Problems. "Science", 1981.

ROBUST STABILITY ANALYSIS FOR PLASMA SHAPE CONTROL SYSTEM Part I

Dmitrii A. Ovsyannikov, Alexei P. Zhabko, Evgeny I. Veremey, Boris A. Misenov, Alexander D. Ovsyannikov, Vladimir L. Kharitonov

St. Petersburg State University, Bibliotechnaya pl., 2, Petrodvorets, St. Petersburg, 198904 Russia
e-mail: veremei@vrm.apmath.spb.su

Summary. The background of the loop-shaping approach to the robust stabilizing controllers synthesis are presented. It may be applied to the plasma shape control problem taking into account unstructured uncertainties in the plant model representation. The main aspects of the LSH-approach to robust stability margin analysis are discussed. It is shown, that optimal robust stability margin for the augmented plant is not equal to that for the initial plant and augmented optimal controller. The method of the controllers comparison is proposed by means of robust stability margin estimation. The results of the computations for the same given controllers are enclosed.

1 Preliminary note

As it is known, analysis and synthesis of dynamic system under the various model uncertainties is a matter of a great importance and hardness.

As for plasma-shape control synthesis, some general remarks concerning this global problem should be noted.

1. For any controller of the power consumption in the working range the eigenvalues of the matrix of full plasma-shape control closed loop system **are located in the neigbourhood** of the imaginary axis.

2. According to this, the stability margin of the closed loop system with respect to eigenvalues, the phase and the magnitude are extremely small (tend to zero).

3. That is why, it's not fully correct in this case to apply the standard MATLAB methods to analyze the robust stability margins of the full closed loop system with 10 control coils.

4. The correct approach to the robust stability margin analysis is to investigate the well controllable part of the system with non-efficient coils excluded. Other way is to use modified MATLAB procedures without H_∞-norm computation.

Taking into account all above remarks it is possible to use various approaches to the problems of robust stability margin analysis, in particular, the methods offered in [1].

2 Background

One of the most effective and suitable methods for the plasma shape control problem is the optimal loop-shaping synthesis (LSH-method) Let us consider its main aspects.

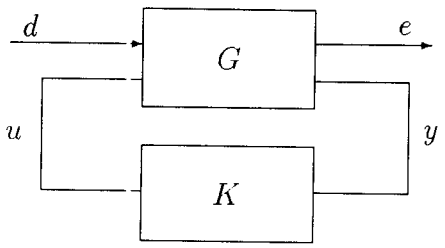

Fig. 1.

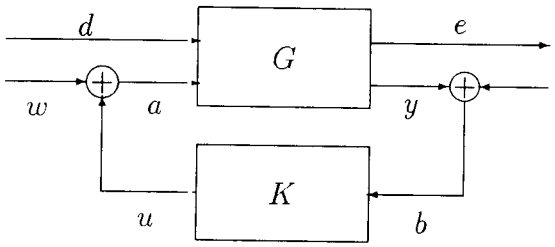

Fig. 2.

The controlled plant in plasma shape stabilization problem could be represented in standard LTI-form

$$\begin{cases} \dot{x} &= Ax + Md + Bu, \\ e &= C_1x + D_{11}d + D_{12}u, \\ y &= C_2x + D_{21}d + D_{22}u. \end{cases} \tag{1}$$

Here $x \in \mathbf{E}^n$ is state-space vector, $u \in \mathbf{E}^m$ is control vector, $y \in \mathbf{E}^{k_2}$ is output vector of measurements, $d = (\varphi(t) \;\; \psi(t))^T$ is vector of external disturbances, $e \in \mathbf{E}^{k_1}$ is tracking error vector.

Let the plant (1) be closed by the arbitrary internally stabilizing controller

$$u = K(s)y. \tag{2}$$

The closed loop interconnection of the system (1), (2) is illustrated by fig. 1. Here G is controlled plant and W is stabilizing controller.

Introduce the two auxiliary signals w and v being supplied both to input and to output of controller in addition to considered interconnection as it is shown in fig. 2.

Let us consider the transfer matrix $F_R(s, G, K)$ of the closed loop system from auxiliary signals (w, v) to input and output signals (b, u) of the controller (2):

$$\begin{bmatrix} u \\ b \end{bmatrix} = F_R(s, G, K) \begin{bmatrix} w \\ v \end{bmatrix}. \tag{3}$$

According to fig. 2 we have

$$b = y + v, \quad y = Ga, \quad a = u + w = Kb + w$$

and therefore $y = G[K(y + v) + w]$. This expression may be considered as the equation with respect to y, from which it follows that

$$y = (E - GK)^{-1}GKv + (E - GK)^{-1}Gw. \tag{4}$$

In accordance with (4) we have the formula for input signal of the controller in the following form

$$b = y + v = y + (E - GK)^{-1}(E - GK)v =$$
$$= (E - GK)^{-1}GKv + (E - GK)^{-1}Gw +$$
$$+(E - GK)^{-1}(E - GK)v = (E - GK)^{-1}[GK + E - GK) + Gw]$$

or

$$b = (E - GK)^{-1}Gw + (E - GK)^{-1}v,$$

therefore

$$u = Kb = K(E - GK)^{-1}Gw + K(E - GK)^{-1}v. \tag{5}$$

Here E is identity $(k \times k)$-matrix.

The expressions (4) and (5) give us

$$\begin{bmatrix} b \\ u \end{bmatrix} = \begin{bmatrix} (E - GK)^{-1}G & (E - GK)^{-1} \\ K(E - GK)^{-1}G & K(E - GK)^{-1} \end{bmatrix} \begin{bmatrix} w \\ v \end{bmatrix}, \tag{6}$$

i. e. the desired transfer matrix F_R may be represented as

$$F_R(s, G, K) = \begin{bmatrix} (E - GK)^{-1}G & (E - GK)^{-1} \\ K(E - GK)^{-1}G & K(E - GK)^{-1} \end{bmatrix} \tag{6a}$$

or in other form

$$F_R(s, G, K) = \begin{bmatrix} E \\ K \end{bmatrix} (E - GK)^{-1}[G \quad E]. \tag{7}$$

As it is noted in [1], [2], the transfer matrix $F_R(s, G, K)$ is of the first importance for LSH-approach. It is determined by the following statement.

Theorem 1. If an arbitrary controller with transfer matrix K belongs to the set Ω of the controllers internally stabilizing the nominal controlled plant (1) with transfer matrix G, then for all model perturbations $\begin{bmatrix} \Delta_1 \\ \Delta_2 \end{bmatrix}$, satisfying inequality

$$\left\| \begin{bmatrix} \Delta_1 \\ \Delta_2 \end{bmatrix} \right\|_\infty < b_m(G, K) = \|F_R(s, G, K)\|_\infty^{-1}, \tag{8}$$

the closed loop system with perturbed plant $\tilde{G} = (N + \Delta_1)(M + \Delta_2)^{-1}$ will be stable. Here $NM^{-1} = G$ is a normalized coprime factorization satisfying the condition

$$N(j\omega)^* N(j\omega) + M(j\omega)^* M(j\omega) = E$$

for the nominal plant. The norm $\|F_R\|_\infty$ is determined as

$$\|F_R(s, G, K)\|_\infty = \max_{\omega \in [0, \infty)} \bar{\sigma}(\omega, G, K), \tag{9}$$

where $\bar{\sigma}(\omega, G, K)$ is the maximal singular value of $F_R(j\omega, G, K)$ matrix.

So the value of $b_m(G, K)$ may be treated as *robust stability margin estimation for the closed loop system with the plant G and controller K*. It is the certain characteristic for the arbitrary controller internally stabilizing the nominal plant.

3 Loop-shaping optimal synthesis

As it was done in [1] on the base of approach presented in the previous section, it is possible to expand robust stability margin. Note that LSH-method takes into account not only the robust stability but also the closed loop system nominal performance. This is accomplished by the use of augmented plant model with the transfer matrix

$$P = W_2 G W_1, \tag{10}$$

where W_1 and W_2 are given transfer matrices of the weight multipliers.

It is proposed in [1] to find the transfer matrix of optimal controller for the plant (10) with respect to $\|F_R\|_\infty$

$$K_\infty = \arg \min_{K \in \Omega} \|F_R(s, P, K)\|_\infty. \tag{11}$$

In accordance with (8), optimal controller (11) provides the best (maximum) robust stability margin for the augmented plant. This margin is determined by the formula

$$b_m(P, K_\infty) = b_m(W_2 G W_1, K_\infty) = \|F_R(s, W_2 G W_1, K_\infty)\|_\infty^{-1}. \tag{12}$$

The final step of LSH-optimal synthesis procedure is to find the transfer matrix of augmented controller as follows

$$\tilde{K} = W_1 K_\infty W_2. \tag{13}$$

It is easy to see that augmented controller (13) stabilizes the initial plant G.

However it should be noted (this fact is not mentioned in [1]) that the optimal robust stability margin for the augmented plant is not equal to that for the initial plant with the augmented controller! So robust stability margin estimation (12) could not be used for real closed loop system, because

$$b_m(P, K_\infty) \neq b_m(G, \tilde{K}), \tag{14}$$

where

$$b_m(G, \tilde{K}) = b_m(G, W_1 K_\infty W_2) = \|F_R(s, G, W_1 K_\infty W_2)\|_\infty^{-1}. \tag{15}$$

The proof of the statement above is based on the formulae (6a), (12), (15) and may be easy carried out for the most simple situation with the following weights

$$W_1(s) \equiv E, \qquad W_2(s) \equiv \gamma E, \quad \gamma = \text{const}. \tag{15a}$$

4 Controllers comparison by means of robust stability margin estimation

As it follows from previous sections the value of

$$b_m(G, K) = \|F_R(s, G, K)\|_\infty^{-1} \tag{16}$$

may be used as one of the most simple robust stability margin estimations for any controller to be tested. This value may be computed with the help of standard procedures [1]. It is evident that the larger is $b_m(G, K)$ the better controller is.

Nevertheless it is necessary to highly stress that such an approach to the controllers comparison for plasma shape control system has essential disadvantages pointed out below.

1. The matrix of closed loop plasma shape control system in superconducting coils tokamaks for any controller in the working range of control power consumption has the eigenvalues located near the imaginary axis. It leads to the singular situation for which standard procedures give incorrect results.

2. The value of estimation $b_m(G,K)$ is too pessimistic—it may be exceeded for the most part of the frequency range. So it is better to use the function $b(\omega,G,K) = 1/\bar{\sigma}(\omega,G,K)$ as the frequency robust stability margin for the given controller and the nominal plant.

3. Besides the general pessimistic essence of the estimation $b_m(G,K)$ it is necessary to say, that experiments show the extremely small its value for all controllers have been tested.

4. The estimation $b_m(G,K)$ does not take into account the closed loop system performance for the certain transient processes. Before the comparison in the sense of this estimation it should be checked that the controllers are comparable in the sense of some performance characteristics.

In accordance with the notes above it is possible to suggest the following procedure for the various controllers comparison.

A. It is necessary to check that all controllers to be tested internally stabilize the nominal plant and have the similar performance characteristics in the sense of stabilization accuracy and control power consumption. The last of them is of a great importance because for the controllers with small power the robust stability margin is large, and otherwise.

B. For each of the comparable controllers to be tested it is necessary to compute the following characteristic

$$b(\omega,G,K) = 1/\bar{\sigma}(\omega,G,K)$$

—frequency robust stability margin for the closed loop system with the nominal plant G and controller K. It may be done with the help of modified MATLAB-procedure **emargin** in which the H_∞-norm computation is excluded [1].

C. The results of computations should be analyzed in different regions of frequency domain to determine the best controllers with the largest values of $b(\omega,G,K) = 1/\bar{\sigma}(\omega,G,K)$ in these regions.

5 The results of controllers testing by means of frequency robust stability margin estimation

As the examples of using the proposed procedure the corresponding computations were performed for the following controllers in FDR2 plasma shape control systems in ITER tokamak:

1. LSH-optimal controller C1 for the augment plant with the weights (15a).

2. LSH augment controller C2 corresponding to C1 for the initial nominal plant.

3. H_∞-optimal controller C3 with respect to the direct transfer matrix of closed loop system from the input signal d to the output signal e (note that this controller is close to the corresponding LQG-controller).

4. Internally stabilizing controller C4.

The analysis of the results leads to the following conclusion.

1. In the region of the low frequencies the controllers C2, C3 and C4 have approximately the same robust stability margins.

2. All the margins achieve their minima at the frequency about $10\,s^{-1}$ and the values of these minima are extremely small.

3. In the frequency range $\omega \in [0.02, 100]$ the controller C4 has the best robust stability margin, but it is also small.

4. For the high frequencies $\omega > 100$ the controllers C2 and C3 have the best robust stability margins. It is very important because the high-frequency plant behavior is usually uncertain.

5. The robust stability margin for the controller C1 is generally best, however this margin may be achieved only for the augmented plant, but not for the real closed loop system.

6 Conclusion

This work is devoted to some questions concerning the robust stability margin analysis for the plasma shape control systems with various feedback controllers. The method of the controllers comparison by means of frequency robust stability margin estimation is proposed. The results of the computations for the several given controllers are obtained and discussed.

References

[1] μ-Analysis and synthesis toolbox: User's guide / G. J. Balas, J. C. Doyle, K. Glover et al.— Natick (Mass.): The MathWorks, Inc., 1995.— 756 p.

[2] McFarlane D. C., Glover K. Robust controller design using normalised coprime factor plant description.— S.l.: Springer Verl., 1989.— (Lecture notes in control and information sciences. Vol. 138).

ROBUST STABILITY ANALYSIS FOR PLASMA SHAPE CONTROL SYSTEM

Part II

V. L. Kharitonov, B. A. Misenov, A. D. Ovsyannikov, D. A. Ovsyannikov, E. I. Veremey, A. P. Zhabko

St.Petersburg State University
Bibliotechnaya pl.2, Petrodvorets, St.Petersburg, Russia, 198904
E-mail: Dmitri.Ovsyannikov@pobox.spbu.ru

1. Introduction

1.1. At the present report we continue the analysis of the plasma shape stabilization that was started in [1,2]. The different approach to open loop system uncertainty modelling based on the systems of equations for the scenario points is proposed.

Let's underline the main especiality of the equations considered. For any controller of the power consumption in the working range the eigenvalues of the matrix of full plasma-shape control closed loop system are located in the neighbourhood of the imaginary axis. Thus the stability radius at the frequency domain and at the space of matrices is very close to zero. This unfortunate fact does not allow to apply the standard MATLAB methods for the admissible perturbation range of the physical parameters of the system. At the present paper the methods which take into account the mentioned especiality of the model are used.

1.2. Let's investigate the stability of the system of equations describing the dynamics of plasma shape deviation from the nominal

$$L_s \frac{d}{dt} X + R_s X = BU, \tag{1}$$

$$Y = C_s X + D_s U, \tag{2}$$

where s=1,2,3,4,5 corresponds to the scenario points XPF, SOF, SOB, EOB and EOC in ITER tokamak. All of the three controllers presented for investigation use at their feedback only the part of the observations (2) for which the corresponding entries of the matrices D_s are equal to zero. So the system (2) has more simple form here

$$Y = C_s X, \qquad s = 1, 2, 3, 4, 5. \tag{3}$$

1.3. Let's construct the parametric model describing the uncertainty of the system (1), (3) at the space of the matrices

$$Q = (L, R, C^{-1}).$$

Introduce the set of the admissible systems

$$\Gamma = \{Q = \sum_{s=1}^{5} \lambda_s Q_s \mid (\lambda_1, \lambda_2\ \lambda_3, \lambda_4, \lambda_5) \in \Lambda\},$$

where Λ - some set at 5-dimensional space. It's natural to propose that the realized scenario points (matrices Q_1, Q_2, Q_3, Q_4, Q_5) belong to the admissible systems set Γ, and therefore

$(1,0,0,0,0) \in \Lambda, (0,1,0,0,0) \in \Lambda, (0,0,1,0,0) \in \Lambda, (0,0,0,1,0) \in \Lambda, (0,0,0,0,1) \in \Lambda.$

Note that the minimal convex polytope at the space of the system matrices containing all the five scenario points is the set

$$\Gamma_0 = \{Q = \sum_{s=1}^{5} \lambda_s Q_s \mid \lambda_s \geq 0, \sum_{s=1}^{5} \lambda_s = 1\}. \tag{4}$$

Let's suppose hereafter that *all the admissible parametric uncertainty* of the system (1), (3) is described by 5 parameters λ_s. At the next sections we will consider the stability problem for the class of the systems (1), (3) closed by the controller under investigation with respect to some set of the admissible parameters Λ .

1.4. The most well-designed methods of the linear systems with uncertain coefficients stability analysis deal with the class of systems whose characteristic polynomials families form the convex polytope at the coefficients space. The results concerning multidimensional systems of differential equations robust stability analysis are far from systematic and the known robustness conditions are usually just sufficient. In particular, that is why the robustness of the system (1), (3) investigation leads to almost zero stability radius at the matrix coefficients space.

At the present report we also used the sufficient conditions of the stability of linear one-parameter matrix family which become necessary for rank one perturbation matrix.

2. Interval stability radius

2.1. The concept of the interval stability radius defined below reflects the admissible perturbation range of the parameters λ_s, introduced in section 1 to describe the set of the systems (1), (3) closed by the same controller. The norm reflecting the closeness of two parameter vectors $(\lambda_{11}, \lambda_{21}, \lambda_{31}, \lambda_{41}, \lambda_{51})$ and $(\lambda_{12}, \lambda_{22}, \lambda_{32}, \lambda_{42}, \lambda_{52})$ is chosen not as Euclidean norm but as a norm induced by the given collection of the matrices $Q_s = (L_s, R_s, C_s)$ for the scenario points.

For unit interval stability radius the new "ball" coinsides with the minimal convex polytope with matrix vertices $Q_s (s = 1, \ldots, 5)$.

2.2. The problem formulation and basic definitions.

Consider the set

$$\Lambda_0 = \{(\lambda_1, \lambda_2, \lambda_3, \lambda_4, \lambda_5) \mid \lambda_s \geq 0, \sum_{s=1}^{5} \lambda_s = 1\}. \tag{5}$$

and the point $l = (\lambda_{10}, \lambda_{20}, \lambda_{30}, \lambda_{40}, \lambda_{50})$, $\lambda_{s0} \geq 0$, $\sum_{s=1}^{5} \lambda_{s0} = 1$.

Definition. Let's call the set of the points as a closed ball of the radius r with the centre at the point $p = (p_1, p_2, p_3, p_4, p_5)$ $(p_1 + p_2 + p_3 + p_4 + p_5 = 1)$

$$V_r(p) = \{p + r(v - l) \mid v \in \Lambda_0\}.$$

Note. For $p = l$ and $r = 1$ $V_1(l) = \Lambda_0$.

Let's also interprete the ball $V_r(p)$ at the space of the matrices of the system (1), (3). Introduce the matrices

$$Q_s = (L_s, R_s, C_s^T), \quad P = \sum_{s=1}^{5} p_s Q_s, \quad G = \sum_{s=1}^{5} \lambda_{s0} Q_s$$

Then the interval matrix family of the radius r and the centre in P corresponding to the set $V_r(p)$ is

$$T_r(P) = \{P + r\sum_{s=1}^{5} \lambda_s(Q_s - G)\} = \{\sum_{s=1}^{5} v_s Q_s\},$$

$$\lambda_s \geq 0, \sum_{s=1}^{5} \lambda_s = 1; \qquad (v_1, v_2, v_3, v_4, v_5) \in V_r(P).$$

Let's also introduce the median matrix of the system (1), (3)

$$P_m = (Q_1 + Q_2 + Q_3 + Q_4 + Q_5)/5.$$

Definition. Let's call the first interval stability radius r_1 of the system (1), (3) closed by the controller

$$U = W(p)Y, \tag{6}$$

where $W(p)$ is the transfer matrix with rational-fraction coefficients, the maximal value for which the system (1), (3), (6) is asymptotically stable if

$$(L, R, C^T) \in T_{r_1}(P_m).$$

Definition. Let's call the second interval stability radius r_2 for the system (1),(3) closed by the controller (6), the maximal value for which the system (1),(3),(6) is asympotically stable if

$$(L, R, C^T) \in T_{r_2}(Q_s), \quad s = 1, \ldots, 5.$$

The analogous definitions are introduced for the closed loop systems in normal form

$$\begin{aligned} dx/dt &= -(L_s^{-1}R_s)x + (L_s^{-1}B)u \\ y &= C_s x \\ dz/dt &= \Gamma_1 z + \Gamma_2 y \\ u &= Kz \end{aligned} \tag{7}$$

and when considering the families of characteristic polynomials of these systems at the space of characteristic polynomial coefficients.

Note. These methods are the evolution of the robust technichs described in [3].

In Appendix we give the results of computation of the first and the second interval stability radii for three presented controllers C1, C2, C3. The computations were carried out with package MATLAB.

3. Preliminary transformations

Here we present the transformations of the controllers to the form that was used for computations.

3.1. Controller C1.

In the controller C1 there were not used the 5, 8 and 9 coils, so 5, 8 and 9 columns of the matrix were treated as zeros. Besides that in the controller there were chosen

$u_{10} = 0.1 * x_{35}$ and only the first 6 components of observations were used. Thus the system (1), (3) was closed by the controller

$$\frac{dz}{dt} = A_c z + B_c \tilde{y} \cdot \tag{8}$$

Let's denote as $\tilde{B}$ — the matrix without 5,8,9 and 10 columns; $\tilde{C}$ — the matrix consisting of the first 6 lines of the matrix ; E — the square [35:35]-matrix whose entries excepting one $e_{10,35} = 0.1$ are zeros.

After that we obtain the characteristic [65:65]-matrix

$$P\begin{pmatrix} L_s & 0 \\ 0 & I \end{pmatrix} - \begin{pmatrix} -R_s - E & \tilde{B}C_s \\ B_c\tilde{C}_c & A_c \end{pmatrix}, \qquad s = 1,2,3,4,5 \cdot$$

3.2. Controller C2.

For the controller C2 there were used the first 17 observations and the derivatives of the first 6 observations. The controller equations are

$$\frac{dz}{dt} = A_c z + B_c \xi, \tag{9}$$

$$u = C_c z + D_c \xi .$$

where the vector ξ has the dimension 23 and equals to

$$\xi^* = (g^*, \frac{dg^*}{dt}, \epsilon^{1*}, \epsilon^{2*}).$$

Let's denote

as B_c^1, D_c^1 — the matrices composed by the 1-6 columns of the matrices B_c and D_c correspondingly.

as B_c^2, D_c^2 — the matrices composed by the 7-12 columns of the matrices B_c and D_c correspondingly.

as B_c^3, D_c^3 — the matrices composed by the 13-23 columns of the matrices B_c and D_c correspondingly.

as C_s^1, C_s^2 — the matrices composed by the 1-6 and 7-17 rows of the matrices C_s correspondingly.

Then the characteristic matrix of the dimension 85 to consider is

$$P\begin{pmatrix} L_s - BD_c^2C_s^1 & 0 \\ -B_c^2 & I \end{pmatrix} - \begin{pmatrix} -R_s + BD_c^1C_s^1 + BD_c^3C_s^2 & BC_c \\ B_c^1C_s^1 + B_c^3C_s^2 & A_c \end{pmatrix}.$$

3.3. Controller C3.

In this controller there are used all the observation components and it has the form

$$\frac{dz}{dt} = A_c z + B_c y, \tag{10}$$

$$u = -C_c z - D_c y \cdot$$

Excluding the variables, we obtain the system whose characteristic matrix of the dimension 87 is

$$P\begin{pmatrix} L_s & 0 \\ 0 & I \end{pmatrix} - \begin{pmatrix} -R_s - BD_cC_s & BC_c \\ B_cC_s & A_c \end{pmatrix}.$$

4. Conclusions

The results of computations of the first and the second interval stability radii given in appendix lead to the following conclusions.

4.1. The methods of computation of the stability radii based on matrix and polynomial models are comparable with each other.

4.2. All the controllers C1, C2 and C3 have the sufficient robustness.

4.3. The methods proposed allow to estimate the parametric stability margin at the space of the initial physical parameters. To take better into account the nonlinear dependence of the system coefficients on the uncertain parameters one should construct the interval methods of the interval radii estimates based on variational theory.

4.4. The algorithms designed give a possibility to take into account the controllers robustness at the early stages of their design.

Appendix

Table 1

Interval Stability Radii of system (1),(3)

	C1	C2	C3
$r_1(Q_0)$	2.1	3.1	3.8
$r_2(Q_1)$	2.8	2.6	3.3
$r_2(Q_2)$	2.1	2.6	3.3
$r_2(Q_3)$	2.1	2.1	3.1
$r_2(Q_4)$	2.6	3.1	3.8
$r_2(Q_5)$	1.1	5.3	4.6

Here Q is a matrix at the space of the matrices of the system (1), (3)

$$Q = (L, R, C^T),$$

$$Q_0 = (Q_1 + Q_2 + Q_3 + Q_4 + Q_5)/5.$$

Table 2

Interval Stability Radii of system (7)

	C1	C2	C3
$r_1(Q_0)$	2.1	3.1	1.0
$r_2(Q_1)$	2.6	2.9	0.0
$r_2(Q_2)$	2.0	2.1	0.0
$r_2(Q_3)$	2.0	2.5	0.0
$r_2(Q_4)$	2.8	2.6	0.0
$r_2(Q_5)$	1.1	4.3	0.0

Here Q is a matrix at the space of the matrices of the system (7) in normal form:

$$Q = (A, \tilde{B}, C),$$

$$A = -L^{-1}R, \tilde{B} = L^{-1}B.$$

Table 3

Interval Stability Radii

at the space of characteristic polynomial coefficients of system (7)

	C1	C2	C3
$r_1(P_0)$	1.5	1.6	1.6
$r_2(P_1)$	0.5	0.6	0.6
$r_2(P_2)$	0.6	0.6	0.6
$r_2(P_3)$	1.6	1.8	1.6
$r_2(P_4)$	0.5	0.7	0.6
$r_2(P_5)$	1.1	4.4	4.3

Here P is a characteristic polynomial of closed loop system (7).

$$P_0 = (P_1 + P_2 + P_3 + P_4 + P_5)/5$$

References

[1] V. A. Belyakov, A. A. Kavin, D. A. Ovsyannikov, E. I. Veremei, A. P. Zhabko. - Tokamak Plasma Shape Control Mathematical Methods. // *Abstracts, Third Int. Workshop "Beam Dynamics & Optimization"* p. 10, 1996, St.Petersburg

[2] B. A. Misenov, A. D. Ovsyannikov, D. A. Ovsyannikov, E. I. Veremei, A. P. Zhabko. -Non-Linear Model of Tokamak Plasma Shape Stabilization // *Intern. conf. on Informatics and Control (ICI&C 97), 1997, St.Petersburg*

[3] V. L. Kharitonov, A. P. Zhabko. - Linear Algebra Methods in Control Problems // 1993, St.Petersburg

EMISSING AND ELECTRON–OPTICAL PROCESSES MODELING FOR ELECTRON GUN WITH THE FIELD CATHODE

N.V. Egorov, E.M. Vinogradova

Bibliotechnaya 2, Department of Applied Mathematics - Control Processes, St.Petersburg State University, St.Petersburg, 198904, Russia
e-mail: vmpu@apmath.spb.su

Abstract

It is presented the mathematical model for electron-optical system as diode system: field cathode (the thin tip on a flat substrate) — anode (a plane equipotential surface). In this paper the field emission gun is under investigation. The field emission gun is described as the rotationally symmetrical cathode lens, the effect of space charge is neglected. The potential of the tip and substrate is set to zero without the loss of generality ($U_0 = 0$). The parameters of physical problem are: the tip radius of curvature (r_0), the tip length (L), the tip shape ($r_0(z)$), the length from substrate to anode (Z_1), the anode potential (U_1).

Rotationally symmetrical potentials $V(r,z)$ without space charge obey Laplace's equation and the boundary values:

$$\Delta V(r,z) = 0, \qquad V\Big|_{r_0(z)} = U_0, \quad V\Big|_{z=Z_1} = U_1, \tag{1}$$

where (r,z) — cylindrical coordinates, $r_o(z)$ — the tip shape; U_0 — the tip potential; $(-\infty < r < \infty,\ z = Z_1)$ — the anode plane; U_1 — the anode potential.

From [1] the potential distribution $V(r,z)$ would be expressible as:

$$V(r,z) = V_0(r,z) + V_1(r,z) + V_2(r,z), \tag{2}$$

where

$$V_0(r,z) = \int_0^{L-\delta} \frac{\rho(z')}{\sqrt{r^2 + (z-z')^2}} dz', \tag{3}$$

and functions V_1 и V_2 are the solutions of the boundary - value problems:

$$\Delta V_1 = 0, \quad V_1\Big|_{z=z_1} = U_0; \tag{4}$$

$$\Delta V_2 = 0, \quad V_2\Big|_{z=z_1} = -V_1\,. \tag{5}$$

It is obvious that $V_1(r,z)$ is the solution of the boundary - value problem without tip. The function V_2 can be represented as:

$$V_2(r,z) = \int_0^{L-\delta} u_2(r,z;z')\rho(z') \tag{6}$$

where function $u_2(r,z;z')$ is defined from:

$$u_2(r,z;z') = -4\pi G(r,z;0,z') - (r^2+(z-z')^2)^{-1/2}.$$

From (3)—(6), this function can be represented as the solution of the boundary - value problem:

$$\begin{cases} \triangle\ u_2(r,z;z') = 0 \\ u_2(r,z;z')\Big|_{z=Z_1} = -\left[r^2+(Z_1-z')^2\right]^{-1/2} \end{cases} \tag{7}$$

From [1] $\rho(z)$ can be written as:

$$\delta = R_0/2 \tag{8}$$

$$\rho(z) = \sum_{k=0}^{\infty} \rho_k(z), \tag{9}$$

where

$$\rho_0(z) = \frac{\psi_0 - U_1(0,z)}{\ln\frac{4z(L-z)}{r_0^2(z)}}, \tag{10}$$

$$\rho_{k+1}(z) = -\left(\ln\frac{4z(L-z)}{r_0^2(z)}\right)^{-1}\left[\int_0^{L-\delta}\frac{\rho_k(\xi)-\rho_k(z)}{|\xi-z|}d\xi + \int_0^{L-\delta} u_2(0,z;\xi)\rho(\xi)\,d\xi\right]. \tag{11}$$

From $V(r,0)=0$ the value–boundary problem (1) can be spreaded to $z<0$.

Then the functions $V_1(r,z)$ and $V_2(r,z)$ are the solutions of the boundary - value problems:

$$\triangle V_1 = 0, \qquad V_1\Big|_{z=\pm Z_1} = \pm U_0;$$

$$\triangle V_2 = 0, \qquad V_2\Big|_{z=\pm Z_1} = -U_1.$$

So to solve the boundary - value problem (1) (according to (6)) we have to solve two boundary - value problems:

$$\triangle V_1 = 0, \qquad V_1\Big|_{z=\pm Z_1} = \pm U_0; \tag{12}$$

$$\triangle u_2(r,z;z') = 0, \qquad u_2(r,z;z')\Big|_{z=\pm Z_1} = -\frac{1}{\sqrt{r^2+(\pm Z_1-z')^2}}. \tag{13}$$

The solution of the boundary - value problem (11) is obvious:

$$V_1(r,z) = \frac{U_1}{Z_1} z \cdot \tag{14}$$

The function $u_2(r,z;z')$ from (13) can be represented as a Hankel transform [2]:

$$u_2(r,z;z') =$$

$$-\int_0^\infty \left[\lambda \frac{\sinh\lambda(z+Z_1)}{\sinh 2\lambda Z_1} A_1(\lambda) + \frac{\sinh\lambda(Z_1-z)}{\sinh 2\lambda Z_1} A_2(\lambda)\right] \cdot \tag{15}$$

$$\cdot J_0(\lambda r)\, d\lambda, \qquad -Z_1 < z < Z_1$$

The unknown coefficients A_1, A_2 are determinated from boundary values (13) for function $u_2(r,z;z')$ from inverse of a Hankel transform:

$$\begin{aligned} A_1 &= \int_0^\infty \frac{r\, J_0(\lambda r)}{\sqrt{r^2 + (Z_1 - z')^2}}\, dr = \frac{1}{e^{-\lambda(Z_1 - z')}} \\ A_2 &= \int_0^\infty \frac{r\, J_0(\lambda r)}{\sqrt{r^2 + (Z_1 + z')^2}}\, dr = \frac{1}{e^{-\lambda(Z_1 + z')}} \cdot \end{aligned} \tag{16}$$

So the function $u_2(r,z;z')$ can be written:

$$\begin{aligned} u_2(r,z;z') = -\int_0^\infty \Bigg[& e^{-\lambda(Z_1 - z')} \frac{\sinh\lambda(z+Z_1)}{\sinh 2\lambda Z_1} + \\ & + e^{-\lambda(Z_1 + z')} \frac{\sinh\lambda(Z_1 - z)}{\sinh 2\lambda Z_1} \Bigg] \cdot J_0(\lambda r)\, d\lambda. \end{aligned} \tag{17}$$

After some transformations (16) can be defined by the series [17]:

$$\begin{aligned} u_2(r,z;z') = -\sum_{k=0}^{\infty} \Bigg\{ & \Bigg[\frac{1}{\sqrt{r^2 + (4kZ_1 + 2Z_1 - (z+z'))^2}} - \\ & - \frac{1}{\sqrt{r^2 + (4kZ_1 + 4Z_1 - (z'-z))^2}} \Bigg] + \\ & + \Bigg[\frac{1}{\sqrt{r^2 + (4kZ_1 + 2Z_1 + (z+z'))^2}} - \frac{1}{\sqrt{r^2 + (4kZ_1 + 4Z_1 + (z'-z))^2}} \Bigg] \Bigg\} \cdot \end{aligned} \tag{18}$$

The functions $V_0(r,z)$ and $V_0(r,z)$ can be represented as:

$$V_0(r,z) = \int_{-(L-\delta)}^{L-\delta} \frac{\rho(z')}{\sqrt{r^2 + (z-z')^2}} dz', \tag{19}$$

$$V_2(r,z) = \int_{-(\breve{L}-\delta)}^{l-\delta} u_2(r,z;z')\rho(z') \ . \qquad (20)$$

Thus the formulas (2),(8)—(11),(14),(18)—(20) are the solution of the value–boundary problem (1).

And so the potential distribution is determined for our diode system.

The emission characteristic values (the field strength for the cathode's top, the current density for the cathode's top, the emission area) are presented on Table 1 and Tabl.2. These values are calculated for various anode potentials (Tabl. 1) and for various distances between the cathode top and anode plane (Tabl.2) from the next parameters: the tip radius of curvature $r_0 = 10^{-6}$cm, the tip length $L = 10^1$cm.

Let
U_1 — the anode potential,
E_0 — the field strength for the cathode top,
J_0 — the current density for the cathode top,
S_{em} — the emission area,
I — the cathode current.

Table 1

The emission characteristic values for the various anode potentials.

U_1 (B)	E_0 (V/cm)	J_0 (A/cm^2)	S_{em} (cm^2)	I (A)
100	$1.55709\cdot10^{7}$	$3.22958\cdot10^{-8}$	$.177319\cdot10^{-12}$	$.572666\cdot10^{-20}$
180	$2.94974\cdot10^{7}$	$2.50354\cdot10^{1}$	$.387450\cdot10^{-12}$	$.968834\cdot10^{-11}$
200	$3.10834\cdot10^{7}$	$8.22359\cdot10^{1}$	$.415330\cdot10^{-12}$	$.341550\cdot10^{-10}$
225	$3.66420\cdot10^{7}$	$2.37240\cdot10^{3}$	$.519888\cdot10^{-12}$	$.123338\cdot10^{-8}$
250	$4.09674\cdot10^{7}$	$1.75878\cdot10^{4}$	$.610108\cdot10^{-12}$	$.107304\cdot10^{-7}$
275	$4.51379\cdot10^{7}$	$8.53180\cdot10^{4}$	$.705440\cdot10^{-12}$	$.601867\cdot10^{-7}$
300	$4.92709\cdot10^{7}$	$3.15338\cdot10^{5}$	$.808786\cdot10^{-12}$	$.255041\cdot10^{-6}$
325	$5.33913\cdot10^{7}$	$9.58303\cdot10^{5}$	$.922394\cdot10^{-12}$	$.883933\cdot10^{-6}$
350	$5.75063\cdot10^{7}$	$2.49093\cdot10^{6}$	$.104732\cdot10^{-11}$	$.260881\cdot10^{-5}$
375	$6.16187\cdot10^{7}$	$5.73000\cdot10^{6}$	$.118578\cdot10^{-11}$	$.679451\cdot10^{-5}$
400	$6.57298\cdot10^{7}$	$1.19396\cdot10^{7}$	$.134014\cdot10^{-11}$	$.160008\cdot10^{-4}$
425	$6.98400\cdot10^{7}$	$2.28392\cdot10^{7}$	$.151187\cdot10^{-11}$	$.345299\cdot10^{-4}$
450	$7.39497\cdot10^{7}$	$4.09775\cdot10^{7}$	$.170714\cdot10^{-11}$	$.699543\cdot10^{-4}$
475	$7.80592\cdot10^{7}$	$6.90683\cdot10^{7}$	$.192641\cdot10^{-11}$	$.133054\cdot10^{-3}$
500	$8.21684\cdot10^{7}$	$1.11109\cdot10^{8}$	$.217866\cdot10^{-11}$	$.242069\cdot10^{-3}$

Table 1 is presented for $z_1 = .11$cm (the anode plane).

Table 2

The emission characteristic values for the various anode planes.

z_1 (cm)	E_0 (V/cm)	J_0 (A/cm^2)	S_{em} (cm^2)	I (A)
.10010	$7.70721 \cdot 10^7$	$6.12427 \cdot 10^7$	$.187134 \cdot 10^{-11}$	$.114606 \cdot 10^{-3}$
.10109	$7.54038 \cdot 10^7$	$4.96178 \cdot 10^7$	$.178178 \cdot 10^{-11}$	$.884078 \cdot 10^{-4}$
.10208	$7.37814 \cdot 10^7$	$4.00599 \cdot 10^7$	$.169869 \cdot 10^{-11}$	$.680495 \cdot 10^{-4}$
.10307	$7.22031 \cdot 10^7$	$3.22287 \cdot 10^7$	$.162143 \cdot 10^{-11}$	$.522566 \cdot 10^{-4}$
.10406	$7.06665 \cdot 10^7$	$2.58312 \cdot 10^7$	$.154939 \cdot 10^{-11}$	$.400225 \cdot 10^{-4}$
.10505	$6.91685 \cdot 10^7$	$2.06198 \cdot 10^7$	$.148200 \cdot 10^{-11}$	$.305585 \cdot 10^{-4}$
.10604	$6.77062 \cdot 10^7$	$1.64551 \cdot 10^7$	$.142012 \cdot 10^{-11}$	$.233682 \cdot 10^{-4}$
.10703	$6.62768 \cdot 10^7$	$1.30736 \cdot 10^7$	$.136189 \cdot 10^{-11}$	$.178047 \cdot 10^{-4}$
.10802	$6.48774 \cdot 10^7$	$1.03337 \cdot 10^7$	$.130685 \cdot 10^{-11}$	$.135045 \cdot 10^{-4}$
.10901	$6.35052 \cdot 10^7$	$8.12207 \cdot 10^6$	$.125470 \cdot 10^{-11}$	$.101907 \cdot 10^{-4}$
.11000	$6.21576 \cdot 10^7$	$6.34435 \cdot 10^6$	$.120515 \cdot 10^{-11}$	$.764586 \cdot 10^{-5}$

Table 2 is presented for $U_1 = 400$V (the anode potential).

References

[1] E. M. Vinogradova, *Mathematical model of electron gun with field cathode* Proc. of The First Inter. Workshop BDO'94, pp. 179—184, St.Petersburg, 1994.

[2] J. Ufliand, *Dual equations method in the mathematical physics problems*, Leningrad, 1977.

The Computer Reconstruction of Dipole Magnetic Field Perturbations for the Synchrotron-Type Accelerator *

E.P.Zhidkov I.E.Zhidkova V.A.Michailov

Laboratory of Computing Techniques and Automation,
Joint Institute for Nuclear Research,
141980, Dubna, Russia

Abstract

The method to reconstruct the dipole magnetic field perturbations for synchrotron-type accelerator is represented.

The deviations of closed orbit are considered. The proposed method is applied to JINR Nuclotron .

The equation of the closed orbit is consider [1]:

$$y'' + K_y(\theta)y = F_{yk}(y, y', \theta), \tag{1}$$

where $K_y(\theta)$ - the frequancy , $\theta \in [0, 2\pi]$ - the azimuth and F_{yk} - the sectionally continuous unknown function. The boundary conditions are :

$$y(0) = y(2\pi), y'(0) = y'(2\pi), \tag{2}$$

where $y(\theta)$ - the unknown function (dipole magnetic field function) ,which must be reconstructed. Besides this , $K_y(\theta) = K = const$ and the constant is known , $F_{yk}(y, y', \theta) = f(\theta)$ and

$$|f(\theta)| \leq K = const > 0. \tag{3}$$

Around the accelerator ring the 20 beam monitors are stated practically proportionally to measure the values of unknown function $f(\theta)$ in these points. The experimental values of such measurements are known :

$$Y = \{y_1(\theta_1), y_2(\theta_2), ..., y_{20}(\theta_{20})\}, \tag{4}$$

* The task was done with the support of RFBI , project numbers : 97 - 01 - 00746,98 - 01 - 00190, and with the support of Federal Center "Integration" , project number K0085/98.

where $\Theta \in \{\theta_1, \theta_2, ..., \theta_{20}\}$ - the coordinates of beam monitors , which are used as boundary conditions .

So we have the uncorrect back problem , which was formulated for Nuclotron of JINR.

The next method to solve the problem (1) – (4) was proposed. The solution of the equation (1) , depends on $f(\theta)$, for $K_y(\theta) = k^2 = const$ is well known and does look like :

$$y(\theta) = \frac{1}{k}\int_0^\theta \sin k(\theta - t)f(t)dt +$$

$$\frac{\cos k\theta - \cos k(2\pi - \theta)}{2k(1-\cos 2\pi k)}\int_0^{2\pi} \sin k(\theta - t)f(t)dt + \qquad (5)$$

$$\frac{\sin k\theta + \sin k(2\pi - \theta)}{2k^2(1-\cos 2\pi k)}\int_0^{2\pi} \cos k(\theta - t)f(t)dt.$$

Then , the experimental values of $y(\theta) \in Y$ are known. So , let conside the functional

$$\Phi(f) = \sum_{k=1}^{20} (y(\theta_k) - y_k)^2, \qquad (6)$$

where $y(\theta_k)$ - the values of solution (5) in θ_k points and y_k - the experimental values of function $f(\theta)$. Let us minimize this functional $\Phi(f)$ with respect to f . In such case we recieve : 1. the right-hand side of equation (1) is reconstructed , as the minimum of the functional is reached just for such $\hat{f}$ function , which is good enough approximated this right-hand side , 2. for this right-hand side function we reconstructed the function $f(\theta)$, using the existing solution (5) .

The values of $y(\theta)$ are equal to values of experimental measered function in points from set Θ

The programs are produced and testing to realize this algorithm. For functional minimization the FUMILI program [2] was used.

References

[1] Kolomensky A.A. The physician basis of charged particles acceleration methods, Moscow University publish. dep., 1980

[2] Silin I.N. The standard program to solve the problem ... , Dubna, 1967, 11-3362.

Proceedings of the 4th International Workshop
BEAM DYNAMICS AND OPTIMIZATION

Международная конференция
Динамика пучков и оптимизация

Д9,11-98-273

Ответственный за подготовку сборника к печати И.П.Юдин

Редактор Э.В.Ивашкевич, Е.Ю.Шаталова. Макет Р.Д.Фоминой

Рукопись сборника поступила 29.09.98. Подписано в печать 21.12.98
Формат 60 × 84/8. Офсетная печать. Уч.-изд. листов 18,0
Тираж 200. Заказ 51049. Цена 50 р.

Издательский отдел Объединенного института ядерных исследований
Дубна Московской области